

МІНІСТЕРСТВО ОСВІТИ І НАУКИ УКРАЇНИ
Карпатський національний університет імені Василя Стефаника
ННЦ «Напівпровідникове матеріалознавство»
АКАДЕМІЯ НАУК ВИЩОЇ ШКОЛИ УКРАЇНИ
НАЦІОНАЛЬНА АКАДЕМІЯ НАУК УКРАЇНИ
Інститут фізики напівпровідників ім. В.Є. Лашкарьова
Інститут металофізики ім. Г.В. Курдюмова
Українське фізичне товариство
Благодійний фонд "Івано-Франківське математичне товариство"

**ХХ МІЖНАРОДНА ФРЕЙКІВСЬКА КОНФЕРЕНЦІЯ З ФІЗИКИ І
ТЕХНОЛОГІЙ ТОНКИХ ПЛІВОК ТА НАНОСИСТЕМ**

Матеріали

Iвано-Франківськ, 06-10 жовтня, 2025 р.

Ivano-Frankivsk, October 06-10, 2025

Materials

**XX INTERNATIONAL FREIK CONFERENCE ON PHYSICS AND
TECHNOLOGY OF THIN FILMS AND NANOSYSTEMS**

MINISTRY OF EDUCATION AND SCIENCE OF UKRAINE
Vasyl Stefanyk Carpathian National University
Science & Educational Centre of Semiconductor Material Science
ACADEMY OF SCIENCE OF HIGH SCHOOL OF UKRAINE

NATIONAL ACADEMY OF SCIENCE OF UKRAINE
V.E. Lashkarev Institute of Semiconductor Physics
G.V. Kurdyumov Institute of the Physics of Metals
Ukraine Physics Society
CO "Charitable Foundation "Ivano-Frankivsk Mathematical Society"

УДК 539.2

Л 80

XX Міжнародна Фреїківська конференція з фізики і технології тонких плівок та наносистем. *Матеріали.* / За ред. Л.І. Никируя, Т. С. Потятинник, М. Д. Крайнова, І. Р. Міщук. Івано-Франківськ : Вид-во Карпатського національного університету імені Василя Стефаника, 2025. 254 с.

Представлено сучасні результати теоретичних і експериментальних досліджень з питань фізики і технології тонких плівок та наносистем (метали, напівпровідники, діелектрики, провідні полімери; методи отримання та дослідження; фізико-хімічні властивості; нанотехнології і наноматеріали, квантово-розмірні структури, наноелектроніка, тощо. Матеріали підготовлено до друку Організаційним комітетом конференції та подано в авторській редакції.

Для наукових та інженерних працівників, що займаються проблемами тонкоплівкового матеріалознавства та мікроелектроніки.

Рекомендовано до друку вченого радою Фізико-технічного факультету Карпатського національного університету імені Василя Стефаника

XX International Freik Conference Physics and Technology of Thin Films and Nanosystems. *Materials.* / Ed. by L.I. Nykyruy, T. S. Potiatynnyk, M. D. Krainova, I. R. Mishchuk. Ivano-Frankivsk : Publisher Vasyl Stefanyk Carpathian National University, 2025. 254 p.

The results of theoretical and experimental researches in directions of the physics and technology of thin films and nanosystems (metals, semiconductors, dielectrics, and polymers; and methods of their investigation; physic-chemical properties of thin films; nanotechnology and nanomaterials, quantum-size structures; thin-film devices of electronics, are presented. The materials preformed for printing by Conference's Organization Committee and Editorial Board, are conveyed in authoring edition.

For scientists and reserchers on the field of thin-film material sciences and nanoelectronics.

© Карпатський національний університет
імені Василя Стефаника, 2025
© Vasyl Stefanyk Carpathian National
University, 2025

ORGANIZING COMMITTEE

Lyubomyr NYKRYUY, *Chair*, CNU, Ukraine

Ihor Horichok, *Co-Chair*; CNU, Ukraine

Volodymyr Kotsyubynski, *Co-chair*; CNU, Ukraine

Ihor Lishchynskyy, *Co-chair*; CNU, Ukraine

Maksym Strikha, *Co-chair*; V.E.Lashkarev Institute of Semiconductor Physics
NAS of Ukraine, Taras Shevchenko National University of Kyiv, Ukraine

LOCAL ORGANIZING COMMITTEE

Viktor BORYK, Volodymyra BOYCHUK, Ivan BUDZULYAK, Roman DZUMEDZEY, Bohdan DZUNDZA, Oksana HOLOVATA, Halyna HURGULA, Roman ILNYTSKYI, Iryna IVANYSHYN, Volodymyr KLANICHKA, Ihor KOHUT, Galyna MATEIK, Volodymyr MANDZYUK, Ostap MATKIVSKIY, Lyubov MEZHYLOVSKA, Bohdanna NAIDYCH, Zhanna OLEKSYN, Bohdan RACHIY, Yaroslav SALIY, Taras SEMKO, Volodymyr TROIANSKYI, Liliya TUROVSKA, Ivanna VAKALYUK, Halyna VOYTKIV, Lyubov YABLON, Ivan YAREMIY, Lilia YAVORSKA, Rostyslav YAVORSKYI, Svyatoslav YAVORSKYI

ORGANIZING COMMITTEE

AHISKA Rasit, *Gazi University*, Turkey

AOKI Toru, *Shizuoka University*, Japan

BABANLY Mahammad, *Institute of Catalysis and Inorganic Chemistry*, Azerbaijan

BELYAEV Oleksandr, *V.E.Lashkarev Institute of Semiconductor Physics NAS of Ukraine*, Ukraine

BORCHA Marjana, *Yuri Fedkovych Chernivtsi National University*, Ukraine

DRUZHYNIN Anatoliy, *Lviv Polytechnic National University*, Ukraine

FEDOSOV Sergiy, *Lutsk National Technical University*, Ukraine

FOCHUK Petro, *Yuri Fedkovych Chernivtsi National University*, Ukraine

FODCHUK Ihor, *Yuri Fedkovych Chernivtsi National University*, Ukraine

GALUSHCHAK Marian, *Ivano-Frankivsk National technical University of Oil and Gas*, Ukraine

GARDONIO Sandra, *University of Nova Gorica*, Slovenija

GASYUK Ivan, *CNU*, Ukraine

GORDIICHUK Pavlo, *Avanti Battery Company*, USA

GUREVICH Yuri, *Centro de Investigacion y de Estudios Avanzados del Instituto Politécnico Nacional*, Mexico

IVASISHIN Orest, *G. V. Kurdumov Institute for Metal Physics NAS of Ukraine*, Ukraine

KABAN Ivan, *Leibniz-Institut für Festkörper- und Werkstoffsorschung Dresden*, Germany

KHARCHENKO Mykola, *B. Verkin Institute for Low Temperature Physics & Engineering of the NAS of Ukraine*, Ukraine

KÖKÉNYESI Sandor, *Debreceni Egyetem*, Hungary

KORBUTYAK Dmytro, *V.E.Lashkarev Institute of Semiconductor Physics NAS of Ukraine*, Ukraine

KOVALENKO Oleksandr, *O. Honchar Dnipro national University*, Ukraine

KYYAK Bohdan, *NAS of Ukraine*, Ukraine

LEPIKH Yaroslav, *I. Mechnikov Odesa National University*, Ukraine

LYSKO Valentyn, *Institute of Thermoelectricity NAS of Ukraine and MES of Ukraine; Yuriy Fedkovych Chernivtsi National University*, Ukraine

LYTVYN Petro, *V.E.Lashkarev Institute of Semiconductor Physics NAS of Ukraine*, Ukraine

MAZUR Myroslav, *Ivano-Frankivsk National technical University of Oil and Gas*, Ukraine

MAZUR Tetiana, *Ivano-Frankivsk National technical University of Oil and Gas*, Ukraine

MOISEENKO Mykola, *Ivano-Frankivsk National Medical University*, Ukraine

MOKLYAK Volodymyr, *Joint Laboratory of Physics of Magnetic Films (G. V. Kurdyumov Institute for Metal Physics NAS of Ukraine and PNU)*, Ukraine

MYRONYUK Ivan, *CNU*, Ukraine

OGORODNIK Yaroslav, *Radiation Monitoring Devices, inc.*, USA

PARASHCHUK Taras, *AGH University of Science and Technology*, Poland

PELESHCHAK Roman, *Lviv Polytechnic National University*, Ukraine

PROKOPENKO Ihor, *V.E.Lashkarev Institute of Semiconductor Physics NAS of Ukraine*, Ukraine

PROTSENKO Ivan, *Sumy State University*, Ukraine

ROGACHOVA Olena, *National Technical University Kharkiv Polytechnic Institute*, Ukraine

RUBISH Vasyl, *Institute for Information Recording NAS of Ukraine*, Ukraine

SHENDEROVSKIY Vasyl, *Institute of Physics NAS of Ukraine*, Ukraine

SHVYDKA Diana, *Ohio State University*, USA

SMERTENKO Petro, *V.E.Lashkarev Institute of Semiconductor Physics NAS of Ukraine*, Ukraine

STOLYARCHUK Ihor, *Ivan Franko Drohobych State Pedagogical University*, Ukraine

STRONSKY Oleksandr, *V.E.Lashkarev Institute of Semiconductor Physics NAS of Ukraine*, Ukraine

SWIATEK Zbigniew, *Instytut Metalurgii i Inżynierii Materiałowej Polskiej Akademii Nauk*, Poland

TATARENKO Valentyn, *G. V. Kurdyumov Institute for Metal Physics NAS of Ukraine*, Ukraine

TIGINYANU Ion, *Technical University of Moldova*, Moldova

TITOVA Lyubov, *Worcester Polytechnic Institute*, USA

TOMASHYK Vasyl, *V.E.Lashkarev Institute of Semiconductor Physics NAS of Ukraine*, Ukraine

UHRIN Robert, *XLight Corporation*, USA

WISZ Grzegorz, *University of Rzeszów*, Poland

WOJCIECHOWSKI Krzysztof, *AGH University of Science and Technology*, Poland

ZAPUKHLYAK Ruslan, *CNU*, Ukraine

ZAYACHUK Dmytro, *Lviv Polytechnic National University*, Ukraine

ZINCHENKO Victor, *A. V. Bogatsky Physico-Chemical Institute*, Ukraine

ОРГАНІЗАЦІЙНИЙ КОМИТЕТ

Голова Оргкомітету

Любомир НИКИРУЙ, завідувач кафедри фізики та астрономії Карпатського національного університету імені Василя Стефаника, Івано-Франківськ, Україна)

Заступники голови Оргкомітету

Ігор ГОРЧОК, професор кафедри фізики та астрономії Карпатського національного університету імені Василя Стефаника, Івано-Франківськ, Україна)

Володимир КОЦЮБИНСЬКИЙ, завідувач кафедри прикладної фізики і матеріалознавства Карпатського національного університету імені Василя Стефаника, Івано-Франківськ, Україна)

Ігор ЛІЩИНСЬКИЙ професор кафедри фізики та астрономії Карпатського національного університету імені Василя Стефаника, Івано-Франківськ, Україна)

Максим СТРИХА, професор кафедри фізичної електроніки факультету радіофізики, електроніки та комп'ютерних систем КНУ імені Тараса Шевченка, г.н.с. Інституту фізики напівпровідників ім. В.Є. Лашкарьова

Члени організаційного комітету

Професор Рашит АХИСКА, Університет Газі, Туреччина;

професор Тору АОКІ, університет Шізуокі, Японія;

член-кореспондент НАН Азербайджану, професор Магомет БАБАНЛИ, Інститут каталізу та неорганічної хімії, Азербайджан;

академік НАН України, професор Олександр БЄЛЯЄВ, Інститут фізики напівпровідників імені В.Є.Лашкарьова НАН України, Україна;

професор Мар'яна БОРЧА, Чернівецький національний університет імені Юрія Федьковича, Україна;

професор Гжеґож ВІШ, Жешувський університет, Польща;

професор Кшиштоф ВОЙЦЕХОВСЬКИЙ, Університет науки і технологій AGH, Польща;

професор Анатолій ДРУЖИНІН, Національний університет «Львівська політехніка», Україна;

професор Мар'ян ГАЛУЩАК, Івано-Франківський національний технічний університет нафти і газу, Україна;

професор Сандра ГАРДОНІО, Університет Нової Гориці, Словенія;

професор Іван ГАСЮК, Карпатський національний університет імені Василя Стефаника, Україна;

д-р Павло ГОРДІЧУК, Avanti Battery Company, Бостон, США;

професор Юрій ГУРЕВИЧ, Національний політехнічний інститут, Мехіко, Мексика;

академік НАН України, професор Орест ІВАСИШИН, Інститут металофізики імені Г. В. Курдюмова НАН України, Україна;

професор Руслан ЗАПУХЛЯК, Карпатський національний університет імені Василя Стефаника, Україна;

професор Дмитро ЗАЯЧУК, Національний університет «Львівська політехніка», Україна;

професор Віктор ЗІНЧЕНКО, Фізико-хімічний інститут імені А. В. Богатського, Україна

професор Іван КАБАН, Інститут Лейбніца, Дрезден, Німеччина;

професор Богдан КИЯК, НАН України, Україна;

професор Олександр КОВАЛЕНКО, Дніпровський національний університет імені О. Гончара, Україна;

професор Шандор КОКЕНЕШІ, університет Дебрецену, Угорщина;
професор Дмитро КОРБУТЯК, Інститут фізики напівпровідників імені В.Є.Лашкарьова НАН України, Україна;
професор Ярослав ЛЕПІХ, Одеський національний університет імені І. Мечникова, Україна;
д-р Петро ЛИТВИН, Інститут фізики напівпровідників імені В.Є.Лашкарьова НАН України, Україна;
д-р Мирослав МАЗУР, Івано-Франківський національний технічний університет нафти і газу, Україна;
д-р Тетяна МАЗУР, Івано-Франківський національний технічний університет нафти і газу, Україна;
професор Микола МОІСЕЄНКО, Івано-Франківський національний медичний університет, Україна;
професор Володимир МОКЛЯК, Спільна лабораторія фізики магнітних плівок (Інститут металофізики ім. Г. В. Курдюмова НАН України та Карпатський національний університет імені Василя Стефаника), Україна;
професор Іван МИРОНЮК, Карпатський національний університет імені Василя Стефаника, Україна;
професор Ярослав ОГОРОДНИК, Radiation Monitoring Devices, Inc., США;
професор Тарас ПАРАЩУК, Університет науки і техніки AGH, Польща;
професор Роман ПЕЛЕЩАК, Національний університет «Львівська політехніка», Україна;
професор Ігор ПРОКОПЕНКО, Інститут фізики напівпровідників імені В.Є.Лашкарьова НАН України, Україна;
професор Іван ПРОЦЕНКО, Сумський державний університет, Україна;
професор Олена РОГАЧОВА, Національний технічний університет Харківський політехнічний інститут, Україна;
професор Василь РУБІШ, Інститут реєстрації інформації НАН України, Україна;
професор Василь ШЕНДЕРОВСЬКИЙ, Інститут фізики НАН України, Україна;
професор Діана ШВІДКА, Університет штату Огайо, США;
д-р Збігнев СВЬОНТЕК, Інститут металургії та інженерії матеріалів ПАН, Польща;
д-р Петро СМЕРТЕНКО, Інститут фізики напівпровідників імені В.Є.Лашкарьова НАН України, Україна;
професор Ігор СТОЛЯРЧУК, Дрогобицький державний педагогічний університет імені Івана Франка, Україна;
професор Олександр СТРОНСЬКИЙ, Інститут фізики напівпровідників імені В.Є.Лашкарьова НАН України, Україна;
академік НАН України, професор Валентин ТАТАРЕНКО, Інститут металофізики ім. Г. В. Курдюмова НАН України, Україна;
віце-президент НАН Молдови, академік, професор Іон ТІГІНЯНУ, Технічний університет Молдови, Молдова;
професор Любов ТІТОВА, політехнічний інститут Вочестеру, США;
професор Василь ТОМАШІК, Інститут фізики напівпровідників імені В.Є.Лашкарьова НАН України, Україна;
Роберт УГРІН, XLight Corporation, США;
професор Сергій ФЕДОСОВ, Луцький національний технічний університет, Україна;
професор Ігор ФОДЧУК, Чернівецький національний університет імені Юрія Федьковича, Україна;
професор Петро ФОЧУК, Чернівецький національний університет імені Юрія Федьковича, Україна;

академік НАН України, професор Микола ХАРЧЕНКО, Фізико-технічний інститут низьких температур ім. Б. Вєркіна НАН України, Україна.

ЛОКАЛЬНИЙ ОРГАНІЗАЦІЙНИЙ КОМІТЕТ

(Карпатський національний університет імені Василя Стефаника)

Володимира БОЙЧУК, д.ф.-м.н., професорка кафедри прикладної фізики і матеріалознавства

Віктор БОРИК, к.ф.-м.н., доцент кафедри хімії середовища та хімічної освіти

Іван БУДЗУЛЯК, д.ф.-м.н., професор кафедри прикладної фізики і матеріалознавства

Іванна ВАКАЛЮК, д-р філософії;

Галина ВОЙТКІВ, к.пед.н., доцент кафедри фізики та астрономії;

Ольга ДАНИЛЮК, інженер кафедри фізики та астрономії

Роман ДЗУМЕДЗЕЙ, к.ф.-м.н., доцент кафедри фізики та астрономії

Богдан ДЗУНДЗА, д.ф.-м.н., професор кафедри комп’ютерної інженерії та електроніки

Роман ІЛЬНИЦЬКИЙ, д.ф.-м.н., професор кафедри прикладної фізики і матеріалознавства

Ірина ІВАНИШИН, к.х.н., завідувачка кафедри теорії та методики фізичної культури

Володимир КЛАНІЧКА, к.ф.-м.н., професор кафедри фізики та астрономії

Юрій КЛАНІЧКА, к.ф.-м.н., доцент кафедри математики та інформатики і методики навчання

Ігор КОГУТ, д.т.н., завідувач кафедри комп’ютерної інженерії та електроніки

Володимир МАНДЗЮК, д.ф.-м.н., завідувач кафедри комп’ютерної інженерії та електроніки

Остап МАТКІВСЬКИЙ, к.ф.-м.н., с.н.с. кафедри фізики та астрономії

Любов МЕЖИЛОВСЬКА, к.ф.-м.н.

Жанна ОЛЕКСИН, аспірантка кафедри фізики та астрономії

Омелян ПОПЛАВСЬКИЙ, к.ф.-м.н., доцент кафедри фізики та астрономії

Богдан РАЧІЙ, д.ф.-м.н., професор кафедри прикладної фізики і матеріалознавства

Ярослав САЛІЙ, д.ф.-м.н., професор кафедри фізики та астрономії

Ірина СВІД, д.ф.-м.н., професор кафедри комп’ютерної інженерії та електроніки

Тарас СЕМКО, к.ф.-м.н.

Володимир ТРОЯНСЬКИЙ, к.ф.-м.н., професор кафедри фізики та астрономії

Лілія ТУРОВСЬКА, к.х.н., заступник декана факультету управління

Любов ЯБЛОНЬ, д.ф.-м.н., професор кафедри фізики та астрономії

Лілія ЯВОРСЬКА, аспірантка кафедри фізики та астрономії

Ростислав ЯВОРСЬКИЙ, д-р філософії, доцент кафедри фізики та астрономії

Ярослав ЯВОРСЬКИЙ, к.ф.-м.н., завідувач лабораторіями кафедри фізики та астрономії

Іван ЯРЕМІЙ, д.ф.-м.н., професор кафедри прикладної фізики і матеріалознавства.

Topic 1

Thin films technology and research methods

Application of machine learning methods for quality and accuracy evaluation of software analysis of x-ray diffraction reflection curves

Yaremiy I.P., Vekeryk D.V., Yaremii H.I., Yaremiy S.I., Tomyn Ya.I.

Vasyl Stefanyk Carpathian National University, Ivano-Frankivsk, Ukraine,
yaremiyip@pnu.edu.ua

Analysis of X-ray diffraction reflection curves (XRC) is one of the key methods for studying the structural properties of single crystals. Traditional approaches are based on complex physical models and iterative fitting algorithms, which require a good initial approximation, long computation times, and expert supervision. Machine learning methods are considered as a promising alternative for automation of this process.

The aim of this research is to develop a methodology for applying convolutional neural networks (CNN) to analyze XRCs and to determine structural parameters of single-crystal samples with defective near-surface layers.

The basis of the study is the generation of synthetic training data reflecting the relationship between deformation profile parameters and corresponding XRCs. Key parameters (D_{max1} , D_{01} , L_1 , R_{p1} , D_{02} , L_2 , R_{p2}) were varied within physically reasonable ranges, with sublayer thickness (dl) and minimum deformation (D_{min}) taken into account. Theoretical XRCs were calculated using the statistical dynamical theory of diffraction, with added noise and varying resolution to approximate experimental conditions.

CNNs were chosen due to their advantages:

- effective detection of local patterns in XRC shapes;
- invariance to horizontal shifts;
- hierarchical extraction of features of different complexity levels;
- robustness to experimental noise.

The proposed CNN architecture consists of an input layer for XRCs, multiple convolutional layers with different kernel sizes, pooling layers, and fully connected layers for profile parameter regression. Initial testing on a limited set of synthetic data showed that the system determines structural parameters with accuracy comparable to traditional methods, but with significantly higher processing speed.

The main challenge remains the optimization of training data generation to ensure sufficient coverage of possible deformation profiles while balancing the volume of data with available computational resources.

Automation of thermoelectric parameter research in thin-film energy converters

Dzundza B.S., Dombrovskyi S.V., Shtun M.V., Morgun A.V.

Vasyl Stefanyk Carpathian National University, Ivano-Frankivsk, Ukraine,
bohdan.dzundza@pnu.edu.ua

The challenge of improving the efficiency of thin-film semiconductor thermoelectric energy converters has led to a significant number of studies in this field. Therefore, enhancing the accuracy and automating the measurement of the Seebeck coefficient, thermal conductivity, and load characteristics of thin-film thermoelectric elements is highly relevant.

An automated setup has been developed for measuring the thermoelectric parameters of thin-film thermoelectric energy converters. The structural diagram of the system is shown in Fig. 1.

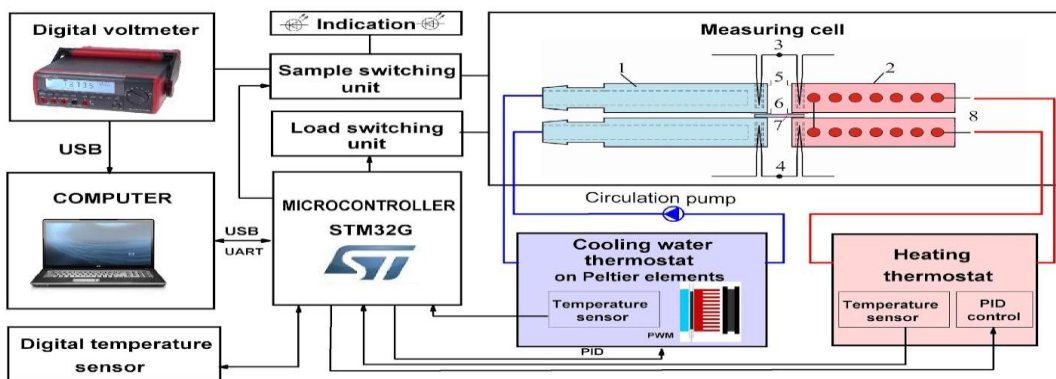


Fig. 1. Structural diagram of the automated setup for measuring thermoelectric parameters of thin films. 1 – water radiator, 2 – electric heater, 3,4 – thermocouples, 5 – load contacts, 6 – measurement contacts, 7 – thin-film sample.

The system is based on the STM32G474 microcontroller, which includes analog modules for temperature measurement and stabilization, as well as load control across a wide current range from $10 \mu\text{A}$ to 100 mA . For measuring the electrical parameters of the sample, a separate galvanically isolated precision voltmeter UTM1805A is used, with data output to a computer. This implementation enables automated selection of optimal load conditions, measurements across wide ranges, and preliminary automated processing of experimental results.

Automatic Defect Recognition of Lithography on Encoder Disk Surfaces

Manko D.Yu¹, Chehil Yu.I².

¹ Institute for information recording NAS of Ukraine, Ukraine,

dmitriy.manko@gmail.com

² Institute for information recording NAS of Ukraine, Ukraine,

y.chehil@gmail.com

Computer vision detects defects through image analysis. While machine learning methods require large datasets, a conventional approach proves more efficient for identifying lithography defects in encoder disks during small-scale production, enabling quick correction.

The video stream is captured via DroidCam and processed frame by frame. Each frame is converted to grayscale for simplified analysis, then smoothed using Gaussian blur to reduce noise. Adaptive thresholding dynamically binarizes the image to handle lighting variations. Morphological operations refine the binary image by filling gaps and removing noise. The resulting mask highlights potential unclean areas when overlaid on the original image. Contour detection identifies the boundaries of non-highlighted regions, whose centroids are then converted to polar coordinates (radius and angle) relative to the image center. The entire process is visualized through a 2x2 grid showing key steps, with polar coordinates displayed in a separate.



Fig. 1. Automatic defect detection using code implemented according to the presented algorithm.

The obtained results demonstrate the feasibility of applying the proposed approach for automated quality control, providing fast and accurate anomaly detection.

Colloidal synthesis and electronic characteristics of CdTe ultrasmall quantum dots

O.G. Kosinov, D.V. Korbutyak, K.S. Dremluzhenko, B.N. Kulchytskyi, O.F. Isaeva, N.V. Mazur, L.I. Trishchuk

V. Lashkarev Institute of Semiconductor Physics, NAS Ukraine, Kyiv, Ukraine,

alex.kosinov.w@gmail.com

The study of ultra-small quantum dots (USQDs) of A_2B_6 semiconductor compounds, with dimensions not exceeding 2 nm, is highly relevant due to their unique properties, such as sharp high-frequency light absorption and almost entirely surface luminescence. These USQDs are promising for applications in light-emitting devices, solar energy, medicine (as "contrast agents" in MRI and for targeted drug delivery), and in high-speed information storage and processing devices. While CdS and CdSe USQDs have been extensively studied, less attention has been paid to CdTe USQDs, despite their importance for the development of long-wavelength photodetectors.

The research focuses on the colloidal synthesis of CdTe nanocrystals (NCs), which is one of the simplest and most accessible methods. The process involves a reaction in a solution of CdI_2 salt, thioglycolic acid (TGA), and NaOH alkali, through which gaseous H_2Te , obtained electrochemically in a galvanostatic cell, is passed. To isolate CdTe USQDs with a size of approximately 2 nm, a centrifugation method was proposed and used. Specific conditions for obtaining these USQDs included low current values (up to 100 mA), short synthesis time (0.5-1 min), and high pH values (8-11) of the reaction medium.

Optical absorption spectra for five CdTe NC samples showed that the maximum absorption bands lie in the range of 300 nm - 310 nm (4.13 - 4.00 eV). This energy significantly exceeds the band gap of bulk CdTe (1.5 eV), which is direct confirmation that these high-energy transitions correspond to ultra-small CdTe quantum dots (clusters) with dimensions ≤ 2 nm. Quantitative studies of CdTe size using the Zetasizer Nano ZS confirmed the presence of USQDs with dimensions of approximately 2 nm.

Photoluminescence (PL) spectra of the CdTe NC samples showed a wide spread of PL maxima in the range of 517 nm - 541 nm. This significant spread, in contrast to the much smaller (10 nm) spread in absorption spectra, indicates that the photoluminescence of USQDs (clusters) is mainly due to surface defects.

Photoluminescence excitation (PLE) spectra, showed that they are significantly determined by the peculiarities of their technological synthesis modes.

In this study, a technology for the colloidal synthesis of CdTe nanocrystals was successfully developed. Optical absorption spectra and photoluminescence excitation spectra of the USQDs confirmed that their size is approximately 2 nm, which was also supported by direct measurements on the Zetasizer Nano ZS. A key conclusion is that the photoluminescence of USQDs is predominantly due to surface defects.

Current-voltage characteristics of films on a patterned silicon substrate from a two-component solution of heterocyclic amines

Kuznetsova D.A.¹, Smertenko P.S.¹, Roshchina N.M.¹, Olkhovik G.P.¹,
Mamykin S.V.¹, Olikh O. Ya²

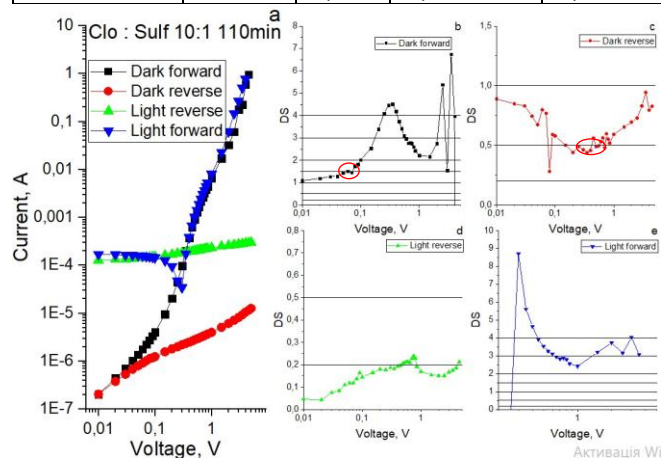
¹V. Lashkaryov Institute of Semiconductor Physics, National Academy of Science of Ukraine,
Kyiv, Ukraine

²Taras Shevchenko National University of Kyiv, Kyiv, Ukraine

Improving the ability of solar cells to capture solar photons and absorb light is crucial for enhancing their energy conversion efficiency. This study proposes an innovative approach to organic-inorganic hybrid structures for thin-film solar cells. They consist of a mixture of two solutions: 10% sulfacyl and $3 \times 10^{-3}\%$ clonidine on the anisotropically etched silicon substrates. Such hybrids are created by depositing aqueous solutions of organic substances at different times (Clo:Sulf – 1:1, 1:2, 2:1, 1:3, 3:1, 1:5, 5:1, 1:10, 10:1) on microprofiled silicon from a chemical bath at room temperature. A preliminary morphological study showed that the concentration ratios $\frac{1}{2}:\frac{1}{2}$, $\frac{1}{4}:\frac{1}{4}$, ... demonstrate a change in structure from point molecules on the surface to the formation of a mesh-like shape [1]. The sample area was 0.25 cm^2 , and the volt-ampere characteristics were measured in darkness and in light at $E = 30 \text{ mW/cm}^2$. The main parameters of the three best and two worst samples, in descending order of efficiency %, are given in Table 1. The typical current-

Tab. 1. Rating of the samples studied in terms of effectiveness

| Ratio CLO:Sulf | Time, min | U_{oc} , V | I_{sc} , A | Eff, % |
|----------------|-----------|--------------|--------------|--------|
| 10:1 | 110 | 0,3 | 1,69E-04 | 0,2547 |
| 1:2 | 90 | 0,25 | 1,39E-04 | 0,1587 |
| ... | ... | ... | ... | ... |
| 2:1 | 100 | 0,25 | 1,82E-07 | 0,0002 |
| 5:1 | 110 | 0,06 | 3,07E-07 | 0,0001 |



The typical voltage dependencies of current (a) and differential slope (b-e). Sample CLO-Sulf 10:1

voltage characteristics (CVC) and their dimensionless sensitivities (DS) are present in Fig. 1. As we can see, the samples have a photovoltaic region, which indicates promise for further research. The presence of a clearly defined $DS = 1.5$ region indicates bimolecular recombination processes and confirms the sufficient availability of both types of charge carriers. Rectifying behaviour is also observed at $U = 0.1 \text{ V}$.

D.A. Kuznetsova et al.. Morphology of films on a patterned silicon substrate from a two-component solution of heterocyclic amines. In X Ukrainian scientific conference on physics of semiconductors (USCPs-10), 2025, Uzhhorod, Ukraine, May 26-30, 2025, p. 85-86.

Dynamic conductivity of silver films deposited on Ge wetting underlayres.

R.I. Bihun, V.H. Apopii, O.M. Koplak

*Ukraine, Lviv, Ivan Franko Lviv national university, 50 Dragomanov st.
roman.bihun@lnu.edu.ua, viktor.apopii@lnu.edu.ua, olha.koplak@lnu.edu.ua*

Optical properties of thin metal films have important information about kinetic parameters of dynamic electron transport. Optical properties of thin silver films have been studied already before, but fundamental analysis of thickness dependencies of effective optical parameters is lacking. We have developed methodology for assessing transport kinetic parameters on the basis of the thickness dependent optical constants of the films. Nanothin silver films in the vicinity of percolation threshold (thicknesses about 8-25 nm) have been studied. The critical thickness d_c of the films, mean linear grain size and grain boundary scattering parameters of charge curriers have been determined from the size dependencies of the effective optical constants. The experimental data are in good agreement with those obtained by structural and electro physical investigations of the samples.

Silver films have been deposited with thermal evaporation on the glass substrate under high vacuum condition ($P \sim 10^{-7}$ torr) at the room temperature. Mass thicknesses of the films have been assessed by the shift of the resonance frequency of the piezosensor. Measuring the resistance of the films was carried out electronically by digital Ohmmeter UT61E. Transmittance and reflectance spectra were measured by broadband spectrophotometer Shimadzu UV 3600. Optical measurements were performed with a normal incidence of the light beam onto the substrate surface.

Dynamic conductivity size dependencies of silver films with thicknesses from 8 to 25 nm in the wavelength range 200-2500 nm were investigated. Optical coefficients n and k have been calculated with Phillips equations [1]. Optical conductivity, effective charge carrier mass, effective relaxation time, skin depth values were calculated. The critical thickness d_c at which metallic phase is formed was found to be 15 nm. It was determined within the framework of the percolation theory [2] (in the vicinity of the percolation threshold transmittance and reflection spectra do not depend on the frequency). This is confirmed by the dynamic conductivity data which are frequency independent for this thickness value of the film. Another proof is the dramatic change of the sign of the first derivative of the dielectric permittivity on frequency ($d\epsilon_1/dv$) around the thicknesses of silver layer 15-16 nm. The effective mass of the charge carrier was around $1,2 \pm 0,2 m_0$, which allowed us to use the free electron model [3] in dielectric constants сфдсгдфешшт. Mean grain sizes were estimated. They proved to be commensurable with film thicknesses. For example, for film thickness 15 nm linear grain size is 22 nm and for thickness

20 nm, D = 25 nm. The skin depth thickness d_{skin} was evaluated [3]. It was shown, that its thickness dependence has descending character up to the percolation region. For thin films with thicknesses above 15 nm this parameter remains constant and approximately 25 nm. Structural investigations of the films showed that grain sizes of the samples similar to those obtained by the optical studies. Within the framework of internal size effect models, the intergrain tunneling coefficient t for thin silver films in the dynamic conduction regime was calculated. The numerical values of the intergrain tunneling parameters t for silver films, both on a clean glass substrate and on a substrate pre-coated with a germanium underlayer with a mass thickness of 1 nm, are close to each other and are 0.65. The data is in good agreement with those obtained by the electro physical investigations of the films in the framework of grain boundary scattering theories.

On the basis of the curried out optical and structural studies was found kinetic charge transport parameters for the silver films with the thicknesses 8-25 nm. Grain-boundary scattering parameters obtained from spectral characteristics are in full agreement with those previously obtained values from electrical resistivity studies of the films. Percolation thickness of silver film was calculated it's 15 nm.

- [1]. Phillips R. T. J. Phys. D: Appl. Phys. 1983. Vol. 16. P. 489–497.
- [2]. R. Bihun, B. Koman. Nanoscale metal film electronics. «Physical and mathematical sciences». Riga, Latvia: Baltija Publishing. 2024. 1-33 p.

M. Dressel, G. Grüner, *Electrodynamics of Solids*, Cambridge University Pres,Cambridge, 2002.

Electric field-induced magnetic anisotropy in multilayer tunnel nanostructures

Krupa, M.M.¹, Korostil, A.M.¹

¹*V. Baryakhtar Institute of Magnetism NAS of Ukraine, Kyiv, Ukraine,
korostilandrii@gmail.com, orostilandrii@gmail.com*

Magnetic tunnel junctions (MTJs) represent a key building block of modern spintronic devices, with their performance critically determined by the interplay between interfacial properties and magnetic anisotropy. A promising route toward low-power control of magnetization is the utilization of voltage-controlled magnetic anisotropy (VCMA), where an applied electric field modifies the orbital hybridization at the ferromagnet/insulator interface. In this work, we investigate VCMA effects in MTJs based on 3d transition metals, with particular attention to CoFeB/MgO and related systems.

The study combines experimental observations with theoretical modeling of spin-dependent charge redistribution at the metal–oxide interface. Applying a gate voltage across the junction modifies the occupancy of 3d orbitals, thereby tuning perpendicular magnetic anisotropy (PMA). The mechanism is linked to the modulation of Fe and Co d-states hybridized with oxygen p-orbitals in the MgO barrier. As a result, voltage control provides a reversible and energy-efficient method of manipulating the easy axis of magnetization without the need for large spin-polarized currents.

Our results reveal a significant anisotropy change, on the order of tens of $\mu\text{J/m}^2$ per volt, which is comparable to or larger than spin-transfer torque switching thresholds in nanoscale devices. We further show that the effect strongly depends on interface quality, crystalline ordering of the oxide barrier, and the choice of the 3d ferromagnet. First-principles calculations support the experimental findings and indicate that the interfacial electronic structure plays a dominant role in determining the voltage response.

This study highlights the potential of voltage-controlled anisotropy as a scalable pathway for spintronic applications, including non-volatile magnetic memory and logic architectures. By reducing energy consumption while maintaining fast switching speeds, VIMA in 3d-metal-based MTJs offers a viable approach toward next-generation low-power spintronic devices.

[1]. Zhan J., Lukashev P.V, Jaswal S.S, Tsimbal E.Y. Model of orbital population for voltage-controlled magnetic anisotropy in transition-metal thin film. *Phys Rev. B.* 2017. V.96. P. 014433.

From electrolyte to material: engineering Ag–Re coatings

Bersirova O.L.^{1,2}

¹ V.I. Vernadsky Institute of General & Inorganic Chemistry NAS of Ukraine,
Department of Electrochemical Materials Science and Electrocatalysis, Kyiv, Ukraine

² Vilnius University, Department of Physical Chemistry, Vilnius, Lithuania

bersibol@gmail.com

The combination of silver's unique electrical and catalytic properties with the mechanical strength of rhenium motivated our interest in Ag–Re materials [1, 2]. Electrochemical deposition offers an efficient and environmentally friendly route to synthesize such alloys with tunable characteristics, particularly relevant for nano- and microelectronics [3].

We developed a novel dicyanoargentate–perrhenate buffered electrolyte for Ag–Re alloy deposition [1]. The effects of bath composition, $[Ag(I)]:[ReO_4^-]$ ratio, current density, temperature, and agitation were studied in relation to alloy composition, structure, morphology, microhardness, and porosity. Compared with conventional silver plating baths [4], Ag–Re alloys up to 15 μm thick and containing up to 13.5 wt.% Re were obtained at $[Ag(I)]:[ReO_4^-]$ ratios from 10:1 to 1:10. Higher Re content led to smaller crystallites, while deposits from Ag-rich baths showed more uniform element distribution. Increasing current density to 15 $mA \cdot cm^{-2}$ decreased Re incorporation and reduced current efficiency to 66%, largely independent of temperature (20–60°C) and stirring.

Ag–Re coatings exhibited strong adhesion to the copper substrate and were nearly pore-free. A clear correlation was established between structural parameters and properties, namely a linear “microhardness–crystallite size” relation in Hall–Petch coordinates.

Electrodeposited Ag–Re coatings with tunable Re content are a promising material offer reliable performance for electrical contacts across wide temperature ranges.

Acknowledgment. O.Bersirova thanks for received funding through the MSCA4Ukraine project, which is funded by the European Union (Project No.1233494).

[1]. Bersirova O., Kublanovsky V., Kochetova S., Bondar O., Electrochemical Synthesis and Characterization of Functional Ag-Re Coatings. *Materials*, 18 (9), 1893 (2025).

[2]. Bersirova O., Kochetova S., Bondar O., Proceedings of the “2nd International Research and Practice Conference “Nanoobjects & Nanostructuring” (N&N-2022)”, 23-25 September 2022, Lviv, 57-58 (2022).

[3]. Farmakovsky B., et al. Patent RU2350673 (2009).

[4]. Bersirova O., Kublanovsky V., Cesiulis H., Electrochemical Formation of Functional Silver Coatings: Nanostructural Peculiarities. *ECS Transactions*, 50 (52), 155 (2013).

Quasiannealing of metamagnetic FeRh film via magnetic field

Lukienko, I.^{1,2}, Uhliř, V.¹

¹ Central European Institute of Technology, Brno University of Technology, Czechia,
lukienko@vutbr.cz

²B. Verkin Institute for Low Temperature Physics and Engineering of NAS of Ukraine,
Kharkiv, Ukraine

Antiferromagnetic (AF) materials that undergo a phase transition to a ferromagnetic (FM) state by the application of an external magnetic field are known as metamagnets. Those featuring a first-order phase transition are promising for applications in spintronics and magnetic refrigeration [1, 2]. In this work, we demonstrate how to improve the quality of metamagnetic thin films by the quasiannealing effect via applying a high magnetic field. We used epitaxial FeRh films, which have the first-order AF-FM phase transition around 360 K, as a model system. After the first magnetic field cycle between -9 T and 9 T, the phase transition temperature was lowered permanently by more than 10 K (Fig. 1). We term this effect “quasiannealing,” as it is related to the release of internal compressive strain in the FeRh crystal lattice, formed during its growth on a MgO(001) substrate, a process with a similar impact as thermal annealing. This transition shift is accompanied by reduction in the out-of-plane lattice parameter, providing structural evidence for our hypothesis. This effect was significant in the 300-nm-thick FeRh films but not in the 30 nm films, where the net compressive strain from the MgO(001) substrate is more prominent. A key ingredient of such prominent quasiannealing effect is the giant ~1% FeRh lattice expansion across the phase transition, which amplifies the common effect of strain release by magnetic field - magnetostriction.

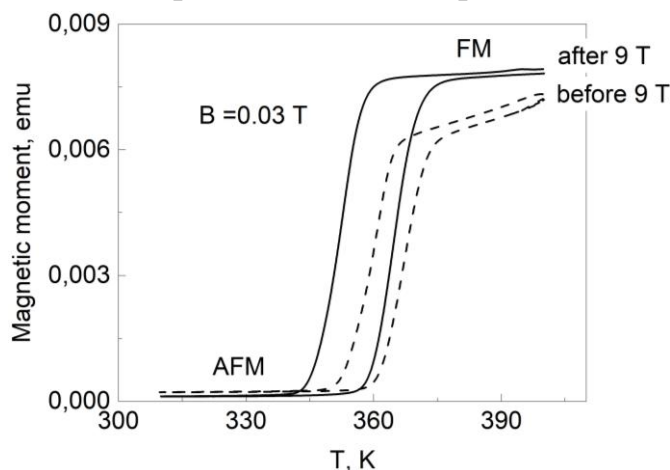


Figure 1. - The phase transition of the 300-nm-thick FeRh film, induced by sweeping temperature before (dashed line) and after (solid line) 9 T magnetic field treatment.

[1]. Chen H., Liu L., Zhou X., Meng Z., Wang X., Duan Z., Zhao G., Yan H., Qin P., Liu Z. Antiferromagnets for Spintronics. *Adv. Mater.* 2024, V. 36, 2310379.

[2]. Magnetocaloric Refrigeration in the Context of Sustainability: A Review of Thermodynamic Bases, the State of the Art, and Future Prospects. Lucia U., and G. Grisolia. *Energies* 2024, V. 17, 3585.

High-accuracy MPPT controller for laboratory research on CdTe thin-film solar cells

Fedenko, V.Y.¹, Dzundza, B.S.¹

¹Vasyl Stefanyk Carpathian National University, Ivano-Frankivsk, Ukraine,
vitalii.fedenkoj@gmail.com

Thin-film samples of CdTe-based photovoltaic cells, due to their small geometric dimension, exhibit relatively low voltage and current values, which significantly complicates the measurement of their characteristics during experimental studies. The nonlinear current-voltage characteristics, which vary under the influence of temperature and illumination levels, cause the operating point to rarely coincide with the maximum power point, resulting in the loss of a significant point of the generated energy. In the case of large-scale solar panels, industrial MPPT controllers are employed to ensure operation at the maximum power point. These controllers dynamically track the optimal voltage-to-current ratio according to a predefined algorithm. [1]. To address this issue, a concept of a highly sensitive specialized MPPT controller is proposed. It is based on an STM32G microcontroller and a controlled electronic load, built using several independent current stabilizers for different ranges, from 10 μ A to 1 A, thereby emulating the load of a photovoltaic converter during research. (fig.1).

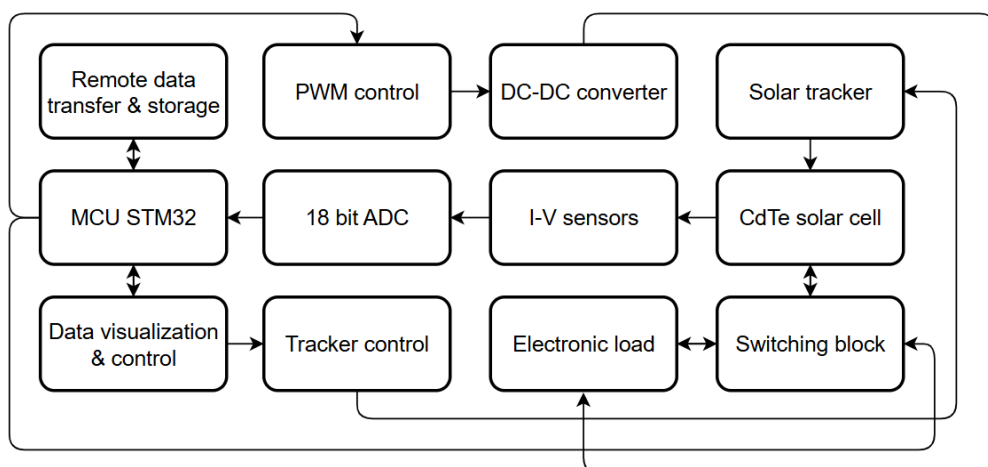


Fig. 1 – Block diagram of the proposed MPPT controller

The use of high-sensitivity measurement sensor in combination with a high-resolution (18-bit) I²C ADC and the selected algorithm for optimal parameter tracking enables the study of thin-film samples at the maximum power point. This approach makes it possible to perform an objective evaluation of a series of samples under identical condition and to establish angular dependencies at a fixed illumination level.

[1]. Affari, B. C., Kahoul, N., Chenni, R., Neçaibia, A., Younes, M., Kherici, Z. High accuracy testing of MPPT proteus model performance for photovoltaic system. Sci. Bull. Electr. Eng. Fac. 2022. V.46, No 1. P. 1-7.

Magnetoresistive and Magnetocapacitive Effects in Tunnel Magnetic Junctions. Problems and Prospects of Practical Application

Krupa M.M.

*Institute of Magnetism National Academy of Science of Ukraine, Kyiv, Ukraine,
03143 Kiev, Vernadsky's bul., 36
lidermyk@i.ua*

Abstract

This work shows that when the magnetic electrodes in magnetic tunnel junctions are magnetized, a strong magnetic field gradient appears in the barrier nonmagnetic layer, which causes a spatial redistribution of the concentration of spin-polarized electrons in the magnetic metal/insulator interface region and leads to the appearance of an uneven distribution of electric charge. Such a magnetically induced charge affects the dielectric characteristics of the barrier nanolayer and leads to a change in the resistance and capacitance of magnetic tunnel junctions. More over, this effect is most pronounced in tunnel magnetic contacts with magnetic electrodes that have perpendicular anisotropy.

The work contains experimental measurements of the tunnel magnetoresistance and tunnel magnetocapacity in magnetic tunnel junctions with perpendicular anisotropy of $Tb_{22-\delta}Co_5Fe_{73}/Pr_6O_{11}/Tb_{19-\delta}Co_5Fe_{76}$ electrodes and in $Co_{80}Fe_{20}/Pr_6O_{11}/Co_{30}Fe_{70}$ contacts, where the magnetic electrodes have uniaxial anisotropy in the plane. The change in resistance during magnetization reversal of $Tb_{22-\delta}Co_5Fe_{73}/Pr_6O_{11}/Tb_{19-\delta}Co_5Fe_{76}$ contacts reached 120% and of $Co_{80}Fe_{20}/Pr_6O_{11}/Co_{30}Fe_{70}$ contacts it did not exceed 40%. The change in capacitance during magnetization reversal of $Tb_{22-\delta}Co_5Fe_{73}/Pr_6O_{11}/Tb_{19-\delta}Co_5Fe_{76}$ contacts reached values of 110%, and of $Co_{80}Fe_{20}/Pr_6O_{11}/Co_{30}Fe_{70}$ contacts it reached values of 45%. In work the scheme and the principle of recording and reading information from an MTJ-based storage medium also is given.

[1]. Prokopiv V.V., Turovska L.V., Nykyryuy L.I., Horichok I.V. Quasichemical modelling of defect subsystem of tin telluride crystals. Chalcogenide Letters. 2016. V. 13, No 7. P. 309-315.

Modification of the CdS Buffer Layer Using Nanofibers to Enhance the Efficiency of Thin-Film CdTe Solar Cells

Yavorskyi R.S.¹, Krychovetskyi M.V.¹, Yavorska L.O.¹

¹*Vasyl Stefanyk Carpathian University, Ivano-Frankivsk, Ukraine*

r.yavorskyi@pnu.edu.ua

Thin-film solar cells based on cadmium telluride (CdTe) are considered among the most promising due to their high efficiency and low cost. However, traditional CdS/CdTe structures have drawbacks, such as a high density of defects at the interface and micro-shunting, which reduces their efficiency. To address these issues, we investigated a new design using nanofibers (nw) in the CdS buffer layer, which improves the element's optical properties.

The modeling of the solar cells was carried out using the SCAPS (Solar Cell Capacitance Simulator) v.3.3.09 software. All simulations were performed under standard conditions: a temperature of 300 K, an AM 1.5 light spectrum, and a radiation power of 1000 W/m². During the modeling, the optimal layer thicknesses were determined to achieve maximum efficiency. The optimal thickness of the CdTe absorbing layer was 3 μm (efficiency η = 12.78%, fill factor FF = 75.81%), the nw-CdS buffer layer was 120 nm (η = 13.16%, FF = 76.18%), and the SnO₂ window layer was 40 nm (efficiency reached 13.33%, FF = 77.39%).

In addition, the study showed that the density of interface defect states (Nit) is a critical parameter. An increase in Nit leads to a significant reduction in photoelectric parameters. It was found that for stable device operation, the density of defect states should not exceed 10¹² cm⁻².

This study demonstrates that nw-CdS nanofibers can improve the optical properties of the element and reduce recombination at the interface, thereby increasing reliability and performance. It was found that minimizing the density of interface defect states is a critical factor for achieving high efficiency, and our analysis suggests a maximum approximate value of Nit = 10¹² cm⁻² for practical applications. The obtained results can serve as a basis for further experimental research and the development of next-generation thin-film solar cells.

This work was supported by the Project for Young Scientists No. 0123U100226 granted by the Ministry of Education and Science of Ukraine.

Modified Probe Method for Measuring the Electrical Resistance of Contact Structures for Thermoelectric Energy Converters

Lysko, V.V.^{1,2}, Razinkov, V.V.¹, Havryliuk, M.V.^{1,2}, Strusovskyi, K.I.²,

¹ Institute of Thermoelectricity of the NAS of Ukraine and MES of Ukraine, Chernivtsi, Ukraine, v.lysko@gmail.com

² Yuriy Fedkovych Chernivtsi National University, Chernivtsi, Ukraine

One of the current tasks in the field of thermoelectricity is the miniaturization of thermoelectric energy converters, which could substantially reduce their cost and expand the scope of practical applications. The primary obstacle to this progress is the relatively high contact resistance, since—as is well established—the influence of contact resistance on the efficiency of a thermoelectric energy converter increases as the device dimensions decrease [1].

Therefore, the development of methods and equipment for analyzing contact structures in thermoelectric energy converters, as well as the creation and optimization of their fabrication technology, is an important task.

A detailed physical model of the process for determining the electrical contact resistance at the “metal–thermoelectric material” interface has been developed based on the probe measurement method [2]. Computer modeling demonstrates that the error in determining the electrical contact resistance, caused by the non-isothermal conditions in the contact structure, can be significantly reduced by thermostabilizing one side of the structure; under such conditions, the error does not exceed 2%.

To implement this measurement technique, a dedicated setup was designed and manufactured at the Institute of Thermoelectricity (Ukraine); its external view is shown in Fig. 1.

A series of experimental investigations was conducted to evaluate the contact resistance of the “nickel–extruded Bi–Te-based thermoelectric material” structure. The results reveal a clear correlation between the surface roughness of the thermoelectric material and the contact resistance: the lowest values of contact resistance are achieved when the thermoelectric surface is polished.

[1]. Vikhor L., Lysko V., Kotsur M., Havrylyuk M. *J. Appl. Phys.*, 2025, 137(9), 094503.

[2]. Anatychuk L., Lysko V., Strusovskyi K. (2023). *J. of Thermoelectricity*, (4), 38–48.

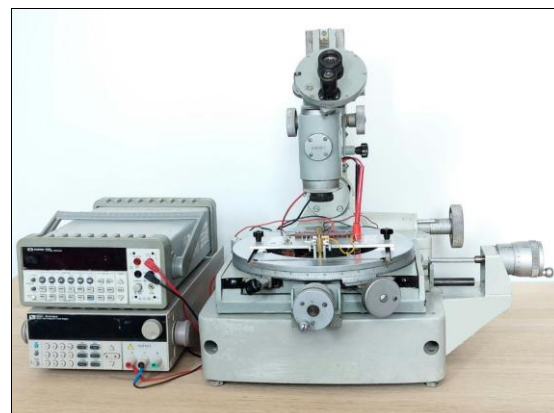


Fig. 1. External view of the measurement setup

Multilayer Porous Silicon Structures: Experimental Insights into Heat Transfer under Controlled Fabrication Conditions

Lishchuk, P.O.¹, Chepela, L.I.², Borovyi, M.O.³, Olikh, O.Y.⁴, Plyushchay, I.V.⁵, Shevchenko, V.B.⁶, Kalyuzhnyi, D.Y.⁷, Popiuk, K.V.⁸, Isaiev, M.V.⁹

¹ Taras Shevchenko National University of Kyiv, Kyiv, Ukraine,

pavel.lishchuk@knu.ua

² Taras Shevchenko National University of Kyiv, Kyiv, Ukraine, lesia.chepela97@gmail.com

³ Taras Shevchenko National University of Kyiv, Kyiv, Ukraine, mborovyi1@gmail.com

⁴Taras Shevchenko National University of Kyiv, Kyiv, Ukraine,

olegolikh@knu.ua

⁵ Taras Shevchenko National University of Kyiv, Kyiv, Ukraine, inna.pl@knu.ua

⁶ Taras Shevchenko National University of Kyiv, Kyiv, Ukraine victoria.shevchenko@knu.ua

⁷ Taras Shevchenko National University of Kyiv, Kyiv, Ukraine, denuasev@gmail.com

⁸ Taras Shevchenko National University of Kyiv, Kyiv, Ukraine, popiuk_kateryna@knu.ua

⁹ Université de Lorraine, CNRS, LEMTA ,
Nancy F-54000, France, mykola.isaiev@univ-lorraine.fr

Multilayer porous silicon (pSi) systems are promising candidates for thermal management applications due to their tunable morphology and controllable transport properties. Previous studies have demonstrated that interfacial thermal resistance between layers plays a decisive role in reducing the effective thermal conductivity of such systems. Building upon these insights, we focus on the fabrication and direct characterization of custom-designed multilayer pSi structures. The samples were prepared by electrochemical etching under varied conditions, allowing systematic modification of layer number, thickness distribution, and porosity. The resulting structures were examined to assess how thermal conductivity evolves as a function of etching parameters and interfacial density. Preliminary results confirm that reducing the number of interfaces leads to measurable changes in effective transport, while maintaining structural stability of the porous network. Thermal conductivity measurements were performed using photoacoustic gas-microphone methods, providing a non-destructive probe of heat transfer. The growing experimental dataset serves as a foundation for machine-oriented approaches, where predictive models could recommend synthesis conditions required to obtain multilayer structures with tailored thermophysical properties. Such integration of experimental design and data-driven characterization is expected to accelerate the development of porous silicon systems optimized for energy-efficient thermal transport.

Authors gratefully acknowledge financial support from the National Research Foundation of Ukraine under Grant No. 2023.03/0252.

Optimizing of CdTe thin film solar cells: a study of spectral and thermal effects

Yavorskyi R.S.¹, Fedenko V.Y.¹, Kashuba A.I.², Gleb V.F.¹,
Semkiv I.V.², Krychovetskyi M.V.¹

¹*Vasyl Stefanyk Carpathian University, Ivano-Frankivsk, Ukraine*

r.yavorskyi@pnu.edu.ua

²*Lviv Polytechnic National University, Lviv, Ukraine*

Photovoltaic converters based on cadmium telluride (CdTe) represent one of the most promising thin-film solar cell technologies due to an optimal band gap (~ 1.5 eV) and a high absorption coefficient. However, the efficiency of these devices is highly dependent on their operating conditions, specifically the spectral composition of light and the working temperature. The study of these dependencies is a crucial task for predicting and enhancing the performance of solar cells in real-world scenarios.

Thin-films heterostructure Au/CdTe/CdS/ITO structures were deposited via RF-magnetron sputtering in a vacuum onto glass substrates coated with a conductive ITO layer. Theoretical analysis and simulation of the photovoltaic characteristics were conducted using the SCAPS-1D software package. Experimental measurements of current-voltage characteristics, along with their spectral and temperature dependencies, were performed using an automated setup equipped with a set of monochromatic LEDs and precise temperature control within the 283–373 K range.

The SCAPS-1D simulation results established that the maximum spectral efficiency of CdTe-based photoconverters is observed in the wavelength range of 600–800 nm. A sharp decrease in efficiency at $\lambda > 830$ nm is caused by the photoelectric effect threshold, which corresponds to the band gap of CdTe.

It was demonstrated that increasing the thickness of the CdTe absorber layer from 1 μm to 4 μm leads to a growth in both the short-circuit current density (J_{sc}) and the open-circuit voltage (V_o). However, the growth of these parameters slows at thicknesses exceeding 3.5 μm . The experimental data show good correlation with the simulation results, confirming that the optimal absorber layer thickness is in the 3–4 μm range.

Investigation of the temperature dependencies revealed a linear decrease in both efficiency and open-circuit voltage as temperature increases. This is attributed to an increase in the diode saturation current and the charge carrier recombination rate. A key finding is the experimental confirmation that the relative efficiency versus temperature curves are nearly identical under both monochromatic illumination ($\lambda \approx 800$ nm) and direct sunlight, which simplifies the process of predicting device performance.

This work was supported by the Project for Young Scientists No. 0124U000760 granted by the Ministry of Education and Science of Ukraine.

Properties of pulsed laser deposited MWCNT thin films

Virt I.¹, Padalka I.¹, Stefaniuk I.², Cieniek B.², Potera P.²

¹*Institute of Physics, Mathematics, Economics and Innovative Technologies
Drohobych State Pedagogical University I.Franko, Ukraine,*

isvirt@dspu.edu.ua

²*Institute of Materials Science and Engineering University of Rzeszow, Poland*

Carbon materials are very promising for modern electronics [1]. Pulsed laser deposition (PLD) is a process that uses a laser to create thin films of these materials. The laser "knocks out" carbon from a target, which then deposits onto a substrate, forming specialized coatings.

PLD is highly valuable in microelectronics and photonics because these fields require high-quality film structures. The experimental system used to create these nanocarbon layers has been previously documented. For depositing the nanocarbon layers, a KGd(WO₄)₂ laser was used with the following radiation characteristics: a wavelength (λ) of 1067 nm, a pulse duration (t) of 20 ns, a beam energy density of 6–8 J/cm², and a repetition rate of 1–0.3 Hz. The laser system utilized a Q-switch to operate in a modulated mode, allowing for the precise control of the laser pulses. The ablation of the target, made from compressed multi-walled carbon nanotube (MWCNT) powder, was carried out in a quartz chamber. This process was performed under a high vacuum, with a final pressure of 10⁻⁶ Pa, to ensure the purity of the final film. The resulting thin films were composed of carbon nanotubes, created through this laser deposition method.

To spectroscopic analyze the films, their absorbance was measured using a spectrometer across a wavelength range of 0.2 to 3.0 mm. The absorption capacity of the material is described by the absorption coefficient, denoted as A . This value is the product of the material's specific absorption and the film's thickness. The absorption is determined by the ratio of the light's initial intensity (I_0) to its final intensity (I) after passing through the film. The relationship is given by the formula: $I=I_0\cdot\exp(-Ad)$. Here, A is a parameter that depends on the light's wavelength. By analyzing absorption as a function of the photons' energy rather than wavelength, it's possible to determine the energy at which light begins to diffuse sharply within the absorbing layer.

The text suggests that the film deposited on the glass surface likely has a graphene-like structure. This conclusion is drawn from a physical effect observed during the analysis, which is a common method for identifying both the material and its structure. Additionally, the presence of a graphene surface film is known to increase the material's microhardness.

[1]. Salah L.S., Ouslimani N., Bousba D. Carbon Nanotubes (CNTs) from Synthesis to Functionalized (CNTs) Using Conventional and New Chemical. *Approaches Journal of Nanomaterials*. 2021. V. 2021, ID 4972770. P. 1-31

Photosensitive Heterostructures Based on Li-doped CdTe for Photodetector Applications

Mazur, M.P.¹, Mazur, T.M.¹, Slyotov, M.M.²

¹Ivano-Frankivsk National Technical University of Oil and Gas, Ivano-Frankivsk, Ukraine, myroslav.mazur@nung.edu.ua

²Yuriy Fedkovych Chernivtsi National University, Chernivtsi, Ukraine

This work presents research aimed at studying the effect of lithium doping on the photoelectric properties of CdTe and developing light-sensitive heterostructures with improved characteristics for use in photodetectors.

Au–CdTe:Li surface barrier diodes were fabricated and studied. Optical absorption, photocurrent spectra, and photoelectric parameters in the spectral range of 1.4–5.0 eV were also analysed. The role of interband transitions and localised LiCd centres in the formation of photosensitivity was evaluated.

The results obtained show that Au–CdTe:Li structures demonstrate increased photosensitivity due to the formation of a high surface potential barrier φ_o . High quantum efficiency ($\eta \approx 12\%$) was achieved. Typical photoelectric parameters were also obtained under AM2 illumination for an open-circuit voltage $V_{oc} \approx 0.7$ V and a short-circuit current density $I_{sc} \approx 10$ mA/cm² (Fig. 1). The energy conversion efficiency of the structures reached 10%. An important result of the work is that the temperature coefficient of CdTe devices was found to be almost four times lower than that of silicon analogues [1].

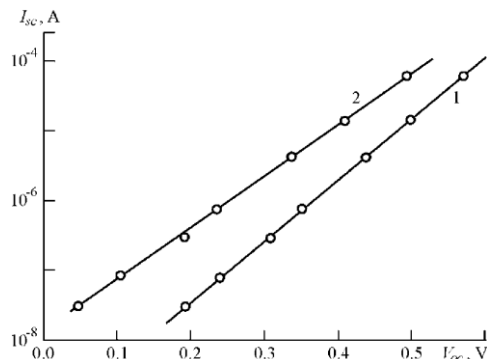


Fig. 1. Dependences of I_{sc} (V_{oc}) at different temperatures: 1 – 300 K, 2 – 400 K

Analysing the results obtained, we can conclude that CdTe doping with lithium and the formation of Au–CdTe:Li heterostructures is a promising approach for the development of efficient, thermally stable photodetectors operating in a wide spectral range, from ultraviolet to near-infrared radiation.

[1]. Slyotov M.M., Mazur T.M., Slyotov O.M., Kinzerska O.V., Mazur M.P. Photodetectors Based on CdTe:Li. *Journal of Nano- and Electronic Physics*. 2024. V. 16, No 5. P. 05031-1–05031-5.

Synthesis of multi-layered nanocomposite polymer films with embedded nanocrystals of PbS

Tokarev, V. S.¹, Korbityak, D. V.², Shevchuk, O. M.¹, Bukartyk, N. M.¹

¹ Lviv Polytechnic National University, Lviv, Ukraine, viktor.s.tokarev@lpnu.ua

²V.E. Lashkaryov Institute of Semiconductor Physics NAS of Ukraine, Kyiv, Ukraine,
dmytro.korbityak@gmail.com

Here, we report on the synthesis and characterization of multi-layer polymer films with embedded Lead sulphide nanocrystals (PbS NCs). Initially, PbS NCs were synthesized via the interaction of Lead acetate with thiourea in poly(vinyl alcohol) (PVA) solutions in a water-propanol mixture with peroxide polymer (PP) added. The latter served as a cross-linking agent for nanocomposite polymer films formed on glass slides via spin-coating. Multi-layered nanocomposite polymer films were formed by repeating the procedures of spin-coating of the nanocomposite polymer layer on a glass slide from the PbS NCs dispersion in PVA+PP solution, followed by crosslinking the formed layer at T=120 °C for 1.5 hours.

The optical spectra of the two- and three-layered nanocomposite films were characterized by the presence of one main very intense maximum in the area of 405-416 nm, which corresponded to the bandgap of 2.10-2.25 eV. The presence of several small peaks in the area of 446 nm, accompanying the main peak, indicated a low polydispersity of the embedded PbS NCs. As expected, the increase in the number of film layers led to the colour intensification of the nanocomposite films, which was proven by enhanced absorption values in their optical spectra.

An X-ray phase analysis of the obtained films was performed. The experimental X-ray patterns are shown in Fig. 1. According to these results, the cubic

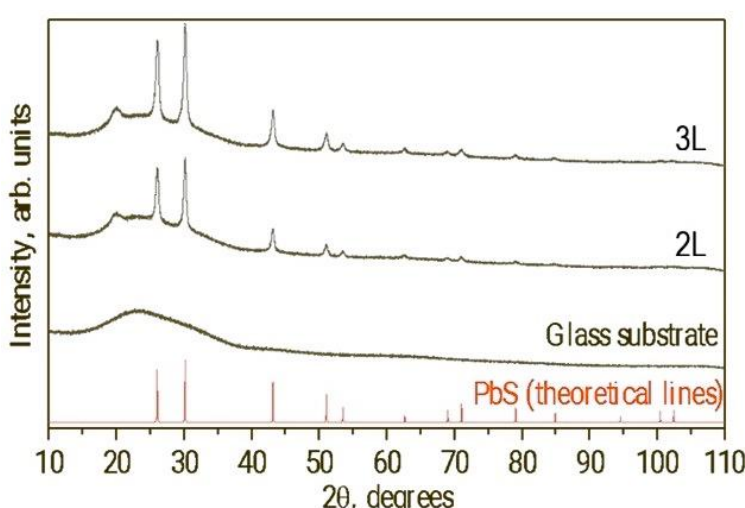


Fig. 1. XRD patterns of two (2L) and three (3L) layered nanocomposite films compared to those of the glass substrate and PbS bulk crystal.

PbS phase was identified by prominent peaks at 2θ : 26°, 30°, 43°, 51°, 53.5°; while only an amorphous halo is present in the XRD pattern of a virgin glass substrate. A broad peak with low intensity, which appeared in the XRD patterns of nanocomposite films in the area of 18-22°, is attributed to the crystalline structure of PVA matrix.

The average crystallite size of the PbS NCs estimated using Scherer equation was 15 ± 1 nm.

Synthesis, structure, and morphology of ZnO-Zn conglomerates growth by the rapid solar evaporation method

Y. Kovalskyi¹, V. Karpyna¹, L. Myroniuk¹, O. Olifan¹, S. Korichev¹,
S. Starik³, V. Strelchuk², I. Danylenko², A. Ievtushenko¹

¹ Frantsevich Institute for Problems of Materials Science, NAS of Ukraine, 3

Omeljana Pritsaka str., Kyiv, 03142, Ukraine, y.kovalskyi@ipms.kyiv.ua

² V. Lashkaryov Institute of Semiconductor Physics, NAS of Ukraine, 45 Nauky av.,
Kyiv, 03028, Ukraine

³ V. Bakul Institute for Superhard Materials, NAS of Ukraine, 2 Avtozavodskaya str.,
04074, Kyiv, Ukraine

Zinc oxide (ZnO) belongs to the class of wide-bandgap semiconductors and has a number of advantages, including the availability of raw materials, chemical stability, and environmental safety. These properties motivate the active use of ZnO in photocatalytic processes [1].

Applying new approaches to the synthesis and structural modification of ZnO opens up prospects for the creation of effective photocatalysts for solving environmental and energy problems. Modern methods to increase photocatalytic activity focus on modifying the structure and morphology of ZnO by optimizing synthesis methods, metals and non-metals doping, and creating composites with related semiconductor materials.

ZnO-Zn conglomerates were synthesized on silicon substrates by carbothermal reduction using the rapid solar evaporation method. During the process, growth conditions were altered by changing the relation of precursors: a mixture of ZnO and carbon powders with a mass ratio of ZnO/C of 1:1 and 4:1, as well as the distance between the precursor and the substrate.

The work presents a comprehensive study the structure, morphology, elemental composition, and their optical and photocatalytic properties of ZnO-Zn conglomerates. Particular attention is paid to the analysis of photoluminescence and Raman scattering, which are informative methods for assessing the quality of the crystal lattice and structural defects. The obtained results allow us to evaluate the influence of synthesis conditions on the photocatalytic activity of ZnO-Zn conglomerates and justify the prospects for their practical application.

[1]. Baibara O.E., Radchenko M.V., Karpyna V.A., Ievtushenko A.I. A Review of the Some Aspects for the Development of ZnO Based Photocatalysts for a Variety of Applications. *Physics and Chemistry of Solid State*. 2021. V. 22, No 3. P. 585-594.

Structure analysis of Co- and Fe-based amorphous thin film produced by magnetron sputtering

Nykyrui Yu.¹, Mudry S.¹, Sembratovych N.¹, Kordan V.²,

¹ Metal Physic Department, Ivan Franko National University of Lviv, Ukraine,

² Department of Inorganic Chemistry, Ivan Franko National University of Lviv, Ukraine, :

yuliya.nykyrui@lnu.edu.ua

Amorphous multicomponent thin films based on cobalt, boron, and silicon are distinguished by unique physicochemical properties, which determine their prospects for application in electronics, sensor technologies, and energy. Due to the amorphous structure, which is characterized by the absence of long-range order, these materials have isotropic magnetic properties, high electrical resistivity, corrosion resistance, as well as mechanical strength and wear resistance. In particular, Co-Si-B films demonstrate soft magnetic properties with low coercive force and high permeability. An important feature is the dependence of magnetic characteristics on film thickness, which is associated with residual stresses and compositional inhomogeneities that arise during deposition. In addition, heat treatment of such films can significantly change their electrochemical behavior, particularly improving corrosion resistance in alkaline environments. Studies have also shown that nanocrystallization in an amorphous matrix of Co-based alloy allows for regulating magnetic and electrical properties, which opens up prospects for creating highly sensitive sensors and microelectronic devices.

Thin films on a glass substrate were obtained by magnetron sputtering. An amorphous Co-based and Fe-based alloys were used as a source for thin films. The sputtering duration varied from 10 to 60 minutes to obtain films of different thicknesses. For a comprehensive analysis of the obtained thin films, several experimental methods were used that allow characterizing both the morphological and physicochemical properties of the material, in particular optical interference, which provides an accurate determination of the thickness of the films by analyzing the interference pattern that occurs when light reflects from the film boundaries; atomic force microscopy (AFM), which allows studying the surface topography with nanometer accuracy, revealing inhomogeneities, roughness and defects; X-ray diffraction (XRD), which allows to identify the crystalline or amorphous nature of the film, as well as to determine the lattice parameters and the degree of ordering. Also, the main attention in this work is paid to energy-dispersive X-ray spectroscopy (EDX), which allows for the qualitative and quantitative analysis of the elemental composition of the films. Combined with electron microscopy, this method provides localized probing with high spatial resolution.

Structural studies of As₂S₃:AgI glasses

Kochubei H.¹, Stronski A.¹, Kavetskyy T.², Balayeva N.³

¹ V.Lashkaryov Institute of Semiconductor Physics NAS Ukraine, Kyiv, Ukraine

² Drohobych Ivan Franko State Pedagogical University, Drohobych, Ukraine

³ Semiconductor Physics and MAIN, Chemnitz University of Technology, Chemnitz, Germany

kochubei.hanna@gmail.com

Chalcogenide glasses are versatile photonic materials used across infrared optics, sensing, optoelectronics, holography, and both passive and active elements in integrated and fibre platforms. Their optical, luminescent, electrical, thermophysical, mechanical, and magnetic responses can be tailored through doping - e.g., with optically active rare-earth and transition-metal ions [1]. Silver doping of As₂S₃ is particularly attractive because it combines the broad glass-forming domain of the As-S network with the high ionic conductivity of Ag⁺ [2]. Modifying this base composition with AgI is likewise relevant for photonics and sensing [3], since the introduced additives provide a handle to tune the structure and, consequently, the material properties.

The diffraction patterns were recorded using a Rigaku SmartLab in parallel-beam geometry with Cu K α radiation ($\lambda = 1.5406 \text{ \AA}$) over $2\theta = 2\text{-}120^\circ$ with a 0.05° step at room temperature. The resulting curves confirm that all samples are amorphous. Based on these XRD data, radial distribution functions and short-range order parameters were computed in RAD GTK+ [4]. The positions of the first (r_1) and second (r_2) maxima were identified, and the bond angle ϕ was calculated using $\phi = 2 \cdot \arcsin(r_2/(2r_1))$ relation.

Table 1. Radial distribution functions and short-range order parameters

| Composition | r_1 | r_2 | r_2/r_1 | ϕ |
|---|-------|-------|-----------|--------|
| As ₂ S ₃ | 2.3 | 3.48 | 1.51 | 98.32 |
| (As ₂ S ₃) ₉₅ (AgI) ₅ | 2.31 | 3.51 | 1.52 | 98.88 |
| (As ₂ S ₃) ₆₅ (AgI) ₃₅ | 2.31 | 3.51 | 1.52 | 98.88 |

Comparison of the short-range order parameters for studied samples shows that the r_1 and r_2 values for (As₂S₃)₉₅(AgI)₅ and (As₂S₃)₆₅(AgI)₃₅ are essentially identical; for pure As₂S₃, a slight shift is observed (for r_1 - within the errors values). Errors were estimated for the RAD GTK+ transform settings and are typically $\pm 0.01 \text{ \AA}$.

- [1]. A.Stronski, O. Paiuk, A. Gudymenko, et.al. Effect Of Doping By Transitional Elements On Properties Of Chalcogenide Glasses. *Ceramics International*, 41, I.6, (2015), 7543-7548.
- [2]. Liu JUN et al. Infrared absorption investigation of glasses in the system As₂S₃-Ag₂S-AgI. *Journal of Non-Crystalline Solids* 111 (1989) 43-47
- [3]. K. Kolev et al. Complex (As₂S₃)_(100-x)AgI_x chalcogenide glasses for gas sensors. *Sensors and Actuators B* 143 (2009) 395 - 399
- [4]. V. Petkov, "RAD, a program for analysis of X-ray diffraction data from amorphous materials for personal computers", *J. Appl. Crystallogr.* 22 (1989) 387-89.

The features of oxide materials for transparent electronics

Ievtushenko A.I.¹, Karpyna V.A.¹, Khyyzhun O.Y.¹, Shtepliuk I.I.¹, Olifan O.I.¹, Myroniuk D.V.¹, Dranchuk M.V.¹, Ovsianikova L.I.¹, Mamykin S.V.², Romanyuk V.R.², Kolomys O.F.², Strelchuk V.V.², Lytvyn P.M.², Korchovyi A.A.², Dusheiko M.G.³, Koval V.M.³, Tkach V.M.⁴, Starik S.P.⁴, Baturin V.A.⁵, Karpenko O.Y.⁵

¹*Frantsevich Institute for Problems of Material Science, NASU, Kyiv, Ukraine,
a.ievtushenko@ipms.kyiv.ua*

²*V. Lashkaryov Institute of Semiconductor Physics, NASU, Kyiv, Ukraine*

³*National Technical University of Ukraine “Igor Sikorsky Kyiv Polytechnic Institute”,
Kyiv, Ukraine*

⁴*V. Bakul Institute for Superhard Materials, NASU, Kyiv, Ukraine*

⁵*Institute of Applied Physics, NASU, Sumy, Ukraine*

Transparent electronics is a modern technological field that employs semiconductors with a wide bandgap ($E_g > 3$ eV). In recent years, transparent electronics has attracted considerable attention from developers because it offers many new and useful applications in the automotive, aerospace, consumer, and environmental industries. With the development of transparent conductive oxides (TCOs) of p-type conductivity, in addition to traditional n-type oxides such as indium tin oxide (ITO), tin oxide (SnO), and zinc oxide (ZnO), it has become possible to manufacture transparent diodes and transistors as essential components for creating transparent electronics devices, circuits, and systems. The prospects for the development of transparent electronics are based on the simultaneous development of effective materials, processes, devices, circuits, and systems.

Our report is devoted to the investigation of the materials science aspects for the growth of high-quality ZnO, NiO, CuAl_xO_y and MoO_x films and nanostructures on different wafers by using reactive magnetron sputtering (MS), the reactive ion-beam sputtering (RIBS) and atmospheric pressure metalorganic chemical vapor deposition (APMOCVD) techniques. The research results covering the influences of the key technological parameters and approaches on the characteristics of oxide thin films will be presented and discussed with the application of advanced research methods.

Topic 2

Theoretical investigation: thin films and nanomaterials.

Absorption of macroporous silicon with two and three layers of macropores

Onyshchenko V.F., Karachevtseva L.A.

*V. Lashkaryov Institute of Semiconductor Physics NAS of Ukraine, Kyiv,
Ukraine, onyshchenkov@isp.kiev.ua*

Two-layer porous silicon is used as an anti-reflective coating. The reflection and absorption spectra of two-layer macroporous silicon are studied [1]. The absorption spectra of three-layer macroporous silicon are calculated using the derived formulas and compared with the absorption spectra of two-layer macroporous silicon. The largest absorption spectra of three-layer macroporous silicon are found by the gradient descent method. The layers of macroporous silicon are considered an effective medium. Multiple reflections from the surfaces and boundaries of macroporous silicon are taken into account.

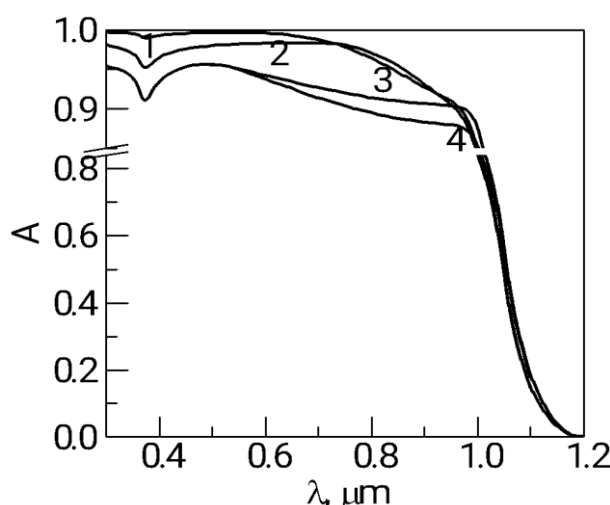


Fig. Absorption spectrum of macroporous silicon with macropore depth, μm : 4–10, 2–120 (two-layer), 3–10, 1–120 (three-layer).

The absorption of three-layer macroporous silicon is greater than that of two-layer macroporous silicon. Adding a layer of macroporous silicon increases the absorption in the long-wavelength region of the spectrum. As the macropore depth increases, the absorption of macroporous silicon increases, due to absorption in the first or second layers of macroporous silicon. The more light with short wavelengths is absorbed in the first or second layers of macroporous silicon, the less it will be reflected from the boundaries between the first and second and second and third layers of macroporous silicon. Optimization of the porosity of the layers leads to an increase in the transmission of the internal surfaces and an increase in the absorption of macroporous silicon.

[1]. Onyshchenko V.F., Karachevtseva L.A. Reflection and absorption of two-layer porous silicon. *J. Nano-Electron. Phys.* 2025. V. 17, No 1. P 01022–6.

Calculation of adhesion strength of thin metal films with metal substrates

Syrovatko Yu.V.

South-Eastern Interregional Centre of the State Institution 'Institute of Soil Protection of Ukraine', Doslidne, Ukraine,
yu.syrovatko@gmail.com

Adhesion is one of the main criteria of the coating quality. Studies of interaction at the coating–substrate interface is an important task to be solved to improve the coating technology. This paper proposes a theoretical approach to determining the values of adhesion strength at the metal–metal interface and comparing the results with the experimental data for electrodeposited coatings of nickel, iron, copper and zinc on the copper and steel substrates.

The concepts allowing us to theoretically evaluate the adhesion energy are based on the quantum-mechanical semi-classical representation implemented in our paper [1]. In this aspect, we used the Wentzel-Kramers-Brillouin (WKB) representations to model the wetting process and the work of adhesion of melts to metal substrates. According to this model, we can evaluate the conditions determining the degree of wetting of the metal substrate, where the determining components are certain numbers similar to the quantum numbers of the WKB theory and the width of the energy barrier. The formation of a potential barrier indirectly characterized the process of interaction between the melt and the substrate through generation of a particle with the reduced mass (atoms of the melt and the substrate). We extended this formalism to modeling of the processes for obtaining thin films. In this aspect, we introduced for consideration a comparative criterion, which allowed us to form an idea of thin film adhesion strength. This criterion expressed some difference in the kinetic energy of the system when the quantum number of the system changed from an integer to a half-integer. In the event when the energy of the system determined by the temperature exceeded this energy difference, we observed good adhesion in the system, according to the calculation data.

The calculated values of adhesion strength for nickel, iron, copper and zinc coatings on the copper and steel substrates satisfactorily agree with the experimental data [2] and with the values of adhesion strength of the same systems calculated with the use of the density functional method in [2].

- [1]. Shtapenko E.Ph., Syrovatko Yu.V. Abnormal Effect of Changing the Wetting Angle in Non-Equilibrium Melt–Solid Metal Systems. *Metallofiz. Noveishie Tekhnol.* 2024. V. 46, No 8. P. 717-737.
- [2]. Shtapenko E.Ph., Voronkov E.O., Zabludovsky V.A., Tytarenko V.V., Kraeva V.S., Kuznetsov V.N. Adhesion strength of electrodeposited metal films with metal substrates. *Journal of Chemistry and Technologies.* 2023. V. 31, No 3. P. 516-521.

Comparison of reflectance of two-layer and three-layer macroporous silicon

Onyshchenko V.F., Karachevtseva L.A.

*V. Lashkaryov Institute of Semiconductor Physics NAS of Ukraine, Kyiv, Ukraine,
onyshchenkovf@isp.kiev.ua*

Porous silicon has found application in solar cells. The reflection spectrum of double-sided macroporous silicon has been calculated [1]. According to the derived formulas, the reflection spectra of two-layer and three-layer macroporous silicon are calculated and compared. The layers of macroporous silicon are considered as an effective medium. Multiple reflections from the boundaries of each layer of macroporous silicon and the monocrystalline substrate are taken into account. The smallest reflection spectrum of two-layer and three-layer macroporous silicon is found.

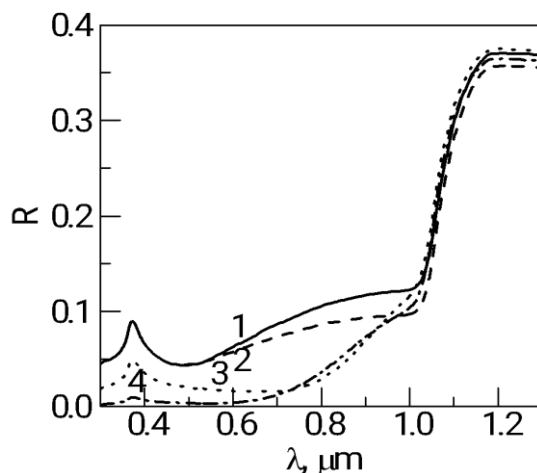


Fig. Reflection spectrum of macroporous silicon with macropore depth, μm : 1–10, 3–120 (two layers), 2–10, 4–120 (three layers).

The reflectance of three-layer macroporous silicon is less than that of two-layer macroporous silicon. Adding a layer of macroporous silicon with an additional reflection boundary reduces the reflection in the long-wavelength region of the spectrum. This occurs due to a decrease in the contrast between the refractive index between adjacent media. As the macropore depth increases, the reflectance of macroporous silicon decreases due to absorption in the first or second layers of macroporous silicon. The more light with short wavelengths is absorbed in the first or second layers of macroporous silicon, the less light will be reflected from the boundaries between the first and second and second and third layers of macroporous silicon.

[1]. Onyshchenko V.F., Karachevtseva L.A. Reflection of bilateral porous silicon with macropores or nanowires. *J. Nano-Electron. Phys.* 2025. V. 17, No 2. P 02015–7.

Density functional theory of resonant inelastic x-ray scattering in the quasi-one-dimensional dimer iridates $\text{Ba}_5\text{AlIr}_2\text{O}_{11}$ and $\text{Ba}_3\text{InIr}_2\text{O}_9$

Kukusta, D.A., Bekenov, L.V., Antonov V.N.

G.V. Kurdyumov Institute for Metal Physics of N.A.S. of Ukraine, Kyiv, Ukraine,

kukustik@imp.kiev.ua

The energy band structure of $\text{Ba}_3\text{InIr}_2\text{O}_9$ and $\text{Ba}_5\text{AlIr}_2\text{O}_{11}$ is investigated within the density-functional theory using the generalized gradient approximation while considering strong Coulomb correlations in the framework of the fully relativistic spin-polarized Dirac linear muffin-tin orbital band-structure method.

For $\text{Ba}_3\text{InIr}_2\text{O}_9$ the resonant inelastic x-ray scattering (RIXS) spectra are obtained theoretically at the iridium L_3 edge for the monoclinic $C2/c$ and hexagonal $P6_3/mmc$ crystal structures [1]. The RIXS spectrum of $\text{Ba}_3\text{InIr}_2\text{O}_9$ at the iridium L_3 edge possesses several sharp features below 2 eV that correspond to transitions within the iridium t_{2g} levels. The excitation located in the range from 2 eV to 5 eV is due to $t_{2g} \rightarrow e_g$ transitions. The third wide structure situated at 5–12 eV appears due to charge transfer transitions. The influence of the momentum transfer vectors \mathbf{Q} and incident photon energy on the iridium L_3 RIXS spectrum is also investigated. To study the role of the core state on the resulting iridium RIXS spectra the RIXS spectra at the iridium K , M_3 , M_5 , N_3 , N_5 , and N_7 edges are discussed. The comprehensive theoretical calculations of the RIXS spectrum at the oxygen K edge are presented as well.

For $\text{Ba}_5\text{AlIr}_2\text{O}_{11}$ RIXS spectra are obtained theoretically at the iridium K , L_3 , M_3 , M_5 and oxygen K edges [2]. The RIXS spectrum at the iridium L_3 edge possesses sharp twelve features below 1.5 eV that correspond to transitions within the iridium t_{2g} levels. The excitations located in the range from 2 eV to 4 eV are due to $t_{2g} \rightarrow e_g$ and $\text{O}_{2p} \rightarrow t_{2g}$ transitions. The high energy peaks situated at 5–11 eV appear due to charge transfer transitions. The theory reproduces well the shape and polarization dependence of the RIXS spectrum at oxygen K edge. The dependence of the RIXS spectrum intensity at the oxygen K edge on the incident photon energy and the momentum transfer vector \mathbf{Q} is much stronger than the corresponding dependence at the iridium L_3 edge.

[1]. Kukusta D.A., Bekenov L.V., Kucherenko Yu., Antonov V.N. Density functional theory of resonant inelastic x-ray scattering in the quasi-one-dimensional dimer iridate $\text{Ba}_3\text{InIr}_2\text{O}_9$. *arXiv*: 2502.18299.

[2]. Kukusta D.A., Bekenov L.V., Antonov V.N. Density functional theory of resonant inelastic X-ray scattering in the quasi-one-dimensional dimer iridate $\text{Ba}_5\text{AlIr}_2\text{O}_{11}$. *Comput. Condens. Matter.* 2025. V. 44 P. e01102.

Domain Morphology, Electrocaloric Response and Negative Capacitance States of Ferroelectric Nanowires Array

Maksym V. Strikha^{1,2}, Anna N. Morozovska³, Oleksii V. Bereznykov³, Zdravko Kutnjak⁴, Eugene A. Eliseev⁵, and Dean R. Evans⁶

¹*Institute of Physics, National Academy of Sciences of Ukraine,
Nauky Avenue 46, 03028 Kyiv, Ukraine, maksym.strikha@gmail.com*

² *Taras Shevchenko National University of Kyiv, Faculty of Radiophysics, Electronics and Computer Systems, Pr. Akademika Hlushkova 4g, 03022 Kyiv, Ukraine,*

³ *V. Lashkariov Institute of Semiconductor Physics, National Academy of Sciences of Ukraine,
Nauky Avenue 41, 03028 Kyiv, Ukraine*

⁴ *Slovenia Jožef Stefan Institute, Ljubljana, Slovenia*

⁵ *Frantsevich Institute for Problems in Materials Science, National Academy of Sciences of Ukraine, Omeliana Pritsaka Street 3, 03142 Kyiv, Ukraine*

⁶ *Air Force Research Laboratory, Materials and Manufacturing Directorate, Wright-Patterson Air Force Base, Ohio, 45433, USA*

We analyzed the domain morphology, electrocaloric response and negative capacitance states in a one-dimensional array of uniformly oriented ferroelectric nanowires, which are densely packed between the flat electrodes. Distributions of the spontaneous polarization and emerging domain structures, electric potential and field, dielectric permittivity and electrocaloric response of the nanowires were calculated by the finite element modelling using the Landau-Ginzburg-Devonshire approach, electrostatic equations, and elasticity theory. Due to the size and depolarization effects, the paraelectric, poly-domain or single-domain ferroelectric states of the wires can be stable depending on their radius and surrounding medium dielectric constant (**Fig.1**).

Both these factors determine the phase state of the wire, which spontaneous polarization is normal to its axis, because they are intertwined via the strong depolarization field. Due to the dipole-dipole interaction between the nanowires, the polar (or anti-polar) state of their array is stable for the wire sizes, which are significantly smaller than the critical size of the paraelectric transition in the single wire. Another important feature is the appearance and stability of the large region of the mixed state of the nanowire array, where the single-domain and the poly-domain ferroelectric states coexist in each wire. The mixed state is almost absent for a single wire.

Let us consider a FeFET system, where a layer of densely packed ferroelectric nanowires is sandwiched between the upper gate electrode and a 2D conductive channel with a small effective screening length λ (e.g., the channel is made from a graphene or a transition metal dichalcogenide). The space between the nanowires is filled by an elastically soft dielectric with a high

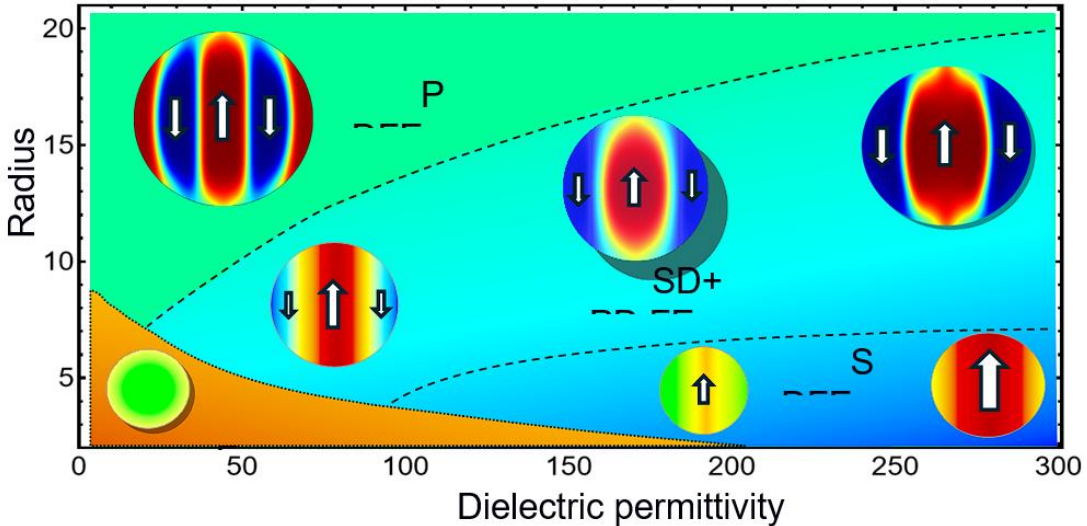


FIGURE 1. The ground state of the BaTiO₃ nanowires as a function of wire radius R and relative dielectric constant of environment ϵ_s for $U = 0$ and room temperature $T = 298$ K. Abbreviations PE, PDFE and SDFE correspond to the paraelectric, polydomain and single-domain ferroelectric states, respectively. Abbreviation “SD+PD FE” corresponds to the coexistence region of the SDFE and PDFE states. Color images with white arrows show schematically the polarization distribution and direction in the XZ cross-section of the nanowire.

permittivity $\epsilon_s \approx \epsilon_f$. The 2D channel is separated from the bottom gate electrode by a dielectric oxide layer of thickness d and relative dielectric permittivity ϵ_d (**Fig. 2(a)**). We assume that ferroelectric nanowires are a wide-gap material close to a dielectric, and therefore the upper gate is electrically separated from the channel. The difference of the geometry shown in **Fig. 2(a)** from the layered geometry considered in the work [1], is that the thickness of the ferroelectric layer here is rigidly determined by the diameter $2R$ of the nanowires. It is important, that we cannot consider connection in series of elements with positive and negative permittivity (such as considered in Ref. [1]), because the wire cores, which have a negative dielectric permittivity, are covered by thick shells with a positive dielectric permittivity.

The spatial distribution of the local dielectric permittivity $\epsilon_{NW}(\vec{r})$ inside the wires is conditioned by the distribution of spontaneous polarization therein: it is maximal in the spatial regions where the spontaneous polarization changes more strongly and it is minimal in the regions where the polarization variation is the smallest. Thus, when the NC state with $\epsilon_{NW}(\vec{r}) < 0$ occurs in certain areas of ferroelectric nanowires at $\epsilon_s \geq \epsilon_f$, the effective capacitance of the nanowires array between the top gate and the conducting channel increases for $0 < \mu < \frac{1}{2}$ or becomes negative for $\frac{1}{2} < \mu < 1$, where μ is the volume fraction of the NC regions. According to the conclusions of Ref. [Помилка! Закладку не визначено.], the domination of the NC states creates conditions for reducing

the subthreshold swing below the Boltzmann limit, which can be of great importance for the scaling of FeFETs and reducing of power consumption.

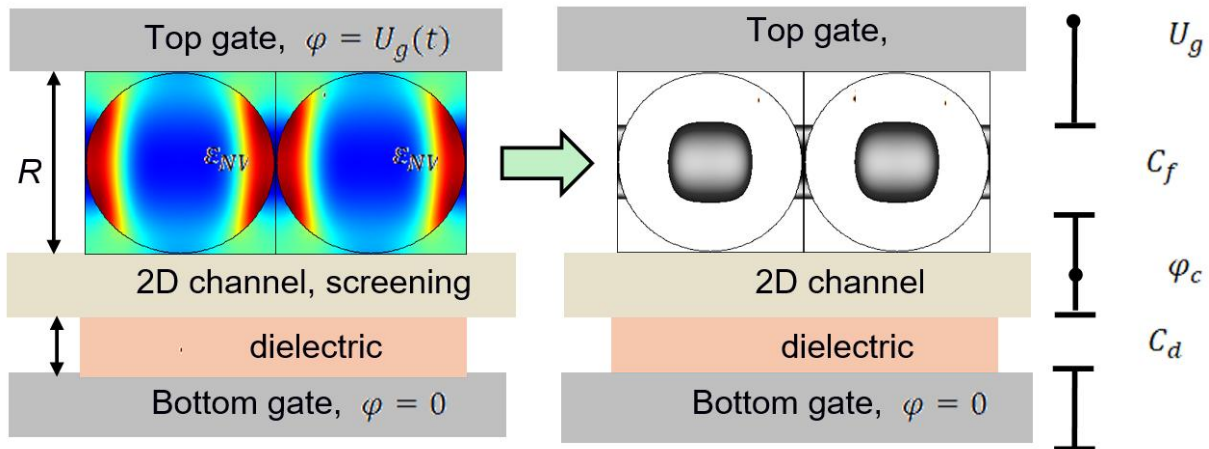


FIGURE 2. (a) Transistor structure “top gate - ferroelectric nanowires - 2D conducting channel - dielectric - bottom gate”. **(b)** Simplified model of the structure (a) in the case of a long channel. **(c)** The equivalent scheme of the NC FeFET.

Acknowledgements. The work of A.N.M. is funded by the EOARD project 9IOE063 (related STCU partner project is P751b) and sponsored by the NATO Science for Peace and Security Program under grant SPS G5980 “FRAPCOM”. The work of E.A.E. is funded by the National Research Foundation of Ukraine (project “Silicon-compatible ferroelectric nanocomposites for electronics and sensors”, grant N 2023.03/0127). The work of O.V.B. is funded by the NAS of Ukraine, grant No. 07/01-2025(6) "Nanosized multiferroics with improved magnetocaloric properties".

A. N. Morozovska, E. A. Eliseev, Y. M. Vysochanskii, S. V. Kalinin, and M. V. Strikha. Size Effect of Negative Capacitance State and Subthreshold Swing in Van der Waals Ferrielectric Field-Effect Transistors, Advanced Electronic Materials, **11**, 2400495 (2025), <https://doi.org/10.1002/aelm.202400495>, <https://doi.org/10.48550/arXiv.2406.13051>.

Effect of Interstitial Boron Atoms on Oxygen Vacancy Mobility in ZnO: A DFT Study

Kazakova O. O.^{1,2}

¹*Chuiko Institute of Surface Chemistry, NAS of Ukraine, Kyiv, Ukraine,*

²*G.V. Kurdyumov Institute for Metal Physics, NAS of Ukraine, Kyiv, Ukraine,*

kazakova.olga@ukr.net

Zinc oxide (ZnO) is a wide-bandgap semiconductor that is promising for use in optoelectronics, transparent electronics, sensors, and photocatalysis. In particular, it is a potential replacement for the widely used indium tin oxide in the formation of current-collecting layers in perovskite-based photovoltaic cells. However, the high mobility of native defects, such as oxygen vacancies (V_O), initiates degradation processes at the ZnO/perovskite interface and reduces the overall stability of the device.

To solve this problem, we propose to reduce the mobility of V_O by introducing impurity boron atoms into the ZnO lattice, which can form stable complexes with vacancies.

Spin-polarized DFT calculations for $2\times 2\times 2$ ZnO supercells with point defects (oxygen vacancy V_O and a B impurity at an interstitial site, B_i) were performed using the Quantum ESPRESSO package. The PBE exchange-correlation functional was used with a Hubbard correction ($U = 7.5$ eV) applied to the Zn d-states. Positional relaxation was performed for all structures, while the lattice parameters were fixed to the values obtained from a full relaxation of the defect-free supercell.

The calculated binding energy of the ($V_O + B_i$) complex is -1.63 eV. This indicates the formation of a thermodynamically stable complex, which should significantly suppress the diffusion of isolated oxygen vacancies and, consequently, increase the stability of the device.

Furthermore, the analysis of the electronic structure shows that the formation of the ($V_O + B_i$) complex leads to the passivation of the vacancy's electronic activity. Unlike an isolated neutral V_O , which introduces a defect level at the Fermi energy and induces metallic behavior in ZnO, the ($V_O + B_i$) complex is a semiconductor with a direct band gap. The projected density of states (PDOS) analysis reveals that the interstitial boron contributes states to the conduction band minimum, which explains the narrowing of the band gap compared to pure ZnO.

Thus, interstitial boron atoms not only physically immobilize oxygen vacancies by forming stable complexes but also electronically passivate them, restoring the semiconducting nature of the material. This makes boron doping a promising strategy for enhancing the stability of ZnO-based electronic devices.

Electrically active oxygen vacancies in BaHfO_3

Balabai, R.M.¹, Pryshliak, O.S.²

Kryvyi Rih State Pedagogical University, ¹balabai@i.ua, ²chronus2011@gmail.com

Oxygen lattice defects in oxides modify the electrical, optical, magnetic, and chemical properties of materials, significantly affecting the functions and properties of oxide-based devices [1]. Perovskite-type oxide, BaHfO_3 is a wide-bandgap oxide and is also sensitive to the concentration of oxygen vacancies. These properties make BaHfO_3 an excellent candidate for memristors.

In the computational experiments of our study, the methods of the electron density functional theory and pseudopotential from first principles were used. A superlattice approach was used in the modeling of the clusters of different sizes with different concentrations of oxygen vacancies (fig. 1).

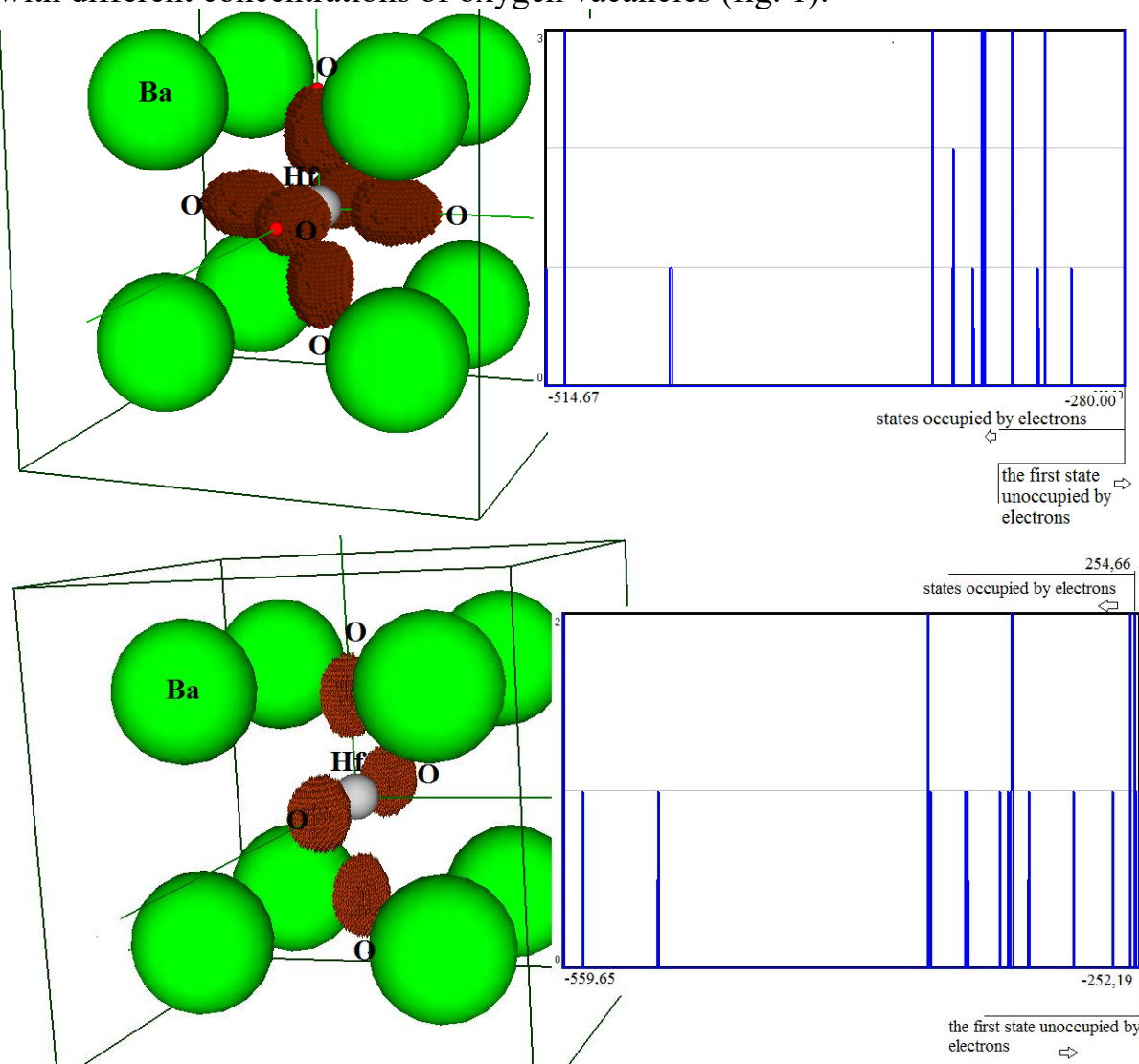


Fig. 1. Electronic structure of 13- and 15-atom clusters of BaHfO_3 with and without oxygen vacancies

[1]. Gunkel F. et all. Oxygen vacancies: The (in)visible friend of oxide Electronics. *Appl. Phys. Lett.* 2020. V. 116. P. 120505.

Electron tunneling through graphene-based double-barrier structure

Sakhnyuk V.E., Zamurujeva O.V., Romanchuk O.M., Ivanovskyi A.V.

Lesya Ukrainka Volyn National University, 13 Voli Ave., 43000 Lutsk, Ukraine

Sakhnyuk.Vasyl@vnu.edu.ua

For the electrons that are incident on the potential barrier in graphene, there are the following values of the angles of incidence, for which the coefficient of passage is equal to one. For electrons with the normal incidence barrier is completely transparent regardless of its height and width. Such an effect for relativistic electrons has long been known as the "Klein's paradox" [1,2] and is associated with the preservation of pseudospin.

We investigated the symmetric double-barrier structure of rectangular shape determined by the function $Vx=V0[H-x-aHx+a+d+Hx-aH-x+a+d]$, there $H(x)$ – Heaviside step function. A massless two-dimensional Dirac equation with potential $V(x)$ was solved to analyze the tunneling of electrons through such a potential barrier.

The main results of the study:

1) A new formula for the dependence of the coefficient of transparency of a symmetric double-potential rectangular barrier on its parameters and on the angle of incidence of electrons has been obtained;

2) Conditions which must satisfy the angles with 100% probability of tunneling of electrons through the barrier have been found;

3) Angles of incidence at which the probability of a tunneling is equal to one have been found from the analysis of the conditions of resonance tunneling for certain values of the barrier parameters. It is shown that with the decrease in the barrier height, the number of resonance angles increases, and the maxima become more acute.

[1] O. Klein, Z. Phys. 53, 157 (1929).

[2] M. I. Katsnelson, K. S. Novoselov, A. K. Geim, Nat. Phys. 2, 620 (2006).

Electronic energy spectrum of a spherical non-concentric inverted core–shell quantum dot

Bilynskyi, I.V.¹, Leshko, R.Ya.², Leshko, O.V.², Ocheretyanyi, A.O.¹,
Popov, M.Yu.¹, Kvyk, M.V.¹, Melnyk, Ya.Yu.¹

¹ Department of physics, Kryvyi Rih State Pedagogical University, 54 Univerytetska
Stret, 50086 Kryvyi Rih, Ukraine

²Department of physics and information systems, Drohobych Ivan Franko State Pedagogical
University, 3 Stryiska Street, 82100 Drohobych, Ukraine,
leshkoroman@gmail.com

ZnS/CdSe quantum dots in a reverse type-I configuration [1] have a CdSe shell bandgap narrower than that of the ZnS core, which leads to the localization of charge carriers specifically in the shell. This enables easier extraction of electrons and holes, which is important for photonic and photovoltaic devices. Such nanocrystals have been successfully synthesized in an aqueous environment and have demonstrated the ability to finely tune the emission wavelength by varying the thickness of the CdSe shell. Thus, their relevance is determined by the flexibility of optical tuning and the potential for integration into biomedical markers or nanophotonic devices.

Spherical core–shell quantum dots of the inverse type-I often turn out to be nonconcentric due to effects arising during their synthesis and subsequent processing. During the growth of the shell on the core, mechanical stresses can develop because of the difference in lattice parameters between the core and shell materials. These stresses lead to structural deformation, which may cause the core to shift relative to the shell, resulting in nonconcentric nanoparticles.

To date, there exists a theory of spherical nonconcentric core–shell quantum dots [2] based on the plane-wave method. According to this theory, matrix elements of the kinetic and potential energies have been obtained analytically for type-I quantum dots. However, this model does not account for the specifics of the inverse type, where the shell bandgap is smaller than that of the core. Therefore, analyzing inverse quantum dots requires a modification of this theory that considers the peculiarities of the energy levels and wave functions in such structures.

In our study, we applied the modified theory to analyze spherical nonconcentric inverse type-I core–shell quantum dots, specifically ZnS/CdSe. Our findings indicate that increasing nonconcentricity leads to the splitting of energy levels and a reduction in the ground-state energy. This behavior contrasts with type-I core–shell quantum dots, where increased nonconcentricity typically results in an increase in ground-state energy.

Furthermore, we observed that the degree of splitting of the excited-state energy levels is influenced by the shell thickness. As the shell thickness decreases, the wavefunction of the electron extends more into the matrix and core regions, leading to a change in the order of energy level splitting. This

Topic 2

phenomenon underscores the complex interplay between structural parameters and electronic properties in nonconcentric quantum dots.

The obtained results open new opportunities for a detailed study of the influence of external electric and magnetic fields on the energy levels and wave functions of charge carriers in inverse type core–shell quantum dots. In particular, it becomes possible to calculate changes in the energies of the ground and excited states when varying the intensity and direction of the external fields [3], allowing the prediction of the behavior of such nanostructures under different conditions. This is important for the development of devices sensitive to external fields, such as sensors or elements for quantum computing. Additionally, the results of the study allow for the evaluation of the effective optical bandgap in inverse type core–shell quantum dots. Increasing the nonconcentricity of the structure leads to the splitting of excited energy levels and a reduction in the ground-state energy. This phenomenon is important for the development of optoelectronic devices, such as lasers, photodiodes, and solar cells, where precise tuning of energy levels is required to achieve the desired performance.

- [1]. Sahu A., Kumar D. Core-shell quantum dots: A review on classification, materials, application, and theoretical modeling. *Journal of Alloys and Compounds* 2016. V. 924, P. 166508:1-22.
- [2]. Leshko R. Ya., Bilynskyi I. V., Leshko O. V., Slusarenko M. A. Electron energy spectrum of the non-concentric spherical core-shell quantum dot. *Micro and Nanostructures* 2023. Vol. 181. P. 207615:1-8.
- [3]. Leshko R. Ya., Bilynskyi I. V., Leshko O. V., Popov M. Yu., Ocheretyanyi A. O. Electron and hole energy spectrum of non-concentric spherical core-shell quantum dot under an externally applied electric field. *Condensed Matter Physics* 2024. Vol. 27, №. 4. P.43703: 1–8.

Engineered by radiation: phase tuning in iron nanoparticles

Shirinyan A.S.¹, Bilogorodskyy Yu.S.¹

¹ Institute of Applied Physics of NAS of Ukraine, Sumy, Ukraine,
aramshirinyan@ukr.net

The influence of radiation-induced defects and their recombination – driven by the energy contribution of point defects such as radiation vacancies – on the stabilization of the low-temperature α -phase in iron nanoparticles at elevated temperatures has been investigated using the Gibbs thermodynamic framework. This analysis involved solving kinetic equations that account for defect generation in different structural phases under irradiation. A specific range of defect generation rates and irradiation doses was identified, within which a size-dependent and temperature-limited zone (2–10 nm wide) enables the existence of the radiation-stabilized α -phase in the temperature interval of 400–530 K. The findings are presented through a phase stability diagram for nanocrystalline iron, constructed under varying irradiation conditions. This diagram delineates three distinct stability regions corresponding to different phases, along with the boundary curves marking phase transitions. It is demonstrated that lowering the rate of defect production shifts the stabilization of the α -Fe phase toward lower temperatures, while preserving the temperature and size range where this phase remains stable. However, increasing the irradiation dose or defect generation rate does not extend the α -phase stabilization zone to higher temperatures or larger particle sizes.

- [1]. Shirinyan A, Bilogorodskyy Y. Effect of radiation-induced vacancy saturation on the first-order phase transformation in nanoparticles: insights from a model. *Beilstein J Nanotechnol.* 2024. V. 15. P. 1453–72.
- [2]. Bilogorodskyy YS, Shirinyan AS, Krit OM. Influence of irradiation on the evolution of radiation defects in nanocrystalline FCC metals: The case of Ni. *Nucl Instrum Methods Phys Res B.* 2025. V. 563(165674): 165674.

Fractality and information basis of structuring in the formation of the gradient-modified thin films of $\langle Ge_2S_3:X \rangle (X-Al, Bi, Pb, Te)$ system: concepts, methods and application

Yurkovych Nataliya¹, Mar'yan Mykhaylo², Seben Vladimir³

¹Uzhhorod National University (Uzhhorod, Ukraine), nataliya.yurkovych@uzhnu.edu.ua

²Uzhhorod National University (Uzhhorod, Ukraine),

mykhaylo.maryan@uzhnu.edu.ua

³University of Presov(Presov, Slovakia), vladimir.seben@unipo

The formation of self-organized structures and fractality in gradient-modified materials of $Ge(As)-Bi(S,Se)$ systems the use of Object-Oriented Modeling (*OOM*) and Artificial Intelligence (*AI*), which are de facto built on the principles of synergetics, is discussed. The principles of *OOM* (encapsulation, inheritance, polymorphism) and Self-Organized Information Structures (*SOIS*) can also be applied to create smart fractal environments based on non-crystalline semiconductor materials [1-3]. These concepts are the basis of the fractal approach to the formation of nanoscale levels of self-organized structures in gradient-modified thin films of $Ge(As)-Bi(S,Se)$ systems, which is demonstrated in the presented materials.

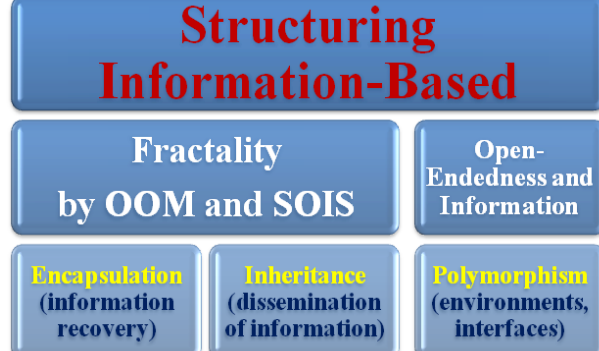


Fig. 1. Fractality and *OOM* of gradient modified structures formation of $\langle Ge_2S_3:X \rangle (X-Al, Bi, Pb, Te)$ system.

In the case of the gradient films formation, encapsulation consists in combining the composition of the system with the film deposition algorithm, which would implement a minimum of energy dissipation (Fig.1). The composition of thin films includes components of the matrix (elements of the vitreous Ge_2S_3) and *components of the modifier* (the atoms of the chemical elements Al , Te , Pb , Bi , etc.). One of the variants of the gradient-modified films deposition algorithm is the inhomogeneous source of the atomic stream

$$G_N = 3.513 \cdot 10^{22} \frac{a_1 P_{evap}}{\sqrt{M_{evap} T_{evap}}} [\text{cm}^{-2}\text{s}^{-1}], \quad (1)$$

where P_{evap} is the equilibrium saturated vapor pressure of the evaporated substance (Al , Bi , Pb , Te), a_1 is an evaporation coefficient, M_{evap} is the molecular weight of evaporating elements – modifiers, T_{evap} is evaporation temperature [1]. Relation (1) contains a significant range of changes in deposition algorithms due to variations in parameters a_1 , P_{evap} , M_{evap} , T_{evap} . In fact, as a result of encapsulation and combining the composition with the deposition

algorithm (1), not just a gradient film is formed, but rather a fractally-gradient one [3]. The information structure that is laid down at the same time determines the self-organized levels of structuring of the obtained films (Fig.1). The distribution of the modifier components across the thickness of the films has a fractal nature (the fractal dimension of the space d_f can be determined for the corresponding modifiers Al , Te , Bi , Pb due to the nature of the component distribution [1,3]). Inheritance within the framework of *OOM* is implemented through an iterative process of changing the physical and chemical properties (we considered the change of optical characteristics) and the formation of attractors phase spaces for the obtained levels of structuring gradient films of various profiles based on the original profile. Polymorphism involves the formation of film morphology surfaces for different modifiers of the chemical elements Al , Te , Bi , etc.

The morphology of the investigated surfaces of inhomogeneous structures $\langle Ge_2S_3:X \rangle (X-Al, Bi, Pb, Te)$ are illustrated. The results show that the surface morphology of the films is depends on the type of the introduced modifier Al, Bi, Pb, Te (Fig. 2).

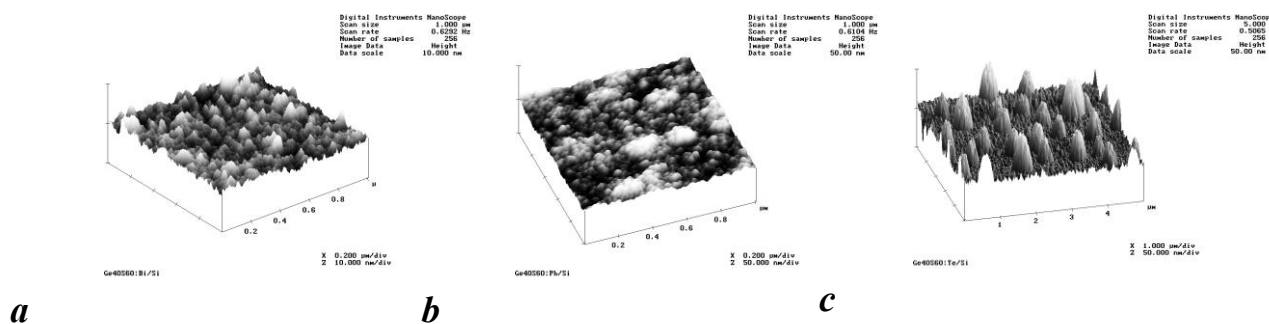


Fig. 2. Axonometric image and sectional analysis of the gradient film surface $\langle Ge_2S_3:Bi \rangle$ (Bi - 14 at.%) (a), $\langle Ge_2S_3:Pb \rangle$ (Pb-12 at.%) (b), and $\langle Ge_2S_3:Te \rangle$ (Te – 30,7 at.%) (c), obtained using AFM.

Investigation of gradient materials on the basis of systems $Ge(As)-Bi(S,Se)$ and nanolevels of formation the ordered fractal structures in them are considered. Development of mathematical model for open-endedness system in formation of gradient structures taking into the use of object-oriented modeling processes of self-organization and depositional flows, heat dissipation are conducted. The possibility of obtaining qualitative modified gradient structures with a given distribution of components by the method of thermal spraying in a vacuum and the possibility of studying the concentration distribution by thickness by mass spectrometry of post-ionized neutral particles has been shown.

- [1]. Yurkovich, N., Mar'yan, M. & Seben, V. (2018). *SPQEo*, **21**(4), 365-373.
- [2]. Mar'yan, M., Yurkovich, N. & Seben, V. (2022). *SPQEo*, **25** (4), 402-412.
- [3]. Yurkovich, N., Mar'yan, M. & Seben, V. Fractality formation of the gradient-modified thin films $\langle Ge_2S_3:X \rangle (X-Al, Bi, Pb, Te)$ by self-organized processes. *21st Conference of Czech and Slovak Physicists, Proceedings*. Published: Slovak Physical Society, EQUILIBRIA, s.r.o., Košice, 2023, pp. 113–114.

Geant4 Simulation of ^{16}O Beam Induced Secondary Electron Emission from ZnO Nanorod Arrays on Si_3N_4

Kotsyubynsky, V.¹, Cholewa, M.², Kindrat, V.¹, Boychuk, V.¹, Mentynskyi, N.¹

¹*Vasyl Stefanyk Carpathian National University, Ivano-Frankivsk, Ukraine,
volodymyr.kotsyubynsky@pnu.edu.ua*

²*Institute of Physics, College of Natural Sciences, University of Rzeszow, Rzeszow, Poland,
mcholewa@ur.edu.pl*

A computational investigation of secondary electron emission (SEE) from ZnO nanorod arrays deposited on Au/ Si_3N_4 substrates under irradiation with ^{16}O ions in the 10–100 MeV energy range was performed. Using GEANT4 Monte Carlo simulations [1], the mechanisms of electronic stopping, electron excitation, and secondary electron yield (SEY) were systematically analyzed as functions of ion energy, nanorod radius, and substrate coverage. The results demonstrate that oxygen ions lose their energy in ZnO predominantly through electronic stopping (>99%), with maximum energy transfer observed at 20 MeV. Analysis of electron spectra showed a coexistence of low-energy secondaries and high-energy δ -electrons, with ZnO nanorod arrays producing broader and more intense distributions than flat ZnO films. The enhanced performance of nanostructured ZnO is attributed to its high surface-to-volume ratio, anisotropic geometry, and localized electric field effects at nanorod tips, which facilitate electron escape [2]. Simulations revealed that SEY is strongly dependent on both ion energy and nanorod morphology. The highest yields were obtained for nanorods with radii of 0.5–1.0 μm and moderate substrate coverage (35–50%), where the balance between interaction volume and escape probability is optimized. In contrast, sparse arrays generate fewer secondaries due to reduced interaction cross-section, while densely packed arrays or continuous films exhibit suppressed yields as a result of recombination losses. The findings confirm that ZnO nanorod arrays provide significant advantages for SEE-based detector applications compared with continuous ZnO films, achieving up to a twofold improvement in SEY. These results emphasize the importance of nanostructure engineering in tailoring SEE performance and offer predictive guidance for the development of advanced detectors and diagnostic devices in plasma physics, ion-beam technologies, and space science.

[1]. Allison J., Amako K., Apostolakis J., Arce P., Asai M., Aso T., Yoshida H. Recent developments in Geant4. Nuclear instruments and methods in physics research section A: Accelerators, Spectrometers, Detectors and Associated Equipment. 2016, V. 835, P. 186-225.

[2]. Cholewa M., Grędysa A., Pozaruk A., Osipowicz T., van Kan J. A., Dou Y. X., Boutachkov P. Investigating the Secondary Electron Emission of Nanomaterials Induced by a High-Resolution Proton Beam. *physica status solidi (b)*. 2022, V. 259, No 4, P. 2100445.

Impact of In, Al, and Ga Doping on the Electronic Properties of (ZnO)₁₂ Nanoclusters: A First-Principles Approach

Dzikovskyi, V.Ye., Kovalenko, M.V., Bovgyra, O.V., Levchenko, B.I.

*Ivan Franko National University of Lviv, Lviv, Ukraine,
mariya.kovalenko@lnu.edu.ua*

Nowadays, zinc oxide (ZnO) is one of the most essential semiconductors for various applications in nanodevices due to its unique properties: wide band gap (3.44 eV at 4.2 K), large exciton binding energy (60 meV) at room temperature, transparency in the visible light region, non-toxicity, and biocompatibility. In addition, ZnO possesses one of the largest families of nanostructures, including nanowires, nanotubes, nanoribbons, nanorings, nanoclusters, and others. As is well known, doping is an essential and effective method for improving metal oxide semiconductors' optical, electrical, and sensing properties. Dopant impurities modify the properties by altering the band structure and morphology of the metal oxide semiconductor.

Among the wide variety of nanostructures, fullerene-like nanoclusters attract significant attention, as their unique properties make them suitable for various applications, including photovoltaic solar cells, gas sensors, and photocatalysis. Previous investigations have demonstrated that (ZnO)₁₂ nanoclusters represent the most stable hollow structure for small clusters and have been successfully synthesized. In this work, we present the results of calculations of the structural and electronic properties of (ZnO)₁₂ nanoclusters doped with In, Al, and Ga atoms.

All calculations, including geometry optimization, electronic spectra, and density of states distributions, were performed for pristine and In-, Al-, and Ga-doped (ZnO)₁₂ nanoclusters within DFT using the CASTEP package. The GGA(PBE) approximation with Hubbard corrections (GGA+U) was employed to describe the exchange- correlation energy of the electronic subsystem. The structural parameters were relaxed through ionic optimization using the efficient BFGS algorithm.

First, we carried out calculations for the undoped (ZnO)₁₂ nanocluster, which revealed a band gap of 4.12 eV, in good agreement with previous theoretical studies employing the hybrid B3LYP functional. For the doped structures, five different configurations of impurity atom incorporation in the (ZnO)₁₂ nanocluster were considered: substitution of a Zn atom; substitution of an O atom; an atom located above the tetragon surface; an atom located above the hexagon surface; and placement inside the nanocluster. All calculations demonstrate that adding In, Al, and Ga atoms into the (ZnO)₁₂ nanocluster structure leads to modifications in the cluster geometry and electronic properties compared to the pristine structure. Based on the results, it can be concluded that such clusters have potential applications in optoelectronic devices.

Investigation of Liquid Crystal Structures for Optical Acetone Vapor Sensors in the Visible and Near-Infrared (NIR) Spectral Ranges

Kremer, I.P.¹, Mykytyuk, Z.M.¹, Ivakh, M.S.¹, Kachurak, Y.M.¹,
Shymchyshyn M.O.²

¹ Lviv Polytechnic National University, Lviv, Ukraine, iryna.p.kremer@lpnu.ua

²European University, Lviv, Ukraine, maryan.shimchyshyn@e-u.edu.ua

In the context of rapid advances in medicine, environmental monitoring, and human safety, there is a growing demand for highly sensitive, selective, and fast-response sensors for detecting volatile organic compounds (VOCs), particularly acetone. Acetone serves as a key marker in fields ranging from the diagnosis of metabolic disorders such as diabetes mellitus to air quality control and fire safety. Organic materials, especially liquid crystal mixtures, have shown strong potential as sensitive layers in gas sensors [1], though their use is limited by insufficient selectivity under real conditions with interfering components such as water vapor, ethanol, and acetaldehyde.

Improving selectivity is therefore critical, especially in biomedical applications such as non-invasive breath analysis [2]. A promising approach involves extending detection into the near-infrared (NIR, 0.9–1.7 μm) spectral range, which is of interest for environmental and biomedical monitoring [3]. Based on CB15 and E7 liquid crystal mixtures, we developed and studied a sensitive structure optimized for optical acetone sensors. The composition provided maximal optical response in the visible region, while NIR characterization broadened the analysis range and enhanced selectivity. The optical properties, particularly NIR absorption, can be tuned through mixture composition and film thickness control.

[1] Mykytyuk, Z. M., Kremer, I. P., Ivakh, M., Diskovskyi, I. S., Khomyak, S. V. Optical sensor with liquid crystal sensitive element for monitoring acetone vapor during exhalation. *Molecular Crystals and Liquid Crystals*. 2021. V. 721, No 1. P. 24–29.

[2] Mykytyuk Z., Fechan A., Shymchyshyn O., Rudyi A., Nazarenko V., Petryshak V. Sensor Network Based on Gas Smart Sensors for Environmental Monitoring. *Modern Problems of Radio Engineering Telecommunications and Computer Science Proceedings of the 11th International Conference Tcset 2012*. P. 503-504.

[3] Hezhuang Liu, Jingyi Wang, Daqian Guo, Kai Shen, Baile Chen and Jiang Wu. Design and Fabrication of High Performance InGaAs near Infrared Photodetector. *Nanomaterials*. 2023. V. 13, No 21. P. 2895.

Machine learning computational framework for structural and electronic analysis of defects in graphene quantum dots

Tuzhykov, A.V.¹, Kiv, A.E.^{1,2}, Soloviev, V.M.^{1,3}, Kavetskyy, T.S.^{1,4,5},
 Šauša, O.^{5,6}, Slusarenko, M.A.³, Korotysh, V.O.³

¹ South Ukrainian National Pedagogical University named after K.D. Ushynsky, Odessa, Ukraine, andrewtuzhykov@gmail.com; vnsoloviev2016@gmail.com

² Ben-Gurion University of the Negev, Beer-Sheva, Israel

³ Kryvyi Rih State Pedagogical University, Kryvyi Rih, Ukraine

⁴ Drohobych Ivan Franko State Pedagogical University, Drohobych, Ukraine,

⁵ Institute of Physics, Slovak Academy of Sciences, Bratislava, Slovakia

⁶ Department of Nuclear Chemistry, FNS, Comenius University, Bratislava, Slovakia

The computational approach presented in this work combines advanced machine learning methodologies [1, 2] with electronic density prediction using deep neural networks. We utilize an architecture that provides a balance between the accuracy of quantum-mechanical methods and the computational efficiency of empirical force fields. The workflow includes structure generation, geometry optimization, defect characterization, and electronic structure analysis. Initial molecular structures of GQDs of various sizes are created using JMOL, and the entire computational pipeline is implemented in Python using the Atomic Simulation Environment (ASE) for structural manipulations and the orb-models package for interatomic potential calculations. The geometry optimization procedure follows a two-stage process. First, structures undergo relaxation using the Orb calculator [3], implemented within the ASE framework. This relaxation uses the FIRE algorithm with a force convergence criterion of 0.01 eV/Å. After obtaining ground-state structures, we systematically introduce various defects (vacancies, substitutions, and bond inversions) using transformation operations defined in specialized utilities. This allows modeling a wide range of defects with high accuracy and controlling their placement in the GQD structure. As an example, Fig. 1 shows typical point defects: vacancy and divacancy.

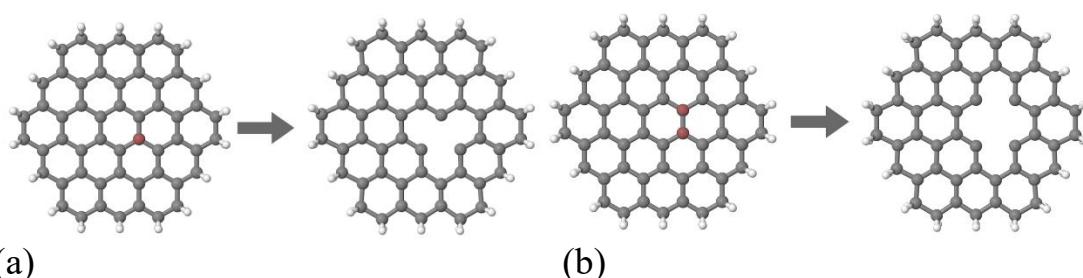


Fig. 1. (a) Formation of monovacancy in GQD. When one carbon atom is removed, a monovacancy is formed, leading to local lattice deformation around the vacancy. (b) Formation of divacancy causes more substantial lattice reconstruction compared to monovacancy.

For electronic structure prediction, we apply DeepDFT [4], which implements a deep learning approach to bypass the computational costs of solving Kohn-Sham equations while maintaining ab-initio accuracy. For GQD systems, the model generates electronic density predictions (Fig. 2) on a regular spatial grid with resolution comparable to standard DFT calculations (typically with a grid step of 0.1-0.2 Å).

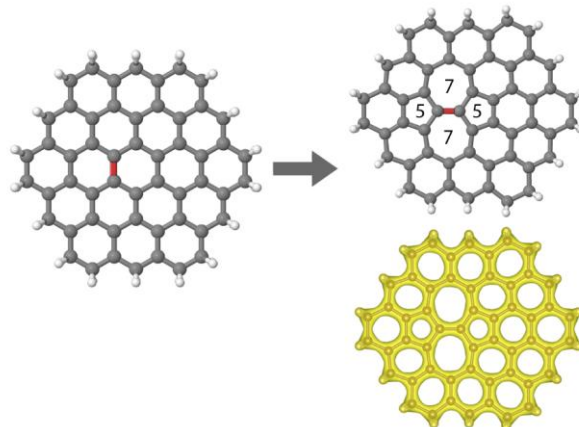


Fig. 2. Stone-Wales defect in graphene quantum dot. Rotation of a C-C bond (marked in red) by 90° causes hexagonal lattice reconstruction with formation of two pentagons (5) and two heptagons (7), significantly changing the electronic density distribution of the material.

Based on the performed calculations, we propose strategies for GQD functionalization through controlled defect introduction. This opens prospects for developing new materials with enhanced characteristics for applications in photovoltaics, quantum optics, bioimaging, and sensing.

Acknowledgments

This work was supported in part by the Ministry of Education and Science of Ukraine (projects Nos. 0122U000850, 0122U000874, 0122U001694, 0125U001054, 0125U002005, and 0125U002033), Slovak Grant Agency VEGA (projects Nos. 2/0166/22 and 2/0131/25), and Slovak Research and Development Agency (project No. APVV-21-0335). T.K. also acknowledges the SAIA for scholarship in the Institute of Physics SAS in the framework of the National Scholarship Programme of the Slovak Republic. This work has also received funding through the MSCA4Ukraine project (grant No. 1128327), which is funded by the European Union.

- [1]. A. Tuzhykov, A. Kiv, V. Soloviev et al., *NATO SPS B*, (2025) 67-83, DOI: 10.1007/978-94-024-2316-7_4.
- [2]. A. Kiv, V. Soloviev, A. Tuzhykov et al., *NATO SPS B*, (2025) 91-104, DOI: 10.1007/978-94-024-2316-7_6.
- [3]. M. Neumann et al., *arXiv*, (2024) 22570, DOI: arXiv:2410.22570.
- [4]. P.B. Jørgensen et al., *arXiv*, (2020) 03346, DOI: arXiv:2011.03346.

Magnetic properties of Josephson junctions with non-sinusoidal current-phase relation

Sakhniuk P.V., Zamurujeva O.V.

Lesya Ukrainka Volyn National University, 13 Voli Ave., 43000 Lutsk, Ukraine

Zamuruyeva.Oksana@vnu.edu.ua

In numerous works devoted to the theoretical description of the behavior of superconducting junctions in a magnetic field, a sinusoidal dependence of current on phase difference is used. However, depending on the junction's parameters, current magnitude, and other factors, the current-phase relation may differ from sinusoidal [1].

This work analyzes two cases of non-sinusoidal dependence of current on phase difference: the first, where a second harmonic is added to the main term, and a more complex form of non-sinusoidal dependence that arises for tunneling superconducting junctions when pair-breaking effects are taken into account. As a result of the study, which primarily focuses on clarifying the effect of deviations from the sinusoidal dependence of current on phase difference on the magnetic properties of Josephson junctions, we can draw the following conclusions:

1. Accounting for the second harmonic in the current-phase relation increases the sensitivity of the critical current to changes in the external magnetic field.
2. When the electron transmission coefficient through the junction increases, the sensitivity of the junction's critical current to a change in magnetic flux also increases. The critical current changes particularly sharply in the region of magnetic flux close to an integer multiple of the elementary flux quantum.
3. Regarding the magnetic field distribution in a fluxon, unlike the sinusoidal dependence where the main flux is concentrated in the vicinity of the fluxon core and the magnetic field rapidly decreases with distance from it, for non-sinusoidal dependencies, the magnetic field is more uniformly distributed throughout the fluxon's area.

[1]. Golubov A.A., Kupriyanov M. Yu., Il'ichev E. The current-phase relation in Josephson junctions. Rev. Mod. Phys. 2004. Vol. 6, p. 411.

Molecular aspects of the mechanochemical activation of bismuth telluride chemical processes by iodine solutions

Rybchakov, D.E.^{1,2}, Manyk, O.M.^{1,2}

¹ *Yuriy Fedkovych Chernivtsi National University, Chernivtsi, Ukraine,*

rybchakov.denys@chnu.edu.ua

² *Institute of Thermoelectricity of the NAS and MES of Ukraine, Chernivtsi, Ukraine*

A comprehensive analysis of the chemical bond formation features in Bi-Te system melts using iodine solutions has been conducted. A theoretical model combining a crystal-chemical approach with modern quantum-chemical methods has been developed, allowing for a more accurate description of complex interactions in multicomponent systems [1].

Calculations of effective radii, redistribution of electron density and energy, and dissociation of non-equivalent chemical bonds depending on the interatomic distances Bi-I and Te-I within the interval of $2,5 \leq d_i \leq 3,5$ (A) are provided in Tables 1-2.

Table 1. Effective charges Δq_i , effective radii R_{Ui} , and dissociation energies of chemical bonds φ_i for the nearest neighbors at non-equivalent distances d_i of the I-Bi structural varieties.

| φ_i | φ_1 | φ_2 | φ_3 | φ_4 | φ_5 | φ_6 | φ_7 | φ_8 | φ_9 | φ_{10} | φ_{11} | φ_{12} |
|-----------------------|-------------|-------------|-------------|-------------|-------------|-------------|-------------|-------------|-------------|----------------|----------------|----------------|
| $d_i(A)$ | 2,5 | 2,6 | 2,7 | 2,8 | 2,9 | 3,0 | 3,1 | 3,2 | 3,3 | 3,4 | 3,445 | 3,5 |
| $R_{Ui}^I(A)$ | 1,317 | 1,370 | 1,423 | 1,475 | 1,528 | 1,581 | 1,633 | 1,686 | 1,739 | 1,791 | 1,815 | 1,844 |
| $\Delta q(\varphi_i)$ | 1,916 | 1,682 | 1,456 | 1,239 | 1,029 | 0,827 | 0,631 | 0,441 | 0,257 | 0,078 | 0 | -0,095 |
| $D_i(ev)$ | 3,134 | 3,014 | 2,903 | 2,798 | 2,718 | 2,613 | 2,551 | 2,448 | 2,374 | 2,304 | 2,28 | 2,27 |

Table 2. Effective charges Δq_i , effective radii R_{Ui} , and dissociation energies of chemical bonds φ_i for the nearest neighbors at non-equivalent distances d_i of the I-Te structural varieties.

| φ_i | φ_1 | φ_2 | φ_3 | φ_4 | φ_5 | φ_6 | φ_7 | φ_8 | φ_9 | φ_{10} | φ_{11} | φ_{12} |
|-----------------------|-------------|-------------|-------------|-------------|-------------|-------------|-------------|-------------|-------------|----------------|----------------|----------------|
| $d_i(A)$ | 2,5 | 2,6 | 2,7 | 2,8 | 2,9 | 3,0 | 3,1 | 3,2 | 3,3 | 3,385 | 3,4 | 3,5 |
| $R_{Ui}^I(A)$ | 1,33 | 1,394 | 1,448 | 1,501 | 1,555 | 1,609 | 1,662 | 1,71 | 1,769 | 1,815 | 1,823 | 1,877 |
| $\Delta q(\varphi_i)$ | 1,71 | 1,488 | 1,275 | 1,07 | 0,872 | 0,681 | 0,496 | 0,317 | 0,143 | 0 | -0,025 | -0,188 |
| $D_i(ev)$ | 2,859 | 2,745 | 2,643 | 2,549 | 2,461 | 2,379 | 2,323 | 2,323 | 2,163 | 2,108 | 2,099 | 2,039 |

As follows from Table 1, for the Bi-I bond, the sign change occurs within the interval of $3,4-3,5$ A, while for the Te-I bonds, it occurs within the interval of $3,3-3,4$ this indicates a transition from donor to acceptor interaction.

The presented results expand the technological capabilities for analyzing phase transformations, which are influenced by factors such as the breaking of existing chemical bonds and the formation of new ones. They also enable calculations of the influence of the initial components' composition on the nucleation of a new phase, the effect of the distribution of phase components on the physical properties of the resulting materials.

[1]. Manyk O.M., Rybchakov D.E., Lysko V.V., Razinkov V.V. Phase equilibria of melts of thermoelectric materials based on Bi-Sb-Se-Te. "Physics and chemistry of solid state" V. 26, No. 3 (2025) pp. 578-583.

Quantum Confinement Effects in Carbon Quantum Dots Synthesized by the Microwave Method

Roman Hladun¹, Roman Ilnytskyi¹, Ivan Budzuliak¹, Nazarii Ilnytskyi²

¹*Vasyl Stefanyk Carpathian National University, Ivano-Frankivsk, Ukraine,*

roman.hladun.24@pnu.edu.com; roman.ilnitsky@pnu.edu.ua; ivan.budzuliak@pnu.edu.ua

²*Ivano-Frankivsk National Medical University, Ivano-Frankivsk, Ukraine,*

tossartombar@gmail.com

The study examines the influence of microwave synthesis conditions on the optical properties of carbon quantum dots (CQDs), focusing on the variation of heating duration and the introduction of sodium bicarbonate (NaHCO_3). These parameters were found to enable controlled modification of quantum confinement effects, which are responsible for the fluorescence characteristics of the nanoparticles.

CQDs were synthesized by microwave-assisted heating of an aqueous citric acid solution (500 W, 6–9 min). Sodium bicarbonate was introduced either before or after thermal treatment. The optical response was investigated under UV excitation at wavelengths of 365 and 395 nm. With increasing heating duration, a systematic redshift of the fluorescence maximum was observed, indicating particle growth and a higher degree of carbonization. Excitation-dependent emission was clearly detected: blue fluorescence dominated under 365 nm excitation, while a shift of the emission peak toward the green spectral region occurred at 395 nm. This behaviour is attributed to multiple emissive centers formed by surface-related emissive states arising from structural defects and diverse functional groups, which create a distribution of energy levels.

The addition of NaHCO_3 significantly affected both the intensity and position of the emission maximum, depending on the timing of reagent introduction. These findings confirm that the chemical composition of the reaction medium is a key factor in defining the optical properties of CQDs, likely through surface functionalization and pH-driven reaction pathways. Overall, the results demonstrate that the optical behaviour of CQDs can be purposefully tuned by adjusting synthesis parameters and excitation conditions. Such controllability provides a valuable approach for the rational design of multifunctional nanomaterials with potential applications in photonics, biomedical imaging, and sensing technologies.

Quantum Size Effects in Thin Films of V₂VI₃ Topological Insulators

Rogacheva E.I.

National Technical University "Kharkiv Polytechnic Institute", Kharkiv, Ukraine,
rogachova.olena@gmail.com

The V₂VI₃ compounds and V₂VI₃-based solid solutions are currently the best thermoelectric (TE) materials for use in refrigerating devices. Interest in studying the TE properties of V₂VI₃ crystals and thin films has grown sharply after it became known that these materials belong to new objects of quantum physics - topological insulators (TIs) whose unique properties are determined by the presence in them of a metallic surface state protected by time reversal symmetry. Many works have appeared suggesting the possibility of using the properties of TIs in spintronics, quantum computing and thermoelectricity. TI thin-film nanostructures are of particular interest because in them the contribution of surface states to the total conductivity increases. The existence of TI states may affect the manifestation of quantum size effects (QSEs) in thin films, e.g., an oscillatory behavior of the dependences of transport properties on film thickness d . The goal of this work is to summarize and analyze our earlier obtained experimental results on the d -dependences of TE properties in n - and p -Bi₂Te₃, Bi₂Se₃, and Bi₂(Te_{1-x}Se_x)₃ polycrystalline thin films prepared by thermal evaporation of crystals in vacuum onto glass substrates (e.g. [1-3]) and to present some our new results. For all films studied, the d -dependences of TE properties exhibit an oscillatory behavior and are well approximated by a sinusoidal function. The obtained results are interpreted within the framework of the model of a rectangular quantum potential well with infinitely high and specularly reflecting walls, considering the peculiar properties of the surface layers of V₂VI₃ films. We believe that a large amplitude, sustained character, and other features of oscillations are associated with the specific boundary conditions in the V₂VI₃ thin films. The results obtained are important for the development of the concepts of solid-state physics and for practical applications of these materials.

- [1]. Rogacheva E.I., Budnik A.V., Sipatov A.Yu., Nashchekina O.N., Dresselhaus M.S. Thickness dependent quantum oscillations of transport properties in topological insulator Bi₂Te₃ thin films. *Appl. Phys. Lett.* 2015. V. 106, No 5, P. 053103.
- [2]. Rogacheva E.I., Budnik A.V., Sipatov A.Yu., Nashchekina O.N., Fedorov A.G., M.S. Dresselhaus, S. Tang. Thickness oscillations of the transport properties in n -type Bi₂Te₃ topological insulator thin films. *Thin Solid Films*. 2015. V. 594. P. 109–114.
- [3]. Rogacheva E.I., Menshikova S.I., Sipatov A.Yu., Nashchekina O.N. Thickness-Dependent Quantum Oscillations of the Transport Properties in Bismuth Selenide Thin Films. *Thin Solid Films*. 2019. V. 684, P.31-35.

Nonlocal dipole polarizability of a spherical metallic nanoshell

Korolkov, R.Yu.¹, Berezhnyi, O.Yu.¹, Korotun, A.V.^{1,2}

¹National University Zaporizhzhia Politechnic, Zaporizhzhia, Ukraine,
romankor@zp.edu.ua

²G.V. Kurdyumov Institute for Metal Physics of the NAS of Ukraine, Kyiv, Ukraine

The study of the optical properties of the two-layer nanoparticles of the type “dielectric core – metallic nanoshell” is of considerable interest from the point of view of their practical importance. In most cases, the Drude model is used to describe the permittivity of the shell metal, in which only the time dispersion is taken into account. However, in such cases as the interaction of two closely located shell particles or the hybrid nanosystems of the type “metallic nanoshell – semiconductor quantum dot”, which have the great practical importance, the nonlocal phenomena can play the significant role, and therefore it becomes necessary to take into account the spatial dispersion. In this case, the effective dielectric function is used instead of the Drude function. In this connection, the comparison of the frequency dependences of the dipole polarizability of the metallic nanoshell according to the local and nonlocal theories is of interest and actual.

Let two-layer nanoparticle of the radius R , which is under the study, consists of the dielectric core of the radius R_c with the permittivity τ_c and the metallic shell with the permittivity $\tau_s(\omega)$, and the entire particle is situated in the medium with the permittivity τ_m . In this case the dipole polarizability of the shell particle is determined by the relation

$$\alpha_{\text{dip}} = 3V \frac{\tau_s \tau_a - \tau_m \tau_b}{\tau_s \tau_a + 2\tau_m \tau_b}, \quad (1)$$

where $V = 4\pi R^3/3$ is the volume of the entire nanoparticle;

$$\begin{aligned} \tau_a &= (1 + 2\beta_c)\tau_c + 2(1 - \beta_c)\tau_s; \\ \tau_b &= (1 - \beta_c)\tau_c + (2 + \beta_c)\tau_s, \end{aligned} \quad (2)$$

and $\beta_c = (R_c/R)^3$ is the bulk content of the dielectric in the nanoparticle.

In the local theory, the permittivity of the shell material is determined by the Drude formula

$$\tau_s(\omega) = \tau^\infty - \frac{\omega_p^2}{\omega(\omega + i\gamma_{\text{eff}})}, \quad (3)$$

where ω_p is plasma frequency; τ^∞ is the contribution of the interzone transitions into the permittivity; γ_{eff} is the effective relaxation rate.

In turn, the expression for the effective dielectric function has the form

Topic 2

$$T_s^{\text{eff}}(\omega) = \frac{1}{T_s(\omega)} + \frac{3}{T^\infty} \left(\frac{\omega_p}{\beta} \right)^2 \left\{ \left[\left(\frac{R_c}{u_1} \right)^2 I_{3/2}(u_1) K_{3/2}(u_1) + \right. \right. \\ \left. \left. + \left(\frac{R}{u_2} \right)^2 I_{3/2}(u_2) K_{3/2}(u_2) \right] \right\}^{-1}, \quad (4)$$

where $\beta = \sqrt{3/5}v_F$, v_F is Fermi electron velocity;

$$u_1 = \frac{R_c}{\beta} \sqrt{\frac{\omega_p^2}{T^\infty} - \omega(\omega + i\gamma_{\text{eff}})}, \quad u_2 = \frac{u_1}{\beta_c^{1/3}}, \quad (5)$$

$I_v(x)$ and $K_v(x)$ are Infeld and Macdonald functions of the order v .

The results of the calculations show the significant differences between the real and imaginary parts of the dipole polarizability according to the above mentioned theories in the infrared range of the spectrum and the adjacent part of the optical range, while at high frequencies the difference between the results is insignificant.

Optical properties of CdSe nanoparticles

Ilchuk H.A., Semkiv I.V., Kashuba A.I.

¹ Department of General Physics, Lviv Polytechnic National University, 12 Bandera Street,
79013 Lviv, Ukraine,
andrii.i.kashuba@lpnu.ua

We report on the optical properties of CdSe nanoparticles (NPs) located in water. The optical parameters are calculated for different concentrations of the CdSe NPs in water (in the interval 0–100 % with the step 5 %). The dependences of the transmission and reflection coefficients of CdSe NPs on the wavelength λ of light are calculated using a known transfer-matrix method [1]. The effective refractive indices of the CdSe NPs in water are calculated using a Bruggeman mean-field approach [2]. The size of the NPs remains much smaller than the wavelength λ (usually up to 0.1λ), which allows for neglecting any scattering effects. The calculations are based on the assumption that the shape of the CdSe NPs does not differ significantly from a spherical one. The particles are isolated, do not stick together, and they form no aggregates.

It is shown that the integral values of the optical transmittance and reflectance increase with decreasing content of the CdSe NPs located in water. The refractive index and the extinction coefficient decrease with decreasing content of the CdSe NPs. The optical dielectric functions ε_1 and ε_2 are calculated from the spectral dependences of the refractive index and the extinction coefficient using the Kramers–Kronig relations. The high-frequency dielectric constant, the ratio of the carrier density to the effective carrier mass (N/m^*), and the relaxation time (τ) are obtained from the dispersion of the optical dielectric function.

Acknowledgement. This work was supported by the Project #0124U000760 for Young Scientists granted by the Ministry of Education and Science of Ukraine.

[1]. Kashuba A.I., Petrus R.Y., Kushnir O.S., Ilchuk H.A., Semkiv I.V., Kashuba N.Y. Optical properties of CdTe nanoparticles in water. Ukr. J. Phys. Opt. 2025. V. 26, No. 2. P. 02001-02009.

[2]. Bergman D.J. Effective medium approximation for nonlinear conductivity of a composite medium. In: Dal Maso, G., Dell'Antonio, G. F. (Eds), Composite Media and Homogenization Theory. Progress in Nonlinear Differential Equations and Their Applications (Birkhäuser, Boston).-1991.-5.

Optical properties of metallic nanoscale truncated spheroids and spheroidal segments on dielectric substrate

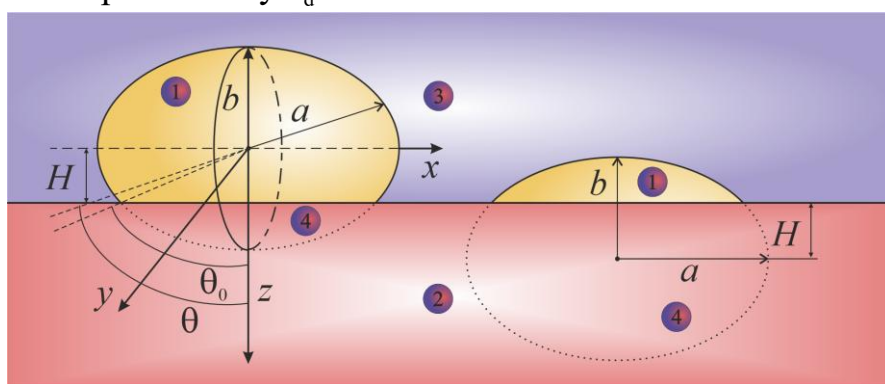
Korotun A.V.^{1,2}, Rubish V.M.³

¹Zaporizhzhia Politechnic National University, Zaporizhzhia, Ukraine,
andko@zp.edu.ua

²G.V. Kurdyumov Institute for Metal Physics of the NAS of Ukraine, Kyiv, Ukraine
³Institute for Information Recording, NAS of Ukraine, Uzhgorod, Ukraine

It is known that metals commonly used in plasmonics such as gold and silver exhibit poor wettability with respect to many dielectrics. As a consequence, instead of the solid films, the island films are formed in many cases. By selecting the material and the substrate parameters, deposition temperature and sputtering rate, films with the islands of the different shapes, sizes and densities can be obtained. This leads to the changes in the scattering and absorption spectra due to the excitation of the surface plasmonic resonances (SPR) at different frequencies. Let us point out that in [1] the case when the islands have the shape of the hemispheres was investigated. However, the shape of the islands may differ from hemispherical. Therefore, the task of studying the optical properties of the islands representing a part of the oblate spheroid (truncated spheroid or spheroidal segment) is actual.

We will study the optical properties of the isolated metallic nanoislands in the form of the truncated spheroid or spheroidal segment with the values of the principal curvatures a , b (Fig. 1) and the permittivity $\epsilon(\omega)$ (domain 1). We consider that the island is located on the dielectric substrate with the permittivity ϵ_d (domain 2), and the permittivity of the surrounding medium is ϵ_m (domain 3). The auxiliary (for the solution of the quasi-static problem) domain 4 in the substrate has the permittivity ϵ_d .



$$1 - \epsilon(\omega), 2 - \epsilon_d, 3 - \epsilon_m, 4 - \epsilon_d$$

Fig. 1. The metallic nanoislands in the form of the truncated spheroid (a) and spheroidal segment (b)

The standard approach for determining the optical characteristics of the nanostructures is to solve the quasi-static problem (due to the small size of the

nanoislands compared to the wavelength), namely, to solve the Laplace equation for four domains using the boundary conditions – the conditions of the continuity of the potential and normal component of the electric induction vector at the interfaces of the domains 1, 2, 3 and 4. Since the studied nanosystems are anisotropic, the quasi-static problem has two independent solutions for the cases of the external field \mathcal{E}_0 perpendicular and parallel to the substrate. Therefore, the dipole polarizability of the studied island nanoparticles will be the diagonal tensor of the second rank. The longitudinal component α_{\parallel} corresponds to the direction of the external field parallel to the axis Oz ($\mathcal{E}_0 \parallel Oz$), and the transverse component α_{\perp} corresponds to the direction perpendicular to the axis Oz ($\mathcal{E}_0 \perp Oz$). In the considered case, the expressions for the transverse and longitudinal dipole polarizabilities will have the following form

$$\alpha_{\perp}^{(\pm)}(\omega) = \frac{12T_m \bar{\alpha}_{\perp}^{(\pm)} V^{(\pm)}}{4 - \bar{\alpha}_{\perp}^{(\pm)} \frac{T_d - T_m}{T_d + T_m}}, \quad \alpha_{\parallel}^{(\pm)}(\omega) = \frac{24T_m \bar{\alpha}_{\parallel}^{(\pm)} V^{(\pm)}}{8 - \bar{\alpha}_{\parallel}^{(\pm)} \frac{T_d - T_m}{T_d + T_m}}, \quad (1)$$

where $V^{(\pm)} = \frac{\pi}{3} (4a_l^2 b_t - 3b_t h^2 \pm h^3)$ is the volume of the island; $h = R - H$ is the height of the segment, and the sign is chosen depending on the shape of the island (Fig. 1) – the truncated spheroid (+) or the spheroidal segment (-);

$$\bar{\alpha}_{\perp(\parallel)}^{(\pm)} = \frac{T_{\perp(\parallel)}^{(\pm)}(\omega) - T_m}{T_m + L_{\perp(\parallel)}^{(\pm)} [T_{\perp(\parallel)}^{(\pm)}(\omega) - T_m]} \quad (2)$$

are the expressions for the diagonal components of the polarizability tensor of the particle (truncated spheroid or spheroidal segment) without the substrate, which coincide in form with the expressions for the dimensionless dipole polarizability of the oblate spheroidal nanoparticle, but the expressions for the depolarization factors $L_{\perp(\parallel)}^{(\pm)}$ and the diagonal components of the dielectric tensor $T_{\perp(\parallel)}^{(\pm)}(\omega)$ will depend on the shape of the island.

It should be pointed out that $\max \left\{ \alpha_{\perp(\parallel)}^{(\pm)} \right\}$ are reached at the frequencies of the transverse and longitudinal surface plasmonic resonance as for the nanoparticles of other forms.

The results of the calculations show that changing the shape of the island leads to the inversion of the frequencies of the longitudinal and transverse surface plasmonic resonances, as well as to the change in the value of the splitting of the plasmonic modes.

[1]. Korotun A.V. Plasmonic phenomena in biconical and bipyramidal metal nanoparticles. *Ukr. J. Phys.* 2023. V. 68, No 10. P. 695-704.

Properties of Polycyclic Aromatic Hydrocarbon complexes with double vacancies functionalized by a single Iron atom within the framework of ligand field theory

Kremen, O. S., Lobanov, V. V., Kartel, M. T.

Chuiko Institute of Surface Chemistry of the NAS of Ukraine,

Oleh Mudrak Str., 17, Kyiv-03164, Ukraine,

kremenoksana@ukr.net

Single-atom functionalization by a transition metal (TM) atom, the creation of different types of vacancies, and the replacement of C atoms with heteroatoms are effective methods of graphene functionalization.

This report presents the results of quantum chemical calculations (DFT, B3LYP/6-31G**/D3) of the complexes of polycyclic aromatic hydrocarbon (PAH) $C_{94}H_{24}$ containing a double vacancy, which have been functionalized by a single Iron atom. The $C_{90}N_4H_{24}$ system, where four carbon atoms were replaced by four nitrogen atoms, was also considered. PAHs were regarded as multifunctional ligands. The method employed to characterize the nature of the ligand-iron bond is based on ligand field theory.

The $Fe-C_{90}N_4H_{24}$ complex has a planar structure with local symmetry D_{4h} . For this case, the diagram of the d -orbitals splitting of the Fe atom in the field of ligands (four nitrogen atoms) would be analogous to a square planar complex (Fig. a). The d_{xz} and d_{yz} orbitals are degenerate and have e_g symmetry; the other orbitals are singly degenerate: the d_{z^2} orbital has a_{1g} symmetry; the $d_{x^2-y^2}$ orbital has b_{1g} symmetry; the d_{xy} orbital has b_{2g} symmetry. The d -orbitals of the Fe atom with lobes on that axis have lower energy due to the lack of ligands on the z -axis of octahedral coordination. The σ -bonding orbitals of the Fe atom have lobes in the x and y directions. The d_{xy} orbital interacts with the p_x orbitals from the nitrogen atoms in the $Fe-C_{90}N_4H_{24}$ complex, and the d_{xz} and d_{yz} (e_g) orbitals interact with the p_z orbitals of the nitrogen atom, as seen in Fig. b.

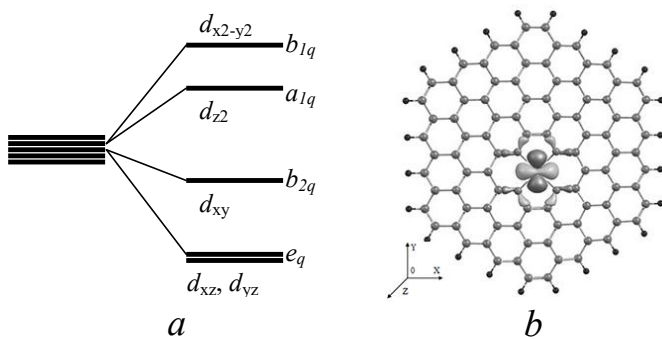


Figure. The d -orbital splitting of levels of the Fe atom in the field of tetragonal symmetry (a), the molecular orbital illustrating the interaction of the d_{xy} orbital of the iron atom with the p_z orbital of the nitrogen atom (b).

The d -orbitals of the TM atom can mix with graphene orbitals of the exact symmetry, which leads to a redistribution of molecular orbitals in energy and, consequently, to a change in the ligand field splitting. The formation of $Fe-C_{90}N_4H_{24}$ complexes with a single Fe atom is possible only due to σ -bonding. Binding with the formation of π -bonds is excluded due to the symmetry conditions.

Quantum size phenomena in transport properties of topological insulator $\text{Bi}_{1-x}\text{Sb}_x$ thin films

Rogachova, O.I.

*National Technical University "Kharkiv Polytechnic Institute", Kharkiv, Ukraine,
olena.rogachova@khpi.edu.ua*

Isostructural and isovalent continuous $\text{Bi}_{1-x}\text{Sb}_x$ solid solutions are, on the one hand, convenient models for solid-state physics due to the high sensitivity of their band structure to changes in composition and other factors, and, on the other hand, promising materials for practical use in thermoelectric (TE) cooling in the 150-200 K range. Besides, the $\text{Bi}_{0.9}\text{Sb}_{0.1}$ solid solution was the first recently discovered 3D-topological insulator, characterized by a surface metallic Dirac layer, which stimulated interest in thin films and surface states and opened new possibilities for applications in spintronics and quantum computing.

The goal of the present report is to review both earlier obtained [1-3] and new results on the kinetic properties of $\text{Bi}_{1-x}\text{Sb}_x$ films as a function of film thickness d and composition x . The films were prepared by thermal evaporation in vacuum from a single source in the Laboratory of Semiconductor Physics and Thermoelectricity at NTU “KhPI” (Kharkiv). The room-temperature dependences of electrical conductivity σ , the Seebeck coefficient, the Hall coefficient, charge carrier concentration and mobility on d (10-400 nm) and x (0-0.1) were measured. For x values in both the semimetallic and semiconducting regions, oscillatory behavior of the d -dependences of the kinetic coefficients with period Δd was observed at room temperature, indicating energy spectrum quantization. The period Δd increased with increasing x , and the theoretical estimates of Δd were in good agreement with experimental values. At $x = 0.09$, high-frequency oscillations were detected in the region of small d , presumably associated with quantization of the topological layer energy spectrum. Several general regularities in the d -dependences were established. It was shown that the monotonic component of the $\sigma(x)$ dependence can be satisfactorily approximated by theoretical calculations based on classical theory. These results demonstrate that studying quantum size effects provides a promising approach to investigating the surface topological layer and can help build a scientific foundation for utilizing the unique properties of TIs in spintronics, quantum computing, and thermoelectricity.

- [1]. E.I. Rogacheva, D.S. Orlova, M.S. Dresselhaus, S. Tang // *MRS Proc. Library*. 2011. P.1314.
- [2]. E.I. Rogacheva, D.S. Orlova, O.N. Nashchekina, M.S. Dresselhaus, S. Tang // *Appl. Phys. Lett.* 2012. 101. P. 023108.
- [3]. E.I. Rogacheva, O.N. Nashchekina, D.S. Orlova, A.N. Doroshenko, M.S. Dresselhaus // *J. Electr. Mater.* 2017. 46, № 7. P. 3821-3825.

Quantum chemical study of the electrostatic potential in the vicinity of active centers on the surface of nanodispersed anatase and its derivative doped with an Ag₂ cluster

Filonenko, O.V.¹, Lobanov V.V.¹, Yavorovsky, O.P.², Riabovol V.M.²

¹ Chuiko Institute of Surface Chemistry, National Academy of Sciences of Ukraine,
Kyiv, Ukraine, oksana.filonenko@isc.gov.ua

²Bogomolets National Medical University, Kyiv, Ukraine

Titanium dioxide nanocomposites doped with nanosilver are characterized by high photocatalytic activity and are widely used, particularly as a disinfecting component in air purification filters and antimicrobial surfaces [1].

In this work, within the framework of quantum chemical modeling, maps of the distribution of molecular electrostatic potential (ρ) in the vicinity of the active centers of the (001) anatase surface and its derivative with adsorbed silver dimer were constructed to substantiate the reasons for the increased photocatalytic activity of TiO₂Ag systems compared to individual nanostructured anatase and nanosilver. The distribution of ρ contains important information about the local electron-donating properties of molecules.

The calculations were performed using density functional theory with the B3LYP exchange-correlation functional and the SBKJC valence basis set, along with an effective backbone potential, within the GAMESS (US) program [2]. To regard the dispersion contributions to the energy of formation of intermolecular complexes, the Grimme dispersion correction D3 was used.

To model the (001) surface of anatase, a cluster with the gross formula Ti₁₅O₄₁H₂₂ was selected. As shown in [3], during the adsorption of Ag₂ on the anatase surface, four Ag–O bonds form with two-coordinated O atoms of the TiO₂ surface, resulting in the elongation of the Ag–Ag bond.

The figure shows the distribution maps of ρ in the plane of three-coordinated oxygen atoms, drawn through the centers of two-coordinated oxygen atoms of the Ti₁₅O₄₁H₂₂ cluster (a) and the Ti₁₅O₄₁H₂₂Ag₂ adsorption complex (b).

The areas adjacent to the three-coordinated O atoms are characterized by relatively insignificant negative values of ~ 20 kJ/mol. Negative values of ρ that are significantly higher in absolute terms are localized in the area between the three-coordinated atoms, opposite the two-coordinated oxygen atoms.

When silver dimer is adsorbed on the anatase surface, the distribution of ρ changes. The area located directly above the silver atoms is characterized by positive values of ρ , which is surrounded by an area of negative potential values; however, these values are significantly lower in absolute value compared to the corresponding values for the pure anatase surface.

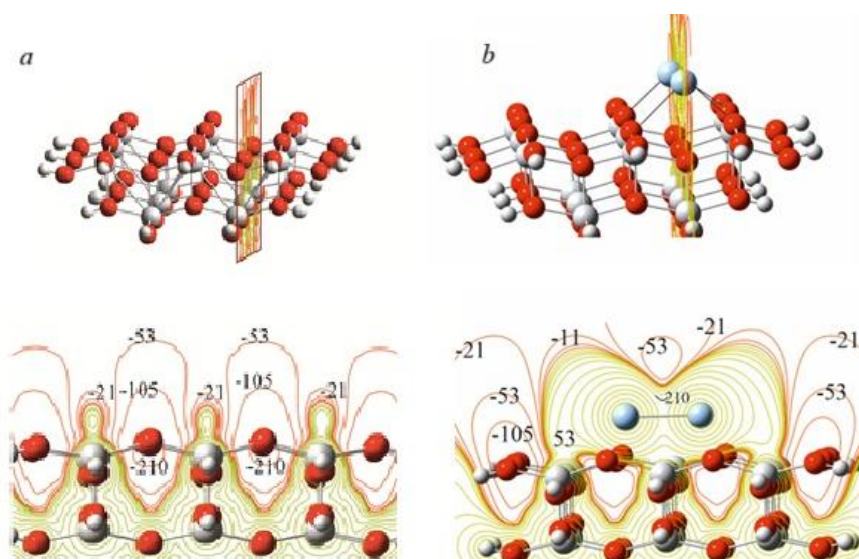


Figure. Distribution of ρ (kJ/mol) in the plane of three-coordinated oxygen atoms of the $\text{Ti}_{15}\text{O}_{41}\text{H}_{22}$ cluster (a) and the $\text{Ti}_{15}\text{O}_{41}\text{H}_{22}\text{Ag}_2$ adsorption complex (b)

Thus, the figure shows that areas of negative values prevail in the distribution of ρ above the surface of the $\text{Ti}_{15}\text{O}_{41}\text{H}_{22}$ cluster, which promotes the adsorption of cations or proton-donating molecules. For $\text{Ti}_{15}\text{O}_{41}\text{H}_{22}\text{Ag}_2$, the regions of negative potential values border on the area of positive values. This nature of the ρ distribution contributes to the fact that (for example) the H atom of a water molecule is localized in the region of negative values, and the O atom is located in the region of positive potential values, contributing to the elongation of the O–H bond until its rupture. Given the distribution of ρ in the vicinity of the Ag_2 molecule adsorbed on the surface of the anatase cluster, it can be assumed that there is a greater probability of OH radicals forming in its presence compared to the pure (001) surface of anatase.

[1]. Yavorovsky O.P., Riabovol V.M., Zinchenko T.O., Zahornyi M.M., Ragulya A.V., Tyschenko N.I., Povnitsa O.Yu., Artiukh L.O., Zahorodnia S.D., Ostapiv D.D. Comparative toxicological-hygienic assessment, structural-morphological, physicochemical characteristics, and virucidal properties of new nanopowder materials TiO_2 and TiO_2Ag . *Medicni perspektivi*. 2024. V.29, No 1. P. 180-192.

[2]. Barca G., et al. Recent developments in the general atomic and molecular electronic structure system. *J. Chem. Phys.* 2020. V.152, No 15. P. 154102.

[3]. Filonenko O., Lobanov, V., Yavorovsky, O., Riabovol, V., Zahornyi M., & Khyzhun O. Quantum chemical study of the spatial and electronic structure of the active centers of the defect-free nano-dispersed anatase surface and it's derivative doped with Ag_2 cluster. *Physics and Chemistry of Solid State*. 2025. V. 26, No 1. P. 35–42.

Quantum chemical study of the interaction between acetylene and fullerene C₇₀ molecules

Kremen, O. S.¹, Bychko, I. B.², Lobanov, V. V.¹, Strizhak, P. E.²

¹Chuiko Institute of Surface Chemistry of the NAS of Ukraine,

Oleh Mudrak Str., 17, Kyiv-03164, Ukraine, kremenoksana@ukr.net

²L.V. Pisarzhevskii Institute of Physical Chemistry of the NAS of Ukraine,
Prospect Nauki, 31, Kyiv-03028, Ukraine

This report presents the results of quantum chemical calculations (DFT, B3LYP/6-31G**/D3) of the chemical interaction between acetylene and fullerene C₇₀ molecules according to eight C–C bond types in C₇₀. The energies of C₇₀•••C₂H₂ reactive complexes (RCs) and C₇₂H₂ reaction products (RPs) formation were calculated. The activation energies of the reaction pathways were determined using transition state (TS) theory.

The initial stage of interaction is the preferential coordination of the C₂H₂ molecule towards the six-membered rings of C₇₀ with an exothermic effect. Next, the formation of C₇₂H₂ occurs through reactions of [2+1], [2+2], and [3+2] cycloaddition, which require high activation energies ranging from 205.67 to 218.02 kJ/mol. The cycloaddition produces various isomers with both closed and open C₇₀ cages. The [2+1] and [3+2] cycloadducts can convert to [2+2] cycloadducts with a high exothermic effect, ranging from -217.11 to -302.75 kJ/mol, and activation energies ranging from 4.55 to 37.59 kJ/mol. For the rest, the [2+2] cycloadduct can transform into the H-C₇₀-C₂H reaction product, where the initial C₂H₂ molecule was represented as -H and -C≡CH fragments attached to neighboring C atoms of the C₇₀ cage. Such a transformation is unfavorable because it requires a high activation energy of 378.35 kJ/mol. The [4+2] cycloaddition reactions were excluded because of geometric restrictions. This research was partially funded by the National Research Foundation of Ukraine (grant 2023.03/0041).

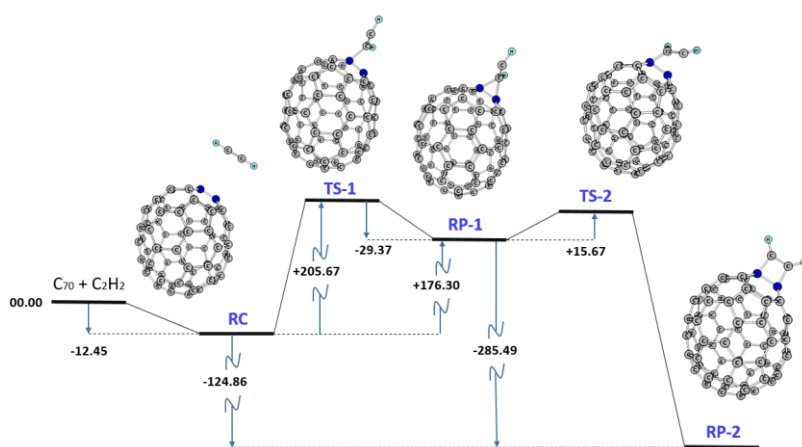


Figure. Reaction profile of acetylene molecule activation by a C₇₀ fullerene molecule with [2+1] cycloadduct formation and subsequent transformation into a [2+2] cycloadduct. Energies are provided in kJ/mol.

Role of the acoustic phonon spectrum components in the formation of thermophysical properties of wurtzite-structure nanofilms

Lutsiuk, Yu.V.¹, Kramar, V.M.^{1,2}, Konstantynovych, I.A.^{1,2}

¹*Yuriy Fed'kovych Chernivtsi National University*

²*Institute of Thermoelectricity of the National Academy of Sciences of Ukraine,
Chernivtsi, Ukraine, v.kramar@chnu.edu.ua*

The temperature changes of heat capacity, entropy, free energy, and coefficients of thermal conductivity and thermal diffusion of nanometer-thick planar structures (nanofilms) were investigated. Numerical calculations were performed on the example of lead iodide nanofilms using dispersion dependences of acoustic phonon frequencies in hexagonal quasi-two-dimensional nanostructures obtained [1] within the approximation of elastic continuum [2]. The dependence of these quantities on the nanofilm's thickness and role of different branches of phonon spectrum in the formation of the thermophysical properties of such structures were also investigated.

It is shown that the greatest influence on thermophysical processes controlled by the values of heat capacity, entropy and free energy have the phonon branches of transverse polarizations (shear and flexural modes of normal vibrations). Their contributions to the values of the indicated quantities are approximately the same and an order of magnitude larger than the contribution of phonons of longitudinal polarization (dilatational modes).

In the processes of thermal conductivity and thermal diffusion, on the contrary, the role of the longitudinal branches of the phonon spectrum is decisive. So, the largest contribution to the lattice thermal conductivity coefficient κ_L is formed by the processes of scattering the longitudinal-polarization phonons. The magnitudes of the partial components of the thermal conductivity coefficient from transverse shear and flexural polarizations phonons are, respectively, 2.6...3.8 and 10...27.5 times smaller, depending on the thickness and temperature of the nanofilm.

Phonons of longitudinal polarization also make the largest contribution to the value of the thermal diffusion coefficient of nanofilm k . The reason for this is that they play a decisive role in forming the value of the thermal conductivity coefficient κ_L and, at the same time, their contribution to the value of the heat capacity c_V is small, while $k \sim \kappa_L/c_V$.

[1].Lutsiuk, Yu., Kramar, V., Petryk, I. Frequency spectrum and group velocities of acoustic phonons in PbI₂ nanofilms. *Phys. Chem. Solid St.* 2022. V. 23, No 3. P. 478–483.

[2].Pokatilov, E.P., Nika, D.L., Balandin, A.A. Phonon spectrum and group velocities in AlN/GaN/AlN and related heterostructures. *Superlattices and Nanostructures*. 2003. V. 33. P. 155–171.

Strain-dependent behaviour of the electronic band gap in phosphorene as a response to its inherent mechanical properties

Los, M.V.¹, Sahalianov, I.Yu.², Radchenko, T.M.¹, Tatarenko, V.A.¹

¹ G.V. Kurdyumov Institute for Metal Physics of the N.A.S. of Ukraine, Kyiv, Ukraine,

los@imp.kiev.ua, tarad@imp.kiev.ua, tatar@imp.kiev.ua

² Linköping University, Norrköping, Sweden,

ihor.sahalianov@liu.se

Black phosphorene has emerged and gained prominence as a quasi-two-dimensional (2D) material since the post-graphene discovery period due to its promising mechanical and electronic properties. Unlike graphene, which is atomically flat, the crystal structure of phosphorene features a corrugated atomic monolayer, where chains of covalently bonded P atoms reside in two different planes. In accord with the anisotropy of the puckered (also called buckled or wrinkled) lattice, phosphorene exhibits high anisotropy in its mechanical, electronic, optical, thermal, and transport properties. Due to its superior mechanical flexibility, phosphorene can sustain extraordinary elastic deformations. These strains can be utilised as a “tool” for tuning the energy gap in phosphorene’s electronic band structure, which is of particular interest in our study.

We simulated the effect of uniaxial and shear tensile strain on the band gap of a phosphorene monolayer of realistic sizes of millions of phosphorus atoms using a tight-binding (TB) model. In this model, the initial hopping integrals are adjusted based on the changes in bond lengths resulting from the in-plane and out-of-plane deformation responses to the applied strain. The unique behaviour of the Poisson’s ratio as a nonlinear nonmonotonic function of strain, as opposed to its more commonly being a constant, is taken into account, resulting in a correspondingly nonlinear nonmonotonic strain dependence of the band gap.

The obtained TB results [1] demonstrate the correlation between mechanical and electronic properties. We conclude that if the response strain is linear and therefore the Poisson’s ratio is constant, then the strain-dependent band gap behaves linearly in phosphorene, similar to graphene. This behaviour contradicts the density functional theory (DFT) based results, which predict that the band gap varies nonlinearly if the phosphorene undergoes expansion (compression) along the armchair or zigzag direction. The disagreement between the TB and DFT findings is overcome by considering the nonlinear contributions in the strain-dependent in-layer and out-of-layer Poisson’s ratios. Moreover, if, in addition to the nonlinearity, the Poisson’s ratio is nonmonotonic with strain, this behaviour of the mechanical characteristic is reflected in its electronic counterpart: the band gap varies nonmonotonically as well.

[1]. Los M.V. et al., Phosphorene as a postgraphene material for straintronics: features of electronic structure and dynamical x-ray diffraction. *Journal of Physical Chemistry C*, Vol. 129, No. 35, p. 15655–15661 (2025); <https://doi.org/10.1021/acs.jpcc.5c02637>

Study of fullerene deposition processes on the free face of single crystals

Schur D.V.¹, Anikina N.S.¹, Savenko A.F.¹, A.P. Pomytkin,
Krivushchenko O.Y.¹, Kotlyar D.A.¹, Gavrilyuk N.A.^{1,2}, Zolotarenko A.D.^{1,2},
Zolotarenko O.D.^{1,2}, Korochkova T.E.^{1,2}, Gabdullin M.T.³

¹ Frantsevich Institute for Problems of Materials Science of NASU, 3, Krzhyzhanovsky Str.,
Kyiv, 03142, Ukraine,

² Chuiko Institute of Surface Chemistry of NASU, 17, General Naumova str., Kyiv, 03164,
Ukraine

³ Kazakh-British Technical University (KBTU) 71, Al-Farabi Str., Almaty, 050040,
Kazakhstan

Experiments have shown that adsorption of fullerenes, depending on the chemical nature of the crystal atoms and the deposition mode (fullerene flux density, their velocity, deposition duration, temperature), can lead to the formation of either a fullerene monolayer, or a layer-by-layer growth of a fullerene film, or the formation of tower-type fullerene crystallites separated by small narrow dips.

The developed statistical theory of equilibrium states of the fullerene deposition processes on the crystal surface made it possible to explain and substantiate the results of experimental data. Possible transformation of the adsorbed fullerene layer is shown. The formation of surface fullerite in the form of tower crystallites during adsorption can, depending on the conditions and deposition mode, lead to thermal desorption, which was observed experimentally. The dependence of the equilibrium concentration of fullerenes on the temperature and height of the tower crystallites is established. It is shown that at a certain temperature, hysteresis effects may appear, leading to a sharp, significant, jump-like increase in the concentration of fullerenes, as a result of which the merging of tower crystallites and the formation of a continuous multilayer fullerite on the surface of the crystal are possible. The increase in temperature depending on the height of the crystallites initially gives an increase in the equilibrium concentration of fullerenes, and this increase due to hysteresis effects may be significant.

Study of multilayer fullerite films

Schur D.V.¹, Shaposhnikova T.I.¹, Anikina N.S.¹, Savenko A.F.^{1,A.P.}
Pomytkin, Krivushchenko O.Y.¹, Kotlyar D.A.¹, GavrilukN.A.^{1,2}, Zolotarenko
A.D.^{1,2}, Zolotarenko O.D.^{1,2}, KorochkovaT.E.^{1,2}, Gabdullin M.T.³

¹*Frantsevich Institute for Problems of Materials Science of NASU, 3, Krzhyzhanovsky
Str., Kyiv, 03142, Ukraine,*

²*Chuiko Institute of Surface Chemistry of NASU, 17, General Naumova str., Kiev,
03164, Ukraine*

³*Kazakh-British Technical University (KBTU) 71, Al-Farabi Str., Almaty, 050040,
Kazakhstan*

Experimental studies of fullerene deposition on a free crystal face allowed us to establish the process patterns, its features, and revealed the manifestation of thermal desorption with increasing temperature.

The statistical theory of adsorption and thermal desorption of fullerenes on a crystalline substrate developed in this work allowed us to establish the nature of these processes, find the temperature dependence of the fullerene concentration for films of different thicknesses, estimate the desorption temperature, its dependence on the film thickness (the number of monolayers s), and find the maximum concentration of fullerenes for different values of s . The nature of the fullerene concentration dependence on the film thickness for different temperatures was established, a significant increase in the concentration of adsorbed fullerenes with increasing film thickness at low temperatures, a weakening of the adsorption process with increasing temperature, and the manifestation of the desorption process at high temperatures were substantiated.

Knowledge of the energy parameters of each specific system from independent experiments can make it possible, using a developed theory, to predetermine the nature of the concentration dependence of fullerenes deposited on the substrate on temperature and the change in this dependence for different film thicknesses.

Surface plasmonic resonances in triangular metal-dielectric nanoprisms

Pavlyshche, N.I.¹, Korotun, A.V.^{1,2}

¹*National University Zaporizhzhia Politechnic, Zaporizhzhia, Ukraine,
andko@zp.edu.ua*

²*G.V. Kurdyumov Institute for Metal Physics of the NAS of Ukraine, Kyiv, Ukraine*

As is well known, the metallic nanoparticles of the various shapes possess the unique optical properties due to the excitation of the localized surface plasmonic resonances. Due to their practical importance, the plasmonic properties of the nanoparticles have been studied theoretically and experimentally for quite a long time. In some cases, when necessary for the practical purposes, such as to reduce the chemical activity, the metallic nanoparticles are coated with the layer of the dielectric material. In addition, some metals oxidize rapidly due to their chemical activity, which leads to the formation of the oxide layer on the surface of the nanoparticles. This circumstance may be the reason for the discrepancy between the results of the theoretical and experimental studies. Among the large number of the nanostructure forms, triangular metallic nanoprisms occupy the special place due to their ability to localize and amplify the electromagnetic field near the surface. It should be pointed out that the excitation of the surface plasmonic resonance in the metal-dielectric nanoprisms has not been sufficiently studied experimentally, and no theoretical studies have been conducted. Therefore, these issues are actual.

Let us consider the nanoscale triangular prism with the side length a and the thickness b , which has the metallic core and covered with the dielectric layer with the thickness t and the permittivity τ_s . Let us assume that the nanoprism is situated in the medium with the permittivity τ_m .

We are going to study the optical properties of the metal-dielectric triangular nanoprisms using the equivalent spheroid approach, the essence of which is as follows. Instead of investigating the optical properties of the low-symmetry nanoparticles (triangular nanoprisms), we will consider the corresponding properties of an equivalent oblate spheroid. In this case, the aspect ratio of the equivalent spheroid (effective aspect ratio) is related to the aspect ratio of the triangular nanoprism by the certain relation, which follows from the condition of the equality of the corresponding axial moments of inertia of the prism and its equivalent oblate spheroid.

Taking into account the above, we will describe the optical properties of the two-layer triangular nanoprism using the relation for the polarizability tensor of the two-layer equivalent spheroid.

$$\alpha_{\perp}^{\perp(\square)} = V \frac{\tau_{\perp}^{\perp(\square)}(\omega) - \tau_m}{\tau_m + L_{\perp(\square)}^{(2)}(\tau_{\perp}^{\perp(\square)}(\omega) - \tau_m)}, \quad (1)$$

Topic 2

in which the diagonal components of the dielectric tensor are determined by the relations

$$T_{\perp}^{(1)}(\omega) = T_s \left[1 + \beta_c \frac{T_s^{(1)}(\omega) - T_s}{T_s + (T_s^{(1)}(\omega) - T_s)(L_{\perp}^{(1)} - \beta_c L_{\perp}^{(2)})} \right]. \quad (2)$$

In formulas (1) and (2)

$$\beta_c = \frac{(a-2t)^2(b-2t)}{a^2b} \quad (3)$$

is the bulk content of metal in the nanoparticle; $L_{\perp}^{(i)}$ ($i=1, 2$) are the depolarization factors of the entire particle and metallic core, which depend on the effective aspect ratios of the metallic core and the whole nanoprism, and the diagonal components of the dielectric tensor of the metallic core

$$T_c^{(1)}(\omega) = T^\infty - \frac{\omega_p^2}{\omega(\omega + i\gamma_{\text{eff}}^{(1)})}, \quad (4)$$

where ω_p is plasma frequency; T^∞ is the contribution of the interzone transitions into the permittivity of metal; $\gamma_{\text{eff}}^{(1)}$ are the diagonal components of the effective relaxation rate tensor.

The size dependence of the transverse/longitudinal surface plasmonic resonance frequencies in the dissipation-free approximation ($\gamma_{\text{eff}}^{(1)} \rightarrow 0$) can be obtained by equating the denominator of the expression (1) to zero. Then, taking into account expressions (2) and (4), we obtain

$$\omega_{sp}^{(1)} = \sqrt{\frac{\omega_p}{T^\infty - T_s + \frac{\frac{T_s}{\beta_c} \left(1 + \frac{1 - L_{\perp}^{(2)}}{L_{\perp}^{(2)}} \frac{T_m}{T_s} \right)}{1 + \left(\frac{L_{\perp}^{(1)}}{\beta_c} - L_{\perp}^{(2)} \right) \left(1 + \frac{1 - L_{\perp}^{(2)}}{L_{\perp}^{(2)}} \frac{T_m}{T_s} \right)}}}. \quad (5)$$

The results of the calculations show that as the aspect ratio $c = a/b$ increases, the distance between the maxima of the optical responses (for example, the maxima of the absorption cross-section) also increases, which means that the frequency splitting of the surface plasmonic resonance $\Delta\omega_{sp} = \omega_{sp}^{(1)} - \omega_{sp}^{(2)}$ also increases.

The energy spectra and band characteristics of two- and three-dimensional superlattices of inhomogeneous quantum

Bandura H.Ya.¹, Leshko R.Ya.¹, Bilynskyi I.V.²

¹ Physics Department, Drohobych Ivan Franko State Pedagogical University, 3 Stryiska St, 82100 Drohobych, Ukraine,

galinka.bandura@gmail.com

² Physics Department, Kryvyi Rih State Pedagogical University, 54 Gagarina Av, 50086 Kryvyi Rih, Ukraine

The modern development of nanophysics and materials science is largely driven by the search for new methods to control the electronic and optical properties of nanostructures. Researchers are particularly interested in superlattices—artificially created periodic systems that, due to quantum effects, give rise to novel spectral and transport characteristics [1]. One of the most promising directions in this field is the use of quantum dots, which exhibit discrete energy levels and enable the design of materials with tailored properties.

In this study, we investigate two- and three-dimensional superlattices composed of quantum dots of identical geometric shape but differing in size and material. This approach makes it possible to create hybrid arrays in which the heterogeneity of the elements plays a pivotal role in shaping the band structure. Such systems open the way to engineering new types of nanostructures that go beyond classical homogeneous lattices.

Numerical modelling methods were employed to determine the energy spectra of the superlattices, calculate the band gap widths, and analyse the mechanisms of level splitting. It was demonstrated that variations in the size and composition of the quantum dots lead to the appearance of additional subbands and significant shifts in energy levels. This enables the tuning of band characteristics and, consequently, the adjustment of the system's electronic and optical properties.

Special attention is devoted to the effect of dimensionality. Distinct spectral formation patterns were identified for two-dimensional superlattices, whereas three-dimensional arrays display a more complex band structure and greater potential for spectral tuning. This approach broadens nanostructural engineering and enables novel functional materials.

The obtained results are relevant for applications in photonics, optoelectronics, and quantum technologies. Inhomogeneous quantum-dot superlattices can form the basis for efficient lasers, sensors, quantum computing elements, and advanced communication systems, opening new possibilities for designing controllable nanostructures and next-generation materials

[1]. Zhonghui Yao, Cheng Jiang, Xu Wang, Hongmei Chen, Hongpei Wang, Liang Qin, Ziyang Zhang. Recent Developments of Quantum Dot Materials for High Speed and Ultrafast Lasers. *Nanomaterials* 2022, V.12, No.7, 1058; <https://doi.org/10.3390/nano12071058>

The steady-state inhomogeneous heat conduction one-dimensional equation

Saliy Ya.P.

*Vasyl Stefanyk Carpathian University, Ivano-Frankivsk, Ukraine,
yaroslav.saliy@pnu.edu.ua*

One of the common methods for measuring the thermal conductivity of solids is the longitudinal heat flow method. In longitudinal heat flow methods, the experimental arrangement is designed in such a way that the heat flow occurs only in the axial direction of the sample. Under steady-state conditions and in the absence of radial heat losses or heat gains, thermal conductivity is determined from the one-dimensional Fourier-Bio thermal conductivity equation [1]. Radial heat losses should be insignificant, which in practice significantly complicates the use of such methods.

The steady-state inhomogeneous heat conduction equation describes the temperature distribution in a body when the temperature does not change with time. We use this equation to find the temperature dependence of the thermal conductivity coefficient [2].

Consider the steady-state equation for the temperature field along a thin rod of diameter d :

$$\frac{d}{dx}(\lambda(T) \frac{d}{dx}T(x)) = \frac{4}{d} \{\sigma(T(x)^4 - T_\infty^4) + \alpha(T(x) - T_\infty)\}, \quad (1)$$

where the Stefan-Boltzmann constant $\sigma = 5.67 \times 10^{-8} \text{ W/m}^2 \cdot \text{K}^4$, T_∞ is the ambient temperature, the heat transfer coefficient α for natural convection in air varies within $3 - 10 \text{ W/m}^2 \cdot \text{K}$.

If the temperature field is well approximated by the dependence

$$T(x) = T_\infty + T_1 \exp(-x/L), \quad (2)$$

then after substituting $t = T/T_\infty$ i $\xi = x/L$ we obtain the equation

$$\frac{d}{d\xi}(\lambda^*(t) \frac{d}{d\xi}t(\xi)) = t^4 - 1 + \alpha^*(t - 1), \quad (3)$$

where $\lambda^* = \lambda d/4L^2\sigma T_\infty^3$, and $\alpha^* = \alpha/\sigma T_\infty^3$.

The solution to equation (3) is

$$\lambda^*(t) = (25 + 12\alpha^* + 13t + 7t^2 + 3t^3)/12. \quad (4)$$

[1]. S. Aksöz, E. Öztürk, N. Marasli, Measurement, *The measurement of thermal conductivity variation with temperature for solid materials* 46, 161 (2013); <https://doi.org/10.1016/j.measurement.2012.06.003>.

[2]. Ya.P. Saliy, B.S. Dzundza Analytical method for determining the temperature dependence of the thermal conductivity coefficient *Physics and chemistry of solid state* V.26, No.2 (2025) pp.307-311

Theoretical Estimation of Carrier Mobility in 2D-InSe Polytypes

Tuziak, O.Ya., Galiy, P.V., Nenchuk T.N., Dziuba, V.I.

Ivan Franko National University of Lviv, Lviv, Ukraine,

tuziak.oksana@gmail.com

The layered crystal InSe as a two-dimensional (2D) structure has been shown to possess high carrier mobility and a tunable bandgap comparable to the best atomically thin dichalcogenides and black phosphorus [1]. This crystal also meets other important requirements for nanoelectronic materials: it can be easily obtained as crystalline samples via mechanical exfoliation, is stable under ambient conditions, and is flexible while remaining resistant to fracture. In addition to their applications in optoelectronics, the cleavage surfaces of these crystals can serve as templates for the formation of indium-deposited nanosystems through solid-state dewetting upon surface heating above the indium melting point [2]. Overall, this crystal exhibits pronounced two-dimensional characteristics, resembling graphene-like semiconductors, and warrants detailed investigation for its further practical applications.

A peculiarity of the InSe crystal structure is that, due to different arrangements of monolayers (four monoatomic sheets in the sequence Se–In–In–Se, with a thickness of approximately 0.4 nm), it exhibits several polytypes, the most common being ε , β , and γ . Previously [3], theoretical DFT investigations were carried out for these three 2D-InSe polytypes, yielding band structures and low effective electron masses for all of them. Here, we present a continuation of these DFT calculations. The deformation potential and elastic constants were obtained, allowing estimation of carrier mobility. Since only acoustic phonon scattering was considered, our result ($3 \div 5 \times 10^3 \text{ cm}^2 \cdot \text{V}^{-1} \cdot \text{s}^{-1}$) should be regarded as an upper estimate, which agrees reasonably well with experimental data available [4].

- [1]. Zheng D., et al. Research progress on two-dimensional indium selenide crystals and optoelectronic devices. *J. Mater. Chem. A*. 2024. V. 12, No 28. P. 16952–16986.
- [2]. Galiy P.V., et al. Self-assembled indium nanostructures formation on InSe (0001) surface. *Appl. Nanosci.* 2020. V. 10, No. 12. P. 4629–4635.
- [3]. Tuziak O.Ya., et al. Calculation of the band structure and its parameters for 2D indium monoselenide. *Ukrainian conference with international participation “Chemistry, physics and technology of surface”/Book of abstracts, 28–29 May 2025.–Kyiv, 2025.* P. 112.
- [4]. Bandurin D., et al. High electron mobility, quantum Hall effect and anomalous optical response in atomically thin InSe. *Nature Nanotechnol.* 2017. V. 12, No. 3. P. 223–227.

Theoretical models of anti-diffusion layers and phase transitions in quaternary systems Fe-Ni-Cr-W

Krechun, M.M.^{1,2}, Manyk, O.M.^{1,2}

¹*Yuriy Fedkovych Chernivtsi National University, Chernivtsi, Ukraine,*

krechun.mariia@chnu.edu.ua

²*Institute of Thermoelectricity of the NAS and MES of Ukraine, Chernivtsi, Ukraine*

Anti-diffusion layers are one of the key elements in the technology of thin films and multilayer coatings used to increase the durability of functional materials at high temperatures and aggressive environments. In previous studies, theoretical models of anti-diffusion barriers in the ternary systems Fe-Ni-Cr [1] and Fe-Ni-W [2] were proposed, which allowed us to identify the regularities of the formation of phase equilibria and stabilization of protective layers.

In this work, these approaches were developed for the more complex quaternary system Fe-Ni-Cr-W, which, due to the unique combination of components, is characterized by high stability and the ability to limit mutual diffusion.

When constructing theoretical models of phase transitions and state diagrams, the results of studies of the physicochemical properties and quantum regularities of the starting elements (Fe, Ni, Cr, W) were summarized. These components are most often used to create reliable anti-diffusion barriers between the branches of p- and n-type thermoelectric materials.

The constructed isothermal cross-sections made it possible to determine the phase equilibrium limits for the eutectic and peritectic type diagrams, which allowed optimizing the technological modes of synthesis of new materials. This creates the prerequisites for the development of effective anti-diffusion barriers in thermoelectric modules designed to operate in high-temperature ranges.

[1]. Manyk O.M., Krechun M.M., Razinkov V.V. Theoretical models of anti-diffusion layers of ternary Fe-Ni-W systems in thermoelectric energy converters.

Journal of Thermoelectricity. 2025. No. 2. P. 25-35.

<https://doi.org/10.63527/1607-8829-2025-2-25-35>.

[2]. Manyk O.M., Krechun M.M., Razinkov V.V. Theoretical models of anti-diffusion layers of ternary Fe-Ni-W systems in thermoelectric energy converters.

Journal of Thermoelectricity. 2025. No. 2. P. 25-35.

<https://doi.org/10.63527/1607-8829-2025-2-25-35>.

Vibrational thermodynamics of $\text{Mo}_{0.5}\text{W}_{0.5}\text{S}_2$ solid solution calculated with finite displacement method

Vasiliev O.O.

Frantsevich Institute for Problems of Materials Science National Academy of Science of Ukraine, Kyiv, Ukraine, o.vasiliev@ipms.kyiv.ua

Solid solutions of MoS_2 - WS_2 are promising for applications in electronics and as solid lubricants. To better understand their controlled synthesis and stability, this work calculates the vibrational thermodynamic properties of the equimolar $\text{Mo}_{0.5}\text{W}_{0.5}\text{S}_2$ ground state (as determined in [1]) and compares them to the end-members, MoS_2 and WS_2 . The calculations were performed using the finite displacement method via the phonopy software package with Quantum Espresso. The convergent parameters of the DFT calculation were the same as in [1], adjusted for the system size where needed.

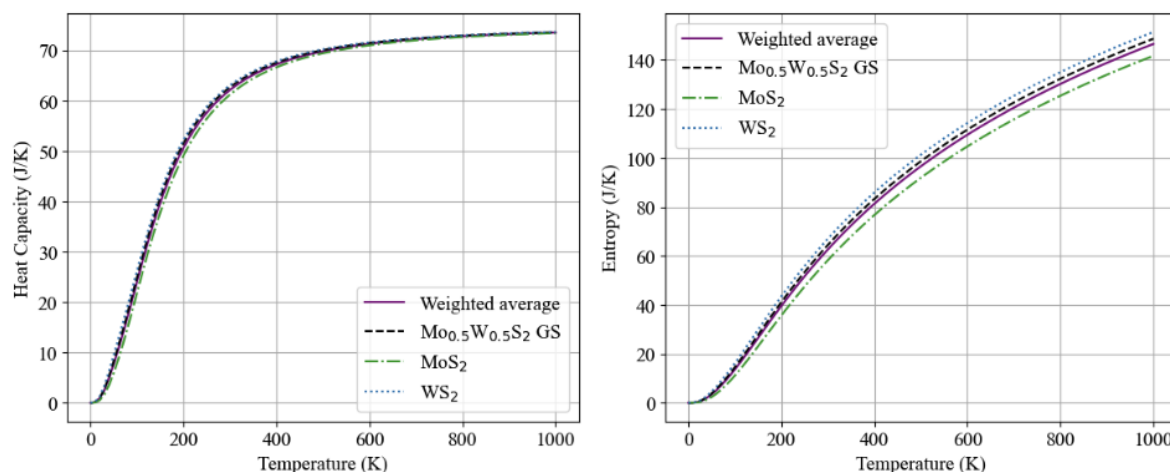


Figure – Vibrational heat capacity and entropy of $\text{Mo}_{0.5}\text{W}_{0.5}\text{S}_2$. Data for the end-members are taken from [2] for MoS_2 and [3] for WS_2 .

The figure shows the calculated temperature dependence of heat capacity and entropy, demonstrating that for practical purposes, the properties of the solid solution can be estimated by the molar-weighted average of its components. The curves for heat capacity are very closely aligned. For entropy, the values for the $\text{Mo}_{0.5}\text{W}_{0.5}\text{S}_2$ solid solution are slightly higher than the weighted average, indicating a small tendency towards the values of tungsten disulfide (WS_2).

- [1]. O. Vasiliev, First-principles study of mixing in the system of layered dichalcogenides MoS_2 - WS_2 , Phys.Chem.Sol.State 26 (2025) 261–266.
- [2]. O. Vasiliev, Thermodynamic Properties of Hexagonal Molybdenum Disulfide, Powder Metall Ceram 58 (2019) 230–236.
- [3]. O. Vasiliev, Thermodynamic Properties of Tungsten Disulfide from First Principles, Powder Metall Ceram 59 (2021) 576–584.

Topic 3
Physical-chemical properties of thin films

Characteristics of electrical conductivity in ferroelectric polyvinylidene fluoride

Sergeeva A., Fedosov S.

Odesa National University of Technology, Odesa, Ukraine, snfedorov@ukr.net

Polyvinylidene fluoride (PVDF) is a typical ferroelectric polymer having potential for creation a new generation of sensors and actuators [1]. We studied the electrical conductivity in PVDF by analyzing its current-voltage (i - V) characteristics. A few processes that determine the form of the i - V characteristic have been considered. In the case of Richardson-Schottky emission

$$i = AT^2 \exp[-(Q - \beta_s \sqrt{V}) / kT], \quad (1)$$

where $\beta_s = \sqrt{e^3 \alpha / 4\pi \epsilon_0 \epsilon x_o}$ is the Schottky coefficient; A is the Dashman constant. For $\alpha=1$, $x_o=26 \mu\text{m}$ and $\epsilon=10$ we obtain $\beta_s/kT=0,088 V^{-1/2}$.

When the current is limited by the space charge (Mott-Gurney law)

$$i = (9/8)\Theta \mu \epsilon_0 \epsilon V^2 / x_o^3, \quad (2)$$

where Θ is the dimensionless carrier capture parameter.

If the Poole-Frenkel emission is stimulated by the field, then

$$i = i_o \exp(\beta_{PF} \sqrt{E} / 2kT), \quad (3)$$

where β_{PF} is the Poole-Frenkel coefficient.

The conductivity mechanism can be identified by the shape of the i - V characteristic [2]. The i - V curve is linear in weak fields in coordinates $\ln i - \sqrt{V}$, and in coordinates $\ln i - \ln V$ in stronger fields with $\beta_s/kT=0,118 V^{-1/2}$ and $\alpha=1,34$. The potential barrier height is $Q=0.72 \text{ eV}$, and the exponent of the i - V dependence is 1.52 instead of 2. Thus, in the ascending part, the current is controlled by both electrode processes and the space charge, with Schottky emission dominating in weak fields and the space charge-limited current in stronger fields. In the second part at $V = 1.2-2.0 \text{ kV}$, the conductivity decrease is observed due to the capture of charge carriers in deep traps, or due to purification of ionic impurities in the field. The ion component makes the greatest contribution to the total current in strong fields, i.e. in the third section.

[1]. *Nathan Ida Sensors, Actuators, and Their Interfaces, 2nd Edition. The Institution of Engineering and Technology. 2020. 928 p.*

[2]. Sergey Fedosov and Alexandra Sergeeva *Formation and relaxation of polarized state in ferroelectric polymers*. Lambert Academic Publishing, Germany, 2020. 165 p.

Chemical polishing of InSb of different crystal orientations with I₂ + HI etching solutions

Malanych G.P., Tomashyk V.M.

V.Ye. Lashkaryov Institute of Semiconductor Physics, National Academy of Sciences of Ukraine, Kyiv, Ukraine, galya.malanich@gmail.com

This paper is dedicated to the development and optimization of new polishing composition based on weaker oxidants. Iodine-containing solutions can be perspective due to low oxidizing ability of iodine, as compared to bromine. The nature and kinetics of chemical dissolution of InSb, oriented in [111]A, [111]B, [110], [100] and [112] crystallographic directions in I₂ + HI etching solutions have been studied.

Investigation was carried out in the interval of solution concentrations: 3–15 mass. % I₂ in HI. It was found that the increasing of iodine concentration in etching solutions results in the increasing dissolution rate (v) of given semiconductor materials. The etching rate is within the range from 15.4 to 31.5 $\mu\text{m}\cdot\text{min}^{-1}$ for the I₂ + HI etchant compositions. It was established that the difference between dissolution rates of different oriented InSb surfaces is insignificant. For all studied I₂ + HI etching solutions the identical sequence to increasing of the InSb etching rate of different surfaces was defined as:

$$v \text{ InSb (112)} < v \text{ InSb (110)} < v \text{ InSb (111)B} < v \text{ InSb (100)} < v \text{ InSb (111)A}$$

For the polishing mixtures of I₂ + HI solutions the dependences of the dissolution rate on the speed of the disk rotation and temperature were obtained and rate-controlling stages of etching processes have been determined. The value of apparent activation energy (E_a) was calculated from temperature dependences, and it didn't exceed 30 $\text{kJ}\cdot\text{mol}^{-1}$.

Surface conditions of crystals after treatment were examined by microstructure investigation by using a metallographic microscope MIM-7 with a digital video camera eTREK DCM800 (8 Mpix). The roughness of the polished surfaces was measured using a NanoScope IIIa Dimension 3000TM scanning probe microscope (Digital Instruments, USA). The chemical composition of the surface was determined by energy dispersive X-ray spectroscopy (EDS/EDX) on a ZEISS EVO 50XVP (Carl Zeiss, Germany) instrument equipped with an INCA PentaFETx3 energy-dispersive X-ray spectrometer for elemental analysis with an accuracy of ~0.1%. It was established that optimized iodine-containing etching compositions are characterized by high-polishing properties. They can be recommended for chemical treatment of the InSb single crystals solid solutions surfaces.

This study was supported by the NAS of Ukraine project #III-10-24. The authors are sincerely grateful to all the defenders of Ukraine and emergency workers who made publication of the research results possible.

Comparison of poling and polarization switching dynamics in nanostructured films of ferroelectric polymers – PVDF, P(VDF-TFE) and P(VDF-TrFE)

Sergeeva A., Fedosov S.

Odesa National University of Technology, Odesa, Ukraine, snfedorov@ukr.net

The most promising materials for replacement of brittle crystalline ferroelectrics in production of pyro- and piezoelectric sensors, detectors and actuators are ferroelectric polymers (FPs), such as polyvinylidene fluoride (PVDF) and its copolymers with tetrafluoroethylene P(VDF-TFE) and trifluoroethylene P(VDF-TrFE) [1]. In this study we compare dynamics of poling, short-circuiting and switching of polarization in PVDF, P(VDF-TFE) and P(VDF-TrFE) thin films.

PVDF was presented by 12.5 μm -thick biaxially stretched films from Kureha Co. with Al electrodes of 0.2 cm^2 area deposited by vacuum evaporation. The polymer contained almost equal portion of crystalline and amorphous phases. The fraction of the ferroelectric β -phase in relation to the non-polar α -phase corresponded to a ratio of 70%:30%. Uniaxially oriented 25 μm thick films of P(VDF-TrFE) copolymer with the entirely β -phase crystalline part were obtained from Solvay et. Cie., Belgium. Samples of P(VDF-TFE) copolymer were from the experimental series of 20 μm thick films composed of 94% of VDF and 6% of TFE. The films had been extruded from melt and uniaxially stretched by the supplier (Plastpolymer). The structure of the P(VDF-TFE) copolymer exhibited 95% of crystalline and 5% of amorphous phases.

Poling and switching experiments were performed utilizing the electrical circuit described elsewhere [2]. Samples were first conditioned by poling at 160 MV/m for 50 s. Then the same DC field was applied in the opposite direction for time from 10^{-6} to 50 s, while the electrical displacement D was recorded. Samples were again conditioned and poled in the same direction after each switching experiment. All four components of the total displacement, namely capacitive, conductive and ferroelectric parts, were extracted from $D(t)$ curves. It was found that the highest switchable polarization ($13 \mu\text{C}/\text{cm}^2$) was in P(VDF-TrTE) films followed by P(VDF-TFE) films ($9 \mu\text{C}/\text{cm}^2$) with the lowest $8 \mu\text{C}/\text{cm}^2$ in PVDF. It appeared that switching time decreased with increasing of the applied field and was 4 order of magnitude longer than the theoretical value. All features of poling and switching were explained by polycrystalline structure of the films [1] and by influence of their intrinsic conductivity [2].

- [1]. H. S. Nalwa (Editor) *Ferroelectric Polymers: Chemistry, Physics, and Applications*, CRC Press, 1995, 912 p.
- [2]. S. N. Fedosov, H. von Seggern Critical Dependence of Polarization Phenomena on Conductivity in Ferroelectric Polymers *Journal of Nano- and Electronic Physics*. 2013. Vol. 5, No 4. P. 04056/1-04056/9.

Controlled formation of Co-Pt alloys in Pt/Co bilayers by Kr⁺ irradiation and post-annealing

Pedan, R.¹, Vladymyskyi, I.¹

¹National Technical University of Ukraine “Igor Sikorsky Kyiv Polytechnic Institute”, Kyiv, Ukraine, roman1pedan@gmail.com

Co-Pt thin films are widely considered for applications in spintronics and magnetic data storage owing to their tunable magnetic anisotropy and high coercivity [1]. Ion-beam processing, as well as its combination with thermal treatment provides a powerful tool for tailoring their structural and magnetic properties [2].

In this study, Pt(10 nm)/Co(10 nm) bilayer stacks were irradiated with 110 keV Kr⁺ ions at fluences ranging from 1×10^{14} ions/cm² to 1×10^{15} ions/cm², followed by post-irradiation annealing at 550 °C for 30 min in vacuum. Structural and magnetic characterization was carried out using X-ray diffraction, secondary ion mass spectrometry, ferromagnetic resonance (FMR), and vibrating sample magnetometry (VSM).

The results demonstrate that ion irradiation alone induces significant intermixing at the Co/Pt interfaces, leading to the formation of Co-Pt solid solutions with fluence-dependent compositions. A small fraction of equiatomic Co-Pt alloy and a dominant Pt-rich Co-Pt alloy was identified, with the composition of the latter evolving from Co₁₀Pt₉₀ to Co₂₅Pt₇₅ as the fluence increases. Subsequent thermal annealing moderately modifies the alloy fraction, promoting the equiatomic phase but not yielding a single-phase state.

Magnetic characterization shows that irradiation enables controlled tuning of effective magnetization (decrease from ~1200 emu/cm³ to ~700 emu/cm³).

The obtained results demonstrating that the ion irradiation, as well as ion irradiation with following annealing can be effective methods for controlled modification of Co-Pt systems. The choice of irradiation parameters enables tuning of structural and magnetic properties over a broad range, making this approach promising for advanced spintronic and nanoelectronic applications.

- [1]. Araki, D., Sonobe, Y., Takahashi, Y. K., Homma, T. Ultrathin CoPt alloy films with fcc (111) orientation and perpendicular magnetic anisotropy fabricated by electrodeposition. *Electrochemistry Communications*. 2025. V. 176, P. 107938.
- [2]. Huang, L.; Wu, H.; Cai, G.; Wu, S.; Li, D.; Jiang, T.; Qiao, B.; Jiang, C.; Ren, F. Recent Progress in the Application of Ion Beam Technology in the Modification and Fabrication of Nanostructured Energy Materials. *ACS Nano*. 2024. V. 18, No 4. P. 2578-2610.

Density of States and Interband Light Absorption in $\text{Ga}_{1-x}\text{Al}_x\text{N}$ ($x=0; 0,03; 0,07$) Thin Films

Bordun O.M.¹, Bordun I.O.¹, Kukharskyi I.Yo.¹, Medvid I.I.¹, Koflyuk I.M.¹,
Protsak M.V.¹

¹ Ivan Franko National University of Lviv, Lviv, Ukraine,

oleh.bordun@lnu.edu.ua

Among new functional materials, GaN-based films occupy an important place, being used in the development of efficient radiation sources, ionizing and UV radiation detectors, and electroluminescent displays. In general, the physical properties of thin films are determined by the methods and conditions of their fabrication, as well as by introduced dopants that purposefully modify the films' properties. Therefore, we investigated of $\text{Ga}_{1-x}\text{Al}_x\text{N}$ ($x=0; 0,03; 0,07$) thin films, in which part of the Ga^{3+} ions were replaced by isovalent Al^{3+} ions.

$\text{Ga}_{1-x}\text{Al}_x\text{N}$ ($x=0; 0,03; 0,07$) thin films with thicknesses of 0.3–1.0 μm were obtained by RF ion-plasma sputtering in a nitrogen atmosphere on sapphire (Al_2O_3) substrates. The structure and composition of the obtained films were studied by X-ray diffraction analysis (Shimadzu XDR-600). A polycrystalline structure with predominant orientation in the (002) plane has been established. Optical transmission spectra were measured with a CM2203 spectrofluorometer equipped with a Hamamatsu R928 measuring head.

The studies showed that for all types of films investigated, the interband absorption edge region is well described by Urbach's empirical rule. The obtained results were analyzed depending on the type of films. To describe the obtained results, a model of a heavily doped or defective semiconductor in a quasi-classical approximation was used, according to which the density of states, associated with fluctuations in the concentration of charged anion vacancies, decreases exponentially into the depth of the band gap. Application of this model made it possible to determine, for different types of films, the reduced effective mass of free charge carriers m^* , the radius of the ground electronic state a , the screening radius r_s , and the root-mean-square potential Δ .

The obtained results were analyzed.

Effect of the interaction of intense low-energy radiation with a ZnO material films

Barchuk N.¹, Virt I.¹, Chekailo M.², Cieniek B.³, Potera P.³

¹*Institute of Physics, Mathematics, Economics and Innovative Technologies
Drohobych State Pedagogical University I.Franko, Ukraine,
nazar.barchuk@gmail.com*

²*Institute of Applied Mathematics and Fundamental Sciences Lviv Polytechnic
National University, Ukraine,*

³*Institute of Materials Science and Engineering University of Rzeszow, Poland*

Thin-film zinc oxide is a key material for the fabrication of ultraviolet photodetectors (UV photodetectors), including photodiodes and photoresistors [1]. UV photodetectors based on transition metal-doped ZnO, in particular nickel-doped ZnO:Ni films, have been reported to exhibit improved photoresponse times compared to pure ZnO.

Laser annealing is a technique used to make oxide functional thin films compatible with various substrates, including flexible materials. This study specifically investigated the effects of optical annealing on Ni-doped ZnO (ZnNiO) thin films. The films were first deposited as polycrystalline layers on sapphire and silicon substrates using pulsed laser deposition.

The deposited films were then annealed using a continuous CO₂ laser. A key advantage of the CO₂ laser is its long-wavelength radiation, which can penetrate deeper into the film compared to shorter-wavelength lasers like UV and IR. The primary goal of this post-growth annealing was to improve the conductive properties of the films. After annealing, the films were analyzed to evaluate changes in their structure and electrical properties: a scanning electron microscope (SEM) was used to analyze both the as-grown and annealed films. The films' electrical properties were measured using the van der Pauw method. Additionally, electrical conductivity and photovoltaic properties of the ZnNiO films were investigated.

The study found that CO₂ laser annealing caused noticeable changes to the films' crystalline structure and surface appearance. Specifically, high-power CO₂ laser annealing led to a degradation of the crystallinity and resulted in a mixed grain size. The annealing process also caused surface nanostructuring, which was confirmed by the SEM analysis. A reduction in the grain size of ZnO films doesn't necessarily improve sensor performance. Our research shows that the crystalline uniformity of the film is a more critical factor for achieving optimal results.

[1]. Li G.; Cheng B. Zhang H.; Zhu X.; Yang D. Progress in UV Photodetectors Based on ZnO Nanomaterials: A Review of the Detection Mechanisms and Their Improvement. *Nanomaterials*. 2025, V. 15, No 9 (644). P.1-16.

Electrical Conductivity of $\text{La}_{1-x}\text{Sr}_x\text{CoO}_3$ Perovskites for Solid Oxide Fuel Cell Cathodes

Kolkovskyi P.I.^{1,2}, Yaremiy I.P.¹, Rachiy B.I.¹, Kotsuybynsky V.O.¹, Ivanichok N.Y.², Kolkovska H.M.¹, Belous A.G.², Boychuk V.M.¹

¹*Department of Applied Physics and Materials Science, Vasyl Stefanyk Precarpathian National University, Ivano-Frankivsk, Ukraine;*

²*Department of Solid State Chemistry, V. I. Vernadsky Institute of General and Inorganic Chemistry, National Academy of Sciences of Ukraine, Kyiv, Ukraine, pkolkovskyy@gmail.com*

Solid oxide fuel cells (SOFCs) represent a promising technology for efficient and environmentally friendly energy conversion.

This study investigates the electrical conductivity of perovskite-type compounds with varying degrees of strontium substitution, aiming to identify compositions that offer improved transport properties while maintaining structural integrity.

Figure 1 shows that electrical conductivity of $\text{La}_{1-x}\text{Sr}_x\text{CoO}_3$ increases with Sr substitution, reaching a maximum at $x = 0.3$. Beyond this point, further Sr addition leads to a slight decrease in conductivity. This indicates an optimal doping level around $x = 0.3$ for achieving the highest electrical conductivity.

The increase in electrical conductivity with Sr substitution up to $x = 0.3$ can be attributed to the creation of more charge carriers. When Sr^{2+} replaces La^{3+} in the LaCoO_3 lattice, it introduces holes (positive charge carriers) to maintain charge neutrality. These holes enhance the mobility of electrons and improve conductivity.

However, beyond $x = 0.3$, the conductivity decreases slightly. This can be due to several factors: Structural Distortion: Higher Sr content can lead to distortions in the crystal lattice, affecting the overlap between Co 3d and O 2p orbitals, which reduces carrier mobility. Carrier Localization: At higher doping levels, the increase in hole concentration may lead to localization of charge carriers due to increased disorder. Phase Separation or Defect Formation: Excessive Sr may induce phase separation or increase oxygen vacancies, both of which can hinder charge transport.

Thus, an optimal Sr concentration (around $x = 0.3$) balances carrier generation and structural stability, resulting in maximum electrical conductivity.

Funding: This work was funded by the NATO Partnerships and Cooperative Security Committee in the framework of the Science for Peace and Security Programme (G6166).

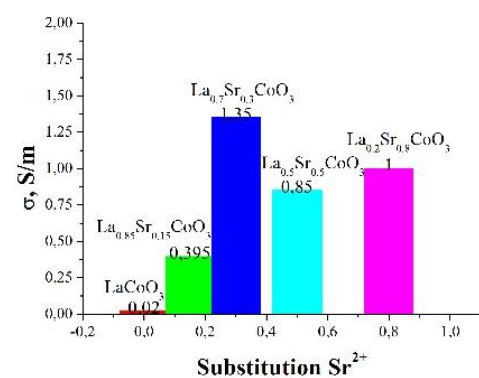


Fig. 1. Electrical Conductivity (σ) as a Function of Strontium Substitution in $\text{La}_{1-x}\text{Sr}_x\text{CoO}_3$ Compounds

Emitting heterosystems $ZnSe$ and ZnO

Slyotov, M.M.¹, Slyotov, O.M.¹, Mazur, T.M.², Chernivchan, V.Ya.¹, Mazur, M.P.²

¹*Yuri Fedkovich Chernivtsi National University, 2 Kotsiubynskoho St., Chernivtsi, Ukraine*

²*Ivano-Frankivsk National Technical University of Oil and Gas, Ivano-Frankivsk, Ukraine,
tetiana.mazur@nung.edu.ua*

At the present stage of functional electronics, selenides and zinc oxides are important for devices operating in the short-wave optical range. A key task is to increase the efficiency of generation–recombination processes in radiation sources and photodetectors. The method of isovalent substitution (IVS) in the reactions $ZnS+Se\rightarrow ZnSe$ and $ZnSe+O_2\rightarrow ZnO$ significantly expands the capabilities of $ZnSe$ - and ZnO -based emitters. Annealing of II–VI substrates in vapors of isovalent elements in a closed volume enables heterostructures (HSs) with a stable structure and a transition layer. Optimal solid-phase substitution occurs at concentrations above 0.1 at. %, which determines HS properties [1].

Optical studies (absorption, reflection, photoluminescence with λ -modulation) revealed the crystal structure and energy parameters ($E_G, \Delta_{CR}, \Delta_{SO}$). The quantum efficiency of luminescence reached 15–17% for $ZnSe/ZnS$ and 20–25% for $ZnO/ZnSe$ heterostructures (compared to ~0.1% for typical $ZnSe$). Emission spectra cover the blue–violet (0.41–0.48 μm , 2.95–2.58 eV) and near-UV (0.35–0.40 μm , 3.10–3.55 eV) ranges, formed by interband recombination and exciton annihilation at isovalent impurities (Fig. 1,2). For $ZnO/ZnSe$ heterostructures, the emission maximum shifts to lower photon energies with increasing excitation L , and the intensity follows $I\sim L^{1.5}$. At high excitation, equidistant sidebands arise due to electron–phonon scattering (Fig. 1,2). Thus, IVS is an effective approach for thin-layer fabrication in optoelectronic devices.

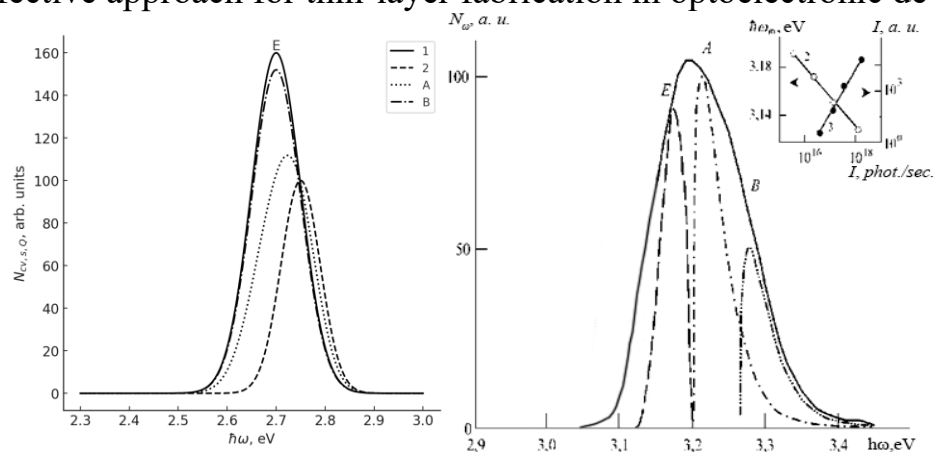


Fig. 1, 2. Spectra of β - $ZnSe/\beta$ - ZnS (1) and ZnO (2) heterostructures. A, B – interband radiative recombination; E – exciton; The inset shows the dependence of the position of the maximum $\hbar\omega_m$ (1) and intensity I (2) of the photoluminescence heterostructures β - $ZnSe$ on the excitation level L . $T=300$ K.

[1]. Mazur, T.M., Slyotov, M.M., Slyotov, O.M., Mazur, M.P. Light emitters based on $ZnSe$. *Low Temperature Physics*. 2025. V. 51, No 2, P. 256–260. <https://doi.org/10.1063/10.0035413>

Faraday effect in ZnSe crystals doped with transition metals

Kinzerka, O.V.¹, Slyotov, M.M.¹, Mazur, T.M.²

¹*Yuri Fedkovich Chernivtsi National University, Chernivtsi, Ukraine,
oksanakinzerka@gmail.com*

²*Ivano-Frankivsk National Technical University of Oil and Gas, Ivano-Frankivsk, Ukraine*

of the Faraday effect in zinc selenide doped with some transition metal impurities, namely Mn, Fe and Co. Fig. 1a shows the spectral dependences (dispersion curves) of the Verde constant, which was calculated using the relation $\Theta = V \cdot H \cdot d$, where H – magnetic field strength, d – sample thickness, V – Verde's constant, which in turn depends on the frequency of light and the nature of the substance.

Measurements of the rotation angle of the plane of polarization were carried out at $T = 77$ K with an intensity of $H = 10000$, and the thickness of the samples was chosen to be $d_0 \approx 0.1$ cm.

As can be seen from fig. 1a, for all the studied samples, an increase in the Verde constant is observed with an increase in the energy of the light quantum, which is characteristic of the diamagnetic state of the substance. It is known that the transition metal impurity is not distributed throughout the entire volume of the sample, but is located in the diffusion layer with a thickness of d , which is less than d_0 .

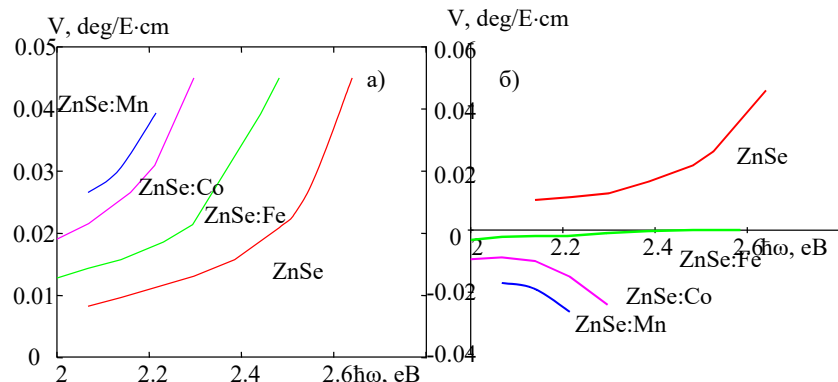


Fig. 1. Spectral dependences of the Verde constant

In this regard, to find the true spectral dependence of the Verde constant for doped samples, it is necessary to find the difference between the value V for ZnSe:Me and its value $\hbar\omega$ at the same for the base ZnSe crystals.

As a result of this action, the dispersion curves of fig. 1 a are transformed into other dependencies $V(\hbar\omega)$, which are depicted in Fig. 1b.

Comparison of the nature of the obtained dependences of the Verde constant on the photon energy with known literature data for other materials allows us to draw the following conclusions. At the temperature of liquid nitrogen, impurity-free ZnSe crystals have diamagnetic properties. Doping of zinc selenide base substrates with Mn and Co impurities leads them to a paramagnetic state, and Fe to a ferromagnetic state.

Figure of merit of Au nanofilms on Ge underlayers near percolation threshold

R. Bihun¹, V. Apopii¹, B. Penyukh¹, A. Fareniuk¹, D. Leonov²

¹*Ivan Franko National University of Lviv, Dragomanova Str., 50, Lviv, 79005, Ukraine*

²*Technical Centre, N.A.S. of Ukraine 13, Pokrovs'ka Str., UA-04070, Kyiv, Ukraine*

The investigation of electron transport in nanometer scale metallic films exposed to electromagnetic radiation is highly relevant to contemporary advancements in micro- and nanoelectronics, as well as transparent electronics [1-3]. Metallic layers with thicknesses in the nanometer range are considered excellent candidates as transparent ohmic conductors, due to their ability to combine high electrical conductivity with substantial transparency in both visible and infrared regions. Unlike conventional materials such as In_2O_3 or ZnO , these metal films provide enhanced thermal and structural stability, which makes them particularly suitable for long-term applications in modern transparent electronic devices.

Metallic thin films can exist either in a continuous phase or as isolated islands (dispersed phase), depending on their thickness and deposition conditions. This dual-phase behaviour results in a wide range of electro-structural properties. The critical percolation thickness [2] is a certain mass thickness of the metal film at which a transition is observed from the island organization of metal clusters to the appearance of the first continuous conduction channel with ohmic charge transport mechanism. In the vicinity of this transition, metallic films often display anomalous optical and electrical behavior, which can be interpreted by percolation theory [3].

Precisely controlled deposition of nanoscale gold layers close to their percolation threshold can address the challenge of developing new transparent conductive materials with controlled parameters. When the film thickness is just below or near the percolation limit (typically in the range of 3 – 9 nm), the deposited gold films can exhibit high conductivity ($\sigma < 10^8 (\Omega \cdot \text{m})^{-1}$) and outstanding optical transmittance ($T \approx 75\text{--}85\%$).

In this study, gold films with nominal thicknesses of 5 nm and 10 nm were deposited at 78 K onto both bare glass substrates and substrates precoated with germanium underlayers in ranging up to 1 nm in thickness. The deposition was carried out under high-vacuum conditions ($P \approx 10^{-7}$ torr) at quench condensation regime [1]. The mass thickness of the Au and Ge films was monitored via shifts in the resonance frequency of a quartz crystal microbalance sensor. The electrical resistivity was determined by two-probe and four-probe (Van der Pauw) methods, and the optical properties were characterized on Shimadzu UV-3600 spectrophotometer.

The analysis of transmittance across different wavelengths (700, 800, 1000, 1200 and 1400 nm) revealed a size-dependent behaviour that varied with the

thickness of the Ge underlayer. It was determined that the percolation threshold of Ge for Au films was approximately 2 nm for the 5 nm thick samples and 1 nm for the 10 nm samples respectively. Notably, the figure of merit of the studied silver films peaked near the percolation threshold, indicating an optimal balance of conductivity and transparency at this critical point.

- [1]. Bihun R. I., Buchkovs'ka M.D., Koman B. P., Leonov D. S. *Nanosystems, nanomaterials and nanotechnologies*. 2022. Vol. 20, № 4. P. 0929-939.
- [2]. Turko B., Sadovyi B., Vasil'yev V., Eliyashevskyy Y., Kulyk Y., Vas'kiv A., Bihun R., Apopii V., Kapustianyk V. *Наносистеми, наноматеріали, нанотехнології*. 2024. Vol. 22, № 2. P. 239-247.
- [3]. R. Bihun, B. Koman. Nanoscale metal film electronics: Scientific monograph. Part 1. «Physical and mathematical sciences». Riga, Latvia: Baltija Publishing. 2024. 1-33 p.
- [4]. Smilauer P. *Contemporary Physics*. 1991. Vol. 32, № 2. p. 89-102.

Films and colloids of Ag–In–Se nanoparticles: photoluminescence features

Nikolaienko A.^{1,2}, Karlash A.¹, Dmytruk A.²

¹ Faculty of Radiophysics, Electronics and Computer Systems, Taras Shevchenko National University of Kyiv, Kyiv, Ukraine, asya.nikolaenko@gmail.com

² Institute of Physics, National Academy of Sciences of Ukraine, Kyiv, Ukraine

Ag–In–Se-based nanoparticles (NPs) are a non-toxic alternative to the well-known Cd-containing quantum dots, exhibiting intense photoluminescence (PL) in the visible and near-infrared spectral ranges. By varying the composition (Ag : In : Se ratio), the position of their absorption edge and PL emission maximum can be tuned, which is crucial for applications in light-emitting diodes, photodetectors, and biomedical imaging.

Recently, we proposed a “green” synthesis of these NPs [1], which was subsequently developed for different ligands (N-acetyl-L-cysteine and L-cysteine hydrochloride). The resulting colloidal solutions of the NPs are transparent but have a rich red color.

In this work, we present the optical properties of colloids as well as films of these NPs obtained on glass substrates by a drop-coating method. The PL spectra of the NPs, recorded three months after the synthesis, showed shifts of approximately 40-50 nm to the red, with emission peaks after aging at ~710 nm. Considering the harsh conditions of applications of luminescent devices based on these NPs, the dependence of PL intensity on elevated temperature was investigated. A nonlinear decrease of the PL intensity was found. The physical mechanisms underlying the observed results may include thermally activated trapping of carrier (electrons or holes) into existing traps - either surface states or bulk defects. As the temperature increases, the probability that a carrier acquires sufficient thermal energy to overcome the potential barrier into the trap also increases, leading to non-radiative recombination and, as a result, a decrease in the photoluminescence quantum yield.

The photoluminescence decay kinetics are in the range of tens to hundreds of nanoseconds and exhibit a strong dependence on wavelength: the longer the emission wavelength, the slower the decay. This can be explained by hybrid mechanisms of self-trapped excitons and donor-acceptor recombination.

Knowledge of the photophysics of the observed phenomena is essential for the effective application of Ag-In-Se-based nanoparticles.

[1]. Nikolaienko, O. Kapshuchenko, A. Karlash, A. Dmytruk, Abstracts of X Ukrainian Scientific Conference on Physics of Semiconductors 2025, P. 397-398.

***In situ* Raman study of photoinduced oxidation of amorphous As₂S₃-based thin films: effect of the light energy and the type of the network modifier**

**Y. M. Azhniuk¹, V. V. Lopushansky¹, V. Y. Loya¹, S. M. Hasynets¹,
V. M. Kryshenik¹, D. Solonenko², I. M. Voynarovych¹,
A. V. Gomonnai¹, D. R. T. Zahn^{3,4}**

¹ Institute of Electron Physics, Nat. Acad. Sci. Ukr., Uzhhorod, Ukraine,
yu.azhniuk@gmail.com

² Silicon Austria Labs GmbH, Microsystem Technologies Research Unit, Villach, Austria

³ Semiconductor Physics, Chemnitz University of Technology, D-09107 Chemnitz, Germany

⁴ Center for Materials, Architectures and Integration of Nanomembranes (MAIN),
Chemnitz University of Technology, D-09107 Chemnitz, Germany

Amorphous arsenic sulphide and related materials are known, in particular, for numerous photostimulated effects, which make them promising for various optical applications. These effects include photostructural transformations, photoinduced material transport as well as photochemical reactions that may occur on the sample surface under illumination by light of appropriate energy and intensity.

The present study is devoted to photooxidation of amorphous As₂S₃, As–Se–S, and As–Bi–S bulk glasses and thin films under illumination by ultraviolet (UV) and visible light. Bulk glasses were synthesised by melting the corresponding elemental components, thin films (1–2 μm thickness) were prepared by thermal evaporation on silicon and silicate glass substrates. The film surface morphology was checked by atomic force microscopy (Agilent AFM 5420).

Raman spectroscopy was employed as a technique serving in this case a dual purpose: (1) providing the light of appropriated energy and intensity, and (2) being an *in situ* means of detection of the photoinduced changes in the material. For this purpose, Horiba LabRAM HR 800 and XploRA Plus spectrometers were used with the excitation wavelengths $\lambda_{\text{exc}} = 325, 514.7, 532$, and 633 nm.

Raman spectra of amorphous As₂S₃ films measured at $\lambda_{\text{exc}} = 514.7, 532$, and 633 nm contained three broad maxima near 180, 220, and 340 cm⁻¹ typical for this material and did not reveal any drastic changes with the variation of the laser power density P_{exc} in a rather broad range (up to 4.3 MW/cm² at $\lambda_{\text{exc}} = 514.7$ nm). Meanwhile, for $\lambda_{\text{exc}} = 325$ nm the spectra were similar at $P_{\text{exc}} \leq 80$ kW/cm² while at an elevated $P_{\text{exc}} = 150$ kW/cm² new intense narrow features emerge in the spectra at 266, 367, and 558 cm⁻¹, which are identified as Raman peaks of arsenolite As₂O₃. Arsenolite is formed on the As₂S₃ film surface due to a photoinduced chemical reaction, which is initiated by the local sample overheating under laser irradiation followed by partial thermal decomposition of the film material, interaction of vaporised arsenic atoms with oxygen from the ambient air and vapour growth of As₂O₃ crystallites [1].

Under illumination by visible light (514.7 or 532 nm) no oxidation of amorphous As_2S_3 occurs since the absorption coefficient for the green light is much lower than for the UV light and the temperature required to vaporise As from the film surface cannot be achieved. However, for amorphous arsenic sulphide films with S partially replaced by Se (above 50 at. %), the Raman features of arsenolite appear in the spectra after illumination by 514.7 nm laser light at a laser power density P_{exc} above 1 MW/cm^2 . The explanation is rather straightforward: with S \rightarrow Se substitution the material bandgap shrinks, the absorption coefficient at λ_{exc} increases and the light absorbed by the sample heats it locally to the temperature sufficient for the vaporisation and subsequent oxidation.

Doping or modification of the amorphous As_2S_3 films by other elements (for instance, Cd, Bi, or Ag) as well results in an absorption edge shift and an increase of the absorption coefficient at λ_{exc} . In this case, when the dopant (or modifier) content did not exceed 10–15 at. %, the bandgap narrowing was hardly noticeable. For the amorphous As_2S_3 films doped by Cd (as well as Zn, In, Ga, or Si) we did not observe surface oxidation under visible light. However, for $(\text{As}_{1-x}\text{Bi}_x)_2\text{S}_3$ films with $0.04 \leq x \leq 0.18$ Raman measurements at $\lambda_{\text{exc}}=532 \text{ nm}$ and $P_{\text{exc}}=4 \text{ kW/cm}^2$ clearly show the signatures of As_2O_3 in the spectra. Since the optical absorption of $(\text{As}_{1-x}\text{Bi}_x)_2\text{S}_3$ with $x=0.04$ does not differ drastically from that of As_2S_3 , there should also be another mechanism contributing to the photooxidation. Raman spectra of the $(\text{As}_{1-x}\text{Bi}_x)_2\text{S}_3$ films immersed in isopropanol (to block the sample contact with ambient air) measured at similar conditions also revealed the Raman features of As_2O_3 . This means that the photooxidation reaction on the surface does not require oxygen from ambient air to be involved. Evidently, oxygen atoms must have been adsorbed on the film surface prior to the sample immersion in isopropanol. The presence of bismuth in the film facilitates the adsorption of oxygen. Additional studies are required to elucidate the role of bismuth in the photochemical reactions leading to the formation of As_2O_3 crystallites.

It is essential that the formation of arsenolite in the $(\text{As}_{1-x}\text{Bi}_x)_2\text{S}_3$ films clearly differs from the photooxidation on the surface of bulk $(\text{As}_{1-x}\text{Bi}_x)_2\text{S}_3$ glasses (with $0.14 \leq x \leq 0.20$) where our Raman measurements at $\lambda_{\text{exc}}=532 \text{ nm}$ and $P_{\text{exc}}=40 \text{ kW/cm}^2$ (a number of new features in a broad spectral range up to about 1000 cm^{-1} increasing in intensity with the exposure time) confirm the formation of units containing arsenate AsO_4^{3-} ions on the sample surface [2].

[1]. Y. Azhniuk, D. Solonenko, V. Loya, I. Grytsyshche, V. Lopushansky, A. V. Gomonnai, D. R. T. Zahn, Appl. Surf. Sci. 2019, 467–468, 119.

[2]. Y. Azhniuk, V. Lopushansky, S. Hasynets, V. Kryshenik, A. V. Gomonnai, D. R. T. Zahn, J. Raman Spectrosc. 2024, 55, 637.

Influence of atmospheric oxygen on the formation of near-surface layers and electrical parameters of SnTe thin films

Mateik, H.D., Mazur, T.M., Mazur, M.P.

*Ivano-Frankivsk National Technical University of Oil and Gas, Ivano-Frankivsk,
Ukraine, galyna.mateik@gmail.com*

The influence of thickness and annealing temperature on the electrical parameters of polycrystalline SnTe thin films deposited from the vapor phase by open evaporation in vacuum on freshly cleaved (0001) mica substrates has been investigated.

A pronounced inhomogeneity of the electrical parameters across the film thickness was observed. It was shown that a hole-enriched near-surface layer is formed due to the acceptor action of atmospheric oxygen. Within the framework of Petritz's two-layer model, the parameters of near-surface and bulk regions were estimated: the thickness of the near-surface layer is $\sim 0.09 \mu\text{m}$ for as-grown films and $\sim 0.18 \mu\text{m}$ for films annealed at 353 K; the carrier concentration in the near-surface layer is an order of magnitude higher than in the bulk; annealing results in an increase in surface hole concentration, an enhancement of thermopower, and broadening of the near-surface region (Fig. 1).

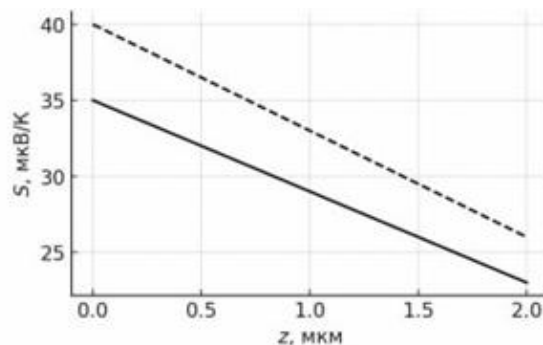


Fig. 1. Thickness distribution profiles of the thermo-EMF of thin SnTe films $S(z)$. The solid line represents freshly grown films, while the dashed line represents films annealed at 353 K.

Annealing of films in air leads to a significant increase in the surface concentration of holes, a slight decrease in conductivity, and an increase in thermo-EMF. The thickness of the surface layer increases approximately twofold. We can conclude that atmospheric oxygen plays a key role in shaping the electrophysical properties of the surface regions of SnTe films, determining their conductivity, mobility, and thermoelectric parameters.

Influence of growth conditions and heat treatment on the properties of thin zinc oxide films obtained by the PVD method

Yavorska, L.O.¹, Nykyrui, L.I.¹

¹*Vasyl Stefanyk Carpathian University, Ivano-Frankivsk, Ukraine*

lilia.katanova@pnu.edu.ua

Zinc oxide (ZnO) has emerged as a highly promising semiconductor material for optoelectronic applications owing to its unique physicochemical characteristics. In particular, its wide band gap (~3.37 eV) and high exciton binding energy (~60 meV) make it an attractive candidate for light-emitting devices and laser diodes operating in the visible and ultraviolet spectral regions. The relatively high exciton binding energy enables ZnO to compete effectively with GaN, ensuring intense luminescence at room temperature. Furthermore, the intrinsic transparency of ZnO in the visible range and its low resistivity expand its potential for integration into thin-film solar cells [1].

ZnO thin films were deposited by pulsed laser deposition (PLD) employing a Nd:YAG laser with a wavelength of 532 nm (second harmonic) under a base pressure of 10^{-7} mbar. For the investigation of their morphological, structural, and optical characteristics, the films were grown on silicon glass and ITO substrates. The results indicate that both deposition parameters and subsequent thermal treatment exert a pronounced influence on the film properties. In particular, analysis of the optical spectra allowed the determination of band gap parameters and relaxation times, thereby confirming the feasibility of tailoring material properties through processing conditions.

It was established that the properties of ZnO thin films are strongly dependent on both fabrication conditions and post-deposition annealing. These findings provide valuable insights for optimizing the fabrication processes of ZnO-based materials intended for advanced optoelectronic devices and photovoltaic applications.

- [1]. Boudjada, Fahima, Hocine Chorfi, and Abdelghani Djebli. "Theoretical approach by the ADF-Band of electronic properties in oxides. Part I: ZnO." Journal of New Technology and Materials 4.1 (2014): 143-146.

Long-wavelength luminescence of CsPbBr₃ crystal

Vitalii Shvets, Andriy Pushak, Taras Demkiv

Ivan Franko Lviv national university, 8 Kyryla i Mefodiy str., vitalii.shvets@lnu.edu.ua

CsPbBr₃ crystal are known for their intense luminescence in the green region of the spectrum (≈ 530 nm), which makes them promising for optoelectronic applications and for use as cryogenic scintillators [1]. However, in some cases the samples exhibit long-wavelength emission in the infrared (IR) range, which may indicate additional charge-carrier recombination mechanisms. Infrared luminescence in CsPbBr₃ crystals in the 800–1050 nm range was observed by Dorenbos [2] under X-ray excitation. This luminescence was absent when the crystal was excited by photons with energies below 10 eV.

In our case, when CsPbBr₃ crystals were excited by synchrotron photons with an energy of 7.5 eV (Fig.), long-wavelength luminescence with a maximum at 920 nm ($h\nu \approx 1.35$ eV) was observed. The spectrum has a characteristic shape: a gradual increase in intensity starting from 750 nm and an asymmetric decline beyond 950–1000 nm. Such a signal profile may be associated with carrier recombination via defect states in the material's band gap, as well as with the possible influence of surface traps and localized excitons.

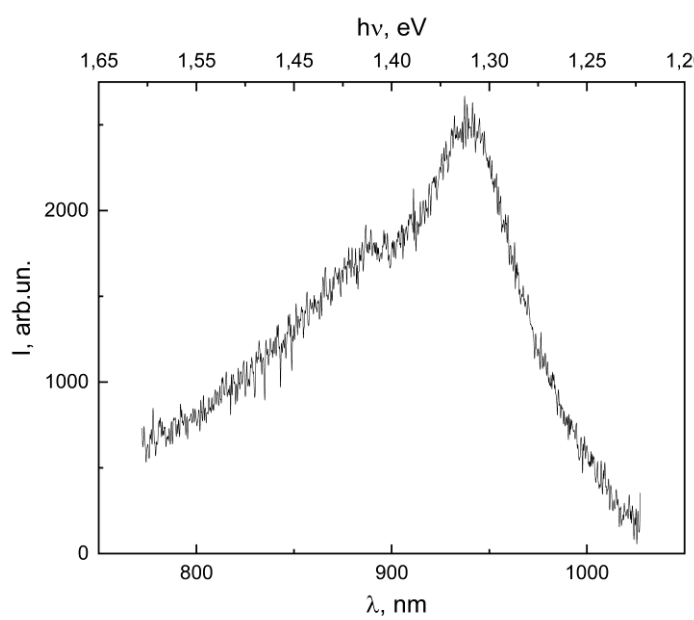


Figure. Luminescence spectrum of a CsPbBr₃ crystal at T = 8.2 K. $h\nu_{\text{ex}} = 7.5$ eV (165 nm).

radiation photons can be explained by the lower efficiency of radiation-defect formation in this case. In particular, the likelihood of such defects increases significantly under X-ray irradiation, which is absorbed throughout the entire crystal volume, whereas synchrotron radiation mainly interacts with its surface layers. This may account for the higher efficiency of radiation-defect formation under X-ray excitation compared with synchrotron excitation.

The intensity of this luminescence is relatively low compared with the visible-range emission of CsPbBr₃ crystals. Its origin may be partly due to excitation by high-energy scattered light. At the same time, the most probable mechanism is emission associated with radiation-induced defects, as suggested in [2] and as demonstrated for F-center luminescence in CsPbCl₃ crystals [2]. Within this interpretation, the weak intensity of the infrared luminescence of CsPbBr₃ under excitation by synchrotron

Topic 3

- [1]. V.B. Mykhaylyk, H. Kraus, V. Kapustianyk, H.J. Kim, P. Mercere, M. Rudko, P. Da Silva, O. Antonyak, M. Dendebera, Bright and fast scintillations of an inorganic halide perovskite CsPbBr_3 crystal at cryogenic temperatures, *Scientific Reports*, vol. 10, p.8601 (2020).
- [2]. J.J. van Blaaderen, D. Biner, K.W. Krämer, P. Dorenbos, The temperature dependent optical and scintillation characterisation of Bridgman grown CsPbX_3 ($X = \text{Br}, \text{Cl}$) single crystals, *Nuclear Instruments and Methods in Physics Research A*, vol. 1064, p.169322 (2024).

Maskless Laser Patterning and Micro-Processing of Thin Films

P. Lytvyn, A. Korchovyii, A. Rusavsky, A. Vasin, K. Svezhentsova,
O. Dubikovskyi, O. Kulbachynskyi, V. Dzhagan

¹ V. Lashkaryov Institute of Semiconductors Physics, National Academy of Sciences of Ukraine, 45 Nauky av., 03028 Kyiv, Ukraine, dzhagan@isp.kiev.ua

Maskless laser direct writing provides an agile alternative to resist-based photolithography for rapid prototyping of micro- and optoelectronic structures [1]. Here we demonstrate a laser-processing toolbox for thin films and 2D materials that combines ns-pulsed infrared-wavelength patterning with continuous-wave (CW) blue-wavelength post-processing. The platform integrates a 1064 nm fiber laser (120 ns pulses, 0.75 mJ) for efficient photothermal ablation of metals and semiconductors, and a 455 nm, 10 W CW diode laser that is strongly absorbed in semiconductors and enables controlled thermal budgets for annealing, recrystallization, and micro-polishing. By tuning fluence, scan strategy, sample preheating, and ambient atmosphere, we achieve clean edge definition, layer-selective removal, and localized modification of conductivity or crystallinity. Representative applications include maskless patterning of metal/semiconductor stacks for contacts and interconnects, laser trimming of 2D-material channels for sensor platforms, semiconductor annealing, and surface nano-structuring. The approach reduces process complexity and turnaround time while remaining compatible with standard characterization (AFM/SEM/Raman and electrical probe). These results position laser direct writing as a versatile route to accelerate device development and low-volume manufacturing.

This study was supported by NRFU project #2023.05/0022

[1]. A Kryuchyn, V Petrov, I Kosyak, S Shanoilo, Ie Beliak, S Kostyukevich, P Lytvyn, M Boltovets, V Strelchuk, K Svezhentsova, O Kolesnikov, A Korchovyi, V Dzhagan. Prospects for the creation of the technology of maskless photolithography based on direct laser recording. Semiconductor Physics, Quantum Electronics & Optoelectronics 28 (2024) 093-101. DOI: <https://doi.org/10.15407/spqeo28.01.093>

Morphological features of gas-sensitive polyaniline films

Dzeryn M.R.¹, Tsizh B.R.^{1,2}, Aksimentyeva O.I.³, Horbenko Yu.Yu.³

¹Stepan Gzytsky National University of Veterinary Medicine and Biotechnologies Lviv,
Ukraine; marjawka232@ukr.net,

²Kazimierz Wielki University in Bydgoszcz, Bydgoszcz, Poland; tsizhb@ukw.edu.pl

³Ivan Franko National University of Lviv, Lviv, Ukraine; aksimen@ukr.net

The introduction of nanoscale fillers into the composites of conducting polymers allows obtaining nanomaterials with high sensitivity of their electrical resistance to the adsorption of various substances. One of the most suitable sensory mediums for detecting gases is polyaniline (PAN) and its derivatives [1, 2].

In this work, we investigated the surface morphology of PAN films obtained by chemical deposition on glass plates, since they have a number of interesting features, in particular, gas-stimulated changes in them occur faster than in films obtained by other methods [3]. These films are characterized by an intense green (emerald) color. Such films are quite uniform and have good adhesion to the surface of the glass plate. In our studies, the thickness of the films, depending on the deposition time, was from 0.3 to 0.6 μm.

Under the influence of gases, in particular ammonia, a change in the color and morphology of the sensor films is observed. In particular, the number of crystalline regions and areas of blue color, characteristic of the main form of emeraldine, increases. Such phenomena indicate the interaction of gas molecules with acid-doped PAN with the formation of both ammonia salt crystals and supramolecular areas of the polymer. The formation of a developed amorphous-crystalline structure of sensor films contributes to an increase in their gas sensitivity due to an increase in the specific surface area and the creation of additional adsorption sites for gas molecules. Such features contribute to the effective use of the studied films in gas sensors.

[1]. Farea M.A., Mohammed H.Y., Shirsat S.M., et al. Hazardous gases sensors based on conducting polymer composites: Review, *Chemical Physics Letters*. 2021, V. 766, 138703.

[2]. Wong Y.C., Bee C.A., Haseeb A.S.M., et al. Conducting Polymers as Chemiresistive Gas Sensing Materials: A Review. *J. Electrochem. Soc.* 2020, V.167, 03503.

[3]. Bohdan Tsizh, Olena Aksimentyeva. Optimization of the Gas-Sensitive Response of Nanostructured Films of Polyaminoarenes, *Molec. Cryst. & Liq. Cryst.* 2025, <https://doi.org/10.1080/15421406.2025.2515635> Thermoelectric Properties of Thin Film Microgenerators

Negative capacitance and dielectric losses in the MIS structures with nanocomposite $\text{Fe}_x\text{O}_y(\text{Fe})$ films

Evtukh A.A.^{1,2}, Pylypov A.I.², Muryi Ya.Yu.¹, Antonin S.V.¹, Pylypova O.V.², Bratus O.L.¹

¹*V. Lashkaryov Institute of Semiconductor Physics, NAS of Ukraine, 41 Nauky Ave., 03028 Kyiv, Ukraine, anatoliy.evtukh@gmail.com*

²*Educational Scientific Institute of High Technologies Taras Shevchenko National University of Kyiv, 4-g Hlushkova Avenue, Kyiv, Ukraine*

The specific capacitance and dielectric losses are among the most important parameters of the capacitors. The negative capacitance has been revealed in the structures with such materials as thin films including ferroelectrics, amorphous chalcogenides, binary oxides, organic/inorganic composites, alloys etc. The structures with negative capacitance are very attractive for applications in modern micro- and nanoelectronics.

In this work the revealing and investigation the negative capacitance effect and dielectric losses in MIS structures with nanocomposite $\text{Fe}_y\text{O}_x(\text{Fe})$ films are described. The nanocomposite films were obtained by ion-plasma sputtering technique. The Fe target was sputtered in O_2+Ar atmosphere. The thicknesses of the films were 46 nm. The impedance and capacitance - voltage ($C-U$) characteristics were measured by Agilent 4294A semiconductor parameter analyzer in the frequency range of the testing signal 10 Hz – 5 MHz. The amplitude of testing signal was 50 mV.

The capacitance-voltage characteristics of the structure with the nanocomposite $\text{Fe}_x\text{O}_y(\text{Fe})$ film exhibit non-monotonic behavior. Initially, in the region of low bias voltages, the capacitance increases with increasing the voltage, and then decreases. In the region of higher voltages, the capacitance is negative. The lower the frequency, the lower the bias voltage required to transition from positive to the negative capacitance. Further increase in bias voltages leads to the increase in the value of negative capacitance.

The dielectric losses demonstrate the nonmonotonous frequency dependence. As a rule, the dielectric losses are remarkably increased after the thermal annealing. The growth of dielectric losses is caused by structure transformation of the films during annealing.

The physical model for explanation of negative capacitance effect and dielectric losses has been proposed. It based on the peculiarities of nanocomposite films polarizations with taking into account as Maxwellian displacement current and the conduction current.

Acknowledgements. This research was supported by the National Research Foundation of Ukraine under the project No. 2025.06/0012.

New materials for interference optics based on the ZnS – EuF₃ system

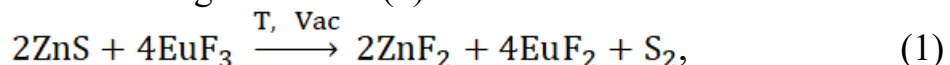
Babenko A.V.^{1,2}, Zinchenko V.F.¹, Mozkova O.V.³, Magunov I.R.¹, Doga P.G.¹

¹*Bogatsky Physico-Chemical Institute NAS of Ukraine, Odesa, Ukraine, yfzinchenko@ukr.net*

²*Odesa I.I. Mechnikov National University, Odesa, Ukraine, anton.octane.sr@gmail.com*

³*State Enterprise for Special Instrument Making «Arsenal», Kyiv, Ukraine olgamozk@ukr.net*

The results of the study of the interaction of Zinc sulfide with Europium (III) fluoride by X-ray phase analysis methods are presented. The obtained X-ray phase analysis results (DRON-3M) indicate the process of reduction of Eu³⁺ to Eu²⁺, which occurs according to scheme (1):



where the starting reagent – ZnS is the result of self-propagating high-temperature synthesis, which has a wurtzite crystal lattice. The synthesis product contains only one phase – EuF_{2+x} based on europium difluoride. The interaction between the components was studied using optical methods – IR transmission spectroscopy (Frontier Perkin-Elmer) and luminescence spectroscopy (Fluorolog FL3-22).

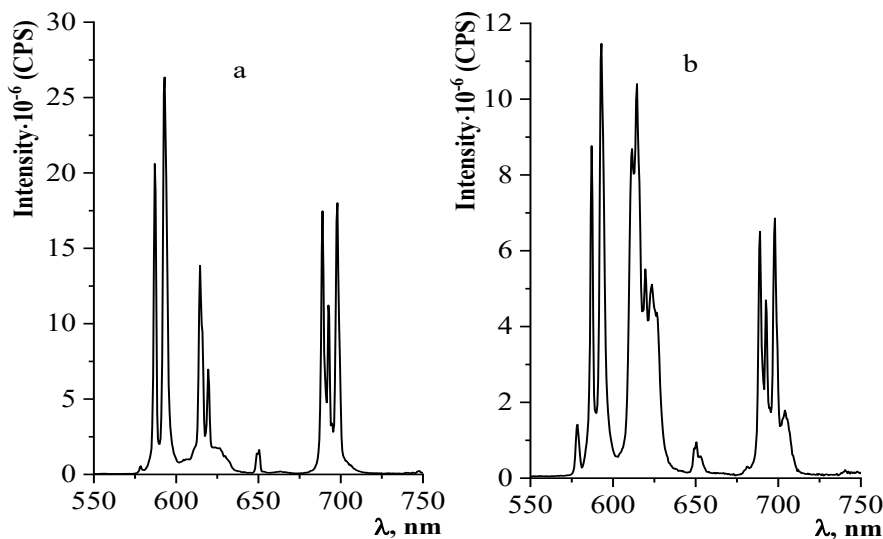


Fig.1. Luminescence spectra at $\lambda_{\text{exc}} = 395$ nm of EuF₃ in the ZnS – EuF₃ system with a slit of 1-1 nm: (a) - mechanical mixture; (b) - heat-treated sample;

Luminescence spectra (fig. 1.) indicate a decrease in the emission intensity of Eu³⁺ ions, which indicates a decrease in their concentration and confirms the hypothesis of the course of the redox reaction.

The samples of the system were studied by thermal evaporation in vacuum (VU-1A). The obtained thin-film coatings showed high mechanical strength of 20000 rotations and intermediate values of the refractive index (1.73). The material is promising for the creation of interference optics.

Optimization of Electrical and Thermoelectric Properties of LAST Films Using XGBoost

Makovyshyn V.I.¹

¹ King Danylo University, Ivano-Frankivsk, Ukraine, makovyshyn.i.volodymyr@ukd.edu.ua

The study focuses on the modeling of thickness-dependent electrical parameters and nanostructure formation in thin films of LAST (Pb-Ag-Sb-Te) compounds. The main objective is to optimize vapor-phase deposition processes to improve the thermoelectric efficiency of nanostructured materials.

Thin films were synthesized by vacuum deposition from pre-synthesized LAST materials. Morphological characteristics were analyzed using AFM, while the XGBoost machine learning algorithm was employed to predict electrical conductivity, charge carrier mobility, and surface roughness as functions of film thickness and deposition parameters.

The modeling revealed that nanocrystallite sizes increase logarithmically with film thickness, directly influencing charge transport. For thinner films (200–300 nm), higher electrical conductivity was observed, making them suitable for electronic applications. Thicker films (~1000 nm) demonstrated enhanced thermoelectric performance due to reduced thermal conductivity and higher Seebeck coefficients. Machine learning predictions closely matched experimental data, confirming the reliability of XGBoost for real-time optimization of deposition processes.

The research demonstrates that machine learning can serve as an effective tool for predicting and controlling the properties of LAST thin films. Optimizing deposition parameters enables tailoring films either for high electrical conductivity (sensors, contacts) or for improved thermoelectric efficiency (energy applications).

[1]. Makovyshyn V. I., Styslo T. R., Ivanov O. O., Styslo O. V. Modeling Thickness Dependencies of Electrical Parameters and Nanostructure Formation in Vapor-Phase Condensates of LAST Compounds Using Machine Learning. Physics and Chemistry of Solid State. 2025. 26(1). pp. 29–34.

Photoinduced transformations in bulk and thin-film Sb₂S₃:Ag

Y. M. Azhniuk¹, A. I. Pogodin², M. J. Filep^{1,3}, V. V. Lopushansky¹, V. Y. Izai⁴, V. M. Kryshenik¹, I. M. Voynarovych¹, A. V. Gomonnai¹

¹ Institute of Electron Physics, Nat. Acad. Sci. Ukr., Uzhhorod, Ukraine,

yu.azhniuk@gmail.com

² Uzhhorod National University, Uzhhorod, Ukraine

³ Ferenc Rákóczi II Transcarpathian Hungarian Institute, Berehovo, Ukraine

⁴ Centre for Nanotechnology and Advanced Materials, Faculty of Mathematics, Physics and Informatics, Comenius University Bratislava, Bratislava, Slovakia

Amorphous Sb₂S₃ belongs to the class of phase-change materials for high-performance non-volatile photonics. It is characterised by extraordinary variation of optical parameters (band gap, refractive index) under reversible phase transitions between the crystalline and amorphous states. An important advantage of Sb₂S₃ is its very low optical absorption ($k < 10^{-5}$) in the near-infrared and even visible spectral range both in the amorphous and crystalline states. This enables its application as a medium for building up neural networks. Thermal transport in Sb₂S₃ is dominated by the contribution of phonons rather than electronic thermal conductivity. This makes it promising for thermoelectric devices. Sb₂S₃ has a noticeable potential for applications in solar energy conversion. Doping Sb₂S₃ with silver, in particular, increases its refractive index, thereby making it attractive for applications in photonics as well as reduces its intrinsic high electric resistivity what is essential for its use as buffer layer in photovoltaics.

Here we present a study of Sb₂S₃ and Sb₂S₃:Ag (up to 10 % Ag) polycrystalline ingots and thin films by X-ray diffraction (XRD), energy-dispersive X-ray fluorescence spectroscopy (EDX), and Raman spectroscopy. Sb₂S₃ was synthesized from high-purity elemental Sb (99.999%) and S (99.9995%) by two-temperature synthesis with the "hot" zone temperature of 650 °C. (Sb₂S₃)_{1-x}Ag_x alloys were synthesized from Sb₂S₃ and colloidal Ag in evacuated quartz ampoules at 650 °C for 4 h with subsequent quenching in air. Thin (2.1–2.5 μm) Sb₂S₃ and Sb₂S₃:Ag films were prepared by flash evaporation at 1200 °C on cold silicon and silicate glass substrates.

For XRD studies an AXRD Benchtop diffractometer with Cu K_α radiation and a Ni filter was used. The chemical composition of the samples was analysed based on the EDX data obtained using a Tescan Vega TS5136MM scanning electron microscope equipped with Oxford Instruments INCAx-act EDX detector. Raman spectra were measured using an XPlora Plus spectrometer (Horiba) with a 532 nm laser and a cooled CCD camera.

Chemical composition of the samples determined by EDX spectroscopy corresponds to the element content in the initial mixture. The element distribution over the samples measured by the EDX mapping is rather uniform with slight inhomogeneities in the silver distribution. XRD data confirm the orthorhombic (stibnite) structure of the synthesised polycrystalline Sb₂S₃:Ag

ingots, the Ag-containing samples exhibiting the presence of the AgSbS_2 (β -miargyrite) phase as well.

Raman spectroscopy data measured at low laser power density ($P_{\text{exc}} = 4 \text{ kW/cm}^2$) assume the possible (although not unambiguous) presence of the AgSbS_2 phase, thereby supporting the XRD data. Raman measurements at increased P_{exc} (40 kW/cm^2) revealed photostructural and photochemical transformations, namely the formation of Sb_2O_3 and elemental Sb phases due to the heating of the sample surface by the tightly focused laser light. Raman measurements performed for the samples immersed in liquid isopropanol prevent the sample oxidation by blocking the air access to the laser spot, hence, contrary to the measurements on air, no features of Sb_2O_3 are observed in the Raman spectra measured at elevated P_{exc} .

Raman spectra of thin $\text{Sb}_2\text{S}_3:\text{Ag}$ films measured at low $P_{\text{exc}}=4 \text{ kW/cm}^2$ unambiguously confirm their amorphous structure. Independent of the silver content, the spectra contain a weak hardly resolved continuum at $100\text{--}150 \text{ cm}^{-1}$ and a single broad (FWHM nearly 100 cm^{-1}) maximum at $286\text{--}287 \text{ cm}^{-1}$ which corresponds to the range of vibrations of Sb–S bonds in the SbS_3 and SbS_5 pyramidal units, existing in the Sb_2S_3 structure. The presence of Ag in amount of up to 10 at. % does not produce any visible effect on the Raman spectra of the $\text{Sb}_2\text{S}_3:\text{Ag}$ films.

Increasing P_{exc} to 40 kW/cm^2 leads to photoinduced crystallisation of Sb_2S_3 in the films (the broad maximum of amorphous Sb_2S_3 is transformed into two maxima at 277 and 297 cm^{-1}), accompanied by the appearance of Raman features of elemental Sb (107 and $144\text{--}145 \text{ cm}^{-1}$) and Sb_2O_3 ($189\text{--}190$, 252 , and $448\text{--}450 \text{ cm}^{-1}$). These photochemical transformations are due to the heating of the sample surface by the tightly focused laser light. Besides, a nonthermal effect of photoinduced material transport from heavily illuminated to less illuminated areas in amorphous Sb_2S_3 leads to the formation of a clearly visible pit in the laser spot. Interestingly, the Raman features related to Sb_2O_3 appear in the spectra measured at an increased P_{exc} even when the sample during the measurement is immersed in isopropanol to prevent access of oxygen from the air. In our opinion, oxygen required for the formation of Sb_2O_3 must come from voids existing in the amorphous film structure where it must have been stored since the film condensation. The photoinduced surface deformation enables oxygen release from the voids and reaction with Sb resulting in the formation of Sb_2O_3 .

The research was supported by the "Advanced Science in Ukraine" grant No. 2023.03/0013 by National Research Foundation of Ukraine.

Photopolymerization of acrylated epoxidized soybean oil polymers

Kavetskyy, T.S.^{1,2,3}, Zubrytska, O.V.¹, Matskiv, O.I.¹, Stievenard, M.⁴, Šauša, O.^{2,5}, Švajdlenková, H.^{5,6}, Soloviev, V.M.^{3,7}, Bielinskyi, A.O.^{7,8}, Ostrauskaite, J.⁹, Kiv, A.E.^{3,10}

¹Drohobych Ivan Franko State Pedagogical University, Drohobych, Ukraine,

²Institute of Physics, Slovak Academy of Sciences, Bratislava, Slovakia,

³South Ukrainian National Pedagogical University named after K.D. Ushynsky, Odesa, Ukraine, kavetskyy@yahoo.com; t.kavetskyy@dspu.edu.ua; kiv.arnold20@gmail.com

⁴Department of Chemistry, IUT de LILLE, Villeneuve d'Ascq, Lille, France

⁵Department of Nuclear Chemistry, FNS, Comenius University, Bratislava, Slovakia

⁶Polymer Institute, Slovak Academy of Sciences, Bratislava, Slovakia

⁷Kryvyi Rih State Pedagogical University, Kryvyi Rih, Ukraine

⁸Kyiv National Economic University named after Vadym Hetman, Kyiv, Ukraine

⁹Kaunas University of Technology, Kaunas, Lithuania

¹⁰Ben-Gurion University of the Negev, Beer-Sheva, Israel

Over the past two decades, research into photostimulated processes in polymeric materials has gained new momentum, driven both by the growing demand for functional polymers with controllable properties and the need to understand their long-term stability under operational conditions. Current approaches combine the development of new materials, such as photopolymerization systems for 3D printing and biosensing, with a deep fundamental study of the mechanisms of photoinduced changes, including the role of free volume and the dynamics of molecular motions.

The course of photopolymerization of acrylated epoxidized soybean oil (AESO) and vanillin dimethacrylate (VDM), AESO:VDM samples, with and without a photoinitiator (PI), 2,2-dimethoxy-2-phenylacetophenone (DMPA), and different content of VDM was studied using positron annihilation lifetime spectroscopy (PALS) [1-3]. The results showed that an increased content of VDM containing aromatic rings led to a decrease in the local free volume in the cured polymer network. This in turn affected the diffusion properties of the polymer, especially in the case of water. Furthermore, an increase in the VDM content led to a decrease in the conversion of double bonds in the cured samples, as determined by near-infrared spectroscopy (NIR). This finding highlights a scenario in which the decrease in free volume is not necessarily related to an increase in the crosslink density of the polymer, but rather is a consequence of the occupation of part of the free space by aromatic rings in the polymer [2].

A combination of PALS, ATR-FTIR and EPR spectroscopy in complementary with computer modeling using recurrence analysis, was further used to obtain information on the network properties of AESO:VDM (1:0.5 mol) polymer matrix with and without a photoinitiator DMPA according to the proposed light on/off protocol in view of long-term UV light exposure.

The following findings were obtained after long-term UV light exposure:

1. According to the continuous and interrupted illumination protocol applied, it is concluded that the cured sample containing photoinitiator exhibits higher light absorption than the cured sample without photoinitiator. This can be attributed to the more complete polymerization and slower consumption of PI, which intensively absorbs UV light, and gradually becomes incorporated into the network, while the sample without PI retains residual absorbing monomers and relatively quickly transits to a state with lower UV light absorption and, consequently, polymerization is less intensive.

2. The photo-induced oxidative degradation was found in the framework of the main principals of the subthreshold radiation effects in polymers, and such oxidative degradation is controllable, i.e., may be reduced or enhanced using a photoinitiator or without it.

3. The EPR results showed that illumination leads to maximum radical generation due to photoinitiator activation, whereas in the absence of light, the radicals gradually decay through polymerization and termination reactions, resulting in a decreased radical concentration.

4. The recurrence analysis used turns raw temperature traces into actionable kinetic markers – pinpointing initiation and quench, tracking predictability and complexity, and enabling closed-loop monitoring of photopolymerization quality.

Acknowledgments

This work was supported in part by the Ministry of Education and Science of Ukraine (projects Nos. 0122U000850, 0122U000874, 0122U001694, 0125U001054, 0125U002005, and 0125U002033), Slovak Grant Agency VEGA (projects Nos. 2/0166/22 and 2/0131/25), and Slovak Research and Development Agency (project No. APVV-21-0335). T.K. also acknowledges the SAIA for scholarship in the Institute of Physics SAS in the framework of the National Scholarship Programme of the Slovak Republic. This work has also received funding through the MSCA4Ukraine project (grant No. 1128327), which is funded by the European Union, and the EURIZON project (grant EU-3022), which is funded by the European Union (EURIZON H2020 project) under grant agreement No. 871072.

- [1]. D.P. Královič, K. Cifraničová, O. Šauša, H. Švajdlenková, T. Kavetskyy, A. Kiv, *Chem. Pap.*, **77** (2023) 7257-7261.
- [2]. D.P. Královič, K. Cifraničová, H. Švajdlenková, D. Tóthová, O. Šauša, P. Kalinay, T. Kavetskyy, J. Ostrauskaite, O. Smutok, M. Gonchar, V. Soloviev, A. Kiv, *J. Polym. Environ.*, **32** (2024) 2336-2349.
- [3]. T. Kavetskyy, O. Zubrytska, M. Stievenard, O. Šauša, H. Švajdlenková, V. Soloviev, A. Bielinskyi, J. Ostrauskaite, A. Kiv, *NATO SPS B*, (2025) 265-284, DOI: 10.1007/978-94-024-2316-7_19.

Photosensitive and electrical properties of CdTe thin films

Mazur, T.M., Mazur, M.P.

Ivano-Frankivsk National Technical University of Oil and Gas, Ivano-Frankivsk,
Ukraine, tetiana.mazur@nung.edu.ua

CdTe is a promising direct-bandgap semiconductor material ($E_g \approx 1.5$ eV at 300 K) that allows for both n-type and p-type conductivity, which is important for photovoltaics and IR devices [1]. In CdTe silicon films, grain structure, defects, and grain boundaries play a significant role.

CdTe films grown by the CSS method have a grain size of $\sim 10\text{--}360\ \mu\text{m}$. Photoluminescence contains intense bands of ~ 1.580 eV (exciton recombination) and components of $\sim 1.4\text{--}1.5$ eV associated with defects (Cd vacancies, antisites). The grain boundary is modelled as a heavily doped compensated semiconductor with a defect concentration $>10^{18}\ \text{cm}^{-3}$. Transverse conductivity is Ohmic, lateral conductivity has barriers of $\sim 0.1\text{--}0.3$ eV (Fig. 1).

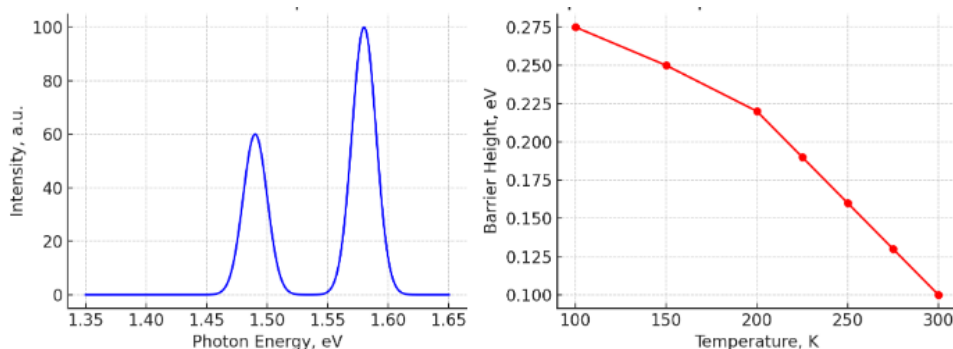


Fig. 1. Photoluminescence spectrum of CdTe (left), temperature dependence of barrier height (right).

Doping CdTe with isovalent Ca causes a conductivity inversion to p-type. Ohmic contacts demonstrate a linear symmetrical I-V curve. A surface p-layer is formed as a result of $\text{Ca}(\text{NO}_3)_2$ doping [2]. Optical studies of CdTe:Ca demonstrate highly efficient photoluminescence ($\eta=8\text{--}10\%$) in the edge region of the spectrum. PL formation is associated with interband recombination and excitons associated with Ca impurities. A separation of the E_g and E_{ex} components is observed in the R_ω spectra, indicating a reduction in defect density and purification of the structure. Ca doping forms a conditionally ‘two-layer’ structure: inner n-CdTe with grains and surface p-CdTe:Ca with high PL efficiency. This allows the creation of heterostructures with an internal electric field.

[1]. Mazur T.M., Prokopiv V.V., Mazur M.P., Pysklynets U.M. Solar cells based on CdTe thin films. *Physics and chemistry of solid state*. 2021. V. 22, No 4. P. 817-827.

[2]. Mazur T.M., Slyotov M.M., Slyotov O.M., Mazur M.P. Light Emitters Based on CdTe Doped with Isovalent Impurities. *Physics and chemistry of solid state*. 2022. V. 23, No 2. P. 317-321.

Physical properties of film high entropy alloys

Protsenko I.Yu., Odnodvorets L.V., Rylova A.K., Shumakova N.I.

Sumy State University, Ukraine, i.protsenko@aph.sumdu.edu.ua

High-entropy film alloys (HEA) with the number of components $n > 4$ can be formed based on Co, Ni, Fe, Cu, Cr, Al, and other elements [1]. The formation of a practically single-phase solid solution (s.s.) of substitution in a multicomponent system contradicts the Gibbs phase rule, but is possible if the requirements for certain values of entropy and enthalpy of mixing and the parameter of the difference in atomic sizes are met [2].

The purpose of our work can be formulated as follows: generalization of previously obtained results regarding dynamic (lattice parameter – a and Debye temperature – θ_D), kinetic (resistivity – ρ , thermal coefficient of resistance – TCR, mean free path of electrons – λ) and magnetic (paramagnetic magnetization – M) characteristics and properties of 5- and 6-component high-entropy alloys in the form of s.s.

Experimental studies of the phase composition, lattice parameter, and electrophysical properties were carried out using the example of HEA thin films with a thickness of 50-70 nm, which were obtained by layer-by-layer condensation of individual components with subsequent annealing or by the method of simultaneous condensation of individual metals.

The obtained results were compared with the calculated ones. In turn, the calculated dependences of a , θ_D , ρ , λ and M on the concentration (x) of the doping element, which was alternately represented by all n elements, were obtained for bulk HEA.

The calculations were carried out in the equiatomic approximation based on the relations written in accordance with the additivity principle. As an example, the relation for the concentration dependence of the parameter a and θ_D from [3] is given below:

$$a = \frac{1-x}{n-1} \sum_{i=1}^{n-1} a_i + x a_n; \quad \theta_D = \frac{1-x}{n-1} \sum_{i=1}^{n-1} \theta_{Di} + x \theta_{Dn}.$$

It should be noted that we have separately analyzed the question of the possibility of applying the additivity principle. It was concluded that such an application would be correct only with respect to the intrinsic characteristics of the HEA atoms. We note a good agreement between the experimental and calculated data in the case of the lattice parameter, resistivity, and paramagnetic magnetization.

[1]. Yeh J.W., Chen S.K., Lin S.J., Gan J.Y., Chin T.S., Shun T.T. Nanostructured high-entropy alloys with multi-principal elements—novel alloy design concepts and outcomes. *Advanced Engineering Materials*. V.6, No 5. P. 299 (2004).

[2]. Tsai M.H. *Physical properties of high entropy alloys*. *Entropy*. V.15. P. 5338 (2013).

[3]. Protsenko I.Yu., Odnodvorets L.V., Shumakova N.I., Protsenko S.I., Shabelnyk Yu.M. A method of predicting the physical properties of multicomponent materials, *European Physical Journal Plus*, 139(3), 252 (2024).

Quantum size phenomena in transport properties of topological insulator Bi_{1-x}Sb_x thin films

Rogachova, O.I.¹

*¹National Technical University "Kharkiv Polytechnic Institute", Kharkiv, Ukraine,
olena.rogachova@kpi.edu.ua*

Isostructural and isovalent continuous Bi_{1-x}Sb_x solid solutions are, on the one hand, convenient models for solid-state physics due to the high sensitivity of their band structure to changes in composition and other factors, and, on the other hand, promising materials for practical use in thermoelectric (TE) cooling in the 150-200 K range. Besides, the Bi_{0.9}Sb_{0.1} solid solution was the first recently discovered 3D-topological insulator, characterized by a surface metallic Dirac layer, which stimulated interest in thin films and surface states and opened new possibilities for applications in spintronics and quantum computing.

The goal of the present report is to review both earlier obtained [1-3] and new results on the kinetic properties of Bi_{1-x}Sb_x films as a function of film thickness d and composition x . The films were prepared by thermal evaporation in vacuum from a single source in the Laboratory of Semiconductor Physics and Thermoelectricity at NTU “KhPI” (Kharkiv). The room-temperature dependences of electrical conductivity σ , the Seebeck coefficient, the Hall coefficient, charge carrier concentration and mobility on d (10-400 nm) and x (0-0.1) were measured. For x values in both the semimetallic and semiconducting regions, oscillatory behavior of the d -dependences of the kinetic coefficients with period Δd was observed at room temperature, indicating energy spectrum quantization. The period Δd increased with increasing x , and the theoretical estimates of Δd were in good agreement with experimental values. At $x = 0.09$, high-frequency oscillations were detected in the region of small d , presumably associated with quantization of the topological layer energy spectrum. Several general regularities in the d -dependences were established. It was shown that the monotonic component of the $\sigma(x)$ dependence can be satisfactorily approximated by theoretical calculations based on classical theory. These results demonstrate that studying quantum size effects provides a promising approach to investigating the surface topological layer and can help build a scientific foundation for utilizing the unique properties of TIs in spintronics, quantum computing, and thermoelectricity.

[1].E.I. Rogacheva, D.S. Orlova, M.S. Dresselhaus, S. Tang // *MRS Proc. Library*. 2011. P.1314.

[2].E.I. Rogacheva, D.S. Orlova, O.N. Nashchekina, M.S. Dresselhaus, S. Tang // *Appl. Phys. Lett.* 2012. 101. P. 023108.

[3].E.I. Rogacheva, O.N. Nashchekina, D.S. Orlova, A.N. Doroshenko, M.S. Dresselhaus // *J. Electr. Mater.* 2017. 46, № 7. P. 3821-3825.

Semiconductor oxide films on the surface of amorphous Co-based alloys

Boichyshyn L.M.¹, Hertsyk O.M.¹, Semeniuk M.V.¹,
Slobodnyj V.A.¹, Pandiak N.L.²

¹ Ivan Franko National University of Lviv, Kyryla and Mefodiya Str. 6,
 79005 Lviv, Ukraine, oksana.hertsyk@lnu.edu.ua

² Ukrainian National Forestry University, Gen. Chuprynska Str. 103,
 79057 Lviv, Ukraine, pandyakn@ukr.net

The practical use of ribbon cobalt amorphous alloys (AMA) $\text{Co}_{75,5}\text{Fe}_{4,6}\text{Si}_{6,0}\text{B}_{16,7}$, $\text{Co}_{66,5}\text{Fe}_{4,0}\text{Mo}_{1,5}\text{Si}_{16,0}\text{B}_{12,0}$, $\text{Co}_{73,6}\text{Fe}_{3,2}\text{Mn}_{3,2}\text{Si}_{5,0}\text{B}_{15,0}$ is determined by the semiconductor properties of the oxide layers that form on their surfaces. Previous voltammetric studies have shown that porous oxide-hydroxide surface layers of heterogeneous structure are formed on the surface of AMA, through which ions with increased reactivity diffuse.

Impedance dependences of the alloy $\text{Co}_{75,5}\text{Fe}_{4,6}\text{Si}_{6,0}\text{B}_{16,7}$ in 0.3 % NaCl after cyclic scanning of the potential in the range -1200 ... -200 mV showed some decrease in the resistance of the oxide film. The protective effect of the films, investigated at potentials -1200, -1100, -600, -550, -290 mV, is significantly lower, i.e. the film is less dense, more porous and defective. This is indicated by the decrease in the charge transfer resistance across the 0.3 % NaCl/(oxide) AMA boundary. Doping of AMA $\text{Co}_{75,5}\text{Fe}_{4,6}\text{Si}_{6,0}\text{B}_{16,7}$ 0.5% Mo leads to an increase in corrosion resistance. The most stable oxide film is at a potential of -577 mV, the resistance to charge transfer across the phase interface is $\approx 2.5 \cdot 10^4 \Omega$, and $Z'' = 1.4 \cdot 10^4 \Omega$. Due to the polarization of the electrode, the destruction of oxide layers occurs, therefore the resistance to charge transfer is $\approx 2 \cdot 10^3 \Omega$ for films studied at potentials of -900 ... -830 mV. Adding $\text{Co}_{75,5}\text{Fe}_{4,6}\text{Si}_{6,0}\text{B}_{16,7}$ Mn to the alloy leads to a decrease in the resistance function of oxide coatings. The most stable were the oxide films tested at a potential of -900 mV, and after polarization of the electrode their resistance does not decrease, Z'' is $\approx 4 \cdot 10^3 \Omega$, and the charge transfer resistance increases from $3 \cdot 10^3$ to $5 \cdot 10^3 \Omega$. Thus, the most stable were the oxide films at potentials of -780 -- 920 mV for the AMA $\text{Co}_{75,5}\text{Fe}_{4,6}\text{Si}_{6,0}\text{B}_{16,7}$, -577 mV before corrosion and -830 -- 900 mV after corrosion for the AMA- $\text{Co}_{66,5}\text{Fe}_{4,0}\text{Mo}_{1,5}\text{Si}_{16,0}\text{B}_{12,0}$, and -900 mV for the AMA- $\text{Co}_{73,6}\text{Fe}_{3,2}\text{Mn}_{3,2}\text{Si}_{5,0}\text{B}_{15,0}$. The best protective effect was obtained by the oxide layers tested at a potential of -900 mV, formed on the alloy $\text{Co}_{73,6}\text{Fe}_{3,2}\text{Mn}_{3,2}\text{Si}_{5,0}\text{B}_{15,0}$.

It has been established that the semiconductor properties of oxide layers, Co-based AMAs at -600 mV, are mainly determined by doping additives, in particular Mo, Mn. In the potential range from -300 to -1000 mV, the conductivity type changes from p- to n-. Therefore, by selecting the potential range and doping additives in AMA, it is possible to change the type of semiconductivity of oxide layers, and accordingly, their scope of application.

SnS₂ nanocrystals formed under illumination in amorphous (As₂S₃)_{1-x}(SnS₂)_x films: a Raman study

V. M. Kryshenik, Y. M. Azhniuk, V. V. Lopushansky,

V. Y. Loya, S. M. Hasynets, A. V. Gomonnai

Institute of Electron Physics, Nat. Acad. Sci. Ukr., Uzhhorod, Ukraine,

yu.azhniuk@gmail.com

Amorphous As₂S₃ and related materials are known for numerous photostimulated effects promising for various optical applications. Modification of the arsenic sulphide composition with Group IV atoms seems interesting in view of the possibility of formation of SnS₂ crystallites, keeping in mind that crystalline SnS₂ is a material with 2D-type structure, promising for thermoelectric applications.

(As₂S₃)_{1-x}(SnS₂)_x films with x up to 0.055 were prepared by flash evaporation and studied by Raman spectroscopy which confirmed their amorphous structure. Raman spectra recorded at a moderate laser power density ($P_{\text{exc}}=4 \text{ kW/cm}^2$) demonstrate rather pronounced (compared to amorphous As₂S₃) maxima at 184 cm⁻¹ and 232 cm⁻¹, their intensities increasing with tin concentration. This is an evidence of rearrangement of the As₂S₃-based amorphous network structure with an increasing number of As₄S₄ units with homopolar As–As bonds responsible for the bands in question. A rather narrow maximum near 270 cm⁻¹ results from As₂O₃ formed due to the photooxidation reaction with oxygen adsorbed on the (As₂S₃)_{1-x}(SnS₂)_x film surface.

Raman measurements performed at a higher P_{exc} (40 kW/cm²) for the (As₂S₃)_{1-x}(SnS₂)_x films with $x \geq 0.04$ show that a pronounced SnS₂-related narrow peak slightly below 310 cm⁻¹ emerges as an evidence for SnS₂ nanocrystals formed on the (As₂S₃)_{1-x}(SnS₂)_x film surface under above-bandgap illumination in the course of the measurement. The nanocrystals are formed due to a drastic drop of the glass viscosity upon above-bandgap illumination which facilitates photoenhanced diffusion of atoms in the laser spot and the nanocrystalline phase separation. This process is considered to be governed by a nonthermal mechanism. Raman spectra of the same samples immersed in isopropanol show the fingerprint of the SnS₂ nanocrystals only when measured at an even higher P_{exc} (100 kW/cm²) which means that heat dissipation by liquid isopropanol inhibits the nanocrystal formation. Thermal effects also contribute to the mechanism of formation of nanocrystals in amorphous chalcogenides.

Illumination of the (As₂S₃)_{1-x}(SnS₂)_x films during the Raman measurements also results in formation of a pit on the film surface. A similar lateral size of the pit measured at the same conditions on air and in isopropanol shows that for the effect of photodeformation of the film surface and photoinduced material transfer the contribution of thermal factors is negligible.

Something about electric field and electromagnetic radiation controlled film elements

Kshevetskyi, O.S.¹

¹Yuriy Fedkovych Chernivtsi National University, Chernivtsi, Ukraine, kshevos@gmail.com

The works [1, 2] describe the control of optical radiation by the properties of photosensitive elements. This work proposes to use electromagnetic (e.g., optical) radiation and an electric field to control the properties of photosensitive film elements. Such control can be used to study the influence of electromagnetic radiation and electric field on the properties of film elements. Also, the specified control can be used for the development, creation and use of various controlled elements (in particular, flexible ones), for example, thermoelectric (for example, position-sensitive temperature sensors or other thermoelectric energy converters) or electronic.

Let us consider an example of implementing the specified control, which is illustrated in Figure 1. In Figure 1: 1 and 2 – different electromagnetic radiations; 3 – photosensitive conductive film; T_1 – T_4 – element temperatures in corresponding positions. Electrical sources and loads, measuring instruments, switching elements, etc. can be connected to contacts 4 – 6. The conductive electrode and dielectric are designed to create an electric field. In this example, short-term processes (pulse modes of operation of the element) can be used.

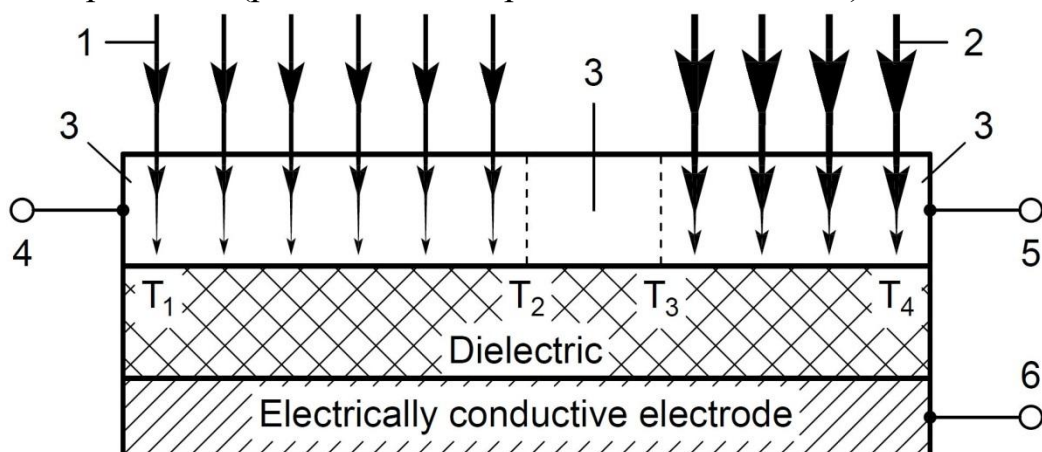


Figure 1. Simplified scheme of an example implementation of controlling the properties of a film element by electromagnetic radiation and an electric field.

[1].Oleg S. Kshevetsky "Estimation of the properties of a position-sensitive photo-thermoelectric temperature sensor", *Proc. SPIE* 11369, Fourteenth International Conference on Correlation Optics, 113690Y (6 February 2020); <https://doi.org/10.1117/12.2553981>

[2].Oleg S. Kshevetsky "About the feasibilities of controlling the properties of thermoelectric energy converters using optical radiation", *Proc. SPIE* 10612, Thirteenth International Conference on Correlation Optics, 106120X (18 January 2018); <https://doi.org/10.1117/12.2303611>

Structural studies of As-S-Se glasses

Kochubei H.¹, Stronski A.¹, Kostyukevich S.¹, Popovych M.¹, Balayeva N.²

¹ V.Lashkaryov Institute of Semiconductor Physics NAS Ukraine, Kyiv, Ukraine

² Semiconductor Physics and MAIN, Chemnitz University of Technology, Chemnitz, Germany

kochubei.hanna@gmail.com

Chalcogenide As–S–Se glasses are widely used in mid-IR photonics, including optical fibres for power delivery and supercontinuum generation, as well as sensing and spectroscopy [1]. In thin-film form, they function as inorganic photoresists for security holography (DOVIDs) and enable micro-optical elements such as axicons and Fresnel zone plates [2].

In this work, the As_{41.24}S_{27.11}Se_{31.65} composition was examined by X-ray diffraction using a Rigaku SmartLab in parallel-beam geometry with Cu K α radiation ($\lambda = 1.5406 \text{ \AA}$) over $2\theta = 2\text{--}120^\circ$ with a 0.05° step at room temperature.

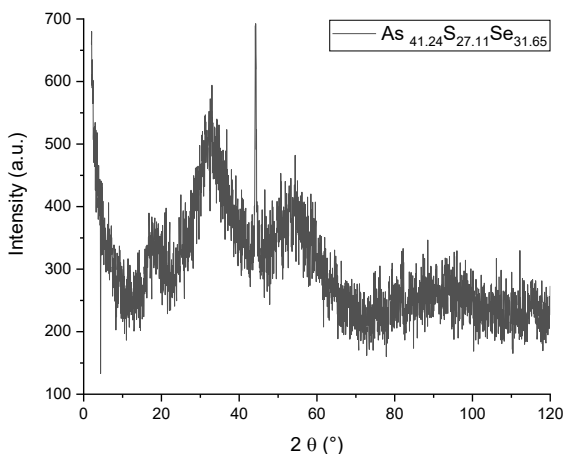


Fig.1. Diffraction pattern of As-S-Se glass.

The radial distribution function (RDF) was computed in RAD GTK+[3], yielding the first- and second-neighbor distances $r_1 = 2.32 \text{ \AA}$ and $r_2 = 3.7 \text{ \AA}$; the bond angle was evaluated as $\varphi = 2 \cdot \arcsin(r_2/(2r_1)) = 100.60^\circ$. These values are typical for As–S/Se networks and are consistent with pyramidal structural units connected via chalcogen bridges. Errors were estimated for the RAD GTK+ transform settings and are typically $\pm 0.01 \text{ \AA}$.

[1]. Z. Feng et al. Mid-infrared single-mode As–S–Se glass fiber and its supercontinuum generation. *J. Non-Cryst. Solids* **557** (2021) 120925.

[2].A. Bulanovs et al. Investigations of As–S–Se thin films as inorganic photoresist for digital image-matrix holography. *Cent. Eur. J. Phys.* **9** (2011) 1103–1109.

[3].V. Petkov, “RAD, a program for analysis of X-ray diffraction data from amorphous materials for personal computers”, *J. Appl. Crystallogr.* **22** (1989) 387-89.

Structural, optical and magnetic studies of ZnCoO thin films and nanoparticles

Stolyarchuk, I.D.¹, Kuzyk O.V.¹, Stefanuk I.², Dan'kiv O.O.¹, Popovych A.V.¹,
Zdyb R.³, Bachynsky O.I.¹, Stolyarchuk A.I.¹

¹ *Ivan Franko Drohobych State Pedagogical University, 82100 Drohobych, Ukraine,
i.stolyarchuk@dspu.edu.ua*

² *University of Rzeszow, 35-310 Rzeszow, Poland*

³ *Maria Curie-Sklodowska University, 20-031 Lublin, Poland*

Oxide based diluted magnetic semiconductors (DMS) have been the subject of recent great interest due to their promising magnetic properties. The main challenge for practical applications of the DMS materials is the attainment of ferromagnetism (FM) above room temperature (RT). Wide bandgap wurtzite-phase semiconductor ZnO ($E_g \approx 3.36$ eV) doped with transition metals (TMs) has been theoretically predicted as one of the promising DMS materials for room temperature spintronic applications [1].

The present work is devoted to preparing of $Zn_{1-x}Co_xO$ thin films and nanoparticles and study of their structural, optical and magnetic properties depending on content of cobalt.

$Zn_{1-x}Co_xO$ thin films have been deposited onto glass and quartz substrates by RF-plasma sputtering technique. $Zn_{1-x}Co_xO$ nanoparticles were produced by pulsed laser ablation of ceramic plates as targets in deionized water. Content of cobalt elements in the obtained samples varied in range of $0 < x < 0.1$. The structures of samples were studied by using X-ray diffraction (XRD), transmission electron microscopy (TEM) and scanning electron microscopy (SEM).

With increasing of cobalt content the optical absorption spectra shown a red shift of the band edge which are caused by to the s, p-d exchange interactions between the band electrons and the localized spins of magnetic impurities both for thin films and nanoparticles. In the room temperature photoluminescence spectra of $Zn_{1-x}Co_xO$ nanoparticles four main peaks were revealed, which are attributed to the band-edge transitions and vacancies or defects.

The EPR spectra of the thin films $Zn_{1-x}Co_xO$ show a broad asymmetric Dyson line, which can be described by a Lorentz-type curve with a Dyson term. The detected anisotropy of the angular dependence of the EPR spectra indicates ferromagnetic ordering at room temperature for the all studied samples.

[1]. Dietl T.; Ohno H.; Matsukura M.; Cibert J.; Ferrand D. Zener model description of ferromagnetism in zinc-blende magnetic semiconductors. *Science* 2000, 287, 1019–1022.

Structure and electrical study of Cu₂XSnS₄ (X=Zn,Fe,Co,Ni) nanocrystal thin films

Datsenko, O.I.¹, Ivakhno-Tselenyk, O.^{2,3}, Kondratenko, S.V.¹, Mazur, N.V.⁴, Dzhagan, V.M.⁴, Zahn, D.R.T.^{2,3}

¹ Physics Department, Taras Shevchenko National University of Kyiv, Kyiv, Ukraine

² Semiconductor Physics, Chemnitz University of Technology, D-09107 Chemnitz, Germany, zahn@physik.tu-chemnitz.de

³ Center for Materials, Architectures and Integration of Nanomembranes (MAIN), Technical University of Chemnitz, Chemnitz, Germany

⁴ V. Lashkaryov Institute of Semiconductors Physics, National Academy of Sciences of Ukraine, 45 Nauky av., 03028 Kyiv, Ukraine, dzhagan@isp.kiev.ua

Cu₂ZnSn(S,Se)₄ (CZTSSe) is among the materials most intensively studied for various potential energy applications [1]. The main advantages are a high absorption coefficient ($\sim 10^4$ cm⁻¹), appropriate bandgaps, nontoxic and affordable constituent elements. Colloidal nanocrystals (NCs) are a promising form for large-area manufacturing of CZTSSe thin-film solar cells, especially on flexible substrates, compatible with printing technologies [2]. However, there is a high probability of defects and impurity phases (Cu_xS, ZnS, etc) in CZTSSe. One of the approaches to stabilize the quaternary phase and eliminate defects is a partial or complete replacement of (one or two) cations.

In this work, we investigated optical, structural and electrical properties a series of Cu₂XSnS₄ (X=Zn,Fe,Co,Ni) NCs were synthesized by means of colloidal chemistry in aqueous solutions. X-ray diffraction and vibrational Raman spectroscopy data reveal that Cu₂ZnSnS₄ and Cu₂CoSnS₄, Cu₂NiSnS₄ NCs were formed without noticeable admixture of secondary (impurity) phases.

Electrical properties were studied in detail on Cu₂ZnSnS₄ and Cu₂NiSnS₄ NC films annealed at various temperatures. In particular, the temperature-dependent spectrum of the real part of the admittance was studied in the range of 85 to 250 K, and in the frequency range from 10³ to 10⁵ Hz. The improvement of the film structure by annealing was observed, which manifested itself in an increase of the electrical conductivity due to the hopping through the states in the bandgap, with the hopping length at 85 K decreasing from about 11 nm in the untreated film to about 5 nm in the film annealed at 220°C.

The work was supported by the DFG project ZA 146/59-1 (517869265).

[1]. Kush P. and Deka S. Multifunctional Copper-Based Quaternary Chalcogenide Semiconductors Toward State-of-the-Art Energy Applications. *ChemNanoMat* 2019, V. 5, PP. 373 – 402.

[2]. Stroyuk, O.; Raevskaya, A.; Gaponik, N. Solar Light Harvesting with Multinary Metal Chalcogenide Nanocrystals. *Chem. Soc. Rev.* 2018, V.7, PP. 5354–5422.

Structure, phase composition, morphology, and magnetism of heavily Cr⁺-implanted CdTe layers for spintronic applications

Popovych, V.D.^{1,2}, Popovych, A.V.¹, Stolyarchuk, I.D.¹, Böttger, R.³, Heller, R.³, Dluzewski, P.⁴, Żywczak, A.⁵, Mroczka, R.⁶, Gołębiowski, M.⁷, Sagan, P.⁷, Zdyb, R.⁷, Kuzma, M.⁸

¹Ivan Franko Drohobych State Pedagogical University, Drohobych, Ukraine
vpopovych@dspu.edu.ua

²Lviv Polytechnic National University, Lviv, Ukraine

³Helmholtz-Zentrum Dresden-Rossendorf, Dresden, Germany

⁴Institute of Physics, Polish Academy of Science, Warsaw, Poland

⁵AGH University of Science and Technology, Krakow, Poland

⁶The John Paul II Catholic University of Lublin, Lublin, Poland

⁷Maria Curie-Skłodowska University, Lublin, Poland

⁸University of Rzeszow, Rzeszow, Poland

Implantation of CdTe single crystals by 500 keV Cr⁺ ions with fluences from 10¹⁶ to 5·10¹⁷ cm⁻² was performed. The dopant depth profiles through SIMS measurements agree with the theoretical prediction using the Schulz-Wittmaack formalism, except for the accumulation of projectile ions at the sample's surface due to their out-diffusion. Strong target sputtering was observed, limiting Cr incorporation into the host lattice. XRD, HRTEM, and EDXS experiments revealed phase separation upon implantation, resulting in the formation of nanocrystals of metallic α-Cr nanoprecipitates with (110)_{Cr}|| (110)_{CdTe} orientation relationship, as well as nanoparticles of chromium telluride compounds. As follows from the RBS spectra, the near-surface layers of the implanted samples were almost not damaged, whereas irradiation-induced disorder extends much further into the crystals than expected from the SRIM calculations. SEM and AFM studies indicated progressive coarsening and increased roughness of the irradiated surfaces as the ion fluence rose. In contrast, RHEED and LEED patterns, and also Raman spectra of the implanted samples, demonstrated improvement of the top-most layers due to the sputtering of the amorphized overlayer, created by the chemo-mechanical polishing of the samples, upon Cr⁺ ion bombardment. Magnetization measurements indicate ferromagnetic behavior for all the implanted crystals, both at liquid nitrogen and room temperature, revealing round-shaped hysteresis loops with a small coercive force, characteristic of soft magnetic materials. The thermomagnetic curves' non-monotonous character suggested several magnetic phases in the materials under study.

In summary, although a much higher dopant content was introduced compared to the conventionally grown CdTe:Cr crystals, the second phase separation and the disorder induced are substantial obstacles to the production of CdTe-based DMS by Cr ion implantation. However, this technique can be used to obtain the perspective magnetic composite, consisting of nanoprecipitates of ferromagnetic chromium tellurides embedded in a semiconducting CdTe medium.

Surface Morphology and Thermoelectric Properties of PbSnTe Nanostructures

Yavorskyi Y.S¹., Shmyhelskyi Y.V¹., Krykhovetskyi M.V.¹, Hleb V.F.¹

¹*Vasyl Stefanyk Carpathian National University, Ivano - Frankivsk, Ukraine,*

yaroslav.yavorskyi@pnu.edu.com

Lead thermotelluride is a promising electrical semiconductor material for the medium temperature range, as well as for devices operating in the infrared part of the optical spectrum. Due to the impurities of antimony and bismuth, it is possible to maintain the concentration of carriers, which provides maximum values of thermoelectric power $S^2\sigma$. The use of thin films and nanostructures significantly expands both the physical properties of PbSnTe compounds and their practical use. At present, many studies of thin films based on lead telluride have been carried out, but nevertheless there are still many open questions regarding the processes of formation and thermoelectric properties for practical use.

In this work, samples for research were grown by methods of open evaporation of pre-synthesized compounds on amorphous (polished glass), polycrystalline (sital and oxide gel films SiO₂, GeO) and single-crystalline (clay (0001) mica-muscovite of the STA brand) substrates under various technological conditions ($T_v = 920\text{--}1020\text{ K}$, $T_p = 320\text{--}520\text{ K}$, $\tau = 15\text{--}600\text{ s}$). The surface morphology and structure were studied by atomic force microscopy (AFM). The phase composition of the condensates was determined by X-ray diffractometry. Absorption and reflection spectra were recorded using a spectrophotometer and an IR-Fourier spectrometer. Electrical parameters were measured by compensation methods at room temperature in a constant magnetic field.

During the research, it was established that the thermal conductivity of Si, Ge substrates, (0001) mica-muscovite cleavages and the deposition temperature have a significant impact on the processes of nanocluster formation in vapor-phase PbSnTe condensates and their optical characteristics. The mechanisms of their formation and the dependence of thermoelectric parameters on the thickness of the condensate were determined. It was shown that the dominant mechanism in this process is the Volmer-Weber nucleation mechanism, and the optimal thermoelectric power is a condensate with a thickness of (0.3 – 0.1) μm . Based on the thickness dependences, resistivity, and carrier mobility for vapor-phase PbSnTe condensates, the dominant scattering mechanisms were determined, which are due to diffuse scattering on the surface and intergrain boundaries. It is shown that their significant contribution depends on both the thickness of the condensates and the size of the nanoclusters in them. Defined the influence of near-surface layers exposed to air nanostructures, on the complex of their thermoelectric parameters.

The effect of short-term annealing on the changes of surfaces of amorphous aluminium-based metal alloys

Kh. Khrushchyk^{1,2}, V. Pihel¹, M. Chava¹, V. Kordan¹, K. Aniołek²,

M. Karolus², L. Boichyshyn¹

¹*Faculty of Chemistry, Department of Physical and Colloidal Chemistry, Ivan Franko National University of Lviv, 6 Kyryla and Mefodiiia Str., 79005, Lviv, Ukraine,*

²*Faculty of Science and Technology, Institute of Materials Engineering, University of Silesia in Katowice, 1A Pulku Piechoty Str., 41500, Chorzow, Poland
khrystyna.khrushchyk@us.edu.pl*

The aim of this work is to study the effect of annealing on the tribological properties of an amorphous metal alloy (AMA) based on aluminium for its further practical application.

The object of the tests were AMAs alloys in the form ribbons with a thickness and width of 20-25 μm and 3 mm, respectively, which were obtained at the G. V. Kurdyumov Institute for Metal Physics of the Ukrainian Academy of Sciences (Kyiv) by melt spinning method in a helium atmosphere on a copper drum rotating at a speed of ~30 m/s. The melt was prepared from pure metals and binary compounds REAl₃ (RE = Y, Gd). The purity of the starting metals was as follows: Al (99.999 wt.%), Ni (99.99 wt.%), Y (99.96 wt.%), Gd (99.96 wt.%) and Fe (99.99 wt. %).

The roughness of the surface and the geometry of wear marks obtained after tribological tests were measured using a Mitutoyo 2D Surftest SJ-500 contact profilometer (Mitutoyo, Tokyo, Japan). The roughness of the samples was measured in the longitudinal direction. Roughness was measured in accordance with ISO 21920 using an elementary cross-section and a measuring cross-section selected according to the surface roughness. The study of changes in the surface of AMAs due to annealing was carried out using a Tescan Vega 3 LMU.

A profile analysis of the surface of the amorphous alloy Al₈₇Y₄Gd₁Ni₈ after various heat treatment modes revealed significant changes in topography. In its as-cast state, the surface is characterised by a relatively uniform profile with an average roughness of $R_a=2.83 \mu\text{m}$, but after short-term annealing (5 min), a decrease in all roughness parameters ($R_a=0.614 \mu\text{m}$, $R_q=0.781 \mu\text{m}$, $R_z=3.09 \mu\text{m}$) is observed, indicating temporary compaction of the oxide film and levelling of minor irregularities.

The effect of structural features of the semiconductive mixed metal (Fe, Zn, Ti) oxides films on their photocatalytic activity

A.S. Kramar¹, A.G. Dyachenko^{1,2}, O.P. Linnik¹

¹*Chuiko Institute of Surface Chemistry, NAS of Ukraine, Kyiv, Ukraine,*

nkramar45@gmail.com

²*Institute of Physical Chemistry, Polish Academy of Sciences, Warsaw, Poland*

The development of new semiconductors for their application in photovoltaics or photo/electro-catalysis is a task of contemporary relevance. The mixed metal oxides or their composites with individual oxides are considered as promising photocatalysts due to the capability of some of them to absorb visible light, inhibition of charge carrier recombination, new surface adsorption centres formation.

The synthesis of mixed metal oxide nonporous three-layered films with a metal molar ratio of Fe:Ti:Zn=0.5:1:0.5 was performed via the sol-gel method (titanium (IV) tetraisopropoxide, chlorides of iron (III) and zinc were used as precursors) with the procedure of the first two layers calcination at 300°C and the last one at 450°C, 500°C or 600°C. The structural characteristics of the films, as defined by XRD and Raman studies, indicate the amorphous nature of the sample obtained at 450°C. The crystallization of pseudobrookite and anatase was fixed in the samples treated at higher temperatures. From our previous studies with the series of the iron-free samples, it is known that the Zn²⁺ ions retard the anatase crystallization, while the cubic ZnTiO₃ phase formation is detected at higher temperatures (600°C). On the other hand, the crystallization of pseudobrookite in the same systems with Fe³⁺ cations instead of Zn²⁺ occurs even at 450 °C. Thus, the amorphous nature of the mixed Fe, Zn and Ti films treated at 450°C (450Fe_aZn_bTi_xO_y) can be explained by addition of zinc cations.

The photocatalytic properties of the films were tested in the process of tetracycline hydrochloride transformation under solar simulated ($\lambda \geq 330$ nm) and visible light ($\lambda \geq 400$ nm) irradiation. The less crystalline films (450Fe_aZn_bTi_xO_y) are characterized by the highest conversion percentage of 63% and 49% under $\lambda \geq 330$ nm and $\lambda \geq 400$ nm, respectively. The photocatalytic activity of the films is decreased in the case of the films treated at 500°C and 600°C. Such behavior can be connected to the adsorption capacity of the films, which is decreased in the range of 450Fe_aZn_bTi_xO_y > 500Fe_aZn_bTi_xO_y > 600Fe_aZn_bTi_xO_y. The formation of the XRD amorphous tiny particles in the case of the 450Fe_aZn_bTi_xO_y sample can be responsible for the highest photocatalytic efficiency due to the highest, among tested materials, specific surface area (120 m²/g), resulting in significant adsorption capacity (32%). In the case of films treated at 500°C and 600°C, the specific surface area is determined to be 57 m²/g and 12 m²/g, respectively, which is reflected in lower adsorption (20% and 6%, respectively) of tetracycline hydrochloride and, in turn, photocatalytic activity (56% and 37%, respectively, under $\lambda \geq 330$ nm).

The Influence of Laser Annealing on the Morphology and Elemental Composition of GeSn Films

Mazur, N.V.¹, Yukhymchuk, V.O.¹, Lytvyn, P.M.¹, Kosulya, O.A.¹,
Gudymenko, O.Yo.¹, Kapush, O.A.¹, Valakh, M.Ya.¹, Yefanov, V.S.¹,
Dmytruk, A.M.², Dzhagan, V.M.¹

¹*V. Lashkaryov Institute of Semiconductors Physics, National Academy of Science of Ukraine,
41 Nauky Ave., 03028 Kyiv, Ukraine, E-mail: nazarmazur1994@gmail.com,*

²*Institute of Physics, National Academy of Science of Ukraine, 46 Nauky Ave., 03028
Kyiv, Ukraine*

GeSn is an extremely promising material for creating next-generation photodiodes, as they can be integrated with silicon technology (CMOS-compatible). When a certain tin content (~ 6 - 8%) is reached, GeSn becomes a direct bandgap semiconductor, which significantly increases its light absorption efficiency and makes it suitable for fabricating not only photodiodes but also lasers compatible with Si technology. Since Sn has very low solubility (0.5 at.%) in Ge under normal conditions, it is necessary to use non-equilibrium deposition methods such as molecular beam epitaxy or chemical vapor deposition. However, these methods are expensive and not suitable for industrial production.

We have formed 150 nm GeSn films on 100 nm Ge buffer layers on Si substrates using the method of sequential thermal deposition of 10 Ge/Sn layers with a thickness ratio of 10:1. After film deposition, the samples were cut into several parts, one of which was implanted with C⁺ or B⁺ ions at a dose of 6.2×10^{15} ion/cm² and an energy of 50 keV. The presence of carbon (boron) atoms in the Ge lattice reduces the local stresses that arise when Sn atoms, which have a significantly larger covalent radius compared to Ge, are incorporated into it. The amorphous GeSn and GeSn:C films were annealed with a femtosecond (800 nm) and a scanning continuous-wave (455 nm) lasers.

Short-term laser annealing, on the one hand, allows for the crystallization of amorphous films, and on the other hand, prevents tin segregation. Raman studies have established that such annealing forms GeSn films with an Sn content of 7 to 8.5 at.% for the scanning continuous-wave and femtosecond lasers, respectively. SEM and AFM showed that during femtosecond laser annealing, so-called LIPSS structures (Laser-Induced Periodic Surface Structures) are formed on the film surfaces. It has been established that the additional incorporation of carbon (boron) leads to the formation of a more stable GeSn structure during thermal annealing.

The work of N.M., V.Yu O.G., O.K., V.Ye. was supported by the National Research Foundation of Ukraine project No. 2023.03/0186. V.D. acknowledges support by NRFU grant No. 2023.05/0022.

Thin film CsPbBr_3 technology research

Orletskyi I.G., Maistruk E.V., Koziarskyi I.P.,
Ulyanytskiy K.S., Koziarskyi D.P.

Yuriy Fedkovych Chernivtsi National University, Chernivtsi, Ukraine
i.koziarskyi@chnu.edu.ua

A review of literary sources showed: firstly, the increased interest in perovskite materials remains, and secondly, the problem of MHPs (Metal Halide Perovskite) stability has also not been solved.

In MHPs, the ionic type of chemical bond prevails, so these materials are well soluble in many solvents, which allows them to be applied from solutions, both from completely synthesized materials and from precursors. On the other hand, this causes certain difficulties during crystal processing, and also affects their stability and resistance to external factors.

In order to establish the possibility of obtaining MHP films (CsPbBr_3), a DMSO solution was used at a concentration of 1 g/5.6 ml. The solution drying mode started at 60 °C with a gradual increase in temperature to 130 °C on glass substrates (cover glass) (Fig. 1-2).



Fig. 1. Result obtained by wetting on glass (40x magnification) - Conventional microscope (CsPbBr_3 MHP film)

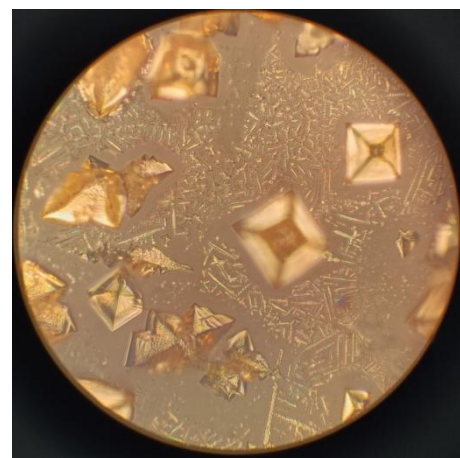


Fig. 2. Result obtained by wetting on glass (magnification 500x) - Metallographic microscope (CsPbBr_3 MHP film)

From Fig. 1-2 it is clear that:

1. On the prepared optical glass, which was cleaned in several stages, a thin film of MHP is deposited by the type of island crystallization.
2. According to the literature, to obtain a continuous film, it is necessary to bring the molarities of the solutions to $>3\text{M}$. Currently, it is possible to dissolve only up to 0.9-1M, after which the problem of inhomogeneity of the CsPbBr_3 solution arises, since PbBr_2 dissolves better than CsBr . This in turn causes the appearance of a green precipitate.

Funding acknowledgement: Supported by the STCU (Project No. 6437).

Wastewater treatment from organic pollutants by polymer based fenton catalysts

Zhyhalo M.M., Demchyna O.I., Yevchuk I.Yu.

*Department of Physical Chemistry of Fossil Fuels of the Institute of Physical-Organic Chemistry and Coal Chemistry named after L. M. Lytvynenko of the NAS of Ukraine
Naukova Str., 3a Lviv, 79060, Ukraine
Zhygaylo@nas.gov.ua*

Nowadays water is one of the most important resources for sustainable life. The need for clean drinking water is increasing at a fast pace. At the same time the contamination of water by inorganic and organic pollutants has become a challenge and requires the development of new efficient approaches to water treatment.

Recently the use of advanced oxidation processes (AOPs) seems to be the efficient method for catalytical degradation of the organic pollutants. The Fenton process is one of the AOPs, therefore the development of the Fenton catalysts with high surface area, good stability and low iron leaching is in the focus of the researches.

In this study we developed new heterogeneous Fenton catalysts consisting of Fe^{+2} ions incorporated in polymeric matrices for wastewater treatment from organic pollutants. Polymeric matrices were synthesized by UV-polymerization of acrylic monomers: acrylonitrile (AN), acrylic acid (AA) and sulfocontaining monomer 2-acrylamido-2-methylpropane-1-sulfonic acid (AMPS) in the presence of photoinitiator and cross-linking agent. The monomer ratio was as follows: the sample P1 AN:AA:AMPS=58.2:14.5:24.4 (wt %) and the sample P2 AN:AA:AMPS=58.2:19.4:19.5 (wt %). After polymerization the synthesized samples were immersed for 90 min in $\text{FeSO}_4 \times 7\text{H}_2\text{O}$ solution, and Fe^{+3} ions were adsorbed by sulfogroups. So, the embedding of iron ions into polymeric matrix was employed through the reaction of the iron salts with sulfo groups of sulfocontaining monomers. Then the materials were placed in methylene blue (MB) solution ($5 \cdot 10^{-5}$ mol/L) and the oxidant H_2O_2 was added to the solution. The MB degradation was determined by monitoring the dye concentration changes at 665 nm using spectrophotometer Spekol 11 (Carl Zeiss Jena, Germany). The kinetic curves for MB degradation are presented in Fig. 1.

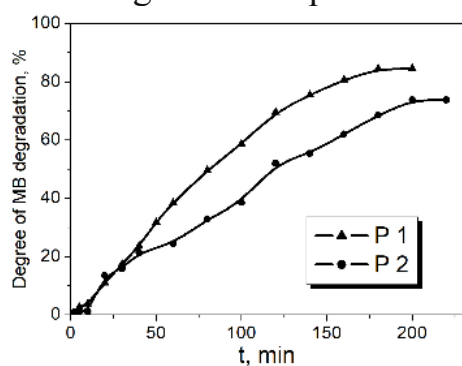


Fig. 1. Kinetic curves for MB degradation

As can be seen from Fig. 1, the degree of dye degradation in the case of using the catalyst P1 reaches 84 %, the catalyst P2 – 74 %. This can be explained by the higher content of sulfo groups in the catalyst P1, respectively, the higher content of Fe^{+2} ions, which act as catalytic centers in the Fenton reaction.

This work was supported by the National Academy of Sciences of Ukraine as part of project No. 0125U002894 (2025–2026).

Topic 4

**Nano- and thin films applications: energy, biotechnology & medicine,
defense, space, etc.**

Adsorption of barium and cobalt cations by titanium dioxide doped with Fluorine

¹I. F. Mironyuk, ^{2*}H.V. Vasylyeva, ¹I.M. Mykytyn, ³I.D. Hnylytsia

¹ Department of Chemistry, Vasyl Stefanyk Precarpathian National University

^{2*} Department of Radiation Safety, Uzhhorod National University,

h.v.vasylyeva@hotmail.com

³Department of Computerized Mechanical Engineering, Ivano-Frankivsk National Technical University of Oil and Gas

Modifier agents that contain atoms with very high electronegativity can be used to develop new ion-exchange adsorbents based on TiO₂. In recent publications, we proposed a new method for obtaining titanium dioxide with a high adsorption capacity for metal cations. The essence of the method lies in the impregnation of the groupings $\equiv\text{TiOPO(OH)}_2$, $\equiv\text{TiOCOOH}$, or $\equiv\text{TiOAsO(OH)}_2$ on the surface of nanoparticle TiO₂, which causes a redistribution of electron density in the Ti-O-Ti bridges and ensures the conversion of titanol groupings into Brønsted acid centers $=\text{TiOH}^{\delta+}$. It is well-known that among the elements, the atom of Fluorine has the highest electronegativity. Research on the adsorption of cobalt and barium cations, as well as radionuclides ¹⁴¹Ba and ⁶⁰Co, is relevant in the context of the removal of heavy metal cations from aqueous solutions. ⁶⁰Co is a well-known radionuclide for medical purposes. This determines the relevance of searching for recycling technologies for its processing and reuse.

In this work, TiO₂ samples doped with Fluorine were synthesized using a titanium aquacomplex solution $[\text{Ti}(\text{OH}_2)_6]^{3+}\cdot 3\text{Cl}^-$, as a precursor, and sodium fluoride NaF as a modifying reagent. Nanoparticle titanium dioxide was synthesized with impregnated groups $\equiv\text{TiF}$ on its surface in amounts of 2, 4, and 8 wt.%. The characteristics of the synthesized samples were investigated using XRD, TEM, and SEM/EDS spectroscopy methods. The specific surface area and porosity were determined using the low-temperature adsorption-desorption isotherms of N₂ molecules.

The adsorption capacity of fluorine-doped TiO₂ samples toward cobalt and barium cations was investigated. The sample of TiO₂ with the highest number of chemisorbed Fluorine atoms (8F-TiO₂) possesses the maximum adsorption capacity for the studied cations. The maximum adsorption capacity of cobalt cations is 156.2 mg/g, and for barium, it is 128.6 mg/g, which is four times greater for Co²⁺ ions than the adsorption capacity of unmodified TiO₂ under equilibrium conditions. The number of adsorption centers on the surface of the synthesized fluorine-doped TiO₂ samples was calculated. It was shown that in the 8F-TiO₂ sample, practically all hydroxylated Ti atoms on the surface convert to the Brønsted acid centers $=\text{TiOH}^{\delta+}$.

Advanced Porous Silicon Systems with Phase Change Materials for Tailored Thermal Properties

Lishchuk, P.O.¹, Chepela, L.I.², Yakovenko, O.S.³, Tsehelnyi, V.A.⁴, Ovsienko, I. V.⁵, Isaiev, M.V.⁶

¹Taras Shevchenko National University of Kyiv, Kyiv, Ukraine, pavel.lishchuk@knu.ua

²Taras Shevchenko National University of Kyiv, Kyiv, Ukraine, lesia.chepela97@gmail.com

³Taras Shevchenko National University of Kyiv, Kyiv, Ukraine, alenka-ya@ukr.net

⁴Taras Shevchenko National University of Kyiv, Kyiv, Ukraine, vladtsegel@knu.ua

⁵Taras Shevchenko National University of Kyiv, Kyiv, Ukraine, iryonaovsienko@knu.ua

⁶Université de Lorraine, CNRS, LEMTA , Nancy F-54000, France, mykola.isaiev@univ-lorraine.fr

Efficient thermal management requires materials with tunable transport properties. Porous silicon (porSi) provides such a platform owing to its controllable porosity, morphology, and compatibility with the infiltration of phase change materials (PCMs). The resulting composites combine the latent heat storage of PCMs with the structural versatility of nanostructured silicon.

In this work, porSi layers of different porosities and thicknesses were fabricated and subsequently infiltrated with PCMs. The composites exhibit pronounced modifications of their thermal and optical response: thermal conductivity increases upon pore filling, while colour shifts indicate changes in the effective refractive index. These effects reflect the interplay between geometry, interfacial resistance, and confinement, which strongly influence heat transport under nanoscale conditions.

Thermal conductivity was evaluated using a photoacoustic gas-microphone technique, providing a non-invasive probe of confined transport. The results confirm that tailoring the structure of porous silicon enables controlled adjustment of composite properties, offering a model system for studying confined phase change behavior and for advancing materials for energy-efficient thermal management.

P.O., L.I., O.S. and V.A. acknowledge the support of the Ministry of Education and Science of Ukraine (project “Development of Advanced Phase Change Composite Systems for Efficient Use of Thermal Energy,” No. 0124U001084). M.I. acknowledges the support of the French National Research Agency (ANR) under the project “PROMENADE” (No. ANR-23-CE50-0008).

AI-Based methodology for predicting thermoelectric material performance from literature data

Korop, M.M.^{1,2}, Prybyla, A.V.^{1,2}, Lysko, V.V.^{1,2}

¹ *Yuriy Fedkovych Chernivtsi National University, Chernivtsi, Ukraine,*
koropmykola@gmail.com

² *Institute of thermoelectricity NAS and MES of Ukraine, Chernivtsi, Ukraine*

Thermoelectric materials based on bismuth telluride (Bi-Te) continue to attract significant attention as highly efficient candidates for waste-heat recovery and solid-state refrigeration due to their favorable transport properties near room temperature. Despite decades of research, further improvement of their figure of merit (ZT) remains a challenge because of the complex interplay between structural, compositional, and processing parameters [1-2]. This work introduces an integrated methodology that combines artificial intelligence (AI) tools with specialized experimental equipment to optimize Bi-Te based thermoelectric materials more effectively. A dedicated AI-driven framework was implemented to process large experimental datasets, discover hidden correlations, and generate predictive models capable of identifying optimal synthesis and processing conditions. The workflow is reinforced by advanced laboratory systems designed for precise measurement of electrical conductivity, Seebeck coefficient, and thermal conductivity across a broad range of operating regimes.

Preliminary results confirm that machine learning models substantially accelerate the exploration of composition property landscapes, reducing the number of experimental iterations required and guiding researchers toward promising material configurations. Moreover, the adaptive nature of the AI approach allows continuous refinement of predictions as new data are incorporated, ensuring higher accuracy and robustness of optimization. This methodology synergy between data-driven modeling and experimental validation not only streamlines the search for improved thermoelectric performance but also lays the foundation for scalable, automated strategies in material design.

- [1]. Korop, M., & Prybyla, A. (2025). Application of LLM to Search and Systematize the Properties of Thermoelectric Materials in Scientific Literature. *Journal of Thermoelectricity*, (1), 16–25. <https://doi.org/10.63527/1607-8829-2025-1-16-25>.
- [2]. Anatychuk, L., & Korop, M. (2023). Application of machine learning to predict the properties of Bi₂Te₃ -based thermoelectric materials. *Journal of Thermoelectricity*, (2), 59–71. <https://doi.org/10.63527/1607-8829-2023-2-59-71>.

Bandpass Filtering of PPG Signals for Heart Rate Analysis

Saliy Ya.P.

Vasyl Stefanyk Carpathian University, Ivano-Frankivsk, Ukraine, yaroslav.saliy@pnu.edu.ua

Photoplethysmography (PPG) is a widely used non-invasive method for monitoring blood pressure [1]. Variations in cardiovascular and autonomic nervous system activity are reflected in changes in PPG signals.

To determine an appropriate cut-off frequency range for a bandpass Butterworth filter, a Fast Fourier Transform (FFT) was applied to several PPG signals. The signals were normalized to unit variance within the range [0, 1].

Figure 1 shows a normalized PPG segment from [2], and Figure 2 its FFT. Excluding the high DC component, the first peak near 1.5 Hz corresponds to the heart rate, while peaks at 3 Hz and 4.5 Hz represent harmonics. Based on this, a 6th-order Butterworth bandpass filter with a passband of 0.5–5 Hz was selected.

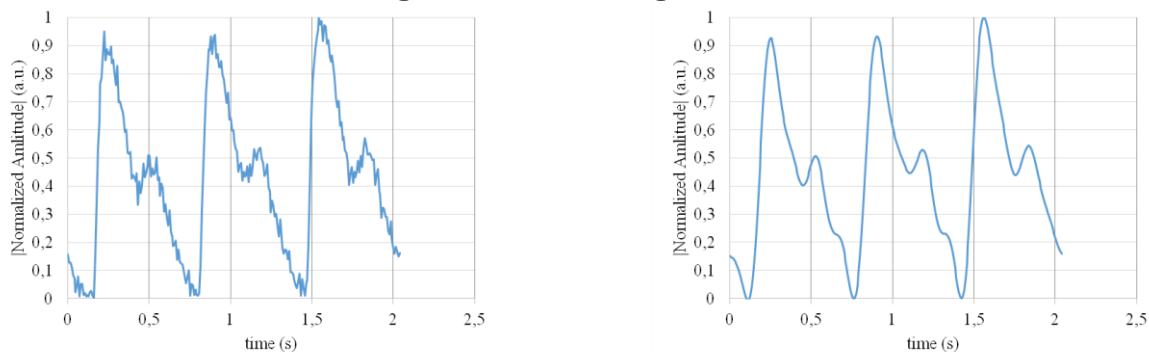


Fig. 1 Normalized raw PPG segment example [2] and filtered PPG signal.

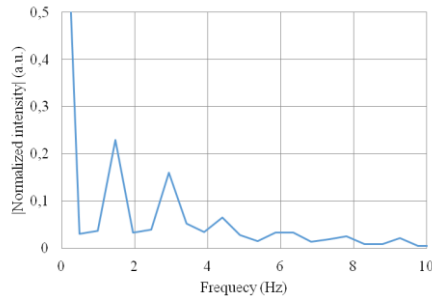


Fig. 2 FFT of raw PPG signal

[1]. Qianyu Liu, Chaojie Yang, Sen Yang, Chiew Foong Kwong, Jing Wang, Ning Zhou Photoplethysmography-based non-invasive blood pressure monitoring via ensemble model and imbalanced dataset processing *Physical and Engineering Sciences in Medicine* (2024) 47:1307–1321

[2]. B.S. Dzundza, S.V. Dombrovskyi, M.V. Shtun, O.O. Chinchoy, A.V. Morgun Software processing features of photoplethysmography signals *Physics and chemistry of solid state* V.26, No.1 (2025) pp.105-110

Computer modeling of output stages of touch microsystems-on-chip based on film CMOS transistor structures

Igor Kohut, Volodymyr Hryha, Vitaliy Martyniuk, Oleksandr Samarchuk,
Andriy Prystaiko

Vasyl Stefanyk Carpathian University, Ivano-Frankivsk, Ukraine igor.kohut@pnu.edu.ua

The creation and development of micro-systems-on-chip (SoC), sensor-type, micro-laboratories-on-chip requires highly efficient input/output cascades that ensure minimal energy loss, high speed, minimal signal delays, and the formation of control signals for external interface devices. Input/output stages based on film (silicon-on-insulator) CMOS structures are more promising due to their low level of parasitic capacitance, radiation and temperature stability, and the possibility of high-level integration on the crystal, creating three-dimensional configurations of transistors and sensitive elements.

Input/output stages of touch microsystems-on-chip, similar to microcircuits, include external housing terminals, microdrone or microball connections between housing crossbars and crystal contact pads, the actual structure and topology of the contact pads themselves, and circuits for protection against electrostatic charges and overvoltage.

The main functions of the input and output stages: input – protection circuits against electrostatic discharges and excessive input signal levels; transmission of input signals to the microsystem core and their processing, and - output – reliable transmission of signals from the microsystem core to the output interface circuits, ensuring the formation of the necessary output signal parameters and optimal delay; performance of level conversion functions from low to high or vice versa, programmable outputs to optimal consumption currents, or three states – log. 0, 1, high impedance. Input/output stages, together with other elements of the microsystem on the crystal, form integrated delay lines.

These elements require significant attention, as they determine the correct operation of the IC or MNC when transitioning to sub- and nanometer sizes (supply voltages: 5, 3.3, 2.5, 1.8, 1.2, 0.6 V). An effective method for solving these problems is computer modeling of input/output stages in PPE – TopSPICE, LT SPICE, MicroWind.

[1]. Microwind 3.1 Lite [Electronic resource]. – Access mode: <https://microwind3-1-lite.software.informer.com/3.1/> (date of access: 05.09.2025)

Computer modeling of ring oscillators in sensor SoC: film CMOS with PLD/FPGA prototyping

Volodymyr Hryha, Vadym Hula, Vitalii Vintoniak, Liudmyla Hryha,
Vitaliy Martyniuk

Vasyl Stefanyk Carpathian University, Ivano-Frankivsk, Ukraine
volodymyr.gryga@pnu.edu.ua

Creating advanced micro-systems-on-chip (SoC), sensor-class devices, and micro-laboratories-on-chip require timing and reference blocks that provide low power, high speed, minimal delay, and reliable delivery of clock and control signals to core logic and external interfaces. In this role, ring oscillators (ROs) are attractive due to their structural simplicity, compact area, and ease of on-die integration; they also demonstrate how supply, temperature, and process changes affect behavior, which makes them valuable teaching and research settings [1].

In sensor microsystems, RO-based timing paths typically encompass the oscillator core (a loop of inverting stages), enable/gating networks, distribution of the generated clock to local domains, optional multi-phase taps, and buffering toward the periphery or pads. Functionally, these stages provide periodic reference generation, timing transfer/conditioning, level adaptation across voltage domains, and programmable operation (enable/disable, tri-state routing). Together with other blocks, they form integrated delay lines for measurement and control. These elements demand attention as technologies scale and supply voltages drop and diversify across multiple on-chip domains [1].

A practical, accessible workflow combines circuit-level exploration with FPGA prototyping. Tools such as TopSPICE, LTspice, or MicroWind support topology studies and layout-driven effects for RO stages. In parallel, PLD/FPGA platforms (e.g., Xilinx Artix-7) enable the rapid hardware validation of qualitative trends, such as how frequency shifts with voltage or temperature, using LUT-based ring oscillators and counter-based readout. Because synthesis tools tend to remove oscillating combinational loops, vendor-documented preservation directives/constraints are applied to retain the structure for measurement. This SPICE-plus-FPGA approach provides clean, reproducible comparisons (df/dV , df/dT) and a foundation for deeper studies of jitter, security primitives (RO-based TRNGs and PUFs), and multi-oscillator arrays for sensing and calibration [2–3].

Digital frequency control on FPGA can be realized via direct interaction with the oscillation path by changing the effective ring length formed by delay elements. The loop is closed through a selectable number of delay cells chosen by the control code applied to a multiplexer (see Fig. 1).

The oscillation frequency is $f_0 = 1/(2Nt_D)$, where N is the number of active delay elements and t_D is the unit delay. The frequency step $\Delta f = 1/(2N(N+1)t_D)$

can be nearly halved to $\Delta f \approx 1/(2N(2N+1) t_D)$ by extending the design with a simple logic transform of the control code [2].

Synthesized on a Xilinx Artix-7 FPGA (xc7a15tcsg324-1) [4], the design used two LUTs and achieved an oscillation frequency of 23.5 MHz.

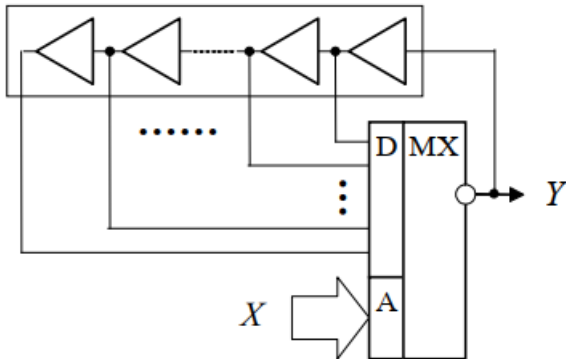


Fig. 1. Direct frequency control via ring-length selection (multiplexer over delay cells)

Figure 2(a) shows the functional block diagram of direct frequency control by varying the ring length, while Figure 2(b) shows the functional timing diagram of this scheme.

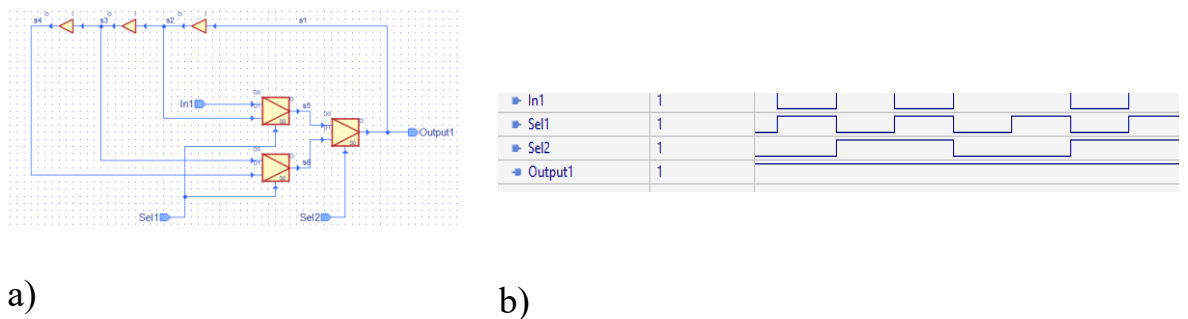


Fig. 2. Direct frequency control of a ring oscillator by varying ring length: (a) functional block diagram; (b) functional timing waveforms.

[1]. B. Razavi, “The Ring Oscillator [A Circuit for All Seasons],” IEEE Solid-State Circuits Magazine, vol. 11, no. 4, pp. 10–81, Fall 2019, doi: 10.1109/MSSC.2019.2939771.

[2]. A. Hajimiri, S. Limotyrakis, and T. H. Lee, “Jitter and phase noise in ring oscillators,” IEEE Journal of Solid-State Circuits, vol. 34, no. 6, pp. 790–804, Jun. 1999, doi: 10.1109/4.766813.

[3]. Microwind, “Introducing 45 nm technology in Microwind3,” Application Note, [Online]. Available: <https://microwind.net/download/21>. Accessed: Sep. 8, 2025.

[4]. AMD, “Artix-7 FPGAs Data Sheet: DC and AC Switching Characteristics (DS181),” [Online]. Available: https://docs.amd.com/v/u/en-US/ds181_Artix_7_Data_Sheet. Accessed: Sep. 8, 2025.

Defect state engineering in chalcogenide materials for efficient energy conversion

Taras Parashchuk*

*Thermoelectric Research Laboratory, Department of Inorganic Chemistry,
Faculty of Materials Science and Ceramics, AGH University of Krakow,
Mickiewicza Ave. 30, 30-059 Krakow, Poland
E-mail: parashchuk@agh.edu.pl

Thermoelectric power generation offers a solid-state pathway for sustainable energy conversion, but its performance is limited by the interdependence of electronic and thermal transport parameters of the semiconductor materials. One of the most promising strategies to overcome these limitations is defect state engineering, which enables precise tuning of carrier concentration while suppressing detrimental thermal transport [1-3].

In this work, I present defect-engineered PbTe as a model system for developing highly efficient thermoelectric chalcogenides. For *n*-type PbTe, simultaneous doping with In and I introduces defect states that act as electron reservoirs. Instead of rigidly increasing the carrier concentration, iodine fills the half-occupied indium level, stabilizing the electronic structure. This mechanism prevents the onset of intrinsic conduction at elevated temperatures and results in high Seebeck coefficients and enhanced power factors. Consequently, a maximum figure of merit $ZT \approx 1.38$ at 723 K and an estimated conversion efficiency of 14.2% were achieved in $\text{Pb}_{1-x}\text{In}_x\text{Te}_{1-y}\text{I}_y$.

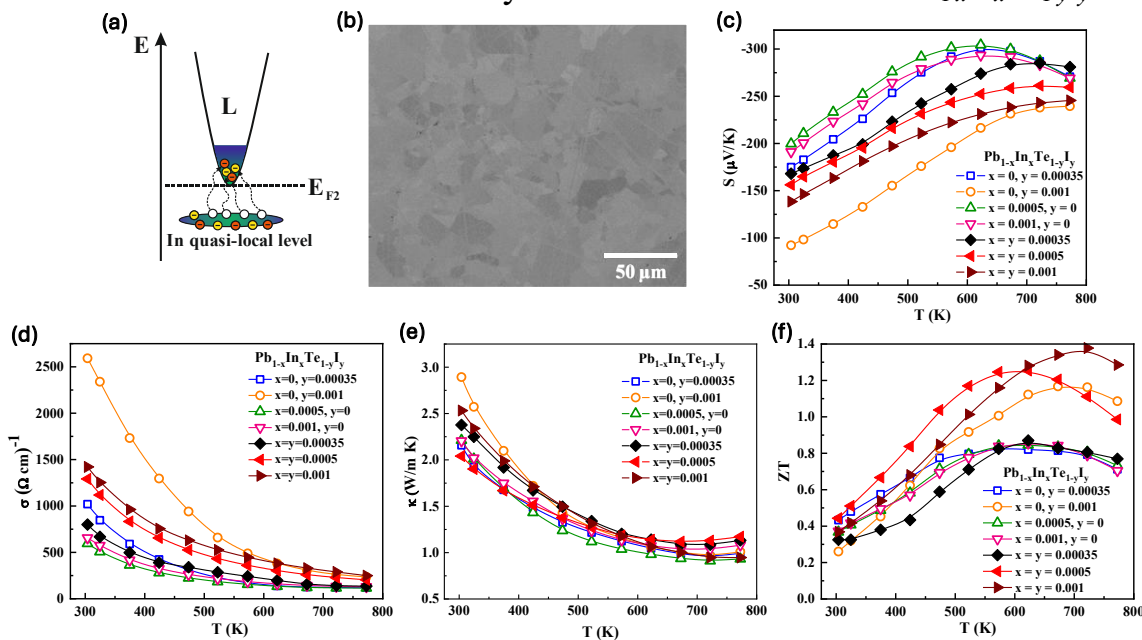


Figure 1. (a) Schematic representation of the PbTe conduction band with the quasi-local defect state occupied by electrons from Indium and Iodine. (b) SEM secondary electron image of the $\text{Pb}_{0.999}\text{In}_{0.001}\text{Te}_{0.999}\text{I}_{0.001}$ sample after SPS processing. Temperature-dependent (c) Seebeck coefficient, (d) electrical conductivity, and (g) thermoelectric figure of merit ZT of $\text{Pb}_{1-x}\text{In}_x\text{Te}_{1-y}\text{I}_y$. Panels are reproduced from [1-2].

Inspired by this success, a similar approach was applied to *p*-type PbTe using Tl and Na co-doping. Here, the synergistic action of resonant scattering (Tl) and rigid-band doping (Na) enhances carrier transport while preserving low lattice thermal conductivity through lattice softening. The resulting materials achieve an outstanding $ZT \approx 2.1$ at 823 K, corresponding to energy conversion efficiency of 15.4%.

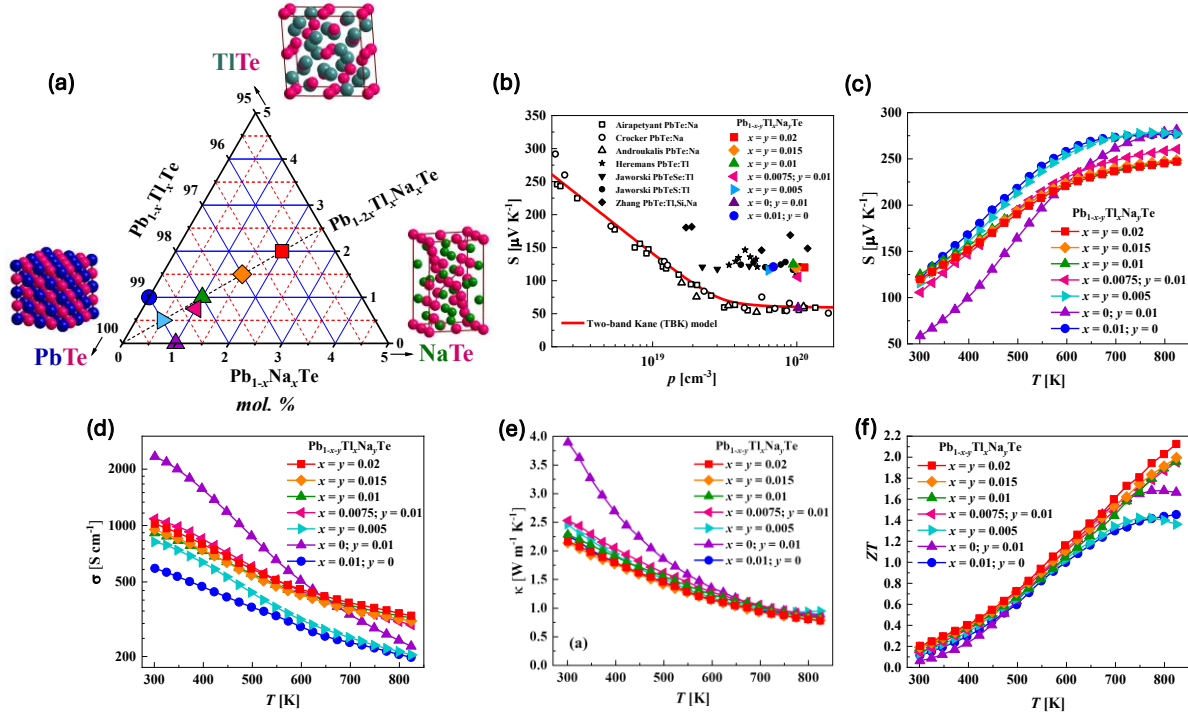


Figure 2. (a) Schematic representation of the proposed defect engineering strategy for designing highly efficient *p*-type PbTe material. (b) Seebeck coefficient as a function of the carrier concentration (Pisarenko plot) in Na and/or Tl doped PbTe. Temperature-dependent (c) Seebeck coefficient, (d) electrical conductivity, and (e) ZT parameter of $\text{Pb}_{1-x}\text{Tl}_x\text{Na}_y\text{Te}$. Panels are reproduced from [3].

These results demonstrate that defect state engineering provides a universal framework for designing high-performance thermoelectric materials. By controlling the electronic structure through targeted co-doping, it is possible to simultaneously optimize transport properties and achieve record energy conversion efficiencies in both *n*- and *p*-type PbTe.

This work was funded by the National Science Center (Poland) under the research project “OPUS-26” UMO-2023/51/B/ST11/00329.

[1]. T. Parashchuk, Z. Dashevsky, K. T. Wojciechowski, Feasibility of a high stable PbTe:In semiconductor for thermoelectric energy applications, *J. Appl. Phys.* 125 (2019) 245103.

[2]. K. T. Wojciechowski, T. Parashchuk, B. Wiendlocha, O. Cherniushok, Z. Dashevsky, Highly efficient *n*-type PbTe developed by advanced electronic structure engineering, *J. Mater. Chem. C* 8 (2020) 13270.

[3]. T. Parashchuk, B. Wiendlocha, O. Cherniushok, R. Knura, K. Wojciechowski, High thermoelectric performance of *p*-type PbTe enabled by the synergy of resonance scattering and lattice softening, *ACS Appl. Mater. Interfaces* 13 (2021) 49027.

Deposition and laser treatment of transparent titanium dioxide films

Dmytruk, I.M.¹, Berezovska, N.I.¹, Yeshchenko, O.A.¹, Hrabovskyi, Ye.S.¹,
Podust, H.P.¹, Romanovska, N.I.², Manoryk, P.A.²

¹Taras Shevchenko National University of Kyiv, Kyiv, Ukraine, igor_dmytruk@knu.ua

²L.V. Pisarzhevsky Institute of Physical Chemistry of NAS of Ukraine, Kyiv, Ukraine

The development of the formation technology of titanium dioxide (TiO_2) films on different substrates and their subsequent treatment with femtosecond laser radiation is presented. The interest in depositing TiO_2 layers on various substrates is largely due to the photocatalytic and self-cleaning properties of TiO_2 that is crucial for optical elements operating under harsh environmental conditions. Different polytypes (brookite, anatase and rutile) of TiO_2 can transform into each other under certain treatment, which, in turn, can improve the functional properties of TiO_2 films. The femtosecond laser treatment provides a simple and fast method for contactless modification of thin films. This kind of processing is resulted in either complete film removal or the modification of its intrinsic structural or electronic states. The film thickness, the laser photon energies, the substrate type influence the processes on the surface/interface and the parameters of laser-induced patterns.

The TiO_2 film obtained by depositing a sol synthesized by a sol-gel method onto substrates (glass, glass with ITO) using spin-coating method followed by drying and calcination at 450°C. After calcination, the TiO_2 film becomes significantly thinner and denser. Further modification has been performed using femtosecond laser irradiation ($\lambda = 800$ nm, the pulse repetition frequency 1kHz, the pulse duration τ of ~ 100 fs, scanning velocity 1 mm/s). During the treatment with linearly polarized femtosecond laser irradiation the pulse irradiation energy density was around $0.32 \text{ J}\cdot\text{cm}^{-2}$ that was under the laser damage threshold fluencies for TiO_2 . Thus, we selected laser treatment conditions to preserve sufficient transparency of the TiO_2 film while achieving the desired hydrophobic–hydrophilic balance. The laser treated area of TiO_2 film on glass demonstrated hydrophilic properties.

For the TiO_2 films on ITO glass, we observed a complex broad and intense emission band in the range of 280–550 nm at 266 nm excitation, originating from the recombination of free and bound excitons. In PL spectra of the TiO_2 films on glass as-grown and laser-treated, the emission bands related to the substrate and defect states emission are more intense compared to the photoluminescence of TiO_2 films.

The present research is supported by the National Research Foundation of Ukraine within the project 2025.06/0087 ‘Nanostructured titanium dioxide films for coating of optical elements’.

Design of SOI transistors taking into account the influence of a floating body and a controlled base

Taras Benko

Vasyl Stefanyk Carpathian University, Ivano-Frankivsk, Ukraine
taras.benko@pnu.edu.ua

Currently, the rapid development of electronics is causing the emergence of new technologies for creating and designing SOI transistors. The process of manufacturing SOI-MON floating-body transistors begins with the creation of active regions in the silicon layer of the device, which will ultimately contain the source, drain, and gate of the transistor. These active regions are created by removing excess silicon through a photolithographic process that serves to isolate the individual active regions from each other. The voids in the device layer created by the photolithographic process are filled with silicon dioxide to restore a flat surface on the substrate.

The proposed structure starts with an n-gate MOS transistor, which is particularly attractive, being widely used with SOI substrate technology. Unlike the conventional, source-bound layout style, the n-gate layout style uses polysilicon gate extensions, parallel, on both sides of the channel, to create insulated contacts between the element surfaces.

Using these contacts, independent body tilt can be applied to individual devices in a partially depleted SOI circuit. In general, the analysis of literature sources and the state of the problem showed the relevance of this topic and the need for further scientific and applied research to improve the design of SOI MOS transistors with a floating body.

This technology can be used to address low-voltage operation without any loss in speed or increase in source leakage. Alternatively, it can be used to speed up the operation of the circuit without any increase in power consumption. The proposed structure starts with an n-gate MOSFB, which is particularly attractive and widely used with SOI substrate technology. Unlike the conventional, source-bound layout style, the n-gate layout style uses polysilicon gate extensions, parallel, on both sides of the channel, to create an isolated contact between the element surfaces.

- [1]. C.F. Edwards. A Multibit Delta-Sigma Modulator in Floating-Body SOS/SOI CMOS for Extreme Radiation Environments. IEEE Journal of Solid-State Circuits, 34, 937. 1999.

Development of a device for recording heart rhythms based on the ESP32 microcontroller and thin film structures

Volodymyr Hryha, Myroslav Pavlyuk, Vitalii Martyniuk

Vasyl Stefanyk Carpathian University, Ivano-Frankivsk, Ukraine

vitalii.martyniuk.20@pnu.edu.ua

The work was carried out within the framework of the MES project “Multifunctional Sensor Microsystem for Non-Invasive Continuous Monitoring and Analysis of Human Biosignals,” State Registration Number: 0124U000384. The development of modern biomedical microsystems, in particular systems for monitoring cardiac activity, requires the use of highly efficient input/output cascades that ensure minimal energy loss, rapid response to changes in the input signal, and the formation of output pulses with specified parameters. In this context, thin film CMOS structures based on silicon-on-insulator (SOI) technology play a significant role, as they are characterized by low parasitic capacitance, high resistance to radiation, and stability under temperature changes. The use of these structures allows the integration of sensor modules, transistor cascades, and auxiliary circuits in a single crystal, which is particularly relevant for medical microsystems designed for autonomous operation and accurate measurement of physiological parameters.

In the case of an ESP32-based heart rate monitoring device, thin film structures are used in sensor elements such as the AD8232, which registers weak electrocardiographic signals. The use of thin film technologies in such sensors provides increased sensitivity, stability, and reduced noise levels, which is critical when analyzing the body's electrophysiological signals. This enables accurate data transmission to the microcontroller for further processing and visualization of cardiac activity indicators in real time.

Input stages of thin film structures provide protection against electrostatic discharges and overvoltage, as well as signal normalization and filtering, while output stages ensure fast and accurate data transmission. Integrating these elements into sensor microsystems enables reliable devices that meet modern medical electronics requirements.

The use of thin film CMOS structures in sensor modules, combined with software methods for data collection, processing, and visualization, ensures system integrity and effective monitoring of physiological parameters such as ECG, pulse, and blood oxygen saturation. An effective way to improve such systems is computer modeling of input and output stages in PPE environments—TopSPICE, LTSpice, MicroWind, VSCode—which helps evaluate thin film behavior and optimize performance for medical electronics.

[1]. Laconte J., Raskin J.-P., Flandre D. Micromachined Thin-Film Sensors for SOI-CMOS Co-integration. – Berlin: Springer, 2006. – 256 p.

Development of a multi-frequency programmable ring oscillator based on NOT logic elements.

Taras Benko, Vladislav Mamroha.

Vasyl Stefanyk Carpathian University, Ivano-Frankivsk, Ukraine
taras.benko@pnu.edu.ua

To build a ring oscillator, you need series-connected inverters, which are available in the standard LT Spice library. A standard inverter has input voltage, output voltage, and control pins that can be used to change the inverter's operating mode depending on the voltage level applied to it[1]. By default, the operating mode input will be grounded.

Among the parameters for the inverter are logic high and low, $V_{high} = 1$ and $V_{low} = 0$ respectively, signal rise and fall times, $T_{rise}=0$ and $T_{fall}=T_{rise}$ respectively, output RC time constant Tau, output capacitance and impedance, $C_{out} = 0$ and $R_{out} = 1$ respectively.

Figure 1 shows the series-connected inverters from the LT Spice library implementing a ring oscillator. In this circuit, the inverter time delay parameter is set to 1 ns.

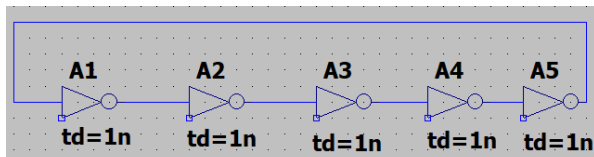


Figure 1. Series-connected inverters in the LT Spice environment.

From the voltage-time diagram in Figure 2. we can determine the period of the signal generated by the inverters, which is 4ns. Hence, if the signal frequency is f.

$$f = \frac{1}{T} f = \frac{1}{T}$$

Then, substituting the value of the period, we get the frequency

$$f = \frac{1}{T} = \frac{1}{4\text{ns}} = \frac{1}{4 \cdot 10^{-9}} = 4 \cdot 10^9 = 4\text{GHz}$$

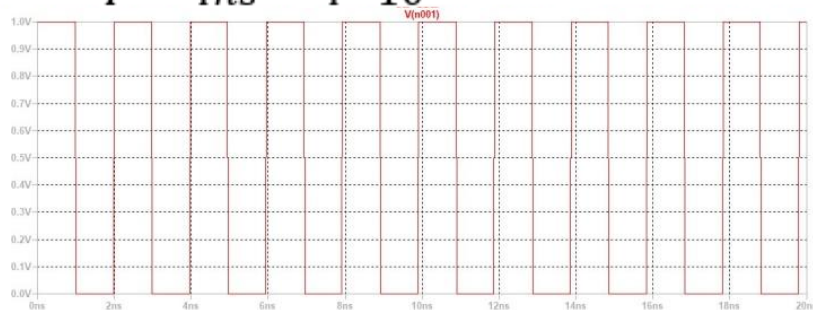


Figure 2. Timing diagram of the ring oscillator signal.

[1]. Akino T. A Clock Generator Driven by a Unified-CBiCMOS Buffer Driver for High Speed and Low Energy Operation / T. Akino, T. Hamahata // 16th International Workshop, PATMOS 2006. – France, 2006. – P. 225-236.

Features of removing anti-reflective coating from the surface of damaged germanium optical elements

Malanych G.P., Tomashyk V.M., Synhaivs'kyi O.F.

V.Ye. Lashkaryov Institute of Semiconductor Physics, National Academy of Sciences of Ukraine, Kyiv, Ukraine, e-mail: galya.malanich@gmail.com

The paper presents the results of one of the important stages of the process of restoring damaged germanium optical elements that have not been mechanically defected, but have experienced degradation of the anti-reflective coating material – chemical removal of the anti-reflective coating from the surface of the optical elements. For the studies, we used whole elements (lenses, optical windows) with damaged anti-reflective coating, which are usually subject to recycling exclusively as secondary raw materials.

Chemical etching compositions were prepared using the following reagents: H_2O_2 , HBr and an organic solvent (ethylene glycol or lactic, oxalic and acetic acids). Surface conditions of crystals after treatment were examined through microstructure investigation by using a metallographic microscope MIM-7 with a digital video camera eTREK DCM800 (8 Mpix). The roughness of the polished surfaces was measured using a NanoScope IIIa Dimension 3000TM scanning probe microscope (Digital Instruments, USA).

The thickness of the removed layer of antireflective coating during the treatment with the optimized etchant composition with the best polishing properties of the germanium surface was 1.5–5 μm and additionally the near-surface germanium layer was $\sim 100 \mu\text{m}$. It was found that chemical treatment reduces the concentration of near-surface acceptor impurities of the anti-reflective coating to $5 \cdot 10^{13} \text{ cm}^{-3}$. Increasing the duration of the etching process resulted only in excessive dissolution of germanium. The roughness parameters of the germanium surface after removal of the antireflective coating material corresponded to the requirements for polished surfaces and did not exceed the values of $R_z \leq 50 \text{ nm}$.

It was established that optimized bromine-evolving etching compositions are characterized by high-polishing properties and can be recommended for chemical removal of a damaged anti-reflective coating from the surface of optical elements.

The work was carried out within the framework of the project 2023.04/0010 “Development of the technology for restoration of germanium optical elements of thermal imaging devices for the repair of armored and aviation equipment” of National Research Foundation of Ukraine. The authors express their sincere gratitude to the defenders of Ukraine and the personnel of the Ministry of Emergency Situations, whose courage and dedication made it possible to conduct this study and share the results with the scientific community.

Heat pipe with induction heating of the Core: mathematical modeling and efficiency analysis

Mazur, T.M.¹, Vashchyshak, I.R.¹, Vashchyshak, S.P.², Mazur, M.P.¹

¹ Ivano-Frankivsk National Technical University of Oil and Gas, Ivano-Frankivsk, Ukraine,
tetiana.mazur@nung.edu.ua

²King Danylo University, Ivano-Frankivsk, Ukraine

The results of mathematical modelling of a wick heat pipe with induction heating of the core, designed for efficient transfer of low-temperature heat flow in conditions of limited dimensions, are presented.

The design includes a thin-walled copper casing, a porous wick structure made of non-magnetic stainless steel, and a magnetic stainless steel core heated by a cylindrical induction coil. A heat balance model was developed that takes into account: induction heating of the core, heat capacity of the elements, and heat loss during free convection.

The electrical part of the system was modelled in Multisim 14 as a parallel resonant circuit. The maximum thermal power was 68.8 W in the vertical position compared to 10 W in the horizontal position. Heat transfer efficiency depends significantly on the angle of inclination. Normal operation is ensured up to 70°; at 80°, operability is maintained, but efficiency decreases due to an increase in gravitational resistance to the movement of the working fluid (Fig. 1). For reliable operation at larger angles, it is advisable to reduce the radius of the wick structure (increasing the capillary pressure), increase the thickness or number of mesh layers, and use working fluids with lower surface tension and better wetting properties.

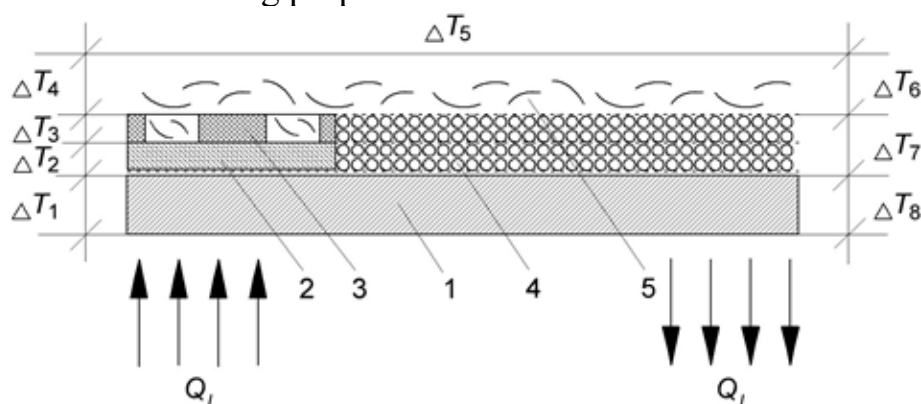


Fig. 1. Temperature differences along the length of a tube with a porous wick

The proposed heat pipe with induction heating of the core is effective and reliable over a wide range of inclination angles. The theoretical results form the basis for further experimental research and optimisation of design parameters.

Impedance spectroscopy of thermoactivated porous carbon material

Solomovskyi, R.V.¹, Nagirna, N.I.², Mandzyuk, V.I.¹

¹ Vasyl Stefanyk Carpathian National University, Ivano-Frankivsk, Ukraine,
volodymyr.mandzyuk@pnu.edu.ua

² Separate Structural Subdivision "Professional College of Electronic Devices",
 Ivano-Frankivsk National Technical University of Oil and Gas, Ivano-Frankivsk, Ukraine

Using the impedance spectroscopy method, an analysis of the kinetics of the electrochemical insertion of lithium ions into a porous carbon material obtained by thermal activation of porous carbon material at 400°C for 2.5 h was carried out. For electrochemical system based on this material, the Nyquist diagram (Fig. 1) were recorded and an equivalent electrical circuit (Fig. 2) was selected that satisfactorily model the impedance spectra in the studied frequency range of 10⁻² - 10⁵ Hz. A physical interpretation was proposed for each element of the circuit and the dependence of these elements on lithium ions insertion degree was analyzed.

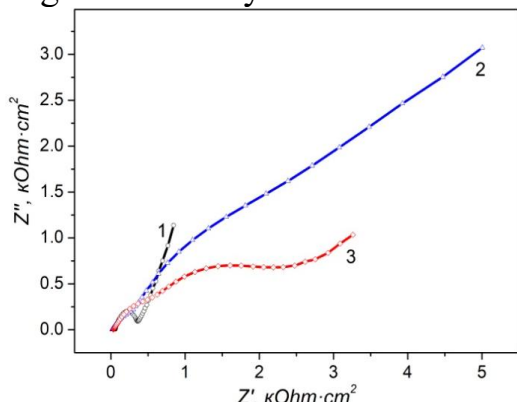


Fig. 1. Nyquist diagrams at different insertion degree of lithium ions: 1 – $x = 0.019$; 2 – $x = 0.187$; 3 – $x = 0.229$.

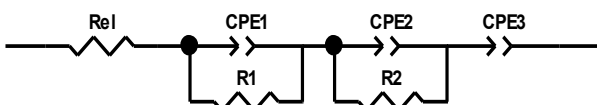


Fig. 2. The equivalent electrical circuit of process of lithium ion insertion into the sample.

proportion of mesopores, and the formation of a solid electrolyte interface more ideal in a structure create more favorable kinetic conditions for the lithium ion insertion into the explored sample, as a result of which the diffusion coefficient of lithium ions exceeds this value for the initial non-activated material more than 2 times and is $5 \cdot 10^{-8} \div 1 \cdot 10^{-11} \text{ cm}^2/\text{s}$ when the insertion degree increases.

The diffusion coefficient D of lithium ions into the structure of electrode material was calculated according the equation

$$\sigma = \frac{RT}{n^2 F^2 A c_{Li} \sqrt{2D}},$$

where σ is the Warburg coefficient, R is the universal gas constant; T is the absolute temperature; n is the number of transferred electrons; F is the Faraday constant; A is the geometric area of the electrode; c_{Li} is the molar concentration of lithium ions transferred through the electrolyte and inserted into the volume of the electrode material or located on its surface.

It is set that the opening of internal porosity, an increase in the

Investigation of Liquid Crystal Structures for Optical Acetone Vapor Sensors in the Visible and Near-Infrared (NIR) Spectral Ranges

Kremer, I.P.¹, Mykytyuk, Z.M.¹, Ivakh, M.S.¹, Kachurak, Y.M.¹,
Shymchyshyn M.O.²

¹*Lviv Polytechnic National University, Lviv, Ukraine, iryna.p.kremer@lpnu.ua*

²*European University, Lviv, Ukraine, maryan.shimchyshyn@e-u.edu.ua*

In the context of rapid advances in medicine, environmental monitoring, and human safety, there is a growing demand for highly sensitive, selective, and fast-response sensors for detecting volatile organic compounds (VOCs), particularly acetone. Acetone serves as a key marker in fields ranging from the diagnosis of metabolic disorders such as diabetes mellitus to air quality control and fire safety. Organic materials, especially liquid crystal mixtures, have shown strong potential as sensitive layers in gas sensors [1], though their use is limited by insufficient selectivity under real conditions with interfering components such as water vapor, ethanol, and acetaldehyde.

Improving selectivity is therefore critical, especially in biomedical applications such as non-invasive breath analysis [2]. A promising approach involves extending detection into the near-infrared (NIR, 0.9–1.7 μm) spectral range, which is of interest for environmental and biomedical monitoring [3]. Based on CB15 and E7 liquid crystal mixtures, we developed and studied a sensitive structure optimized for optical acetone sensors. The composition provided maximal optical response in the visible region, while NIR characterization broadened the analysis range and enhanced selectivity. The optical properties, particularly NIR absorption, can be tuned through mixture composition and film thickness control.

[1]. Mykytyuk, Z. M., Kremer, I. P., Ivakh, M., Diskovskyi, I. S., Khomyak, S. V. Optical sensor with liquid crystal sensitive element for monitoring acetone vapor during exhalation. *Molecular Crystals and Liquid Crystals*. 2021. V. 721, No 1. P. 24–29.

[2]. Mykytyuk Z., Fechan A., Shymchyshyn O., Rudyi A., Nazarenko V., Petryshak V. Sensor Network Based on Gas Smart Sensors for Environmental Monitoring. *Modern Problems of Radio Engineering Telecommunications and Computer Science Proceedings of the 11th International Conference Tcset 2012*. P. 503-504.

[3]. Hezhuang Liu, Jingyi Wang, Daqian Guo, Kai Shen, Baile Chen and Jiang Wu. Design and Fabrication of High Performance InGaAs near Infrared Photodetector. *Nanomaterials*. 2023. V. 13, No 21. P. 2895.

Investigation of the radiation-induced process of the titanium silicate surface using Raman spectroscopy

A. Zaporozhets*, H. Vasylyeva, K. Skubenych, M. Pop

Uzhhorod National University, Uzhhorod, Ukraine, anatolii.zaporozhets@uzhnu.edu.ua

The removal of radionuclides from aqueous solutions is an important scientific task that remains relevant. Many scientific works are dedicated to the creation of new effective adsorbents, the study of their structure and morphology, as well as their adsorption capacity for cations of heavy metals and radionuclides [1-3]. For example, in the publication [2], the organic adsorbent based on the activated carbon for Sr^{2+} and Ba^{2+} removal is described. The recent publication [3] reports effective adsorption of Iodine anions by a hollow ball of oxidized graphene. Inorganic adsorbents such as ferrites, zeolites, aerogels, or TiO_2 -based adsorbents [1] have also been the subject of many publications.

It is well known that all isotopes of the same element have identical chemical properties. That is why researchers often use stable isotopes of potentially harmful radionuclides that emit a certain type of radioactivity for their studies. Based on the research results, conclusions are drawn about the suitability of adsorbents for the removal of radionuclides from aqueous solutions. However, the resistance of adsorbents to the effects of intense ionizing radiation remains underexplored. Only a few publications are dedicated to studying the radiation resistance of adsorbents. Although the radiation resistance of materials is an important parameter [4, 5]. According to the publication [6], irradiation of adsorbents in the air or in some inert gas atmosphere does not always provide a clear pattern of the changes in the adsorbent's surface under the influence of ionizing radiation in real conditions, that is, during the adsorption of radionuclides from aqueous solutions.

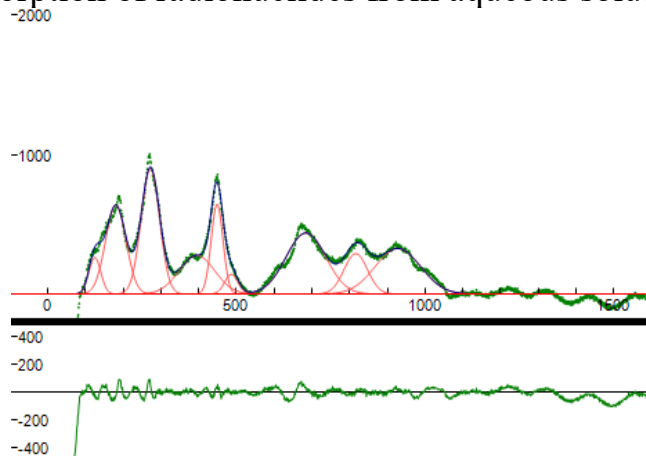


Fig.1. Raman spectrum of the titanium silicate irradiated in a 0.1 M nitric acid medium.

The aim of this work is to investigate the radiation-induced changes in the surface of titanium silicate under the influence of intense beta radiation in an aqueous solution with pH=1 and pH=7 using Raman spectroscopy.

The irradiation of titanium silicate was carried out using the 'Sirius' facility. Samples of the adsorbent before and after irradiation were studied using a Raman spectrometer [6]. The Raman spectra were analyzed using the software application Fityk-1.3.1 setup.exe. An example of the Raman spectrum is presented in Fig. 1.

The results of the work show that irradiation with high-energy electrons in a 0.1 M nitric acid medium significantly affects the surface state of titanium silicate.

The results of the work also show that irradiation with high-energy electrons in a 0.1 M nitrate acid medium reduces the adsorption capacity of titanium silicate for divalent metal cations. This fact must be taken into account when using titanium silicate for the adsorption of radionuclides from aqueous solutions, as this adsorbent loses its adsorption capacity when irradiated in an acidic environment.

- [1]. H.Vasylyeva, I. Mironyuk, I. Mykytyn, Kh. Savka, *Equilibrium studies of yttrium adsorption from aqueous solutions by titanium dioxide*, Applied Radiation and Isotopes, 168, 109473 (2021).
<https://doi.org/10.1016/j.apradiso.2020.109473>
- [2]. S. Zuhara, G. McKay, *Single and binary pollutant adsorption of strontium and barium on waste-derived activated carbons: Modelling, regeneration and mechanistic insights*, Environmental Technology & Innovation, 39, 104220 (2025). <https://doi.org/10.1016/j.eti.2025.104220>.
- [3] I. Mironyuk, J.-C. Grivel, et al., *Structural-morphological and adsorption properties of hollow balls of oxidized graphene obtained by auto-combustion of saccharose*, Nano-Structures & Nano-Objects, 41, 101462 (2025).
<https://doi.org/10.1016/j.nanoso.2025.101462>.
- [4]. Y. Petrenko, V. Kotsyubynsky, L. Turovska, L. *Powder-Filled Epoxy Resin as a Promising Material for Cosmic Radiation Shielding* (In: Kołodziejczyk, A., Pyrkosz-Pacyna, J., Grabowski, K., Malinowska, K., Sergijenko, O. (eds) Selected Proceedings of the 6th Space Resources Conference. SRC 2023. Springer Aerospace Technology. Springer, Cham. 2024)
https://doi.org/10.1007/978-3-031-53610-6_11
- [5]. K. Filak-Mędoń, K.W. Fornalski, M. Bonczyk, et al. *Graphene-based nanocomposites as gamma- and X-ray radiation shield*. Sci. Rep. 14, 18998 (2024). <https://doi.org/10.1038/s41598-024-69628-5>
- [6]. H. Vasylyeva, et al., *Radiation-Induced Processes in Commercially Available Samples of Activated Carbon Under the Influence of Gamma- and Beta-Radioactivity*. J. Nano- Electron. Phys. 17 (3) 03028 (2025)
[https://doi.org/10.21272/jnep.17\(3\).03028](https://doi.org/10.21272/jnep.17(3).03028)

Ion-conducting membranes based on double hydrophilic block copolymers

Kunytska, L.R., Permiakova, N.M., Nesin S.D., Klepko V.V.

*Institute of Macromolecular Chemistry of the NAS of Ukraine, Kyiv, Ukraine
larisa_kunitskaya@ukr.net*

In recent years, significant attention has been devoted to the development of alternative energy sources, among which fuel cells (FCs) have emerged as particularly promising. A key component of FCs is polymer proton-conducting membranes (PPCMs), which enable high-efficiency conversion of chemical bond energy into electrical energy. Most of the work is dedicated to ion-conducting PPCMs based on polyethylene oxide (PEO), however, the high crystallinity of PEO leads to low ion conductivity at room temperature, which affects the high rate capability of energy sources.

As it was shown, one of the promising approaches to reduce the crystallinity PEO-chains is to create block copolymers, which amorphous side chains are able to cooperatively interact with the central PEO block and form intramolecular polycomplexes (IntraPC). We also established recently that electrolyte membranes based on block copolymers of polyethylene oxide and polyacrylamide exhibit a high degree of ion conductivity, and the introduction of additional ionogenic groups -COOH through partial hydrolysis of polyacrylamide blocks leads to an improvement in the conductive properties of the membranes [1].

In the present work, an attempt to completely replace the amide groups of acrylamide units with carboxyl ones is considered. With this aim in mind, diblock- and triblock copolymers comprising polyethylene oxide and polyacrylic acid PAAc-*b*-PEO and PAAc-*b*-PEO-*b*-PAAc have been synthesized. Two series of membranes based on mentioned block copolymers were prepared by using a solution casting technique, and their ion (proton) conductivity was examined at the ambient temperature and in the present of LiPF₆.

It was established that the best conductivity, which is in the range of $4.2 \cdot 10^{-5}$ – $9.8 \cdot 10^{-5}$ S·cm⁻¹, corresponds to the films obtained on the basis of PAAc-*b*-PEO-*b*-PAAc block copolymer. PAAc-*b*-PEO membranes had a conductivity two orders of magnitude lower, however, the introduction of 3-9 weight % of LiPF₆ made it possible to increase conductivity to $4.49 \cdot 10^{-6}$ – $1.98 \cdot 10^{-5}$ S·cm⁻¹. Obtained results demonstrate the possibility of using commercially available, nontoxic solid polymer electrolytes in electrochemical devices.

[1]. Kunytska L.R., Zheltonozhska T.B., Nesin S.D., Klepko V.V. Polymeric conducting membranes based on PEO-containing intramolecular polycomplexes. *Polymer Journal*. 2024. V. 46, № 3. P. 186-194.

Methods and models for metasurface modelling for application in biosensors

Politanskyi, R.L.¹, Vistak, M.V.², Andrushchak, A.S.³, Mykytyuk, Z.M.³, Diskovskyi, I.S²

¹*Yuriy Fedkovych Chernivtsi National University, Chernivtsi, Ukraine,*
r.politanskyi@chnu.edu.ua

²*Danylo Halytsky Lviv National University, Lviv, Ukraine, vistak_maria@ukr.net.*

³*National University Lviv Polytechnik, Lviv, Ukraine, zynovii.m.mykytiuk@lpnu.ua*

One of the methods for modelling metasurfaces is the Floquet method. This method can be used for interaction of electromagnetic waves and a flat surface with periodically changing properties. The spatial period of these changes is much smaller than the wavelength. In some cases, the Floquet method allows to simplify task. One of such problems is the problem of the field formed by linear currents distributed on a flat surface. Fig. 1a shows a surface model, Fig. 1b represents the distribution of the current density, at which the metasurface creates a plane wave with a frequency of 3 GHz.

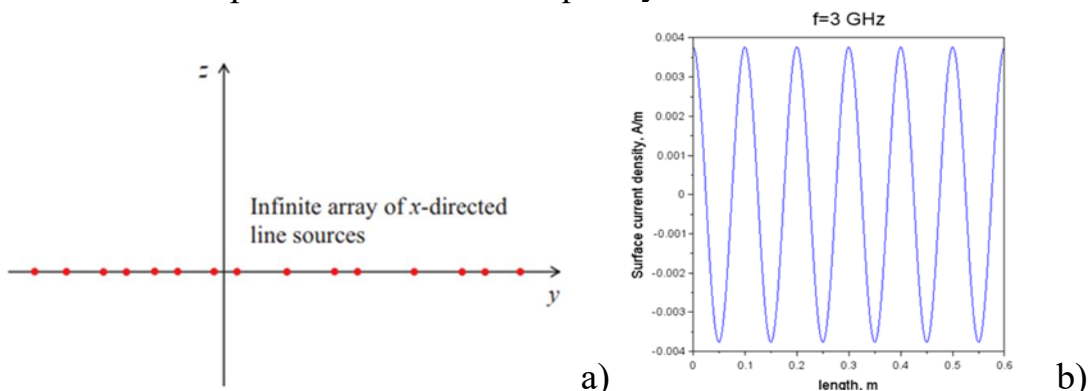


Fig. 1. a) model of a metasurface with linear currents ([1]), b) the distribution of current density, at which the metasurface generates a plane wave

As a result of the research, an algorithm is developed for determining the distribution of currents on a metasurface that generates a given field. The developed methods can be used to model and detect weak fields sensitive to the presence of biomolecules (biosensors). This research has received funding from the Ministry of Education and Science of Ukraine in the frames of 'Nanoelectronics'(No. 0123U101695).

- [1]. Thorkild B. Hansen. Array of line sources that produces preselected plane waves. Wave Motion. Volume 106, 2021, 102791.
- [2]. Sjöberg, D., Engström, C., Kristensson, et al. (2003). A Floquet-Bloch decomposition of Maxwell's equations, applied to homogenization. (Tech. Rep. LUTEDX/TEAT-7119)/1-27/(2003). Dept. of Electroscience, Lund University.
- [3]. L. Ma, B. Wang, S. Wang, L. Li, et al. Tunable quasi-bound states in the continuum in reflective secondary grating metasurfaces for biochemical sensing. Appl. Phys. Lett. 127, 061703 (2025).

Modeling of Signal Converters for SoC Microsystems Based on Thin-Film SOI Devices

Igor Kohut, Oleksandr Samarchuk, Andriy Prystaiko

Vasyl Stefanyk Carpathian University, Ivano-Frankivsk, Ukraine igor.kohut@pnu.edu.ua

System-on-Chip (SoC) represents one of the key directions in the development of modern micro- and nanoelectronics. Essential components of such systems are signal conversion units: analog-to-digital (ADC) and digital-to-analog (DAC) converters, which ensure an optimal balance between speed, accuracy, and power consumption. A promising approach to implementing these functional blocks is the use of thin-film transistors (TFTs), which enable cost-effective, scalable, and energy-efficient solutions. An additional advantage of TFTs is their compatibility with flexible or non-traditional substrates, opening new opportunities for applications in sensor devices.

Modeling of such converters requires consideration of the specific properties of TFT-based resistors, capacitors, and transistors fabricated on thin SOI films: limited carrier mobility, parameter drift over time and under temperature variations, increased leakage currents, and noise effects. These factors directly affect the accuracy, stability, and dynamic range of ADCs and DACs, which are critical for the reliable operation of sensor microsystems.

Various types of ADCs and DACs are used to implement signal conversion in TFT-based microsystems, and their selection determines the trade-off between speed, accuracy, and power consumption. SAR and Delta-Sigma ADCs provide high precision and energy efficiency for sensor inputs, while flash and pipeline ADCs are employed in high-speed or multi-channel systems. Common DAC architectures include R-2R, binary-weighted, current-steering, and charge-redistribution designs, which enable precise analog signal generation within a compact integrated area.

Thus, modeling of TFT-based signal converters using various types of ADCs and DACs is a key step in the development of next-generation sensor systems. It enables the optimization of architectures, the selection of appropriate conversion methods, and the achievement of required accuracy and power consumption, as well as the analysis of frequency and temperature dependencies at the given technology level. The modeling was carried out using Microwind and LTspice, which allow simulation of electrical and temporal characteristics of converters while taking into account the specific properties and technologies of TFTs.

This work was carried out within the framework of the Ministry of Education and Science of Ukraine project “Multifunctional Sensor Microsystem for Non-Invasive Continuous Monitoring and Analysis of Human Biosignals,” State Registration Number: 0124U000384.

Modified Probe Method for Measuring the Electrical Resistance of Contact Structures for Thermoelectric Energy Converters

Lysko, V.V.^{1,2}, Razinkov, V.V.¹, Havryliuk, M.V.^{1,2}, Strusovskyi, K.I.²

¹Institute of Thermoelectricity of the NAS of Ukraine and MES of Ukraine, Chernivtsi, Ukraine, v.lysko@gmail.com

²Yuriy Fedkovych Chernivtsi National University, Chernivtsi, Ukraine

One of the current tasks in the field of thermoelectricity is the miniaturization of thermoelectric energy converters, which could substantially reduce their cost and expand the scope of practical applications. The primary obstacle to this progress is the relatively high contact resistance, since – as is well established – the influence of contact resistance on the efficiency of a thermoelectric energy converter increases as the device dimensions decrease [1].

Therefore, the development of methods and equipment for analyzing contact structures in thermoelectric energy converters, as well as the creation and optimization of their fabrication technology, is an important task.

A detailed physical model of the process for determining the electrical contact resistance at the “metal-thermoelectric material” interface has been developed based on the probe measurement method [2]. Computer modeling demonstrates that the error in determining the electrical contact resistance, caused by the non-isothermal conditions in the contact structure, can be significantly reduced by thermostabilizing one side of the structure; under such conditions, the error does not exceed 2%.

To implement this measurement technique, a dedicated setup was designed and manufactured at the Institute of Thermoelectricity (Ukraine); its external view is shown in Fig. 1.

A series of experimental investigations was conducted to evaluate the contact resistance of the “nickel-extruded Bi-Te-based thermoelectric material” structure. The results reveal a clear correlation between the surface roughness of the thermoelectric material and the contact resistance: the lowest values of contact resistance are achieved when the thermoelectric surface is polished.

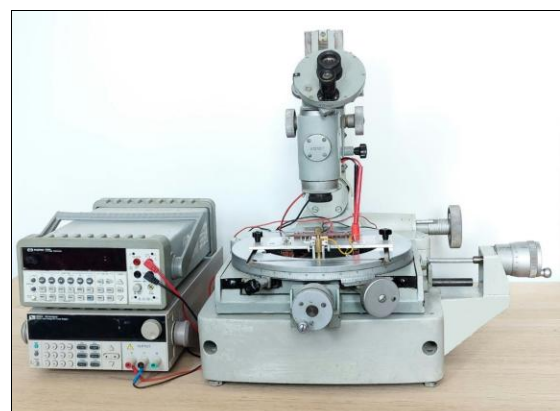


Fig. 1. External view of the measurement setup

[1]. Vikhor L., Lysko V., Kotsur M., Havrylyuk M. *J. Appl. Phys.*, 2025, 137(9), 094503.

[2]. Anatychuk L., Lysko V., Strusovskyi K. (2023). *J. of Thermoelectricity*, (4), 38–48.

Multi-channel thermoelectric heat meter for medical applications

Kobylianskyi, R.R.^{1,2}, Boichuk, V.V.^{1,2}

¹*Yuriy Fedkovych Chernivtsi National University, Chernivtsi, Ukraine,*
boichuk.vadym.vi@chnu.edu.ua

²*Institute of Thermoelectricity of the NAS and MES of Ukraine, Chernivtsi, Ukraine*

The paper presents the development of a multi-channel device for simultaneous measurement of temperature and heat flux density on the human body surface using contact methods [1]. The device incorporates advanced thermoelectric sensors to achieve high sensitivity, stability, and miniaturization [2]. The integration of nanoscale thermoelectric materials significantly enhances the device's measurement accuracy ($\pm 0.1^\circ\text{C}$ for temperature and 5% for heat flux density) while maintaining minimal dimensions [3].

A specialized computer program has been developed for processing data from the electronic registrator, accumulating measurements, and displaying results in real-time on a personal computer. This enables continuous monitoring of a person's temperature and thermal state, which is crucial for early detection of inflammatory processes and various diseases. The device's structure includes thermoelectric sensors with built-in temperature detectors, analog-to-digital converters, a multiplexer for digital signal commutation, and a microcontroller for signal processing.

This approach represents a significant advancement in medical diagnostics technology, allowing for express diagnostics during mass patient examinations [4]. The device's capability to simultaneously measure heat emissions from multiple body areas using up to 10 thermoelectric sensors makes it particularly valuable for improving diagnostic methods and increasing the reliability of obtained results.

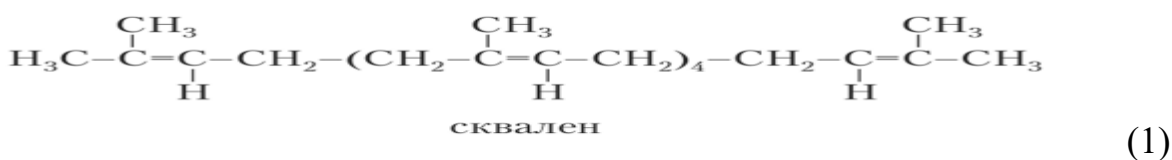
- [1]. Mishra S., Satpathy S., Dehury J. Recent advances in thermoelectric materials and devices for medical applications: A comprehensive review. *Journal of Materials Science*. 2021. Vol. 56. P. 16105-16132.
- [2]. Zhang X., Zhao L.D. Thermoelectric materials: Energy conversion between heat and electricity. *Journal of Materomics*. 2022. Vol. 8. No. 2. P. 251-271.
- [3]. Wang Y., Yang L., Shi X.L. Flexible thermoelectric materials and devices: From materials to applications. *Advanced Materials*. 2020. Vol. 32. No. 49. P. 2003557.
- [4]. Kobylianskyi R.R., Prybyla A.V., Konstantynovych I.A., Boychuk V.V. Results of experimental research on thermoelectric medical heat flow sensors. *Journal of Thermoelectricity*, 2022, (3-4), pp. 68-81.

Nanostructure and biochemical properties of vegetable squalene for cosmetics speeches and drugs

Sergiy Kurta, Olha Khatsevych, Sofiya Fedorchenko, Ihor Mykytyn Cristsna
Kushmeliuk

¹ Department of Chemistry Vasyl Stefanyk Precarpathian University, Ivano-Frankivsk,
Ukraine, sergiykurta@pnu.edu.ua

Hexaoligomeric isoprene (squalene) is an organic unsaturated compound with the formula C₃₀H₅₀. It is a liquid oligodienic hydrocarbon, an acyclic triterpene composed of six isoprene units with a freezing point of -55 °C and boiling point of +203 °C, predominantly found in the surface tissues of plants, animals, and human skin. It is a colorless hydrocarbon, and its hydrogenated derivative is called squalane (C₃₀H₆₂), with most commercial samples having a natural origin.[1]. Unlike unsaturated squalene, due to the complete absence of double bonds, squalane is resistant to autoxidation. This, combined with its lower cost and desirable physical properties, has led to its wide use in cosmetics and perfumery.[2].



Squalene-2,6,10,15,19,23-hexamethyltetracosane-2,6,10,14,18,22-hexaene.[3].

Traditionally, squalene was obtained from shark liver. Approximately 3,000 sharks are needed to produce one ton of squalene. [4]. Due to environmental concerns, alternative sources such as amaranth and olive oil, rice, and sugarcane have been commercialized and as of 2021, they supply around 40% of the total industry volume [5]. One highly valuable property of squalene is its ability to react with water molecules and release oxygen, converting to squalane through the following reaction:



At the chemistry department of the Faculty of Natural Sciences of Vasyl Stefanyk Precarpathian National University in Ivano-Frankivsk, Ukraine, applied research was conducted on various technological methods for the extraction and deparaffinization of squalene and squalane from amaranth oil (amaranthus seed oil). The amaranth oil was extracted from the seeds of two species of the Amaranthus genus - A. cruentus and A. hypochondriacus, which grow in the botanical garden and dendropark of the Precarpathian University. [10]. This is a transparent liquid ranging in color from light to dark yellow. In cosmetology, it is used as a softening, nourishing, and rejuvenating agent. Amaranth, or amaranthus (Latin: Amaránthus), is a widely distributed genus of mainly annual herbaceous plants with small flowers gathered in dense spike-like

Topic 4

or corymbose inflorescences. There are over 100 known species that grow in warm and temperate regions.

As a result of experiments conducted by scientists, three methods for isolating squalene and squalane from amaranth oil were proposed. The first method involves neutralization and precipitation of salts of higher carbon acids, which make up up to 90% of amaranth oil, and isolation and rectification of squalene. However, large losses of squalene, exceeding 50%, were observed with this method. The second method, which we tested, is deparaffinization - precipitation of squalene and squalane using urea, which we previously used for deparaffinization and increasing the octane and cetane numbers of motor fuels [11]. With this method, only paraffinic and olefinic hydrocarbons with a chain length greater than C10 are separated from amaranth oil, making it suitable for squalene and squalane, which have a carbon content of up to C₃₀H₆₂. As a result, losses of squalanes decreased, and we were able to separate up to 90% of squalene and squalane from amaranth oil. However, the amount of squalene decreased to 1%, and the amount of squalane increased to 7%, according to the reaction (1) which we previously presented in our work. As a result of our work, we proposed a new, improved method for isolating saturated squalane from amaranth oil by converting unsaturated squalene through hydrogenation in an aqueous environment.

[1]. Application for registration of a patent of Ukraine No. a202401405.: Method of obtaining squalene and squalane from vegetable oils and animal fats. Authors: Kurta Serhiy Andriyovych, Zhadan Anastasia Yevgeniyevna, Tina Reiterer, Jan Josef Felix From. Application number Vh. No. 334431 Date of filing of the patent application - 03/18/2025.

[2]. Application for registration of a patent of Ukraine. Application number a202502440: Cosmetic composition with natural squalene or "composition of protective and prophylaxis lotion and cream with natural squalene/ Serhiy Kurta, Khatsevych Olga Myroslavivna, Guzio Natalia Mykolaivna, Stetsyuk Yulia Olegivna. Date of filing of the patent application - Vh. No. 869176 dated 05/26/2025.

Nanostructured Cu- and W- doped titania films as self-cleaning coatings with photoinduced hydrophilicity

Petrik I.S.¹, Smirnova N.P.¹, Eremenko A.M.¹, Borysenko M.V.¹, Vorobets V.S.², Kolbasov G.Ja.², Kolomys O.F.³

¹ Chuiko Institute of Surface Chemistry of NAS of Ukraine. Oleg Mudrak Str., 17, Kyiv-03680, Ukraine E-mail: smirnatali@gmail.com

² Institute of General & Inorganic Chemistry of NAS of Ukraine, Acad. Palladin Str. 32/34, Kyiv-03680, Ukraine

³ V. Lashkaryov Institute of Semiconductor Physics of NAS of Ukraine, pr. Nauki, 41, Kyiv-03028, Ukraine

Self-cleaning surfaces (hydrophobic or hydrophilic) are example of smart coatings – new developments of materials engineering for surface protection from corrosion, organic pollutants and microorganisms. Stable, optically transparent coatings capable of self-cleaning are highly desirable for solar panels and windows, sensor devises. The purpose of this work was the development of sol-gel synthesis of W^{6+}/TiO_2 and Cu^{2+}/TiO_2 films and the study of their photoinduced hydrophilicity and photocatalytic activity in the process of palmitic acid photodecomposition under the influence of UV irradiation, investigation of electrocatalytic properties of TiO_2 and M^{n+}/TiO_2 electrodes in the process of oxygen electroreduction.

Mesoporous nanoscale TiO_2 and W^{6+}/TiO_2 and Cu^{2+}/TiO_2 (0.1% - 10%) films applied to the surface of glass or metal (food grade steel 08X18N0, titanium foil) were synthesized by the templated sol-gel method. Raman spectra of M^{n+}/TiO_2 films showed anatase nanocrystalline phases. Band gap energy and the position of flat band potentials were estimated by direct photoelectrochemical measurements. Electrocatalytic properties of TiO_2 and W^{6+}/TiO_2 electrodes were investigated in process of oxygen electroreduction. It has been shown that modified TiO_2 films increase the catalytic activity of electrodes based on them in the oxygen electroreduction reaction, compared to unmodified TiO_2 , which is manifested in a decrease in the oxygen reduction overvoltage ΔE .

Under the influence of near-UV light, doped films acquire hydrophilic properties, more pronounced than demonstrate undoped TiO_2 coatings, the surfaces of W^{6+}/TiO_2 films are characterized by the smaller wetting angle compared to Cu^{2+}/TiO_2 . The example of palmitic acid shows their high photocatalytic activity in fatty acid photodecomposition reactions, which characterizes surfaces capable of self-cleaning under the influence of UV irradiation. The films synthesized in this work, deposited on plates of food-grade steel, which are widely used for the equipment for the food industry, showed corrosion resistance after exposure for 2000 hours in a climatic “salt chamber”.

Such films can be offered to obtain corrosion-resistant, bactericidal surfaces capable to self-cleaning.

Obtaining activated carbon from biomass by thermal activation

Ivanichok, N.Y.^{1,2}, Rachiy, B.I.², Mokliak, M.G.², Lysiv, T.², Mokliak, V.V.^{1,3}

¹ G. V. Kurdyumov Institute for Metal Physics, NAS of Ukraine, Kyiv, Ukraine,

²Vasyl Stefanyk Carpathian University, Ivano-Frankivsk, Ukraine,

natalia.ivanichok@pnu.edu.ua , mvvmcv@gmail.com

³Ivano-Frankivsk National Technical University of Oil and Gas, Ivano-Frankivsk, Ukraine

A straightforward activation approach was applied to derive porous carbon material from walnut shells. Study examined how varying the activation time at 400 °C under limited air exposure affects the structural, morphological, and electrochemical characteristics of the resulting carbon. Structural and morphological analyses of samples were conducted using SAXS, low-temperature adsorption porosimetry, SEM, and Raman spectroscopy. The carbon material obtained at 800 C [1] was placed in a ceramic container and subjected to further thermal activation using a muffle furnace. This process was carried out at 400 °C, with activation times of 1, 2 and 3 hours.

The results of the research SAXS show that extending the activation duration at a constant temperature decreases the interlayer spacing (d_{002}) from 0.38 to 0.36 nm and reduces the lateral size of graphite crystallites from 3.79 to 2.52 nm. Thermal activation nearly doubles the specific surface area (S_{BET}) of the initial carbon material and promotes the formation of a mesoporous structure, characterized by a mesopore content of around 75–78% and an average pore diameter near 5 nm (Table). The fractal dimension increases in activated samples (2.52 and 2.69) compared to the raw sample (2.17).

Table

| Sample, activ. times | Surface Area (m ² /g) | | Pore Volume (cm ³ /g) | | V _{meso} /V _Σ (%) | d Pore (nm) |
|-------------------------|----------------------------------|--------------------|----------------------------------|-------------------|--|----------------|
| | S _{BET} | S _{micro} | V _Σ | V _{meso} | | |
| raw sample | 238 | 133 | 0,133 | 0,014 | 10,5 | 2,2 |
| 1 hours | 421 | — | 0,576 | 0,445 | 77,3 | 5,5 |
| 2 hours | 431 | — | 0,521 | 0,390 | 74,9 | 4,8 |
| 3 hours | 400 | — | 0,498 | 0,387 | 77,7 | 5,0 |

Electrochemical evaluations, performed in a 6 M KOH aqueous solution, included cyclic voltammetry, galvanostatic charge/discharge, and impedance spectroscopy. The results indicate that carbon activated at 400 °C for 2 hours delivers a specific capacitance of about 110–130 F/g at discharge current densities ranging from 4 to 100 mA/g.

[1]. Ivanichok, N.Y, et al. Effect of the carbonization temperature of plant biomass on the structure, surface condition and electrical conductive properties of carbon nanomaterial. *Journal of Physical Studies*, 2021, 25.3.

Acknowledgments: The authors are grateful to the NATO Partnerships and Cooperative Security Committee for the grant to implement project G6166.

Peculiarities of creating cryogenic temperature sensors based on SOI-structures

D.Lisnykh, Yu.Khovorko, A.Druzhinin,

LvivPolytechnic National University, Lviv, Ukraine, anatolii.o.druzhynin@lpnu.ua

The work evaluates the possibility of creating cryogenic temperature sensors based on silicon-on-insulator structures with different levels of doping of the starting material. A sufficiently strong dependence of the negative temperature coefficient of resistance (NTC) opens up the possibility of creating sensitive elements of cryogenic temperature sensors with stable thermistors due to laser recrystallization of polysilicon. Since the material of the sensitive elements of the sensors was subjected to laser recrystallization, which involves minimizing trap centers in the thickness of the polycrystalline film of the SOI structures, it is possible to propose the use of such material in devices for two temperature ranges: for the cryogenic temperature interval $T=4,2\text{--}50\text{ K}$ $\beta_{\text{NTC}} = -(1\text{--}2,5)\% \times {}^\circ\text{K}^{-1}$ and for the interval $T=50\text{--}300\text{ K}$ $\beta_{\text{NTC}} = -(0,1\text{--}0,5)\% \times {}^\circ\text{K}^{-1}$. Instead, films with a positive temperature coefficient of resistance (PTC) can be used in sensitive elements of sensor devices that operate over a wide temperature range. SOI structures with a free charge carrier concentration $N_B = 1,7 \times 10^{20} \text{ cm}^{-3}$ in polysilicon films for the temperature range 4,2 – 300 K, have $\beta_{\text{PTC}} < 0,1\% \times {}^\circ\text{K}^{-1}$. It should be noted that NTC and PTC were evaluated for polysilicon resistors in SOI structures formed by laser recrystallization for the transverse direction with respect to the scanning of the laser beam during recrystallization.

[1]. Druzhinin A.A., Ostrovskii I.P., Kogut I.T., Khovorko Yu.M., Koretskii R.M., Kogut I.R. Magneto-transport properties of poly-silicon in SOI structures at low temperatures. *Materials Science in Semiconductor Processing*. 2015. V.31. P. 19–26

Polymer/inorganic hybrid nanomaterials consisting silica nanoparticles, polyacrylic acid and metal ions

Permyakova1 N.M., Klepko2 V.V.

Department of Polymer Physics, Institute of Macromolecular Chemistry of the NAS of Ukraine. Kyiv, Ukraine, permyakova@ukr.net

The present work demonstrate the synthesis and characterization of polymer/inorganic hybrid (PIH) nanomaterials consisting silica nanoparticles and polyacrylic acid ($\text{SiO}_2\text{-g-PAAc}$), which can be used as pH stimuli-responsive platforms for drug carrier systems, as well as effective matrices for the different metal nanoparticle encapsulation.

PIH samples with different number and molecular weight of the grafted PAAc chains were synthesized by free-radical polymerization of PAAc from the unmodified surface of SiO_2 nanoparticles. The presence of PAAc grafted chains in the chemical structure of PIH confirmed by ^1H NMR and FTIR spectroscopy. The molecular weights of PAAc grafts for four synthesized PIH samples, which determined by viscometry, were 20.4, 77.3, 231.2 and 250.9 kDa. The electrochemical behavior of the PIH samples in water and the acidic properties of carboxyl groups of the grafted PAAc chains were studied by potentiometric titration. The values of pK_0 for carboxyl groups of the grafted PAAc chains were determined in the range of 4.11–4.49, which was in the good agreement with the pK_0 value for individual PAAc. Thermal stability of PIH samples was studied by DTGA method. The PIH interaction with metal ions, in particular, cobalt and nickel ions, was investigated by FTIR spectroscopy and viscometry. It was revealed that grafted polymer “corona” from PAAc chains effective encapsulated Co and Ni ions, which was resulting in the formation of a water-stable $\text{Co}^{2+}/\text{PIH}$ and $\text{Ni}^{2+}/\text{PIH}$ nanocomposites.

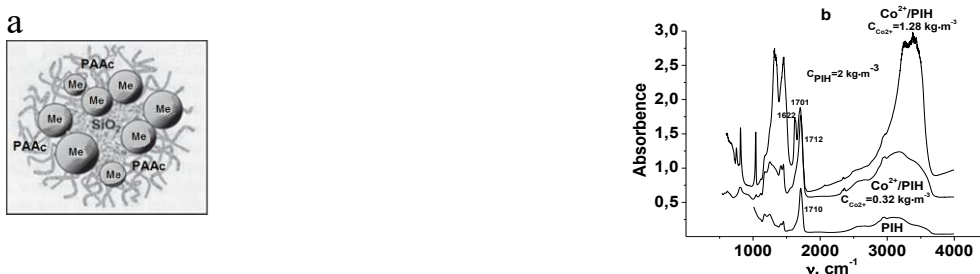


Figure 1. a - Shematic structure for Me/PIH nanocomposition. b - FTIR spectra of thin films of PIH samples and its compositions with Co salt cast from aqueous solutions on fluorite and irtran glasses.

It should be note that these PIH samples proved to be effective matrices for *in situ* synthesis of MeNPs by borohydride reduction of corresponding Me-salt to nanoparticles in aqueous PIH solutions.

Progress in positron annihilation and AI-technology for creation of highly sensitive biosensors of water pollution

Kavetskyy, T.S.^{1,2,3}, Kukhazh, Y.Y.¹, Hoivanovych, N.K.¹, Šauša, O.^{2,4},
Švajdlenková, H.^{4,5}, Zgardzińska, B.⁶, Warowna, J.⁶, Tuzhykov, A.V.³,
Soloviev, V.M.^{3,7}, Kiv, A.E.^{3,8}

¹*Drohobych Ivan Franko State Pedagogical University, Drohobych, Ukraine,*

²*Institute of Physics, Slovak Academy of Sciences, Bratislava, Slovakia,*

³*South Ukrainian National Pedagogical University named after K.D. Ushynsky, Odesa, Ukraine, kavetskyy@yahoo.com; t.kavetskyy@dspu.edu.ua*

⁴*Department of Nuclear Chemistry, FNS, Comenius University, Bratislava, Slovakia*

⁵*Polymer Institute, Slovak Academy of Sciences, Bratislava, Slovakia*

⁶*Institute of Physics, Maria Curie-Sklodowska University, Lublin, Poland*

⁷*Kryvyi Rih State Pedagogical University, Kryvyi Rih, Ukraine*

⁸*Ben-Gurion University of the Negev, Beer-Sheva, Israel*

Free volume plays a special role in polymeric materials, which are the basis for creating electrochemical biosensors. An important stage in obtaining high sensitivity and high quality of the biosensor as a whole is to ensure good adsorption of the enzyme, i.e. to ensure optimal geometric and energy characteristics of the adsorption centers in meso- and nanopores. Therefore, in the process of manufacturing the device, it is necessary to pay attention to the structural aspects associated with free volume and adsorption properties in the sample that have specified structural and electronic characteristics. Linseed or soybean oil and vanillin-based photocross-linked and ureasil-based polymers, microporous carbon fibers and mesoporous titanium dioxide doped with sulfur nanocomposites were selected as immobilizing matrixes in construction of amperometric biosensors for the analysis of phenolic derivates in water [1-13].

Among the photocross-linked polymers, the best sorption/desorption properties are demonstrated by the sample AESO:VDM=1:1 (mol) and is the most promising matrix in the design of amperometric biosensors. At the same time, the ureasil-based polymers containing chalcogenide clusters (As_2S_3 and/or S) showed the highest biosensor's sensitivity but the reason is still under research. The network properties (free volume and crosslinking) of the investigated polymers studied using positron annihilation lifetime spectroscopy and swelling measurements, were taken into account for comparative analysis. A correlation of network properties of polymer matrixes with parameters of amperometric biosensors is found to be fundamental in origin. The topological and chemical mechanisms for effective enzyme immobilization at the construction of xenobiotic amperometric biosensors are established using the investigated materials as holding matrixes.

Artificial intelligence (AI) technology was applied to enhance the design and characterization of the amperometric laccase biosensor. Our computational approach employs machine learning of interatomic potentials (MLIP) to model enzyme-polymer interactions at the molecular level [14]. Using a deep neural

network architecture similar to DeepDFT, we generate electron density predictions for various polymer matrixes to identify optimal enzyme binding sites. The workflow includes structure generation, geometry optimization, and electronic structure analysis implemented in Python with the Atomic Simulation Environment (ASE). Initial polymer-enzyme configurations are created and then relaxed using the FIRE algorithm with a force convergence criterion of 0.01 eV/Å. This computational framework enables prediction of structural and electronic changes upon enzyme immobilization, correlating directly with biosensor sensitivity parameters. By applying this AI-driven methodology, we can efficiently screen candidate materials for specific analyte detection and optimize the functional characteristics of the biosensor for real-time monitoring of water pollution without extensive experimental testing.

Acknowledgments

This work was supported in part by the Ministry of Education and Science of Ukraine (projects Nos. 0122U000850, 0122U000874, 0122U001694, 0125U001054, 0125U002005, and 0125U002033), Slovak Grant Agency VEGA (projects Nos. 2/0166/22 and 2/0131/25), and Slovak Research and Development Agency (project No. APVV-21-0335). T.K. and Y.K. also acknowledge the SAIA for scholarships in the Institute of Physics SAS in the framework of the National Scholarship Programme of the Slovak Republic. This work has also received funding through the MSCA4Ukraine project (grant No. 1128327), which is funded by the European Union, and the EURIZON project (grant EU-3022), which is funded by the European Union (EURIZON H2020 project) under grant agreement No. 871072.

- [1]. T. Kavetskyy et al., *J. Appl. Polym. Sci.*, **134** (2017) 45278.
- [2]. T. Kavetskyy et al., *Acta Phys. Pol., A*, **132** (2017) 1515-1518.
- [3]. T. Kavetskyy et al., *Gold Bull.*, **52** (2019) 79-85.
- [4]. T. Kavetskyy et al., *Eur. Polym. J.*, **115** (2019) 391-398.
- [5]. T. Kavetskyy et al., *Mater. Sci. Eng. C*, **109** (2020) 110570.
- [6]. T. Kavetskyy et al., *Acta Phys. Pol., A*, **137** (2020) 246-249.
- [7]. T. Kavetskyy et al., *J. Appl. Polym. Sci.*, **138** (2021) e50615.
- [8]. M. Goździuk et al., *Acta Phys. Pol., A*, **139** (2021) 432-437.
- [9]. T. Kavetskyy et al., *Bioelectrochemistry*, **147** (2022) 108215.
- [10]. M. Goździuk et al., *Materials*, **15** (2022) 6607.
- [11]. M. Goździuk et al., *Acta Phys. Pol. B Proc. Suppl.*, **15** (2022) 4-A5.
- [12]. T. Kavetskyy et al., *Microchem. J.*, **201** (2024) 110618.
- [13]. T. Kavetskyy et al., *Phys. Chem. Solid State*, **25**(3) (2024) 461-470.
- [14]. A. Kiv et al., *NATO SPS B: Phys. Biophys.*, (2025) 91-104, DOI: 10.1007/978-94-024-2316-7_6.

Solid Oxide Fuel Cells as a part of ISRU for extra-terrestrial missions

Kotsuybynsky V.O., Boychuk V.M., Rachiy B.I., Kolkovskyi P. I.,
Ivanyshyn I.P., Pylypez M.M.

Department of Applied Physics and Materials Science, Vasyl Stefanyk Carpathian National University, Ivano-Frankivsk, Ukraine

In-Situ Resource Utilization (ISRU) is essential for sustainable space exploration, enabling the use of local resources to support long-term missions. Solid oxide fuel cells (SOFCs) provide efficient and reliable power by operating on lunar-derived oxygen and hydrogen, working alongside photovoltaic (PV) modules in hybrid energy systems. During the lunar day, PV panels generate electricity for mission operations and ISRU processes such as water electrolysis, while stored hydrogen and oxygen are later used by SOFCs to produce power through high-efficiency electrochemical reactions. This cycle generates heat and water, which can be recycled to sustain a closed-loop system, ensuring continuous power during the two-week lunar night. SOFCs not only deliver electricity but also provide useful heat for habitats and ISRU, with their modular design allowing scalability.

Oxygen extraction from lunar regolith is a critical ISRU process. Regolith is rich in oxides such as SiO_2 , FeO , TiO_2 , and Al_2O_3 , which can be reduced to release oxygen. Three main methods are considered: molten salt electrolysis, hydrogen reduction, and carbothermal reduction. Among these, molten salt electrolysis is the most efficient for large-scale use, requiring about 8–12 MJ per kilogram of oxygen. To produce 1 kg of oxygen per hour, the process demands roughly 3 kW of power, corresponding to about 7–8 m^2 of PV panels under lunar conditions. Hydrogen for ISRU can be obtained from water ice in permanently shadowed craters, with electrolysis providing both hydrogen and oxygen for fuel cells. Producing 1 kg each of hydrogen and oxygen per hour requires about 12 kW, or 30 m^2 of PV panels on the Moon, while on Mars the same process would need about 70 m^2 due to lower solar irradiance. Water electrolysis appears even more promising for Mars, where abundant ice deposits have been confirmed. In closed-loop systems, hydrogen can be recovered after SOFC operation, while the water produced can be re-electrolyzed, minimizing resource use and maintaining sustainability.

Overall, integrating SOFCs with ISRU and PV technologies enables reliable, scalable, and self-sufficient energy systems, providing continuous power for habitats, scientific equipment, and mobility during lunar and Martian missions.

Funding: *This work was funded by the NATO Partnerships and Cooperative Security Committee in the framework of the Science for Peace and Security Programme (G6166) and Project 2024-1-PL-KA220-HED-000252474 of programme ERASMUS+*

Structural stability of lithium battery cathodes based on core ($\alpha\text{-Fe}_2\text{O}_3$) - shell ($\gamma\text{-FeOOH}$) nanocomposites

Mokliak, V.V.^{1,2}, Chelyadyn, V.L.¹, Halushchak, M.O.², Mokliak, M.G.³

¹G. V. Kurdyumov Institute for Metal Physics, NAS of Ukraine, Kyiv, Ukraine,
mvvmcv@gmail.com

²Ivano-Frankivsk National Technical University of Oil and Gas, Ivano-Frankivsk, Ukraine

³Vasyl Stefanyk Carpathian University, Ivano-Frankivsk, Ukraine

In work present the results of structural stability cathodes based on nanocomposites core ($\alpha\text{-Fe}_2\text{O}_3$) - shell ($\gamma\text{-FeOOH}$) synthesized by the method of deposition [1]. For this purpose, the method of XRD analysis and the method of Mössbauer spectroscopy were used. During battery discharge, the formation of two plateaus was recorded, reflecting the two-phase composition of the cathode. The discharge capacity indicators are 325 Ah/kg at deep discharge to 0.5 V. XRD analysis shows almost complete amorphization of the cathodes for samples with a dominant phase of $\gamma\text{-FeOOH}$ (Figure, a). After discharge, the main reflections (111) and (200) of the LiF phase and the reflection (110), which corresponds to the formation of metallic iron, are recorded.

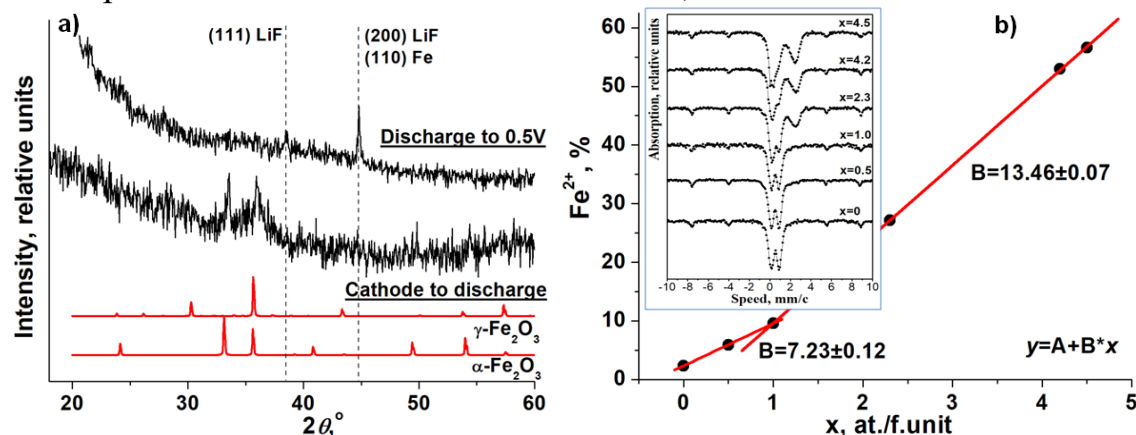


Figure – XRD analysis (a) and Fe^{2+} ions content (b) for cathodes after discharge.

Mössbauer studies show (Figure, b) the stable existence of the hematite phase throughout the range of changes in the values of intercalation of x . The formation of the LiF and Fe^0 phases is due to intercalation-stimulated transformations of amorphous iron hydroxide, which are accompanied by a decrease in the degree of oxidation of Fe^{3+} ions. Starting from the value of $x = 1.0$, which corresponds to 10% of the formed Fe^{2+} ions, the rate of linear growth of the number of these ions doubles. This provides the formation of 57% of Fe^{2+} ions and about 5% of the Fe^0 phase in the cathodes at a deep discharge of up to 0.5 V. This blocks the electrochemically active regions of the cathodes and reduces the diffusion coefficients of lithium ions by 2 orders of magnitude.

[1]. Ostafiychuk, B. K., et al. Low-temperature Mossbauer studies of the phase composition and structural stability of iron (III) oxide/hydroxide nanocomposite. *Physics and Chemistry of Solid State*, 2025, 22.2: 307-312.

Study of the interaction of components of nanocomposite materials in the process of forming film elements of sensors

Lepikh Ya.I., Sadova, N. M.

*Research Institute of Physics at Odesa I.I. Mechnikov National University, Odesa, Ukraine,
ndl_lepikh@onu.edu.ua*

Nanocomposite systems based on "glass-metal compounds" are widely used in microelectronics, in particular as materials for film elements of sensors and hybrid integrated circuits (HIC). As is known, nanocomposites are formed by annealing a mixture of powders of a functional material, a glass binder and an organic binder. During the annealing of pastes, glass powders are melted and sintered into a glass matrix, in which particles of the functional phase are fixed, creating conductive paths. Thus, the complex of electrophysical properties of nanocomposite elements is largely determined by the properties and composition of the glass component and its interaction with compounds of the functional material.

The work investigated the interaction of lead borosilicate glass compounds and functional material compounds (ruthenium compounds) and the processes occurring during heat treatment. The films were made on the basis of lead borosilicate glass powders PbO, SiO₂, B₂O₃, Al₂O₃ with fixed particle sizes of 0.5 μm, 1 μm, 3 μm, 5 μm and ruthenium oxide RuO₂ with particle sizes of 0.05-0.1 μm. The conductivity of the nanocomposite system is influenced by both the electrical resistance of individual conductive grains and the resistance of individual contacts. Technological annealing modes, the ratio of components, the interaction of the glass component and the conductive phases also have a significant impact. The introduction of impurities into the composition of such nanocomposites changes the amount of ruthenium oxide formed. An oxide with strong acidic properties reduces the amount of RuO₂ in the system, and an oxide with alkaline properties promotes the almost complete conversion of lead ruthenate into ruthenium oxide, thereby changing the ratio of components.

Analyzing the obtained results, it can be noted that the use of impurities creates a different effect on the properties of nanocomposites. Thus, oxides TiO₂; Al₂O; Nb₂O₅ increase the surface resistance ρ_s and change the TKR value of the films from the range of positive values to the range of negative values. The NiO impurity leads to a decrease in ρ_s and an increase in TKR. Oxides WO₃; Bi₂O₃ practically do not change ρ_s and TKR of the film. Such a change in properties is explained by the fact that during the annealing of the composite system, the impurity oxides form new crystalline phases with the properties of a semiconductor or dielectric.

The impact of nanomaterials on human life

O.P.Poplavskyy, I.M. Lishchynskyy, I.P. Poplavskyy

*Vasyl Stefanyk Carpathian National University, Ivano-Frankivsk, Ukraine,
omelian.ooplavkyy@pnu.edu.ua*

One of the earliest products of nanotechnology are metallic nanoparticles and nanoclusters. These substances exhibit a multifaceted range of physical and chemical properties, as well as pronounced biological effects, which often differ substantially from those observed in their bulk phases or macroscopic dispersions. Metallic nanoparticles and metal-containing nanomaterials possess distinct physicochemical characteristics and biological activities. This has prompted their consideration as a separate category of materials that necessitates an assessment of their potential risks to human health and the environment.

The prevailing hypothesis regarding the principal pathways by which nanoparticles enter the human body identifies three routes: inhalation (from air), oral ingestion, and transcutaneous absorption. It has been demonstrated that nanoparticles are capable of crossing standard protective barriers, including those of the stomach, placenta, and blood–brain barrier, as well as penetrating neuronal processes, blood vessels, and lymphatic vessels.

The selective accumulation of nanoparticles in organs and tissues, different types of cells, and certain cellular structures can result in their damaging effect, with the severity of damage depending on the target organ and the shape of the nanoparticle.

To assess the potential hazards associated with nanoparticles and nanomaterials, a three-tier classification system has been developed. A high level of potential hazard is indicated by the presence of genotoxic, cytotoxic, mutagenic, and immunotoxic effects, as well as adverse impacts on key biochemical parameters and the overall physiological condition of the organism. A medium level of potential hazard is characterized by the absence of genotoxic and mutagenic effects and by a lack of significant influence on key biochemical parameters, but with some cytotoxic effects or deterioration of the organism's overall physiological state. A low level of potential hazard denotes the absence of genotoxic, cytotoxic, and mutagenic effects, as well as no adverse influence on essential biochemical and immunological parameters or on the general physiological condition of the organism.

The toxic effects of nanomaterials depend on their size and structural organization, physical nature, production method, and surface modification. Therefore, the physicochemical properties of metallic nanoparticles and their compounds determine their biological activity.

The influence of the type of conductive additive on the electrochemical properties of activated carbon material

Ivanichok, N.Ya.^{1,2}, Rachiy, B.I.², Lysiv, T.O.², Borchuk, D.S.², Moklyak, V.V.^{1,3}, Lisovskiy, R.P.⁴, Bedriy, T.R.², Sklepova, S-V.S.²

¹*G.V. Kurdyumov Institute for Metal Physics, N.A.S. of Ukraine, Ukraine,*
ivanichok.nataliia@gmail.com

² *Vasyl Stefanyk Carpathian National University, Ukraine,* bogdan.rachiy@pnu.edu.ua

³ *İvano-Frankivsk National Technical University of Oil and Gas, Ukraine,*
mvvmcv@gmail.com

⁴ *İvano-Frankivsk National Medical University, Ukraine,* rlisovsky@ifnmu.edu.ua

The present work investigated the electrochemical properties of activated carbon material/conductive additive composites as electrodes for electrochemical capacitors in an aqueous electrolyte. The influence of the type of conductive additive on the specific capacitance characteristics of the obtained activated carbon material has been established. The activated carbon material was obtained by thermochemical activation of plant-based raw material (walnut shells) using potassium hydroxide. The influence of the type of conductive additive on the electrochemical properties of the activated carbon material was studied by means of electrochemical impedance spectroscopy, cyclic voltammetry, and galvanostatic charge/discharge measurements.

The study demonstrated that the choice of conductive additive significantly affects the performance of electrochemical capacitors, particularly the specific capacitance of the electrode material and its stability during cycling. Among the tested conductive additives, Super-P carbon black proved to be the most promising, as its combination with the activated carbon material provides optimal electrochemical characteristics. The resulting composite exhibits the highest specific capacitance (~100-120 F/g), stable performance at high charge-discharge rates, and a significant reduction in internal resistance, which is crucial for enhancing the energy and power efficiency of electrochemical capacitors.

Acknowledgment

This research was (in part) sponsored by the NATO Science for Peace and Security Programme under grant id. (G6166) and the Ministry of Education and Science of Ukraine under grant id. (M/41-2025).

Topic 5
Functional crystalline materials and materials with nanoinclusions

Calculation of Charge Carrier Mobility in PbTe Based on Empirical Thermoelectric Parameters

Kulyk, O.H.¹, Halushchak, M.O.², Horichok, I.V.¹

¹ *Vasyl Stefanyk Carpathian National University, Ivano-Frankivsk, Ukraine,*
Ihor.Horichok@pnu.edu.ua.

² *Ivano-Frankivsk National Technical University of Oil and Gas, Ivano-Frankivsk, Ukraine*

Mobility is an important parameter of the electronic subsystem used to assess the thermoelectric quality of materials. The main experimental method for measuring the carrier mobility u is the study of the Hall effect. However, conducting such studies is often a relatively difficult task, in particular at high temperatures. A separate difficulty also arises when the concentrations of the majority and minority carriers are of the same order of magnitude, which is also often the case at high temperatures. Therefore, in [1] a relatively simple method of calculating u was presented. The mobility expression presented by the authors was obtained in the approximate Drude-Sommerfeld model of free electrons and involves the use of experimentally measured values of the Seebeck coefficient and specific electrical conductivity for calculations:

$$u_w = \frac{3h^3\sigma}{8\pi e_0(2m_0k_0T)^{3/2}} \left[\frac{\exp\left(\frac{|S|}{k_0/e_0} - 2\right)}{1 + \exp\left(-5\left(\frac{|S|}{k_0/e_0} - 1\right)\right)} + \frac{\frac{3|S|}{\pi^2 k_0/e_0}}{1 + \exp\left(-5\left(\frac{|S|}{k_0/e_0} - 1\right)\right)} \right]. \quad (1)$$

Here, m_0 is the mass of a free electron. According to [1], the thus determined mobility u_w (w – weighted) is related to the Hall mobility u_H through the effective mass of the density of states: $u_w = u_H \left(m_{d,0}^*/m_0 \right)^{3/2}$.

In this work, we compared the mobilities obtained by formula (1) and by sequential calculation in the relaxation time approximation. We also analyzed the possibility of using another expression for the mobility u as a function of σ and S , obtained for non-degenerate semiconductors with parabolic zones. The results were compared with experimental data.

1. Snyder, G. J., Snyder, A. H., Wood, M., Gurunathan, R., Snyder, B. H., Niu, Ch.. (2020). Weighted Mobility. *Adv. Mater.*, 32, 2001537. DOI: 10.1002/adma.202001537.
2. Horichok, I., Halushchak, M., Kulyk, O., Potyatynnyk, T. (2025). Calculation of Charge Carrier Mobility in PbTe Based on Empirical Thermoelectric Parameters // *Journal of Thermoelectricity*, (2), 39–48. <https://doi.org/10.63527/1607-8829-2025-2-39-48>

Chemical polishing of CsPbBr₃ in dimethyl sulfoxide – methanol solutions

Ivanitska V.G., Pylypko V.G., Fochuk P.M.

*Yuriy Fedkovych Chernivtsi National University, Chernivtsi, Ukraine,
v.ivanitska@chnu.edu.ua*

The condition of the perovskite surface is one of the determining factors for the reliable operation of devices based on it. A perfect, defect-free surface guarantees the quality of processes occurring at the phase boundary. Accordingly, surface treatment is one of the key issues in modern perovskite materials technology.

In our study, anhydrous dimethyl sulfoxide was used to remove the damaged layer on the CsPbBr₃ surface. In order to reduce the perovskite dissolution rate, methanol was added to dimethyl sulfoxide in various volume ratios. The methanol content in the solutions was varied from 0 to 80 per cent by volume. The dissolution rate was determined by the decrease in sample thickness, measuring it before and after etching. The samples were washed in n-hexane, and solvent residues on the surface were removed with a stream of compressed air. The dependence of the thickness of the removed surface layer on the composition of dimethyl sulfoxide–methanol solutions is shown in Fig. 1.

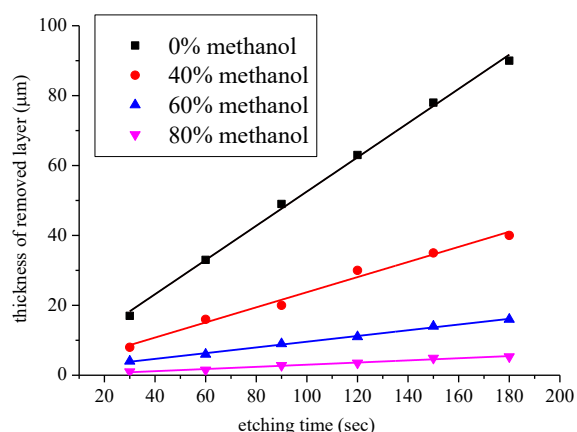


Fig. 1. Dependence of the thickness of the removed surface layer of CsPbBr₃ on the methanol content in dimethyl sulfoxide.

Adding 40 vol.% methanol to dimethyl sulfoxide reduces the dissolution rate of perovskite by almost half. In solutions, containing 60 and 80 vol.% methanol, slight etching is observed, but a whitish film appears on the surface of the samples, which is more intense in the case of a higher methanol content. Therefore, such solutions are unsuitable for removing the damaged layer and obtaining a high-quality CsPbBr₃ surface. The dependence of the rate of perovskite etching on the disc rotation speed determined in this study indicates that the rate of the process is influenced by both the rate of interaction of the solvent with the sample surface and the rate of diffusion processes. Therefore, it can be concluded that, in general, the process occurs according to a mixed mechanism.

Controlling the parameters of nanostructuring the surfaces of IV-VI compounds by beams of charged particles

Zayachuk D.M.¹, Slynsko V.E.², and Csík A.³

¹*Lviv Polytechnic National University, Lviv, Ukraine*

²*Institute for Problems of Material Science NASU, Chernivtsi, Ukraine*

³*Institute for Nuclear Research, (ATOMKI), Debrecen, Hungary*

zayachuk@polynet.lviv.ua

The formation of structures on solid surfaces under ion beam irradiation is a common phenomenon. In some cases, surface texturing is desirable, while in others, it is not. The surface structuring that occurs during ion–solid interactions can be beneficial for various technologies and experimental methods—particularly in solar energy conversion. In this context, the ability to produce surfaces covered with dense arrays of nanostructures of various shapes is highly valuable.

In this report, we discuss in detail the possibilities of controlling surface nanostructuring processes on sputtered IV–VI telluride crystals. We demonstrate that sputtering different tellurides of the IVB group (PbTe, SnTe, and GeTe) results in completely different surface morphologies.

When sputtered with argon ions, SnTe surfaces are consistently covered with dense arrays of cone-like surface structures. These cone arrays appear to consist of multiple generations, each characterized by its own average geometry – specifically, height and apex angle. The surface topography of sputtered SnTe is always significantly different from that of other IVB tellurides, such as PbTe and GeTe, even under identical sputtering conditions. In contrast to SnTe, no "undergrowth" of new cones is observed on previously sputtered PbTe and GeTe surfaces. Our sputtering experiments suggest that these differences in surface morphology under Ar⁺ ion bombardment are due to differences in preferential sputtering behaviour.

We found that the formation of surface structures under Ar⁺ ion impact strongly depends on the presence of easy-cleavage planes. As a result, the conical structures initially formed on PbTe surfaces gradually transform into hybrid structures with a conical base and a pyramidal apex. With continued sputtering, the pyramidal apex grows while the conical base shrinks, eventually resulting in the complete transformation of the cone into a pyramid, which then disappears altogether.

For the first time, we also demonstrate that surface structures on PbTe crystals formed by Ar⁺ ion bombardment can be further modified by electron beam exposure. This effect could serve as a useful tool in solar energy conversion applications.

Correlating crystal structure and thermoelectric performance of Cu₂FeSnS_{4-x}Se_x compounds

Hanna Donyk¹, Taras Parashchuk¹, Oleksandr Cherniushok¹, Dariusz Wieczorek², Oleksandr Smitiukh³, Oleg Marchuk³, Bartłomiej Wiendlocha², Krzysztof T. Wojciechowski¹

¹ Thermoelectric Research Laboratory, Department of Inorganic Chemistry, Faculty of Materials Science and Ceramics, AGH University of Science and Technology, Mickiewicza Ave. 30, 30-059 Krakow, Poland

² Faculty of Physics and Applied Computer Science, AGH University of Krakow, Mickiewicza Ave. 30, Krakow 30-059, Poland

³ Department of Inorganic and Physical Chemistry, Lesya Ukrainka Volyn National University, Voli Ave 13, Lutsk, 43025, Ukraine

hannadonyk@agh.edu.pl

Thermoelectric technologies are attracting more and more attention as a sustainable solution to overcome the global energy challenge and reduce greenhouse gas emissions.¹ By enabling the direct conversion of heat into electricity, thermoelectric materials are promising for power generation and solid-state cooling.² The most common thermoelectric materials, such as Bi₂Te₃ and PbTe or GeTe tellurides, often contain rare and toxic elements, and therefore the development of highly efficient and eco-friendly TE materials for energy conversion remains a significant challenge.³. Diamond-like chalcogenides, such as Cu₂FeSnS_{4-x}Se_x, are prospective due to their content of earth-abundant and non-toxic elements, high thermal stability and their tunable properties.

This study focuses on investigating a new promising eco-friendly material, Cu₂FeSnS_{4-x}Se_x ($x = 0, 1, 2, 3, 4$) with enhanced thermoelectric performance achieved by tuning the sulfur (S) and selenium (Se) content. The material shows structural stability, inherently low thermal conductivity ($\sim 0.7 \text{ W}\cdot\text{m}^{-1}\cdot\text{K}^{-1}$ at 773 K), combined with a promising value of Seebeck coefficient 212 – 300 $\mu\text{V K}^{-1}$ at , and optimal value of carrier concentration $\sim 1.38\times 10^{20} \text{ cm}^{-3}$ making it a potential candidate for thermoelectric applications. Rietveld refinement revealed that the material belongs to the tetragonal crystal structure system (space group $I\bar{4}2m$), while sulfide adopts a related tetragonal structure with space group . The single-phase structure provides structural homogeneity and is reliable to estimate the intrinsic thermoelectric properties of the material. The substitution of selenium leads to an improvement in the power

factor (PF), which consequently results in an enhancement of the dimensionless figure of merit (ZT).

The significance of this work lies in introducing a new perspective on diamond-like structure (DLS) materials and demonstrating their potential as efficient and environmentally friendly candidates for thermoelectric energy conversion.

- [1]. T. Parashchuk, (2025). *J.Phys.Chem.C*.129,3272 – 3284.
- [2]. Chen, P., Xie, H. & Zhao, L. D. *Acta Metall. Sin. English Lett.* (2024).
- [3]. Parashchuk, T., Wiendlocha, B., Cherniushok, O., Knura, R. & Wojciechowski, K. T. *ACS Appl. Mater. Interfaces*, (2021), 13, 49027–49042.

This work was funded by the National Science Center (Poland) under the research project “OPUS-26” UMO-2023/51/B/ST11/00329.

Determination of the Fermi energy of electrons in lead telluride based on measurements of the Seebeck coefficient

Potiatynnyk, T., Matkivskyi, O., Hovdiak, V., Horichok, I.

*Vasyl Stefanyk Carpathian National University, Ivano-Frankivsk, Ukraine,
ostap.matkivskyi@pnu.edu.ua.*

Analysis of the electronic subsystem of thermoelectric materials is an important aspect of the study of new and modification of the properties of known semiconductors. One of the most urgent issues is the determination of the dominant carrier scattering mechanism and the calculation of the Fermi energy μ . The parameter μ can then be used to calculate almost all thermoelectric parameters of the material, in particular, the Seebeck coefficient S , the charge carrier concentration n , the carrier mobility u , the Lorentz number L_0 .

In this work, the possibilities of using the model of dominance of one carrier scattering mechanism for calculating the Fermi energy μ using experimental values of the Seebeck coefficient S_{\exp} were analyzed. The specific electrical conductivity of n -PbTe:I was calculated in the relaxation time approximation with simultaneous consideration of many scattering mechanisms. The obtained Fermi energy values were compared with the values calculated as $\mu(S_{\exp})$. The influence of corrections to the Bloch form of wave functions and screening of scattering centers by carriers on the numerical values of mobilities and numerical values of Fermi energies determined in the model of dominance of one scattering mechanism was investigated.

According to the results of the calculations, the numerical values of μ obtained within the framework of the scattering dominance model on the deformation potential of acoustic phonons DA, when further used to calculate the main thermoelectric parameters (Seebeck coefficient, specific electrical conductivity, and Lorentz number), lead to results that differ from the experimental ones by 10-50%. Taking into account three scattering mechanisms simultaneously allows achieving significantly better agreement between the calculated and experimental material parameters. Moreover, according to the obtained results, for the studied material PbTe:I, the partial contributions of the DA and PO mechanisms in the temperature range 300-600 K are practically the same.

[1]. Potiatynnyk T., Matkivskyi O., Hovdiak V., Horichok I. Determination of the Fermi energy of electrons in lead telluride based on measurements of the Seebeck coefficient. Physics and Chemistry of Solid State. 2015. V. 25, No. 3. P. 584-591. DOI: [10.15330/pcss.26.3.584-591](https://doi.org/10.15330/pcss.26.3.584-591).

Dynistor effect in *n*-CdSb crystals

Fedosov S.A., Koval Yu.V., Zakharchuk D.A., Yashchynskyy L.V.

Lutsk National Technical University, Lutsk, Ukraine,
y.koval@lntu.edu.ua

Along with the currently existing materials, such as Si, Ge GaAs, for the production of the widest class of electronic devices in semiconductor electronics, an intensive search for new ones is ongoing. Doping CdSb crystals with some compensating impurities or radiation irradiation leads to a strong increase in photosensitivity in the low-temperature range. In particular, photoresistors with *n*-CdSb doped with tellurium cooled to 80 K are not inferior in sensitivity to known IR radiation receivers based on PbS and Ge. This opens up the possibility of using photodiodes based on CdSb:Te as IR radiation detectors.

Of great interest are the studies of nonlinear *I-V*-characteristics not only in devices, but also in materials. They have both applied significance and provide an opportunity to explain from a physical point of view the causes of the manifestation of nonlinearity. The nonlinearity of the *I-V*-characteristic is strongly influenced by various external actions: temperature change, mechanical deformation, magnetic field, lighting, etc. The nonlinearity of the *I-V*-characteristic is a characteristic feature not only of many semiconductor devices that have p-n junctions, but also of many semiconductors.

The *I-V*-characteristics of cadmium antimony crystals doped with tellurium (*n*-CdSb:Te) were studied. Specific changes in the *I-V*-characteristics of *n*-CdSb with different dopant contents and different levels of illumination intensity at temperatures from liquid nitrogen and slightly higher were found. The nature of the *I-V*-change had an S-shaped form (dynistor effect). For all groups of samples, the dependences of the current *I* flowing through the crystal on the applied voltage *U* showed a switching of the material from a low-conductive to a high-conductive state. In the process of switching to a high-conductive state, a slight increase in the current was accompanied by a rapid decrease in the voltage on the sample.

With increasing dopant concentration, an increase in the limiting values of the applied electric field voltage was found, which is associated with different ionization of the tellurium impurity level. On the contrary, an increase in temperature above 78 K and an increase in the level of crystal illumination intensity reduces the switching voltage.

From the analysis of S-shaped *I-V*-characteristics, the values of the parameters of the quantities that are important in the development of controlled sensor devices of semiconductor electronics with predetermined characteristics have been established. By changing the dopant content, temperature and illumination intensity in *n*-CdSb:Te, it is possible to control the values of the U_{BO} turn-on voltage.

Effect of carbon nanotubes concentration on IR absorption and strength of composites

Karachevtseva L.A.¹, Kartel M.T.², Lytvynenko O.O.¹

¹*V. Lashkaryov Institute of Semiconductor Physics of the NAS of Ukraine, Kyiv, Ukraine,
lytvo1e@gmail.com*

²*O. Chuiko Institute of Surface Chemistry of the NAS of Ukraine, Kyiv, Ukraine.*

We investigated influence of multiwalled carbon nanotubes (CNTs) on the characteristics of composites based on polymers, rubber, and thermally expanded graphite. Some coincidences were noticed in the effect of CNTs on the properties of the resulting composites, which became the subject of study.

The introduction of CNTs in an amount of 0–5% by weight of the composites leads to a significant increase in the strength characteristics and thermal stability of the composites. This result indicates that CNTs are an ideal filler for composites of various chemical composition and structure.

The dipolar IR absorption measured after the addition of carbon nanotubes to the composites has a negative IR absorption in the spectral positions of the sp₃ hybridization bonds. The light absorption increases by a factor of 102–105 when the frequencies of local oscillations of the surface bonds in the carbon nanotubes coincide with the gap modes along the boundaries of the nanotube and the medium, which leads to the splitting of photon beams and the interference of two photons. Measurements of giant dipolar oscillations with a very small half-width of 0.5 cm⁻¹ indicate a strong interaction of surface polaritons with photons.

Effect of embedded metal nanoparticles on the characteristics of triboelectric nanogenerators

Korotun, A.V.^{1,2}, Moroz, H.V.¹, Kurbatsky, V.P.¹

¹*National University Zaporizhzhia Politechnic, Zaporizhzhia, Ukraine, andko@zp.edu.ua*

²*G.V. Kurdyumov Institute for Metal Physics of the NAS of Ukraine, Kyiv, Ukraine.*

The use of various intelligent platforms requires the availability of sustainable and maintenance-free energy sources. Electronic devices based on the pyroelectric, piezoelectric and triboelectric effects are used to collect energy from the environment, and devices operating on the triboelectric effect demonstrate higher output characteristics. Triboelectric nanogenerators (TENGs) convert the energy of mechanical vibrations (usually low-frequency) into electrical energy and are used as both power sources and various sensors with autonomous power supply. However, modern TENG designs still have a number of drawbacks, the most significant of which is low output power. Therefore, research aimed at eliminating this drawback is relevant.

One of the methods for increasing the output power of TENGs is doping the triboelectric layer, which in the vast majority of cases is polydimethylsiloxane (PDMS), with metal nanoparticles. In this case, the triboelectric layer acquires the properties of a nanocomposite with a frequency-dependent effective dielectric function. The surface density of the charge induced in the TENG is determined by the relationship [1]

$$\sigma' = \frac{\sigma d' T_1 T_2 T_3}{d_1 T_2 T_3 + d' T_1 T_2 T_3 + d_2 T_1 T_3 + d_3 T_1 T_2}, \quad (1)$$

where T_2 and T_3 are the permittivities of the electrode and substrate materials (TiO_2 and glass); d_1 , d_2 and d_3 are the thicknesses of the metal – PDMS composite, TiO_2 and glass layers; σ is the surface density of the triboelectric charge; d' is the interlayer distance in a given state. The effective dielectric function of the metal – PDMS nanocomposite within the framework of the size-corrected Maxwell – Garnett model [2] is determined by the expression

$$T_l = T_{eff}(\omega) = T_m \frac{T(\omega)(1+2\beta) + 2T_m(1-\beta) + (T_m - T(\omega))(1-\beta)\Delta}{T(\omega)(1-\beta) + T_m(2+\beta) + (T_m - T(\omega))(1-\beta)\Delta}, \quad (2)$$

where T_m is the dielectric constant of PDMS; β is the volume fraction of metal nanoparticles in the triboelectric material; the size factor is

$$\Delta = x^2 + \frac{2}{3}ix^3 \quad x = \sqrt{T_m} \frac{\omega R}{c}; \quad (3)$$

ω and c are the frequency and speed of the light wave; R is the radius of the metal particle. Dielectric function of the particle within the Drude model

$$T(\omega) = T^\infty - \frac{\omega_p^2}{\omega(\omega + i\gamma_{\text{eff}})}. \quad (4)$$

In formula (4), ω_p is the plasma frequency; T^∞ is the contribution of interband transitions to permittivity; γ_{eff} is effective relaxation rate.

The above considerations indicate that the charge redistribution between the electrodes and the increase in the surface density of the induced charge can be achieved both by changing the interlayer distance d' and by changing the effective permittivity of the metal-PDMS composite. Note that to control the effective permittivity $T_{\text{eff}}(\omega)$, it seems appropriate to embed a nanoscale light source into the composite.

[1]. Lin Z.-H., Cheng G., Yang Y., Zhou Y.S., Lee S., Wang Z.L. Triboelectric nanogenerator as an active UV photodetector. Advanced Functional Materials. 2014. V. 24, No 19. P. 2810–2816.

[2]. Korotun A.V., Smyrnova N.A., Titov I.M., Shylo H.M. Optical Absorption of a Nanocomposite with Spherical Hybrid Nanoparticles. Metallofizika i Noveishie Tekhnologii. 2023. V. 45, No 5. P. 569–591.

Effect of high-temperature loading (up to 1085 °C) on the phase composition and microstructure of high-strength concrete modified with microsilica (20%) and metakaolin (5%)

I. M. Fodchuk, V. F. Romankevych, V. V. Dovhaniyk, E. V. Novak

Yuriy Fedkovych Chernivtsi National University, Ukraine
v.romankevych@chnu.edu.ua

This study analyzes the effect of high-temperature loading (up to 1085°C) on the phase composition and microstructure of high-strength concrete modified with microsilica (20%) and metakaolin (5%). X-ray diffraction (XRD), scanning electron microscopy (SEM), and energy-dispersive spectroscopy (EDS) were used to investigate the temperature-induced phase transformations and structural evolution of the cement paste depending on the degree of hydration. Samples heated to 505 °C after 28 days of curing suffered explosive destruction due to excessive pore pressure. In contrast, heating to 1085 °C (365 days) resulted in the formation of a dense, thermostable structure. The key role of C–S–H phase dehydration, and the formation of β -C₂S, wollastonite, and anorthite was established. A quantitative elemental analysis (Ca/Si, Al/Si) and microstructural comparison were conducted for each temperature condition.



Fig. 1. SEM analysis of high-strength concrete microstructure:

- (a) 20 °C (28 days), initial structure
- (b) 505 °C (28 days), explosive spalling
- (c) 1085 °C (365 days), porous crystallization

Microstructural analysis by SEM and EDS

Fig. 1a represents control sample at 20 °C. SEM analysis revealed a homogeneous gel-like structure of the cement paste with a dominance of C–S–H phases, hexagonal portlandite Ca(OH)₂, as well as residual quartz and calcite (CaCO₃) crystals. The matrix is characterized by high density, low porosity, and the absence of signs of degradation. This microstructural profile is expected for high-strength concrete at an early stage of hydration and is stable under moderate thermal loading [1], [2].

Heating the sample to 505 °C after 28 days of curing (Fig. 1b) leads to significant microstructural changes: therm-induced porosity, development of

microcracks, and local destruction of the C–S–H gel matrix were detected. These changes are consistent with the dehydration of C–S–H phases and the decomposition of Ca(OH)₂. As a result, a predominantly anhydrous structure with signs of structural instability is formed [3], [5]. These effects are precisely what caused the explosive spalling of the sample observed experimentally.

After prolonged curing (1 year) and subsequent heating to 1085 °C, (Fig. 1c), SEM analysis reveals a predominantly crystalline microstructure dominated by wollastonite (CaSiO₃), β-C₂S, and anorthite. Despite the presence of thermally induced porosity, the structure demonstrates high density and phase stability. The presence of thermostable silicate phases indicates microstructural stabilization at ultra-high temperatures, which is also confirmed by XRD analysis results [2], [4]. As a result of thermal exposure at 1085 °C, the sample's microstructure underwent significant transformations, acquiring a characteristic morphology similar to a dense ceramic material.

Conclusions

Heating above 450 °C leads to the dehydration of C–S–H phases, the decomposition of Ca(OH)₂, and the formation of new phases like β-C₂S, wollastonite and anorthite [4,5].

In samples, cured for 28 days and heated to 505 °C, explosive destruction is observed due to excessive steam pressure and incomplete hydration [1].

Samples, cured for 365 days, after heating to 1085 °C show a stable microstructure – a result of the complete recrystallization of hydrates [2,3].

EDS analysis demonstrates the stabilization of the Ca/Si ratio at ~2.5, which corresponds to the presence of β-C₂S and other calcium silicates [4].

References

- [1] Kim Y., Lee T., Kim G. An experimental study on the residual mechanical properties of fiber-reinforced concrete with high-temperature and load, *Materials and Structures*, 2013, Vol. 46, pp. 607–620. <https://doi.org/10.1617/s11527-012-9916-2>
- [2] Kodur V.K.R. Fire resistance design guidelines for high strength concrete columns, National Research Council Canada.
- [3] De la Torre A.G., De Vera R.N., Cuberos A.J.M., Aranda M.A.G. Crystal chemistry of belite phases in Portland clinkers, *Cement and Concrete Research*, 2008. <https://doi.org/10.1016/j.cemconres.2008.06.002>
- [4] Kurdowski W. *Cement and Concrete Chemistry*. Springer, 2014. <https://doi.org/10.1007/978-94-007-7945-7>
- [5] Cyr M., Idir R., Escadeillas G. Use of metakaolin to improve the resistance to temperature of cement pastes containing silica fume, *Cem. Concr. Res.*, 2008. <https://doi.org/10.1016/j.cemconres.2008.01.002>

Effect of Pressing on Concentration Anomalies in the Kinetic Properties of $(Bi_{1-x}Sb_x)_2Te_3$ Solid Solutions

Martynova, K.V., Rogachova, O.I.

*National Technical University "Kharkiv Polytechnic Institute", Kharkiv, Ukraine,
Kateryna.Martynova@khp.edu.ua*

The problem of heavy doping is one of the key issues in semiconductor physics. The transition from weak to heavy doping is accompanied by the formation of an impurity band and the appearance of anomalies in the concentration dependencies of properties. Such anomalies, observed in many solid solutions have been interpreted in terms of percolation theory and attributed to critical phenomena accompanying the transition to heavy doping [1]. In [2], we reported such anomalies for the mechanical and kinetic characteristics of cast samples of the $(Bi_{1-x}Sb_x)_2Te_3$ solid solutions, which are among the best thermoelectric materials for use in refrigerating devices. For thermoelectric applications, these materials are typically used in the pressed form.

The aim of this study was to determine the effect of pressing on the manifestation of concentration anomalies accompanying the transition from weak to heavy doping, using the $(Bi_{1-x}Sb_x)_2Te_3$ system as an example. The objects of research were pressed samples in the range $x = 0\text{--}0.05$ with particle size $\sim 200 \mu\text{m}$. The dependencies of the Hall coefficient R_H , the Seebeck coefficient S , the charge carrier concentration n , the electrical conductivity σ , and the Hall mobility μ_H on the composition of the solid solution were obtained at room temperature. All the dependencies exhibited distinct extrema near $x = 0.01$, indicating the presence of a phase transition.

The discovered extrema of properties in pressed samples of the $(Bi_{1-x}Sb_x)_2Te_3$ provide further evidence in support of the hypothesis of universality of concentration anomalies, which manifest regardless of the sample preparation method. Considering the growing use of $(Bi_{1-x}Sb_x)_2Te_3$ -based materials in the form of thin films, one can expect that similar anomalies will also appear in film structures, affecting their thermoelectric characteristics.

- [1]. E.I. Rogacheva Percolation effects and thermoelectric materials science // *J.Thermoelectricity*. 2007. № 2. P. 61–72.
- [2]. E.I. Rogacheva, K.V. Martynova, A.S. Bondarenko Thermoelectric and mechanical properties of $(Bi_{1-x}Sb_x)_2Te_3$ ($x = 0 \div 0.07$) semiconductor solid solutions // *J. Thermoelectricity*. 2016. № 5. P. 47–56.

Electric field as a factor regulating the binding of HSA protein to A²B⁶ quantum dots

O. Kuzyk, O. Dan'kiv, I. Stolyarchuk, A. Stolyarchuk,
R. Peleshchak and M. Rehei

Drohobych Ivan Franko State Pedagogical University, Drohobych, Ukraine
olehkuzyk@dspu.edu.ua

When using colloidal quantum dots (QDs) as fluorescent markers in both in vitro and in vivo studies, there is a need for bioconjugation. It should be noted that the surface area of the nanoparticle is sufficient for simultaneous binding to it of several biomolecules. The possibility of conjugating semiconductor nanoparticles with protein molecules, for example, human serum albumin (HSA) or bovine serum albumin, has been experimentally tested. The formation of stable biocomplexes between HSA and nanomaterials, in particular QD, is of great importance for improving the biocompatibility, solubility, and controllability of delivery of these nanoparticles in the human body.

Typically, solutions of A²B⁶ nanocrystals with HSA are prepared by adding a defined amount of QDs to a fixed volume of protein solution followed by stirring for a short time. However, this method is relatively uncontrolled and does not provide precise control of the binding process. The binding of HSA to QDs or other nanoparticles is a complex process that is accompanied by a number of problems. First, the stability of the complex often depends on the physicochemical conditions of the environment, such as pH and temperature, which can lead to the disassociation of the complex in biological systems and reduce the efficiency of nanoparticle delivery. Secondly, uncontrolled binding of proteins on the surface of nanoparticles can adversely affect their physicochemical properties and the formation of a protein shell (protein corona), which leads to a decrease in biocompatibility and the efficiency of targeted delivery in the body, which is a significant limitation for therapeutic applications. Thirdly, interaction with nanoparticles can cause conformational changes in the structure of HSA, which negatively affects its natural functions, in particular transport properties and interaction with cell receptors. Thus, to date, the process of formation of QD–HSA biocomplexes remains poorly controlled, with variable and poorly predicted thermodynamic parameters of binding.

In the present investigation, efforts have been made to establish stable and functionalized HSA–A²B⁶ nanoparticle corona (conjugates) using an electric field. A model of the interaction between QDs and proteins was developed taking into account dipole polarization and orientational ordering in an electric field, and the influence of a constant electric field on the thermodynamic parameters of HSA protein binding to A²B⁶ QDs was investigated.

Electrical properties of the laser and ultrasound irradiated TiS₂/C electrode material

Budzuliak I. M., Yablon L. S., Budzuliak I. I.

*Vasyl Stefanyk Carpathian University, Ivano-Frankivsk, Ukraine,
ivan.budzuliak@gmail.com*

TiS₂ belongs to the narrow-gap semiconductors group having $2.8 \cdot 10^{20} \text{ cm}^{-3}$ charge carriers' concentration at the room temperature. But crystalline titanium disulfide is a semi-metal due to its S-p-Ti-d orbitals overlapping near the Fermi level. We investigated the dependence of specific conductivity of the materials under study on their composition and temperature using AUTOLAB PGSTAT12 measurement complex.

Measuring of Z' – real and Z'' – imaginary parts of the complex resistance $Z = Z' - jZ''$ was conducted within $f = 10^2 \dots 10^5 \text{ Hz}$ frequency range at 1 mV. Specific resistance values were calculated according to the equation: $\rho = \rho' - j\rho''$, where $\rho' = \frac{Z'S}{l}$ – real and $\rho'' = \frac{Z''S}{l}$ – imaginary part of the specific complex resistance, l – thickness of the sample, S – sample surface area. Specific complex conductivity was determined by

$$\sigma = \frac{1}{\rho''} = \sigma' + j\rho''\sigma''$$

where $\sigma' = \frac{\rho'}{M}$ – real part and $\sigma = \frac{\rho}{M}$ – imaginary part of the specific complex conductivity. These parts were calculated using parameter $M = |Z|^2 \left(\frac{S}{l}\right)^2$.

Specific conductivity was calculated according to the formula $\sigma = \sqrt{\sigma'^2 + \sigma''^2}$

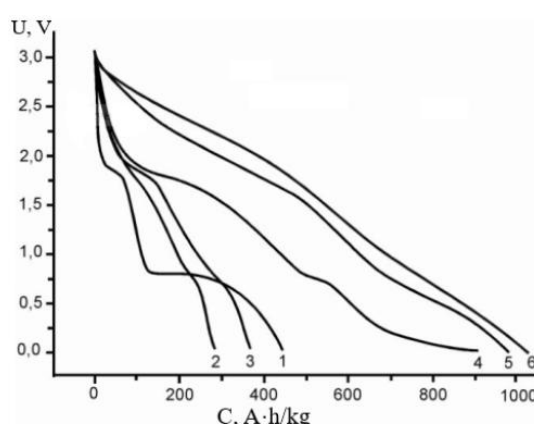


Fig. 1. Discharge curves during the first cycle at a discharge current of 0.3C for LPS with cathode materials: 1 – TiS₂, 2 – TiS₂/C=20/80, 3 – TiS₂/C=80/20, 4 – TiS₂/C=50/50, 5 – laser-irradiated TiS₂/C=50/50, 6 – TiS₂/C=50/50 obtained by ultrasonic dispersion.

Topic 5

Laser irradiation leads to the local temperature growth in the composites that in turn provokes graphite inclusions formation in the PCM (porous carbon material) and the ordered graphite layers' buildup. Since the size and orientation of the crystallites do determine material's texture and its conductivity mechanisms, there is a probability that laser irradiation causes PCM conductivity mechanism change. And accordingly, this change also manifests in the composite as a whole, showing the conductivity increase.

It is established that the conductivity value ≈ 290 ($\text{Ohm}\cdot\text{m}$) $^{-1}$ for the TiS₂/C=50/50 composite obtained by ultrasonic dispersion in the acetonitrile exceeds similar value for the laser irradiated composite (same TiS₂/C=50/50) that was obtained by mechanochemical method.

Electrochemical method for the synthesis of fullerene derivatives in the crystalline state

Khora O.V.^{1,2}, Demianenko E.M.^{1,2}, Shaposhnikova T.I.¹, Anikina N.S.¹,
Savenko A.F.¹, Pomytkin A.P.¹, Krivushchenko O.Y.¹, Kravchuk A.V.¹,
Kotliar D.A.¹, Gavrilyuk N.A.^{1,2}, Zolotarenko A.D.^{1,2}, Zolotarenko O.D.^{1,2},
Schur D.V.¹, Gabdullin M.T.³

¹ *Frantsevich Institute for Problems of Materials Science of NASU, 3, Krzhyzhanovsky Str., Kyiv, 03142, Ukraine, o_khora@ukr.net*

² *Chuiko Institute of Surface Chemistry of NASU, 17, Oleha Mudraka Str., Kyiv, 03164, Ukraine.*

³ *Kazakh-British Technical University (KBTU) 71, Al-Farabi Str., Almaty, 050040, Kazakhstan.*

We use the electrochemical method to synthesize fullerene derivatives, in particular, to synthesize salts of C60 fullerenes with alkali metals that crystallize on the cathode. At present, there are no data on the electrochemical deposition of fullerides on electrodes from fullerene solutions in aromatic solvents, although this method for producing fulleride coatings on metals is undoubtedly of practical interest. As experiments have shown, the films deposited on the electrodes differ from each other not only in thickness, but also in structure, composition, and other physicochemical properties. For example, thick films obtained by electrolysis of a TFE solution dissolve in toluene completely within a fairly short time (20–30 min.), while thin films do not dissolve in either toluene or water. Thick films electrodeposited from a TFE solution with additives of alkali metal salts or bases dissolve partially in toluene and do not dissolve at all in water.

Increasing the concentration of fullerenes in the TFE solution leads to the formation of a product in the form of thick films on the anode with a pronounced polycrystalline structure characteristic of fullerites.

Thick films of fullerites and fullerene-containing compounds obtained in one case on the anode, and in the other - on the cathode, have some similarity in appearance: they consist of individual conglomerates measuring ~140 × 450 μm. The films crack during drying after washing.

Thus, the structure of films electrodeposited from TFE solutions with various additives depends both on the type of additive in the solution and the concentration of the constituent components in the solution, including fullerenes.

Electrochemical properties of the β -Ni(OH)₂ / C / MoO₃ composites

Budzuliak I. M., Yablon L. S., Budzuliak I. I.

Vasyl Stefanyk Carpathian University, Ivano-Frankivsk, Ukraine,
lyubov.yablon@pnu.edu.ua

Hybrid capacitors (HC) based on nickel hydroxide and carbon electrode in the water electrolytes attract attention of researchers due to low price and successful commercialisation. However, low specific (10^{-17} Ohm⁻¹·cm⁻¹) electronic conductivity of nickel hydroxide decreases electron exchange efficiency that leads to specific power drop in corresponding HC. These disadvantages can be compensated by using porous carbon and transition metals' oxides (MoO₃ for instance) when forming composites [1]. In such composites hexagonal close packed structure of nickel hydroxide ensures fast redox reactions and molybdenum oxide layered structure provides possibility to a wide-range intercalation of ions. Additionally, carbon porous structure provides low-resistance paths for the ions (K⁺ in particular) into the material's pores and creates large specific area with electric double layer (EDL) formation.

Cathode peaks that are registered by cyclic voltammetry (CVA) of the studied materials (intervals 0.2-0.5 V and 1-1.3 V) do represent fast reversible faradaic processes. CVA form of electrode materials that contain MoO₃ is almost rectangular that indicates that main contribution into the specific capacitance is provided by EDL. And steep increase of current that is observed at the upper voltage boundary value is probably connected with the hydrogen emission on the nanoporous carbon material's surface. At the discharge currents of 10 and 20 mA, discharge curves start showing plateaus that exhibit fast redox reactions or electrochemical adsorption/desorption that is confirmed by CVA. Charge/discharge curves for composites with molybdenum trioxide are also non-linear like for electrochemical capacitors that indicates pseudocapacitance contribution. During discharge current's increase the HC specific capacitance value shows a sharp decline. This decline depends on two factors: 1) the carbon material itself that has large ohmic resistance increase after discharge current growth due to micropores that restrict access to the inner material's surface; 2) probably irreversibility of redox reactions at large discharge currents. It is established that Coulomb efficiency for HC that has cathode made of laser-irradiated β -Ni(OH)₂ / C composite can reach value of 97% at 50th cycle and remains practically unchanged until 500th cycle. And for the HC with ultrasound-processed β -Ni(OH)₂ / C / MoO₃ cathode material, the Coulomb efficiency grows up to 99% at 100th cycle and doesn't change until 500th, proving it as a perspective composite for the future practical use.

[1]. Olha Popovych, Ivan Budzulyak, Mariia Khemii, Roman Ilnytskyi, Lyubov Yablon. Electrochemical Behavior of Nanocrystalline NiMoO₄ Hydrate Modified by Ultrasound/ Journal of Nano Research. 2023. V. 77. P. 145 – 154.
<https://www.scientific.net/JNanoR.77.145>

Electrophysical parameters of solution-grown CsPbBr_3 perovskite

V. Sklyarchuk, M. Pecherkin, P. Fochuk

*Chernivtsi National University, 2, Kotsiubynskoho, Chernivtsi, Chernivtsi, Ukraine
v.skliarchuk@chnu.edu.ua*

The electro-physical properties of CsPbBr_3 were investigated. Two types of symmetrical structures were created: with a potential barrier In/CsPbBr₃/In and with ohmic contacts Ag/CsPbBr₃/Ag. From measurements of optical transmission spectra, the bandgap width of CsPbBr₃ at T=300 K was determined and was equal to $E_g=2.27$ eV. By measuring the dependence of the collected charge on the applied voltage, using the Hecht equation, the mobility-lifetime product $\mu \cdot \tau$ was determined. This critically important parameter of the semiconductor material is $\mu \cdot \tau \approx 2.8 \cdot 10^{-4} \text{ V}^{-1} \cdot \text{cm}^2$ for the Ag/CsPbBr₃/Ag structure and, accordingly, $\mu \cdot \tau \approx 1.2 \cdot 10^{-4} \text{ V}^{-1} \cdot \text{cm}^2$.

We fabricated two types of structures with contacts close to ohmic - Ag/CsPbBr₃/Ag and with contacts close to rectifying - In/CsPbBr₃/In. The contacts were applied to plates measuring 5x5 mm² and with a thickness of 1.5 mm. The metal was applied by thermal spraying in vacuum over the entire surface of the semiconductor. To estimate the differential resistivity and its dependence on voltage, we constructed the dependences $\rho_{\text{dif}} = \rho_{\text{dif}}(U)$, where ρ_{dif} is equal to:

$$\rho_{\text{dif}} = dU/dI \cdot S/d$$

where dU/dI is the first derivative of voltage from current, d is the crystal thickness, S is the contact area. The corresponding dependence is shown in Fig.1

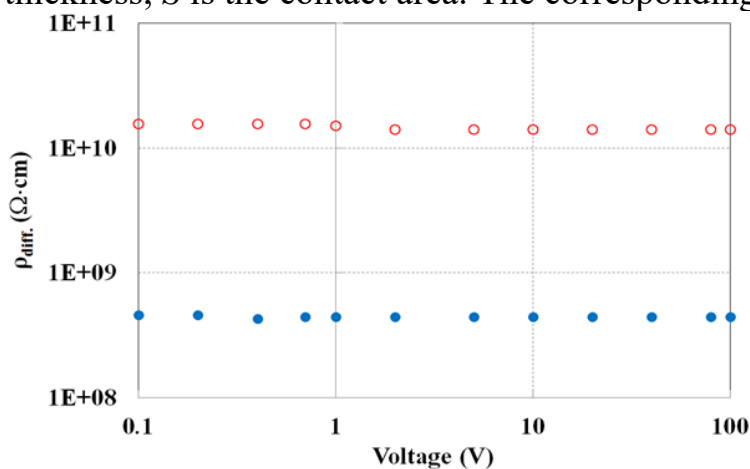


Fig. 1. Dependence of differential resistivity on voltage. Filled circles – the Ag/CsPbBr₃/Ag structure, unfilled circles – the In/CsPbBr₃/In structure (T=300 K).

For the Ag/CsPbBr₃/Ag structures, the equilibrium resistivity was determined, which at T=300 K was equal to $\rho \approx 5 \times 10^8 \Omega \cdot \text{cm}$. It is important that for the In/CsPbBr₃/In structures with barrier contacts, the differential resistivity was obtained, which is significantly higher than the equilibrium one and is equal to $\rho_{\text{dif}} \approx 2 \times 10^{10} \Omega \cdot \text{cm}$. For the Ag/CsPbBr₃/Ag and In/CsPbBr₃/In structures, an important parameter was obtained by the Hecht method – the product $\mu \cdot \tau$, which is equal to $\mu \cdot \tau \approx 2.8 \cdot 10^{-4}$ and $\approx 1.2 \cdot 10^{-4} \text{ V}^{-1} \cdot \text{cm}^2$, respectively.

Extraction of terbium ions from aqueous solutions using a magnetic core nitrogen-functionalised polysilsesquioxane particles

Stoliarchuk N.V.¹, Korobeinyk A.V.¹, Tkachenko O.², Budnyak T.M.²

¹ *Chuiko Institute of Surface Chemistry, NAS of Ukraine, 03164, 17 O. Mudrak Str., Kyiv, Ukraine; stonata@ukr.net*

² *Uppsala University, Villavägen 16, 752 36, Uppsala, Sweden; tetyana.budnyak@angstrom.uu.se*

Rare earth elements (REEs), collectively comprising 17 elements, have professed an emerging popularity [1] due to their significant role in generating solar cells, wind turbines, and electric vehicles. Even though called “rare”, they are quite abundant, however highly dispersed, in the Earth crust, and never as a pure metal [2]. Irregularity in naturally occurring and high requests leads to dependence on secondary sources. Thus, recovery of REEs from wastewaters, E-waste, slags, fly ash, and mine tailings, etc., offers a sustainable solution. Among the REEs, the heavy rare earth elements (HREEs) called special attention for use in high technologies and renewable energy, however they are least abundant in nature. By all of HREEs, terbium is outstanding not only due to versatile utilisation in small electric motors and electronic sensors for the standard automotive industry, including starter motors, wind turbines, and solar technologies [3, 4] but also terbium can substitute other REEs in high applications, i.e., dysprosium [5]. Terbium has less than 1% content in ores outside of South China [6], so it's crucial to find the most effective method for terbium recovery from secondary sources.

Described herein is a technology for the recovery of terbium from aqueous solution via magnetically controlled adsorbents with a HREEs target's functional groups; while terbium is extracted from the solution by chemical adsorption, the application of an external magnetic field facilitates the separation of the sorbent and the media. Core-shell samples of the magnetic core and shell of polysilsesquioxane functionalised with nitrogen-containing groups (able to interact with the HREEs ions) were synthesized via the modified Stober method [7]. Structure and properties of synthesized samples were analyzed using SEM, XRD, magnetic susceptibility tests, IR, and nitrogen adsorption-desorption (Fig.). XRD confirms magnetite formation (Fig., a), and the presence of functional groups was confirmed by IR and element analysis (EA). Content of functional groups of the functionalised polysilsesquioxane shell was calculated from EA (Fig., Table). All samples show super-paramagnetic properties with magnetic susceptibility values in a range 6.03 to 8.80 ($\times 10^{-5}$ SI). Fig.(b, c) displays kinetic curves and adsorption isotherms of Tb^{3+} ($Tb(NO_3)_3 \cdot 5H_2O$) for all samples under investigation. For Samples 1, 2 and 4 the adsorption equilibrium can be reached within 30 min (Fig., b). Highest adsorption values (110 mg/g) were obtained in extraction of Tb^{3+} for Sample 3.

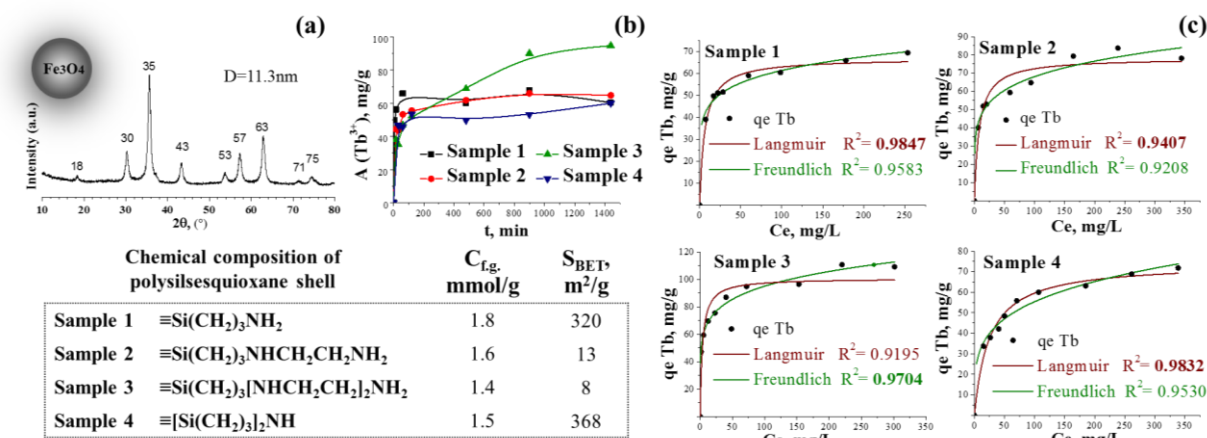


Fig. 1. Sample characteristics: XRD of magnetic sample (a), kinetics (b) and adsorption (c) isotherms for Tb^{3+} (with Langmuir and Freundlich models fitting, and R^2 values); table of chemical composition of samples polysilsesquioxane shell and S_{sp} values.

Conclusions

It is clear that there is a high correlation between the adsorption of Tb^{3+} and the chemical composition of the polysilsesquioxane shell. Since adsorption isotherms for Samples 1, 2 and 4 better fit the Langmuir model, those samples are defined by localized character over isolated adsorption centers. Sample 3 fits a Freundlich model, which indicates the presence of irregular adsorption centres on the adsorbent surface, and also explains the extended period for adsorption equilibrium. However, it is necessary to consider the occurrence of desorption as well as a change of T and pH.

Acknowledgements:

This research was financially supported by the Swedish Institute Foundation through the project EduSustRec4Ukraine (Baltic Sea Neighbourhood Programme, BSNP 01257-2023).

References

- [1]. Dutta, A., et al., *Impact of news and social media sentiments on rare earth investments*. Resources Policy, 2025. **107**: p. 105655.
- [2]. Balaram, V., *Rare earth elements: A review of applications, occurrence, exploration, analysis, recycling, and environmental impact*. Geoscience Frontiers, 2019. **10**(4): p. 1285-1303.
- [3]. Grandell, L., et al., *Role of critical metals in the future markets of clean energy technologies*. Renewable Energy, 2016. **95**: p. 53-62.
- [4]. Alves Dias, P., et al., *The role of rare earth elements in wind energy and electric mobility*. European Commission: Luxembourg, 2020.
- [5]. Alves Dias, P., et al., *The role of rare earth elements in wind energy and electric mobility – An analysis of future supply/demand balances*. 2020: Publications Office.
- [6]. *Mineral commodity summaries 2022*, in *Mineral Commodity Summaries*. 2022: Reston, VA. p. 202.
- [7]. Lapresta-Fernández, A., et al., *Magnetic core-shell fluorescent pH ratiometric nanosensor using a Stöber coating method*. Analytica Chimica Acta, 2011. **707**(1): p. 164-170.

Faraday effect in ZnSe crystals doped with transition metals

Kinzerska, O.V.¹, Slyotov, M.M.¹, Mazur, T.M.²

¹ *Yuri Fedkovich Chernivtsi National University, Chernivtsi, Ukraine,*
oksanakinzerska@gmail.com

² *Ivano-Frankivsk National Technical University of Oil and Gas, Ivano-Frankivsk, Ukraine.*

of the Faraday effect in zinc selenide doped with some transition metal impurities, namely Mn, Fe and Co. Fig. 1a shows the spectral dependences (dispersion curves) of the Verde constant, which was calculated using the relation $\Theta = V \cdot H \cdot d$, where H – magnetic field strength, d – sample thickness, V – Verde's constant, which in turn depends on the frequency of light and the nature of the substance.

Measurements of the rotation angle of the plane of polarization were carried out at $T = 77$ K with an intensity of $H = 10000$, and the thickness of the samples was chosen to be $d_0 \approx 0.1$ cm.

As can be seen from fig. 1a, for all the studied samples, an increase in the Verde constant is observed with an increase in the energy of the light quantum, which is characteristic of the diamagnetic state of the substance. It is known that the transition metal impurity is not distributed throughout the entire volume of the sample, but is located in the diffusion layer with a thickness of d , which is less than d_0 .

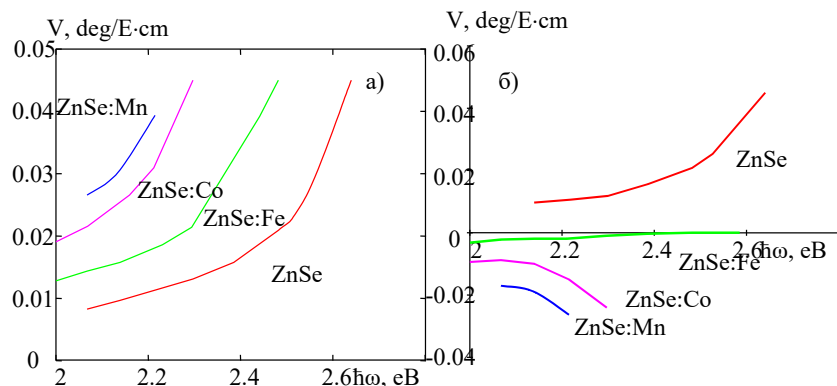


Fig. 1. Spectral dependences of the Verde constant

In this regard, to find the true spectral dependence of the Verde constant for doped samples, it is necessary to find the difference between the value V for ZnSe:Me and its value $\hbar\omega$ at the same for the base ZnSe crystals.

As a result of this action, the dispersion curves of fig. 1 a are transformed into other dependencies $V(\hbar\omega)$, which are depicted in Fig. 1b.

Comparison of the nature of the obtained dependences of the Verde constant on the photon energy with known literature data for other materials allows us to draw the following conclusions. At the temperature of liquid nitrogen, impurity-free ZnSe crystals have diamagnetic properties. Doping of zinc selenide base substrates with Mn and Co impurities leads them to a paramagnetic state, and Fe to a ferromagnetic state.

Far-infrared emission induced by hot carriers in silicon

Mazur, M.P., Mazur, T.M., Bandura, A.I.

*Ivano-Frankivsk National Technical University of Oil and Gas, Ivano-Frankivsk, Ukraine,
myroslav.mazur@nung.edu.ua*

The paper investigates the mechanism of hot carrier emission in silicon in the far-infrared (FIR) region of the spectrum. It is shown that intense excitation of electrons in the conduction band leads to a non-equilibrium energy distribution, which causes effective FIR emission.

The research methodology was based on the analysis of spectral characteristics of radiation and kinetic processes of hot carrier relaxation. Particular attention was paid to the interaction of electrons with phonons and the effect of scattering on radiation dynamics. It was established that the intensity of radiation depends on the excitation energy of carriers and the temperature of the crystal (Fig. 1). A significant increase in the FIC signal is also observed when a critical injection level is reached [1]. The characteristic energy scales of relaxation processes were determined.

The results obtained are important for the development of semiconductor physics and the creation of new radiation sources in the far IR region of the spectrum.

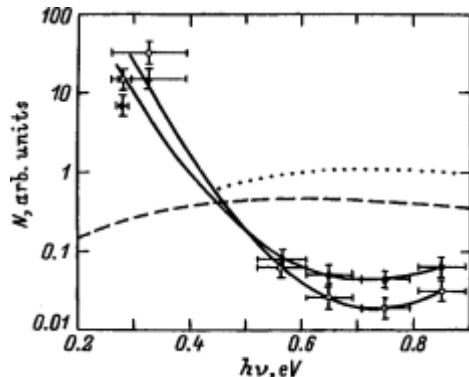


Fig. 1. Spectral distribution of the number of photons $N(h\nu)$ radiated by n–p–n (solid circles) and p–n–p (open circles) transistors at an accelerating voltage of 4 V and injected current of 100 mA. The dashed and dotted curves correspond to the theoretical spectral distributions of radiative electron intersubband transitions.

These effects open prospects for the use of silicon as an active medium for integrated optoelectronic systems. In particular, the identified patterns of hot-carrier radiation can be used as a basis for the development of compact solid-state sources in the far-infrared range, compatible with modern silicon microelectronics technologies.

[1]. Kosyachenko L.A., Mazur M.P. Hot-carrier far infrared emission in silicon. *Semiconductors*. 1999. V. 33, No 2. P. 143-146.

Features of the fullerite films synthesis by the electrophoretic method

Gavrilyuk N.A.^{1, 2}, Shaposhnikova T.I.¹, Anikina N.S.¹, Savenko A.F.¹,
Pomytkin A.P., Krivushchenko O.Y.¹, Kotliar D.A.¹, Zolotarenko A.D.^{1, 2},
Zolotarenko O.D.^{1, 2}, Bezsmertna V. I. 1, Mashira V. A.^{1, 2}, Schur D.V.¹,
Gabdullin M.T.³

¹ Frantsevich Institute for Problems of Materials Science of NASU, 3, Krzhyzhanovsky Str., Kyiv, 03142, Ukraine,

² Chuiko Institute of Surface Chemistry of NASU, 17, General Naumova str., Kiev, 03164, Ukraine

³ Kazakh-British Technical University (KBTU) 71, Al-Farabi Str., Almaty, 050040, Kazakhstan.

Fullerene C₆₀ is a new type of π-acceptor and has a number of significant differences from other acceptor molecules: large size, spherical shape, unique electronic structure, high symmetry and polarizability. These features introduce a certain specificity into donor-acceptor interactions in fullerene compounds.

As experiments have shown, the working solution of toluene-fullerene-ethanol (TFE) both with additives and without them has a fairly high electrical conductivity and was used in the work both for studying the electrochemical properties of fullerenes and for electrodeposition of fullerenes in the form of coatings or obtaining a large amount of the product in the form of fullerites or their compounds on electrodes.

The presence of fullerenes in the solution leads to some change in the volt-ampere characteristic compared to that of the toluene-ethanol (TE) solution. The dependence I(U) becomes practically linear in the region of measured voltages, and the current value, all other things being equal, is slightly lower for the TFE electrolyte, and higher for the TFE solution with the addition of KOH compared to that for the TE solution. In this case, the total electrical resistance of the cell for the TFE electrolyte with the above composition and experimental conditions, determined from the dependence I(U) according to Ohm's law for a section of the circuit, corresponds to ~ 2.9 10⁵ Ohm, for the electrolyte with the addition of KOH - 0.7 10⁵ Ohm. In general, the electrical resistance of the cell strongly depends on both the composition of the electrolyte and the concentration of the constituent components of the solution.

First-Principles Study of Electronic Spectra and Mechanical Properties of Nonstoichiometric ZrC_x

Plyushchay, I.V.¹, Ovsiienko, I.V.¹, Plyushchay, A.I.²

¹ Taras Shevchenko National University, Kyiv, Ukraine, inna.pl@knu.ua

² Kyiv Academic University, Kyiv, Ukraine, plyushchay@gmail.com

³ Institute for Metal Physics of the N.A.S. of Ukraine, Kyiv, Ukraine, plyushchay@gmail.com

The results of ab initio modelling of the electronic structure and mechanical properties of nonstoichiometric zirconium carbide ZrC_x are presented. The calculations were performed within the density functional theory in the generalized gradient approximation using the ABINIT software package. Transition metal carbides with the NaCl-type (B1) structure were modeled using a 24-atom supercell, containing three (111) planes of zirconium and carbon atoms each, with four atoms per plane. Substoichiometry was introduced by removing one or more carbon atoms from the supercell, thus simulating different concentrations of carbon vacancies. The applicability of the chosen supercell was verified by comparison with a larger 96-atom cell with random distribution of vacancies, which did not significantly change the main features of the electronic spectra.

The calculations of pressure for the determination of mechanical moduli were carried out on $\text{Zr}_{12}\text{C}_{12}$, $\text{Zr}_{12}\text{C}_{11}$, and $\text{Zr}_{12}\text{C}_{10}$ supercells under isotropic compression and tension. The obtained electronic spectra show that the Fermi level lies in the vicinity of a local DOS peak resembling a Van Hove singularity. This peak originates from flat regions in the electronic dispersion and leads to a strong sensitivity of the electronic structure to deviations from stoichiometry. The introduction of carbon vacancies shifts the Fermi level toward the minimum of the pseudogap, thereby reducing the occupation of antibonding states and stabilizing the structure. As discussed in our previous work on TiC_x [1], this feature is closely related to the intrinsic nonstoichiometry of group IV transition metal carbides and correlates with the experimentally observed equilibrium concentration of carbon vacancies, explaining the absence of strictly stoichiometric compositions in these materials.

[1]. Plyushchay I.V., Tsaregradska T.L., Plyushchay O.I. Modelling of Electronic Structure and Mechanical Properties of Substoichiometric TiC_x . *Metallofiz. Noveishie Tekhnol.* 2018. V. 40, No 8. P. 1113–1121.

Formation of surface films on component particles during free sintering of B₄C with oxide and boride impurities

Kotliar D.A.¹, Mashira V.A.^{1,2}, Kravchuk A.V.¹, Savenko A.F.¹, Khora O.V.^{1,2}, Demianenko E.M.^{1,2}, Kopylova L.I.¹, Gavrilyuk N.A.^{1,2}, Zolotarenko A.D.^{1,2}, Zolotarenko O.D.^{1,2}, Bezsmertna V.I.¹, Schur D.V.¹, Gabdullin M.T.³

¹ *Frantsevich Institute for Problems of Materials Science of NASU, 3, Krzhyzhanovsky Str., Kyiv, 03142, Ukraine, o_khora@ukr.net*

² *Chuko Institute of Surface Chemistry of NASU, 17, Oleha Mudraka Str., Kyiv, 03164, Ukraine.*

³ *Kazakh-British Technical University (KBTU) 71, Al-Farabi Str., Almaty, 050040, Kazakhstan.*

Despite the significant amount of research conducted, the complex problem of creating dense ceramic materials with increased fracture toughness characteristics remains unsolved.

To successfully establish the optimal manufacturing technology and composition of the composite in order to obtain a material with the highest functional indicators, it is necessary to know the processes occurring in the material during manufacturing, processing into products and subsequent operation. During the formation of a composite material, there is a physical and chemical interaction of components in different aggregate states, which leads to the formation of phases and interfaces between the constituent parts. The phase interface zone determines most of the properties characterizing the composite material.

B₄C ceramics are successfully used in various industrial fields. Pressureless sintering is widely used due to the relatively low cost of producing complex-shaped parts. Sintering additives increase the density and mechanical properties of B₄C ceramics. The paper considers examples of the use of some metal oxides and borides and the formation of surface films on component particles during free sintering of B₄C with impurities of oxides and borides. Experiments have shown that when sintering a mixture of B₄C powders with TiO₂ in the temperature range of 1900–2050°C, the relative density of B₄C ceramics reaches more than 99% of the theoretical value.

It was found that during sintering, TiO₂ forms a thin film and then transforms into TiB₂. The bending strength and fracture toughness at 15 vol% TiO₂ were 513 MPa and 3.7 MPa•m^{1/2}, respectively.

The use of CrB₂ in an amount of 20 mol% at a sintering temperature of 2030°C promotes compaction of samples up to 98.1%. Flexural strength and fracture toughness were 525 MPa and 3.7 MPa m^{1/2} respectively.

Frequency-Dependent Conductivity of Reduced Graphene Oxide: A Comparison of Drude–Smith and Drude–Lorentz Approaches

Zapukhlyak R., Boychuk V., Kotsyubynsky V., Tatarchuk T., Hoy.V.,
Klymyuk M., Frolyak V.

*Vasyl Stefanyk Carpathian National University, Ivano-Frankivsk, Ukraine,
ruslan.zapukhlyak@pmu.edu.ua*

Reduced graphene oxide (rGO) exhibits a complex mechanism of electrical conductivity caused structural heterogeneity, graphene-like domains, residual oxide groups, and interdomain barriers. rGO was obtained by a hydrothermal method on the base of GO synthesized by Tour's approach [1]. The pH of the GO colloid was adjusted to 10.0 using a NaOH solution prior to treatment at 180°C for 5 hours. Pressed cylindrical pellets with a diameter of 25 mm and thickness of 1.0 mm were prepared under a 20 kN. Frequency-dependent electrical conductivity was measured in the range 10^{-2} – 10^5 Hz at 25–200 °C. Experimental data were analyzed using two theoretical frameworks: the Drude–Smith (DS) and Drude–Lorentz (DL) models, which account for different aspects of carrier transport in disordered systems. The DS model, which incorporates partial backscattering and restricted motion of carriers, provided a good description of the conductivity spectra at low and intermediate frequencies (10^2 – 10^3 Hz). The analysis revealed a characteristic dc plateau, thermally activated conductivity with activation energy of 0.120 eV, and frequency-dependent suppression at high ω due to carrier localization and interfacial polarization (Maxwell–Wagner mechanism). Deviations were observed above 10^3 Hz, where DS failed to capture the full frequency response, especially for the imaginary component of conductivity. To address these limitations, the DL model was applied. By introducing two oscillators, representing contributions from mobile carriers in graphene domains and localized oscillations at defect-rich or functionalized regions, the DL model achieved significantly better fits across the entire frequency range. The extracted plasma frequencies and damping parameters displayed distinct temperature trends: one oscillator reflected delocalized carriers in graphene-like regions, while the other described localized or defect-driven transport. The DL-based Arrhenius analysis yielded an activation energy of 0.129 eV, consistent with the DS result, thus validating the robustness of both approaches while highlighting the broader applicability of DL. This comparative data demonstrates that rGO conductivity arises from a hybrid mechanism combining percolative transport, interfacial polarization, and localized oscillations. The results offer new insights into tailoring electrical properties of rGO for electronic, sensing, and energy storage applications through controlled synthesis and defect engineering.

[1]. Kotsyubynsky V., Khimyak Y. Z., Zapukhlyak R., Boychuk V., Turovska L., Hoi V. NaOH-assisted hydrothermal reduction of graphene oxide. *Journal of Physics: Condensed Matter*, 2024, V.36, No 49, P.495701.

Functional phosphor-in-glass films with microcrystalline inclusions

Zozulia, V.O.¹, Terebilenko, K.V.¹, Slobodyanik, M.S.¹

¹ Taras Shevchenko National University of Kyiv, Kyiv, Ukraine, valeria.zozulia@knu.ua

The rapid development of laser technologies, plasma displays and white LEDs requires efficient phosphor materials and suitable hosts for them. Phosphor in glass (PIG) technology offers better thermal stability, improved light quality, longer life span compared to polymer based encapsulants [1]. Moreover, inorganic oxide matrices based on phosphate, tungstate, molybdate are believed to be capable of transferring excitation energy to luminescent centers [2]. Therefore, this work focuses on synthesis and optical properties nanoscale phosphors prepared by both melt-quenching, and solid-state techniques. Both techniques apply alkali metal phosphates, transition metal oxides such as molybdenum or tungsten oxides, and rare earth oxides to enable luminescent properties.

To analyze and confirm the composition, structure features and optical properties of phosphor materials, a combination of techniques was applied, including infrared spectroscopy, X-ray diffraction, photoluminescence spectroscopy and X-ray crystallography. These methods provide detailed insight into the chemical bonding, crystalline phases, and luminescence behavior which is crucial for optimizing material performance.

[1]. He M., Jia J., Zhao J., Qiao X., Du J., & Fan X. Glass-ceramic phosphors for solid state lighting: a review. *Ceramics International*. 2021. T. 47. No 3. P. 2963-2980.

[2]. Laguna M., Nuñez N. O., Becerro A. I., Lozano, G., Moros M., de la Fuente J. M., ... & Ocaña M. et al. Synthesis, functionalization and properties of uniform europium-doped sodium lanthanum tungstate and molybdate ($\text{NaLa}(\text{XO}_4)_2$, X = Mo, W) probes for luminescent and X-ray computed tomography bioimaging. *Journal of Colloid and Interface Science*. 2019. T. 554. P. 520-530.

High-temperature transformation of surface fullerite

Gavrilyuk N.A.^{1,2}, Shaposhnikova T.I.¹, Anikina N.S.¹, Savenko A.F.¹, Pomytkin A.P.¹, Kravchuk A.V.¹, Krivushchenko O.Y.¹, Kotliar D.A.¹, Zolotarenko A.D.^{1,2}, Zolotarenko O.D.^{1,2}, Bezsmertna V. I.¹, Mashira V. A.^{1,2}, Schur D.V.¹, Gabdullin M.T.³

¹ *Frantsevich Institute for Problems of Materials Science of NASU, 3, Krzhyzhanovsky Str., Kyiv, 03142, Ukraine,*

² *Chuko Institute of Surface Chemistry of NASU, 17, General Naumova str., Kiev, 03164, Ukraine.*

³ *Kazakh-British Technical University (KBTU) 71, Al-Farabi Str., Almaty, 050040, Kazakhstan.*

Carbon materials are widely used in science and technology, since, as is known, carbides of many metals have high hardness and strength. The need for materials for work in high-temperature conditions is increasing. Nanotechnologies are already used and nanocarbon compounds will find wide application in the future.

The developed statistical theory of the sprayed fullerenes destruction processes on the free surface of a crystal and the study of the temperature transformation of the carbon coating on the crystal made it possible to explain and justify the temperature dependence of the equilibrium concentration of carbon, which is experimentally manifested during the formation of surface graphite, surface carbide on the crystal face in different temperature ranges, as well as the formation of bulk carbide at sufficiently high temperatures. In the latter case, the temperature dependence of the carbon solubility in the metal was actually obtained.

The resulting formula for the concentration of carbon made it possible, in accordance with the experimental data, to obtain the conditions that the energy parameters of the studied phases must satisfy and then estimate the energy constants of these phases.

The graphs of the temperature dependence of the carbon equilibrium concentration, constructed for the found energy parameters, show a decrease in the concentration of carbon in the surface graphite and surface carbide and an increase of the bulk carbide with increasing temperature. This result is in qualitative agreement with the experimental data obtained in the process of spraying fullerenes onto the surface of a molybdenum crystal with an increase in the temperature of the latter.

Hopping conductivity in SiGeSn thin films

Kondratenko S.V.¹, Datsenko O.I.¹, Lytvyn P.M.

¹ Taras Shevchenko National University of Kyiv, 64 Volodymyrs'ka St. 01601, Kyiv, Ukraine,
kondratenko@knu.ua

² V.E. Lashkaryov Institute of Semiconductors Physics, NAS of Ukraine, 41 pr. Nauki, 03028, Kyiv, Ukraine

(Si)GeSn are promising materials for Si-compatible IR photoelectronics, as they have a lower bandgap that may be direct at high Sn content. Therefore, their electric properties are being studied extensively.

This work studied films of Si0.12Ge0.71Sn0.09 alloys deposited on Ge/Si substrates by admittance spectroscopy within 1-1000 kHz at different temperatures. GaZn eutectic electrodes were applied to the structures with 100, 150 and 200 nm thick films.

Photoelectric spectra of the studied structures in Fig. 1 demonstrate a dominant contribution of Si above 1.2 eV, the photocurrent in Ge corresponds to energies above 0.7 eV, while the impact of the SiGeSn film below 0.7 eV is negligible.

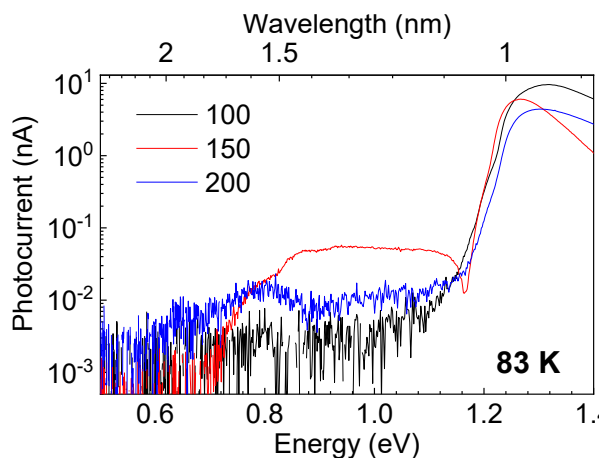


Fig. 1. Photocurrent spectra of the studied SiGeSn/Ge/Si structures at 83 K

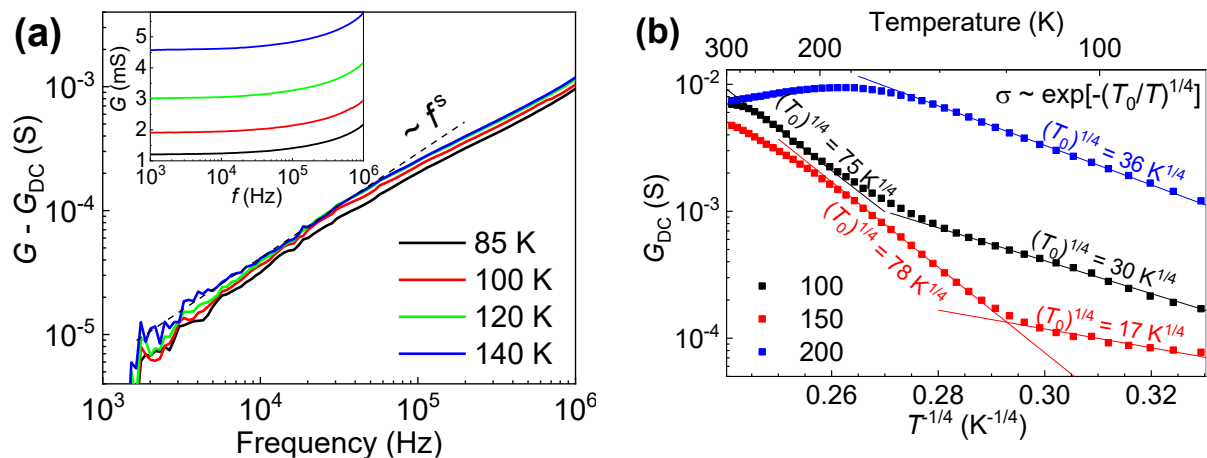


Fig. 2. (a) Frequency-dependent term of the admittance real part (and full data in the inset) for the sample with 200 nm thick film at different temperatures and fitting by Jonscher equation (dash), (b) temperature dependencies of the DC resistance for the

studied films as well as fitting following Mott

Spectra of admittance $A = G + jB$ were obtained, the real part G within the frequency range 1-10 kHz was fitted by Jonscher power dependence $G(\omega) = G_{DC} + Q\omega^s$ (Fig. 2a), where G_{DC} is the DC resistance, Q is a constant, and $0 < s \leq 1$.

The DC resistance revealed sections following Mott theory characteristic for hopping conductivity, $\sigma = \sigma_\infty \cdot \exp[-(T_0/T)^{1/4}]$ (Fig. 2b), while the parameter T_0 allows to estimate the density of localized states near the Fermi level $N(E_F)$, hopping length R_{hop} and hopping activation energy W . The parameters for the studied films are collected in Table 1. We should first pay attention to the parameter R_{hop} . The values about ~ 20 nm are too high and unreliable; thus, they should be ignored, and the respective slopes of the dependencies obviously belong to other kinds of conductivity, such as thermally-activated ones. The rest data marked in bold may be analyzed.

Table 1.

Hopping parameters in the SiGeSn films calculated with Mott theory

| Film thickness (nm) | $(T_0)^{1/4}$ (K ^{1/4}) | $N(E_F)$ ($\times 10^{19}$ eV ⁻¹ cm ⁻³) | R_{hop} (nm) at 85 K | W (eV) at 85 K |
|---------------------|-----------------------------------|---|------------------------|------------------|
| 100 | 29.8 | 60.1 | 7.9 | 0.095 |
| | 74.9 | 1.51 | 19.8 | 3.77 |
| 150 | 17.1 | 561 | 4.52 | 0.010 |
| | 77.5 | 1.32 | 20.5 | 4.33 |
| 200 | 35.8 | 28.9 | 9.49 | 0.198 |

The shortest hopping distance $R_{hop} = 4.52$ nm is observed for 150 nm thick film, whereas that in the thickest (200 nm) film increases to 9.49 nm. The former sample exhibits the highest density of states, which agrees with the RSM and AFM observations (Fig. 3) that indicate cluster formation and increased structural disorder. At the same time, the thickest film appears to accumulate additional disorder, which broadens the distribution of localized states and simultaneously reduces their spatial overlap. This competition results in an increased hopping distance and decreased density of localized states near the Fermi level.

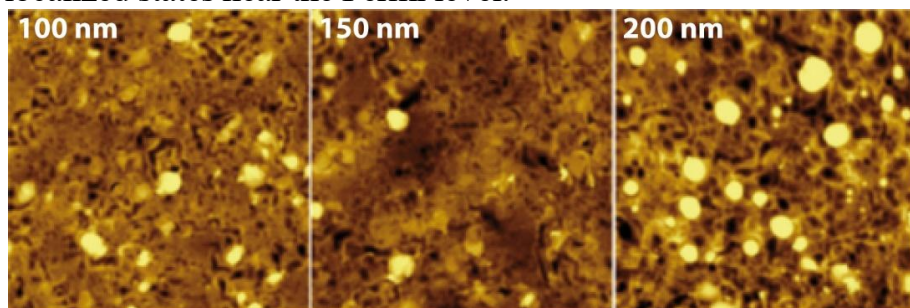


Fig. 3. $10 \times 10 \mu\text{m}^2$ AFM images of the studied SiGeSn films.

This work was supported by the National Research Foundation of Ukraine [2023.03/0060].

Hough transform-based algorithm for Kikuchi band Detection

Fodchuk I., Balovskyak S., Solodkyi M., Borchia M., Kroitor O., Kuzmin A., Hutsuliak I.

Yuriy Fedkovych Chernivtsi National University, Chernivtsi, Ukraine
m.solodkyi@chnu.edu.ua

Given the complex structure of diffraction patterns, the analysis of Kikuchi bands for strain distribution assessment remains insufficiently accurate, particularly in crystals with low symmetry. The classical Hough transform method enables the detection of only well-defined, high-contrast bands. In light of the need to improve the accuracy of diffraction pattern analysis, the development of efficient algorithms for automated image processing is a timely and relevant objective. Automating the characterization of Kikuchi bands contributes to greater objectivity in analysis and reduces the influence of subjective factors during result interpretation.

The study presents a method for preprocessing digital images of Kikuchi bands obtained from synthetic diamond crystal regions [1], which includes noise removal by oriented filtering along the directions of the bands using an oriented Gaussian filter and local contrast enhancement. Such preprocessing enables more precise extraction of band edges as linear segments.

The orientation of the filter kernel was determined by analyzing the orientation for the local brightness distribution of the image. This approach improves the accuracy of band edge detection by enhancing their representation as straight-line segments. A two-level approach to edge description is proposed.

At the first level, the band edges are approximated by straight lines. At the second level, these approximations are refined using hyperbolic curves. The parameters of the hyperbolas are determined by minimizing the mean square error between the hyperbolic curve and the detected band contour points. It is demonstrated that hyperbolas provide significantly more accurate approximations of Kikuchi band edges compared to straight lines.

A Python-based software tool has been developed to enable automatic detection of Kikuchi bands.

[1]]. I. Fodchuk, S. Balovskyak, M. Solodkyi, M. Borchia, D. Băilă, R. Labudzki, and M. Bonilla, “Spatial distributions of local strains in synthesized diamond crystals from the normalized parameters of Kikuchi patterns”, Physics and Chemistry of Solid State, 2024, Vol. 25(4), P. 773–781.

Acknowledgments

This work was partially supported by Ministry of Education and Science of Ukraine (grant number 0125U000832, authors M. Solodkyi, A. Kuzmin; grant number 0125U001483, authors I. Fodchuk, M. Borchia, S. Balovskyak, I. Hutsuliak).

Hydrogen adsorption on the surface

Kopylova L.I.¹, Savenko A.F.¹, Demianenko E.M.^{1,2}, Khora O.V.^{1,2},
Kravchuk A.V.¹, Kotliar D.A.¹, Gavrilyuk N.A.^{1,2}, Zolotarenko A.D.^{1,2},
Zolotarenko O.D.^{1,2}, Korochkova T.E.^{1,2}, Mashira V.A.^{1,2}, Schur D.V.¹,
Gabdullin M.T.³

¹ Frantsevich Institute for Problems of Materials Science of NASU, 3, Krzhyzhanovsky Str.,
Kyiv, 03142, Ukraine, Demianenko_en@ukr.net

² Chuiko Institute of Surface Chemistry of NASU, 17, Oleha Mudraka Str., Kyiv, 03164,
Ukraine

³ Kazakh-British Technical University (KBTU) 71, Al-Farabi Str., Almaty, 050040,
Kazakhstan

In this work, a theoretical calculation of the solubility isostere for adsorbed hydrogen on the (0001) face of an hcp crystal was performed. The calculation of the surface free energy was carried out on the basis of molecular kinetic concepts. The equilibrium equations made it possible to obtain relations that determine the P-T-c diagrams of the crystal surface state. Isotherms, isobars, and isosteres of the adsorbed hydrogen solubility are constructed, their analysis is carried out, and their possible course is established [1, 2].

In this case, the energies of hydrogen atoms in the surface interstices were estimated using experimental isosteres for a ruthenium crystal. The obtained theoretical isosteres confirmed the possibility of the appearance of jumps and kinks in the graphs due to the phase transition of the crystal from an isotropic to an anisotropic state. This result is in full agreement with the experimental data on the solubility isosteres of adsorbed hydrogen on ruthenium.

Of interest is the experimental construction of isotherms and isobars for the adsorbed hydrogen solubility on crystals during their transition from an isotropic to an anisotropic state, accompanied by ordering of hydrogen atoms, in order to possibly reveal the regularity of their behavior and, in particular, the possible detection of an extreme dependence of the atomic order, on temperature and pressure, as predicted by theory.

[1]. Schur D.V., et al. Features of hydrogen storage in a compact state. I. Hydrogen atoms in crystalline solids. LAMBERT Academic Publishing 632 p, (2025).

[2]. Schur D.V., et al. *J. Alloys and Compounds*. 2002. V. 330-332. P. 81-84. & P. 309-315.

Influence of hydromechanical synthesis conditions on the morphology transformation of V₂O₅ nanobelts

Kolomiiets D. I., Pasichnyy M. O.

*The Bohdan Khmelnytsky National University of Cherkasy, Cherkasy, Ukraine,
denyskolomiiets95@gmail.com, pasichnyy@vu.cdu.edu.ua*

One-dimensional nanostructures have gained considerable attention due to their exceptional physical properties and wide range of potential applications in nanoelectronics, optoelectronics, and energy technologies.

The research focuses on the influence of key system parameters — including pH, temperature, viscosity, mixing intensity, sodium chloride (NaCl) and vanadium pentoxide (V₂O₅) concentration — on the hydromechanical synthesis of V₂O₅ nanobelts from commercial V₂O₅ powder. During synthesis, changes in pH, viscosity, and electrical conductivity were monitored. Two main experimental parameters were investigated in detail: mixing speed and NaCl concentration. The results demonstrated that higher mixing speeds promoted the formation of elongated nanostructures by modifying the crystallization kinetics. NaCl acted as a catalyst accelerating the transformation of V₂O₅ agglomerates into nanobelts.

The morphology of the synthesized nanobelts was analyzed using scanning electron microscopy (SEM) (Fig. 1.) and X-ray diffraction (XRD).

Fig. 1. SEM image of the formed V₂O₅ nanobelts



The scalability, reproducibility, and material efficiency of the method enhance its attractiveness for large-scale production. This contributes to the further development of V₂O₅ nanobelts for applications in energy storage, catalysis, and emerging electronic and photonic technologies.

[1]. Xianhong R., Yuxin T., Malyi O., Gusak A., Zhang Y. Ambient dissolution-recrystallization towards large-scale preparation of V₂O₅ nanobelts for high-energy battery applications. *Journal of Nano Energy*. 2016. V. 22. P. 583-593.

Infrared extinction and photoluminescence of highly doped CdTe:Cr single crystals

Popovych, A.V.¹, Popovych, V.D.^{1,2}, Potera, P., Karpii, V.R.¹, Stoliarchuk, I.D.¹

¹*Drohobych Ivan Franko State Pedagogical University, Drohobych, Ukraine,*

andriy.popovich@dspu.edu.ua

²*Lviv Polytechnic National University, Lviv, Ukraine*

³*University of Rzeszow, Rzeszow, Poland*

Significant research and practical interest in the doping of CdTe with Cr impurity have been stimulated in the last several decades by the prospect of CdTe:Cr crystals' use as a gain medium in tunable mid-infrared (IR) solid-state lasers [1] and by their great potential in the field of spintronics [2].

The effect of heavy doping with Cr on the infrared extinction at RT and low-temperature photoluminescence of vapour-grown CdTe single crystals [3] was investigated in the present work. The results indicate a substantial modification of the spectral properties of the crystals within the optical transparency region of CdTe, resulting from the rearrangement of the point defect system and doping-induced precipitation. A Bonch-Bruevich model was used to explain the spreading and redshift of the Urbach absorption edge, enabling the determination of the effective concentrations of point-charged defects and the mean strength of the electric field created as a consequence of their random distribution in the host lattice. The extinction of CdTe:Cr crystals in the near-IR was found to be a sum of the selective absorption arising from the intra-shell transition within the $3d^4$ configuration of substitutional ions, $\text{Cr}_{\text{Cd}}^{2+}$, and the light scattering by the Cr-related nano-precipitates. The concentration of the ions, calculated from optical spectra, was less than half of the total dopant atoms dissolved in the CdTe matrix through secondary ion mass spectroscopy measurements. The extinction in the mid- and longwave IR range of the spectra is determined by the scattering on the dense array of Cr_3Te_4 quasi-2D precipitates developed on the {111}-oriented planes of CdTe due to the exceeding of the Cr solubility limit in this compound.

Low-temperature PL spectra demonstrate the absence of the donor-acceptor emission at 1.45 eV, characteristic of CdTe, obviously due to a decrease in the number of the corresponding centers. Besides, progressive extinction of the exciton and edge emission with the rise of point-charged defect concentration was detected, which may be related to the band-tailing effect [4], also responsible for the spreading and shift of the fundamental absorption edge.

- [1]. Shah R.T. et al., *J. Electron. Mater.* 2002 V. 31 806-810
- [2]. Blinowski J. et al., *Phys. Rev. B* 1996. V. 53 952-957
- [3]. Popovych V.D. et al., *J. Cryst. Growth* V. 426 173-179
- [4]. Shklovskii B.I., Efros A.L. *Electronic Properties of Doped Semiconductors*. Springer-Verlag Berlin Heidelberg, 1984

Investigation of new thermoelectric material based on **Ti_{1-x}Nb_xNiSn_{1-y}Sb_y** solid solution

Romaka V.A.¹, Stadnyk Yu.V.², Romaka L.P.²,
Horyn A.M.², Zelinskiy A.V.²

¹*National University "Lvivska Politehnika", Lviv, Ukraine,
e-mail: volodymyr.romaka@gmail.com:*

²*Ivan Franko National University of Lviv, Lviv, Ukraine,*

Study of the semiconductor solid solution $n\text{-Ti}_{1-x}\text{Nb}_x\text{NiSn}$ showed that it is a promising thermoelectric material and at a concentration $n\text{-Ti}_{0.99}\text{Nb}_{0.01}\text{NiSn}$ and $T \approx 650$ K $ZT = 0.76$ [1]. It was found that Nb atoms can occupy different crystallographic positions, generating energy states of acceptor and donor nature. In this case, the Fermi level ε_F remained near the percolation level of the conduction band ε_C . To obtain maximum values of thermoelectric figure of merit, it was necessary to bring the Fermi level ε_F closer to the conduction band ε_C . For this purpose, $n\text{-Ti}_{1-x}\text{Nb}_x\text{NiSn}$ was doped with a donor impurity Sb, replacing Sn atoms. A new thermoelectric material $\text{Ti}_{1-x}\text{Nb}_x\text{NiSn}_{1-y}\text{Sb}_y$ with high efficiency of converting thermal energy into electrical energy was synthesized.

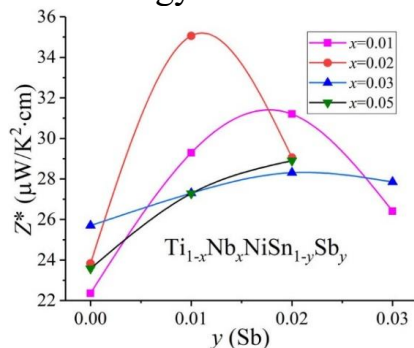


Fig. Change of the thermoelectric power coefficient Z^ of $n\text{-Ti}_{1-x}\text{Nb}_x\text{NiSn}_{1-y}\text{Sb}_y$ at $T=300$ K*

The result of the study of the crystal and electronic structure, electrokinetic and energy properties of $n\text{-Ti}_{1-x}\text{Nb}_x\text{NiSn}_{1-y}\text{Sb}_y$ is the establishment of the nature of the generated energy states and mechanisms of electrical conductivity, which made it possible to establish the parameters of the synthesis of the material with the maximum efficiency of converting thermal energy into electrical energy.

1. Romaka V.A., Stadnyk Yu.V., Romaka L.P., Horyn A.M., Romaka V.V., Haraniuk P.I. *J. Thermoelectricity*. 2025. № 1. P. 5-15.

This research was supported by the Ministry of Education and Science of Ukraine under Grant No. 0124U000989. Authors also thank the Simons Foundation (SFI-PD-Ukraine-00014574) for financial support.

Kinetics of crystallisation of $\text{Ge}_2\text{Sb}_2\text{Se}_{5-x}\text{Te}_x$ phase-change materials

V. M. Kryshenik¹, S. M. Hasynets¹, M. J. Filep^{1,2}, V. Y. Loya¹,
V. V. Lopushansky¹, Y. M. Azhniuk¹, A. V. Gomonnai¹.

¹ Institute of Electron Physics, Nat. Acad. Sci. Ukr., Uzhhorod, Ukraine,
kryshenik@gmail.com

² Ferenc Rákóczi II Transcarpathian Hungarian Institute, Kossuth Sq. 6, Berehovo 90200, Ukraine

Ge–Sb–Se–Te compounds belong to the class of optical phase-change materials which demonstrate high differences of optical parameters (refractive index and reflectivity) upon reversible phase transitions between the crystalline and amorphous phases combined with low optical loss in a broad spectral range (1–18 μm) for both phases.

$\text{Ge}_2\text{Sb}_2\text{Se}_{5-x}\text{Te}_x$ glasses with $0 \leq x \leq 1.1$ were prepared from stoichiometric amounts of elemental components in evacuated quartz ampoules heated to 973 K at a rate of 30 K/h followed by the mixture heating to 1273 K at a rate of 20 K/h with the subsequent aging for 20 h and cooling at 25 K/h down to 873 K and rapid quenching in cold water.

The structure of samples was studied by X-ray diffraction (XRD) using an AXRD Benchtop diffractometer with Cu K_α radiation and a Ni filter and confirmed to be completely amorphous without any crystalline inclusions. This conclusion is supported by the data of Raman spectroscopy (XPloRa Plus spectrometer, $\lambda_{\text{exc}} = 532$ nm, $P_{\text{exc}} = 4$ kW/cm²). Raman measurements performed at elevated laser power density (40 kW/cm²) show that, even in view of the photoinduced deformation of the sample surface, no crystalline phases appear in the unheated as-prepared samples.

Kinetic analysis of non-isothermal crystallisation in $\text{Ge}_2\text{Sb}_2\text{Se}_{5-x}\text{Te}_x$ was performed using differential thermal analysis data obtained at a fixed set of heating rate values β ranging from 2 to 15 K/min. This enabled us to determine the glass-forming temperature T_g , the phase transformation onset temperature T_{ons} , and the exothermic crystallisation peak temperature T_p . For all the samples under study, thermally stimulated crystallisation is governed by a one-step mechanism. Formation of crystalline inclusions in the amorphous matrix is confirmed by the XRD measurements, the crystalline phase being identified as $\text{Ge}_2\text{Sb}_2\text{Se}_5$ (for $x = 0$) or $\text{Ge}_2\text{Sb}_2\text{Se}_4\text{Te}$ (for $x > 0$).

The activation energy E_c of the amorphous-to-crystalline transformation under study was determined by the Kissinger method. With increasing Se content in $\text{Ge}_2\text{Sb}_2\text{Se}_{5-x}\text{Te}_x$ from 0 to 1, the crystallisation peak temperature T_p at $\beta = 6$ K/min gradually varied from 599 to 622 K with E_c decreasing from 178 to 142 kJ/mole. A similar trend was observed for other heating rate values.

Magnesium impurities in hydrogen storage alloys

Savenko O.F.¹, Demianenko E.M.^{1,2}, Khora O.V.^{1,2}, Kopylova L.I.¹,
Anikina N.S.¹, Pomytkin A.P.¹, Krivushchenko O.Y.¹, Kotliar D.A.¹,
Gavrilyuk N.A.^{1,2}, Zolotarenko A.D.^{1,2}, Zolotarenko O.D.^{1,2}, Schur D.V.¹,
Gabdullin M.T.³

¹ Frantsevich Institute for Problems of Materials Science of NASU, 3, Krzhyzhanovsky Str., Kyiv, 03142, Ukraine, Demianenko_en@ukr.net

² Chuiko Institute of Surface Chemistry of NASU, 17, Oleha Mudraka Str., Kyiv, 03164, Ukraine

³ Kazakh-British Technical University (KBTU) 71, Al-Farabi Str., Almaty, 050040, Kazakhstan

Lanthanum-nickel alloys attract the attention of scientists in connection with the possibility of their use as accumulating and storage devices of hydrogen as an energy source. Much attention was paid to the study of LaNi₅, LaNi₇ alloys and multi-component alloys created on their basis. In the latter, lanthanum atoms are partially replaced by atoms of rare earth elements R = Er, Gd, Nd, Pr, Sm, Y, and nickel atoms -by metal and nonmetal atoms M = Al, B, Co, Cu, Fe, Mg, Mn, Si, Sn. In our works, La_{1-x}RXNi_{5-y}My alloys [1-2] were studied, the solubility of hydrogen in them was calculated.

Recently, intensive studies of lanthanum-magnesium-nickel alloys have been carried out. It has been established that magnesium improves the kinetic characteristics of alloys.

The structure and electrochemical properties of La_{2-x}Mg_xNi₇ (x = 0.3-0.6) alloys were systematically studied. The formation of three phases in the system was established: 1) La_{2-x}Mg_xNi₇, 2) LaNi₅, 3) La_{1-x}Mg_xNi₃ depending on the concentrationx of magnesium. In this case, for different values of x, a mixture of phases is formed from two alloys: at x = 0.3–0.5, the samples are a mixture of alloys La_{2-x}Mg_xNi₇ and LaNi₅, at x = 0.6 – a mixture of the first alloy with La_{1-x}Mg_xNi₃. The content of the first alloy in the mixture of phases is set as follows: X1 = 81.5; 93.7; 96.8; 60.7 wt.%, respectively, at x = 0.3; 0.4; 0.5; 0.6.

This paper develops a statistical theory of hydrogen solubility through a thin hydride film in magnesium-containing alloys with L22, D2d, L6O structures.

[1]. Schur D.V., et al. Features of hydrogen storage in a compact state. I. Hydrogen atoms in crystalline solids. LAMBERT Academic Publishing 632 p, (2025).

[2]. Schur D.V., et al. *J. Alloys and Compounds*. 2002. V. 330-332. P. 81-84. & P. 309-315.

MAX-functionalized polypyrrole composites: structure and electrical properties

Horbenko, Y.Y., Aksimentyeva, O.I., Kovalskyi, Y.P., Zhytskyi, A.K., Kordan, V.M.

Ivan Franko National University of Lviv, Lviv, Ukraine, yuliia.horbenko@lnu.edu.ua

The MAX phases are nanolayered, hexagonal, machinable, early transition-metal carbides and nitrides, combining metallic and ceramic properties [1]. This structure allows materials with high mechanical strength, heat resistance [2], and electrical conductivity [3] to be obtained. They serve as precursors for MXenes, which have recently gained significant interest, making the MAX phases even more valuable. However, the effect of the MAX phases on the properties of conducting polymers has not been studied enough. Polypyrrole (PPy) is a heterocyclic positively charged conducting polymer known for easy synthesis, environmental stability, and high electrical conductivity. Therefore, this research aimed to study the effect of the MAX phase, specifically Ti₂AlC, on the structure, electrical properties, and thermal stability of polypyrrole.

Powder samples of PPy/MAX composites with various filling concentrations were synthesized via *in situ* chemical oxidative polymerization. The structural and morphological characteristics of the composites were examined using scanning electron microscopy, infrared spectroscopy, and X-ray diffraction analysis. The effect of the Ti₂AlC filler content on the electrical properties of PPy was studied. The activation energy of electrical conductivity was calculated for samples of various compositions. It was established that a Ti₂AlC content of 5 wt% has the most significant impact on the structure and electrical features of PPy-based composites. Moreover, the incorporation of 5 wt% Ti₂AlC resulted in an enhancement of the thermal stability of PPy, thereby enabling the potential for high-temperature applications.

This work was partly supported by the Simons Foundation (SFI-PD-Ukraine-00014574).

- [1]. Sokol M., Natu V., Kota S. On the chemical diversity of the MAX phases. *Trends Chem.* 2019. V. 1, Iss. 2. 210-223.
- [2]. Jaiswal S., Vishwakarma J., Bhatt S., Karak S., et al. Layered titanium carbide-mediated fast shape switching and excellent thermal and electrical transport in shape-memory-polymer composites for smart technologies: MAX versus MXene. *Adv. Eng. Mater.* 2023. V. 25, Iss. 17. 2300233.
- [3]. Salvo C., Chicardi E., Hernández-Saz J., Aguilar C., et al. Microstructure, electrical and mechanical properties of Ti₂AlN MAX phase reinforced copper matrix composites processed by hot pressing. *Mater. Charact.* 2021. V. 171. 110812.

Micromechanical properties of Cd_{1-x}Zn_xTe single crystals grown in a hydrogen atmosphere by sublimation

A. Tymkiv, V. Brytan, Yu. Pavlovskyy

Drohobych Ivan Franko State Pedagogical University, 24, Ivan Franko Str. Drohobych,
Ukraine, vbrytan2@gmail.com

With the growing demand for efficient and environmentally friendly materials, research and development of CdTe and Cd_{1-x}Zn_xTe are becoming strategically important [1]. CdTe and CdZnTe solid solutions are widely used in laser systems and optoelectronics due to the ability to adjust the bandgap width, which makes these materials suitable for operation in the infrared (IR) and visible spectral ranges. The high performance characteristics of such devices directly depend on the mechanical stability and micromechanical properties of the crystalline material. One way to improve the properties of CZT single crystals is hydrogen treatment, which can be technologically implemented by treating the crystal in a gas discharge of a hydrogen atmosphere [2]. However, the mechanisms of hydrogen treatment's influence on the micromechanical behavior of single crystals remain insufficiently studied.

This paper presents the results of a study of the micromechanical properties of CdZnTe single crystals with a Zn content of 10%, which were grown by sublimation in a hydrogen atmosphere, compared with similar crystals grown in a vacuum. Based on the analysis of experimental data, it has been established that crystals grown in a hydrogen atmosphere are characterized by significantly higher microhardness compared to similar samples grown in a vacuum. Moreover, the crystals obtained in a hydrogen atmosphere showed increased crack resistance: microcracks caused by the indenter were not detected until loads exceeded 120 g, whereas in vacuum-grown samples, they appeared already at 15-20 g. This indicates a reduction in material brittleness and suggests an improvement in its mechanical stability.

The increase in crack resistance is probably associated with the passivation of electrically active defects by hydrogen, which contributes to a reduction in the number of structural defects and the restoration of covalent bonds in the crystal lattice. This, in turn, leads to an increase in the concentration of valence electrons and an improvement in micromechanical properties.

[1]. [S.M. Sze, K.Ng. Kwok,](#) Physics of Semiconductor Devices, Wiley-Interscience, 815, (2007). DOI:10.1002/0470068329

[2]. V.B. Britan, R.M. Peleshchak, D.I. Tsyutsyura, D.V. Korbutyak, The effect of treatment of Cd_xZn_{1-x}Te single crystals in a hydrogen atmosphere on electrically active centers, Solid State Physics and Chemistry, 10(1), 41 (2009). https://pnu.edu.ua/inst/phys_chem/start/pcss/vol10/1001-05.pdf

Nonmonotonic defect formation in surface layers of silicon single crystals under weak effect of cavitation erosion

Gorelov, B.M.¹, Korotchenkov, O.O.², Nadtochiy, A.B.², Podolian, A.O.²,
Kuryliuk, A.M.², Yukhymchuk, V.O.³, Klishevich, G.V.⁴,

¹*Chuiko Institute of Surface Chemistry of NAS of Ukraine, Kyiv, Ukraine, bgorel@ukr.net*

²*Taras Shevchenko National University of Kyiv, Kyiv, Ukraine*

³*V. Lashkaryov Institute of Semiconductor Physics of NAS of Ukraine, Kyiv, Ukraine*

⁴*Institute of Physics of NAS of Ukraine, Kyiv, Ukraine*

Surface erosion was achieved by water cavitation via a Langevin transducer operating at 26–28 kHz and producing a power density of ~1 W/ml. We report the kinetics of defect formation in the surface layers of mm-sized Si (111) crystals. Measurements included Vickers microhardness (HV), X-ray diffraction (XRD), Raman scattering, and defect photoluminescence in the 380–600 nm range. Selected results are presented in Fig. 1.

Initially, during the early stages of cavitation erosion, the surface hardness increases sharply due to the formation of defects in the subsurface layer caused by high-energy impacts of cavitating bubbles; see Fig. 1(a). This process induces a hardening effect similar to that seen in materials under mechanical loading. As the treatment progresses, defects migrate and rearrange, leading to a decrease in HV, which then stabilizes at a nearly constant value as the defect structure reaches equilibrium. The increased XRD intensity with erosion time seen in Fig. 1(b) suggests an enhancement in the crystallinity of the Si surface. As cavitation-induced defects gradually migrate and order themselves over time, interatomic interactions become more structured, improving the material's overall atomic alignment. The broadening of the XRD line at prolonged treatment indicates a degree of disorder or strain within the lattice, likely due to the redistribution of defects, but still within an ordered framework. The interplay between defect migration and ordering in the subsurface layer leads to these changes in both surface hardness and crystallinity. Thus, the combined effects of defect migration, reordering, and increased interatomic interactions explain the observed Si erosion trends.

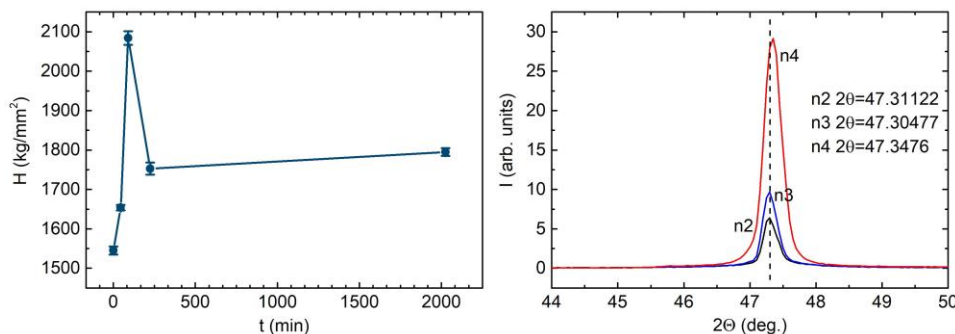


Fig. 1. HV of Si vs cavitation time (a) and XRD peaks after 2, 6, and 24 h treatment (b).

Optical properties of the CdI₂ thick film: experimental and theoretical studies

Rybak O.V., Solovyov M.V., Kashuba A.I.

*Department of General Physics, Lviv Polytechnic National University, Lviv, Ukraine,
oksana.v.rybak@lpnu.ua*

CdI₂ thick film was obtained by cleaving from a bulk sample. The average thickness of the CdI₂ thick film is 2 μm. The optical properties of CdI₂ thick film were investigated by optical absorption spectra. The spectral dependence of the optical absorption and transmission spectra of the obtained CdI₂ thick film in the visible regions is studied at room temperature (AvaSpec-ULS2048-UA-50 (Avantes)). The obtained value of integral transmission is ~57.2 % (a= 360 nm, b= 1000 nm). The absorption spectrum fitting method was applied to estimate the optical band gap and Urbach energy of the CdI₂ thick film. The optical band gaps and Urbach energy obtained for the CdI₂ thick film are 3.05 and 5.17 eV.

Electronic band structure and optical properties are studied for the CdI₂. The theoretical calculations were performed within the framework of the density functional theory (DFT). We calculated the electron dispersion at high symmetry directions, density of electron state and optical properties estimated with the generalized gradient approximation (GGA). A Perdew–Burke–Ernzerhof functional for solids (PBEsol) was utilized. To study the optical properties was use a complex dielectric function $\epsilon(\hbar\omega)$. The refractive index (n) was obtained from the Kramers–Kronig relation. We obtained $n \approx 1.89$ at $\lambda = 700$ nm and $n \approx 1.83$ at $\lambda = 1100$ nm, if comparisons this value with known data from literature ($n \approx 2$ [1] at $\lambda = 700$ nm (500 nm film thickness) and $n \approx 1.93$ at $\lambda = 1100$ nm (1444 nm film thickness) [2]) can be see good agreement. In order to compare the experimental results with the theoretical ones, the spectral behavior of the transmission coefficient (T) was calculated. The main difference between the theoretical and experimental spectral dependence of the transmission coefficient lies in the sharper fundamental absorption edge observed in the theoretical calculation. The experimentally ($T_{\text{aver}} \approx 57.2\%$) and theoretically ($T_{\text{aver}} \approx 70.7\%$) determined values of the normalized integrated transmission is negligible ($\Delta T_{\text{aver}} = 13.5\%$).

- [1]. Tyagi P. and Vedeshwar A.G. Grain size dependent optical properties of CdI₂ films. *Eur. Phys. J. AP*. 2002. V. 19, No 1. P. 3-13.
- [2]. Kariper İ.A. Structural, optical and porosity properties of CdI₂ thin film. *Journal of Materials Research and Technology*. 2016. V. 5, No 1. P. 77-83.

Peculiarities of photoluminescence of ZnO/MnO nanostructures synthesized by ultrasonic spray pyrolysis

Korbutyak, D.V.¹, Berezovska, N.I.^{2,3}, Yukhymchuk, V.O.¹, Kovalenko, O.V.⁴,
Vorovsky, V.Yu.⁴, Dmytruk, I.M.^{2,3}

¹*V. Lashkaryov Institute of Semiconductor Physics, NAS of Ukraine, Kyiv, Ukraine*

²*Taras Shevchenko National University of Kyiv, Kyiv, Ukraine, nataliya.berezovska@knu.ua*

³*Institute of Physics, NAS of Ukraine, Kyiv, Ukraine*

⁴*Oles Honchar Dnipro National University, Dnipro, Ukraine*

Present report deals with the study of peculiarities of secondary emission of ZnO nanocrystals (NCs) doped with a magnetic Mn impurity of different concentrations. ZnO relates to semiconductors with multiple applicability in various fields from electro-optical devices, including solar cells, lasers or varistors, to biological applications. Addition of magnetic impurities such as Mn, Co or Fe can lead to the formation of ferromagnetic properties of ZnO. The solubility of dopants in ZnO lattice depends on many factors (preparation method, annealing temperature, dopant concentration, etc.) and, in turn, affects structural defects in ZnO NCs.

The method of ultrasonic spray pyrolysis was used for the synthesis of ZnO and ZnO:Mn NCs. An atomic concentration of Mn in ZnO:Mn NCs was 2% and 4%. Dry granules are the final product of the synthesis. The synthesized particles have a spherical shape with a hole. They are hollow inside that is the result of leakage of gaseous products of thermal decomposition reactions. The size of spherical particles increases from 0.3÷1.0 μm to 1.0÷3.0 μm with increasing zinc nitrate concentration during synthesis.

A detailed study of the nature of low temperature (at T=77 K) photoluminescence (PL) near fundamental absorption edge and impurity regions of the spectrum of ZnO NCs have been carried out. For ZnO NCs with different Mn concentration we observed the emission bands around 3.467 - 3.352 eV due to the recombination of free excitons. The bands in the energy region 3.33 – 3.12 eV correspond to the bound exciton complexes. The most pronounced fine exciton structure was observed for the ZnO:Mn NCs synthesized at twice the liquid flow rate demonstrating how optimization of technological regimes can form structurally perfect ZnO NCs. In PL spectra some other emission bands attributed to intrinsic defects have been observed, namely it is clearly defined a band at 2.84 eV associated with oxygen vacancies on the surface of ZnO NCs, a broad structural PL band in the region of 2.5 -1.7 eV attributed to the oxygen vacancies, interstitial zinc, etc. The disappearance of the 2.84 eV band after a short exposure of the samples to air is a result of adsorption of oxygen by ZnO NCs. The observed quenching of so-called “yellow” (2.0 eV) PL band elucidates that an increase in the concentration of the Mn impurity leads to the blocking of radiative donor-acceptor transitions in ZnO:Mn NCs.

Phase interactions and solid solution formation in the Ag₆PS₅I – Ag₇SiS₅I system

Shender I.O.¹, Pogodin A.I.¹, Filep M.J.², Malakhovska T.O.¹, Molnar K.A.², Kokhan O.P.¹, Stasiuk Yu.Yu.¹

¹ Uzhhorod National University, Pidgirna St. 46, 88000, Uzhhorod; Ukraine,

² Ferenc Rákóczi II Transcarpathian Hungarian College of Higher Education, Kossuth Sq. 6,90200, Beregovo, Ukraine, iryna.shender@uzhnu.edu.ua

Argyrodites belong to the class of complex chalcogenides with a tetrahedrally close-packed structure, a characteristic feature of which is a high degree of disorder in the cationic sublattice. This structural peculiarity gives rise to enhanced mobility of silver cations, making them promising materials for applications in superionic conductivity and thermoelectrics. As a result, argyrodites attract considerable scientific and practical interest in the context of designing new functional materials. To investigate the features of solid solutions in the Ag₆PS₅I – Ag₇SiS₅I system, samples were synthesized by melting quaternary halogenosulfides in vacuum-sealed quartz ampoules in the corresponding stoichiometric ratios. The process was carried out at temperatures up to 1223 K, which ensured the complete formation of equilibrium phases. The obtained polycrystalline samples were studied using differential thermal analysis (DTA) and X-ray diffraction (XRD). Based on the experimental data, the nature of the physicochemical interactions in the Ag₆PS₅I – Ag₇SiS₅I system was established, and it was determined that this system is partially quasi-binary within the temperature interval of stability of the Ag₆PS₅I phase. In particular, the presence of a peritectic point was identified, characterized by coordinates of 6 mol.% Ag₇SiS₅I and 1035 K.

Thus, the results of the present study demonstrate that the Ag₆PS₅I – Ag₇SiS₅I system enables the formation of continuous solid solutions with an argyrodite-type structure, which opens prospects for further tailoring of these materials with the aim of enhancing their ionic conductivity and thermoelectric performance.

- [1]. Kuhs W.F., Nitsche R., Scheunemann K. The argyrodites - a new family of the tetrahedrally closepacked structures. *Mat. Res. Bull.* 1979, 14, 241–248.
- [2]. Nilges T., Pfitzner A. A structural differentiation of quaternary copper argyrodites: Structure – property relations of high temperature ion conductors. *Z. Kristallogr.* 2005, 220, 281–294.

Phase transitions in Ag_8SnSe_6 : Mössbauer and X-ray Study

Chekaylo, M.V.¹, Yushchuk, S.I.¹, Yuryev, S.O.¹,
Akselrud, L.G.², Mokliak, V.V.^{3,4}

¹ Lviv Polytechnic National University, Lviv, Ukraine, s.o.yuryev@gmail.com

² Ivan Franko National University of Lviv, Lviv, Ukraine

³ G. V. Kurdyumov Institute for Metal Physics, NAS of Ukraine, mvvmcv@gmail.com

⁴ Ivano-Frankivsk National Technical University of Oil and Gas, Ivano-Frankivsk, Ukraine

The structural transformations accompanying the low-temperature phase transition $\beta' \rightarrow \gamma$ in the argyrodite Ag_8SnSe_6 characterized by mixed electron-ionic conductivity, have been studied using Mössbauer spectroscopy and XRD.

XRD patterns of powdered Ag_8SnSe_6 were recorded at 295 K and 393 K. Sn atoms in the γ -phase of Ag_8SnSe_6 are located at the centers of regular tetrahedra coordinated by four Se atoms, whereas in the β' -phase of Ag_8SnSe_6 , the tetrahedra are distorted, as evidenced by differences in Se–Sn–Se bond lengths and angles. The deformation parameters for bond lengths and bond angles, calculated according to [1], are 0.042 Å and 2.60°, respectively.

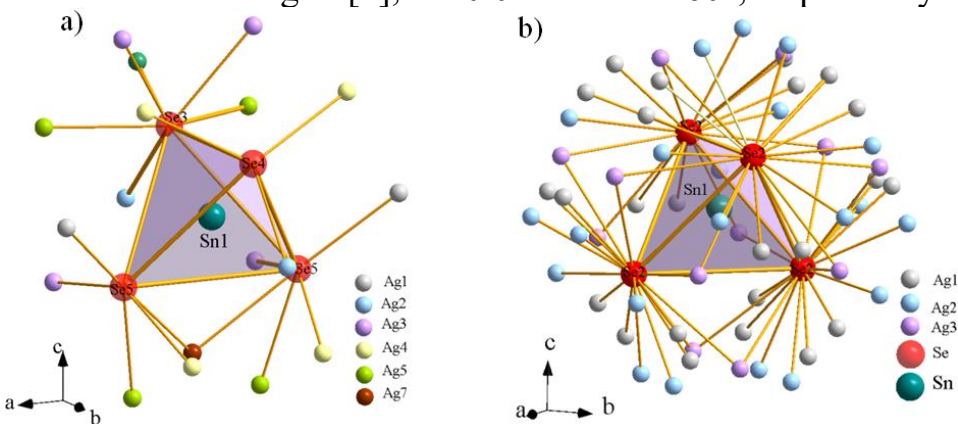


Figure – Spatial models of the first and second coordination spheres of Sn- atoms in the β' - phase (a, 295 K) and γ - phase (b, 393 K) of Ag_8SnSe_6 .

An abrupt decrease in the probability of the Mössbauer effect and isomer shifts was observed in argyrodite near 356 K, corresponding to a phase transition in this compound. It is shown that during the $\beta' \rightarrow \gamma$ phase transition in Ag_8SnSe_6 , an abrupt increase in the root-mean-square vibrational amplitudes of Sn atoms occurs. It is hypothesized that an increase in Ag-site occupancy within the second coordination sphere of γ -phase argyrodite influences the energy state of Sn nuclear levels. In the γ -phase of Ag_8SnS_6 , a homogeneous electric field at the tin nuclei is observed, whereas in the β' -phase of Ag_8SnSe_6 , possible electric field gradients associated with local distortions of the crystal lattice are present. Spatial models of the first and second coordination spheres of Ag_8SnSe_6 in the β' and γ -modifications were proposed (Figure).

[1]. Chekailo, M. V., et al. Temperature dependence of the structures of β' -and γ - Ag_8SnSe_6 argyrodite. *J. Solid State Chem.* , 2024, 332: 124541.

Resonance phenomena in gaps between metallic nanoparticles from the perspective of transformational plasmonics

Korolkov, R.Yu.¹, Shyrokopoias, O.O.¹, Reva V.I.¹, Korotun, A.V.^{1,2}

¹National University Zaporizhzhia Politechnic, Zaporizhzhia, Ukraine, romankor@zp.edu.ua

²G.V. Kurdyumov Institute for Metal Physics of the NAS of Ukraine, Kyiv, Ukraine

As is well known, the concentrating of light energy in the subwavelength volume is an important task for the applications such as nanosensors, single-molecule detection, nanolaser creation, and improved higher harmonic generation. Therefore, it is necessary to localize light on a micron scale and to focus its energy in the nanoscale hot spot. The nanoparticles of noble metals (Au, Ag, Cu) are often used for this purpose. The localized plasmonic resonances are excited on the surfaces of such nanoparticles under the action of light, making it possible to “compress” electromagnetic energy to the dimensions of the order of several cubic nanometres. It should be pointed out that for the vast majority of the nanosystems, the obtaining of the size dependencies of the resonance frequencies using “traditional” approaches is a rather difficult task. Therefore, the search for new approaches to solve these problems is actual.

Over the past two decades, an approach based on transformational optics, that uses the form invariance of Maxwell's equations and conformal (quasi-conformal) coordinate transformations [1] has been developed. Since this approach allows us to obtain the multipole resonance conditions for the big number of the nanosystems, it can be safely called the transformational plasmonics.

Using the transformational plasmonics, let us consider the resonance phenomena in long, co-aligned metallic nanocylinders with the equal base diameters D , located in the dielectric medium with the permittivity ϵ_m . Let us assume that the shortest distance between them is δ (Fig. 1). The multipole resonance condition for the specified system has the form

$$\left(\frac{\epsilon(\omega_{\text{res}}) - \epsilon_m}{\epsilon(\omega_{\text{res}}) + \epsilon_m} \right)^2 = \eta^{4l}, \quad (1)$$

where l is the order of the multipolarity, Drude dielectric function in the dissipation-free approximation

$$\epsilon(\omega_{\text{res}}) = \epsilon^\infty - \frac{\omega_p^2}{\omega_{\text{res}}^2}, \quad (2)$$

and the size-dependent function

$$\eta(c) = \frac{\sqrt{2+c} + \sqrt{c}}{\sqrt{2+c} - \sqrt{c}}. \quad (3)$$

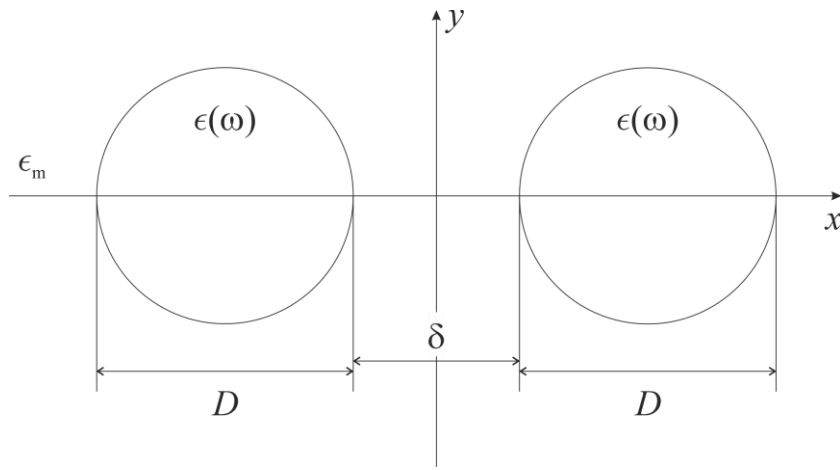


Fig. 1. Geometry of the problem

In formulae (2) and (3), ω_p is plasma frequency; T^∞ is the contribution of the crystal lattice into the permittivity, and $c = \delta/D$.

Substituting the expression (2) into (1), we obtain the size dependencies of the multipole resonance frequencies

$$\omega_{\text{res}}^{(\pm)} = \frac{\omega_p}{\sqrt{T^\infty - \frac{1 \pm \eta^{2l}}{1 \mp \eta^{2l}} T_m}}. \quad (4)$$

Thus, the fact of the resonance frequency splitting in any order of the multipolarity has been established. The calculations have shown that the frequency splitting increases as the distance between the nanocylinders decreases as in the case of the dipole resonances in the dimer of the spherical metallic nanoparticles [2].

[1]. Aubry A., Lei D.Y., Maier S.A., Pendry J.B., Conformal Transformation Applied to Plasmonics beyond the Quasistatic Limit. *Phys. Rev. B.* 2010. V. 82. id. 205109.

[2]. Abramenko L.O., Korotun A.V., Matiushyn V.M. Optical Properties of “Left-Handed” Media Based on a Cubic Lattice of Metallic Nanodimers. *V International Conference «Condensed Matter and Low Temperature Physics 2024»*. (2 – 6 June 2025, Kharkiv). P. 140

Ring ensembles of metallic nanodisks in the optical frequency range

Korolkov, R.Yu.¹, Korotun, A.V.^{1,2}

¹ National University Zaporizhzhia Politechnic, Zaporizhzhia, Ukraine, romankor@zp.edu.ua

² G.V. Kurdyumov Institute for Metal Physics of the NAS of Ukraine, Kyiv, Ukraine

As is well known, the excitation of the toroidal modes contributes to the emergence of the unique properties of materials associated with the artificial magnetism. In turn, the artificial magnetism is extremely important for the design of innovative metamaterials. It should be pointed out that these resonant modes can be excited both in toroidal particles and in the ensembles of the particles, which consist of the different numbers of the disks arranged in a circular configuration (ring ensemble of the nanodisks). At the same time, if the disks are made of ceramic materials, the structures, which are under the consideration, operate in the microwave range, and the radius of the ring must be relatively great ($R \sim 10^{-3}$ m) [1]. It is interesting to scale the available results for the ring ensembles of the particles to the optical (visible) frequency range. In this case, the characteristic sizes of the structure (ring (torus) radius, height and diameter of the disks) will be of the order of $10^{-8} \div 10^{-7}$ m, and the disks themselves must be metallic. It should be pointed out that there are no studies of the properties of such structures in the scientific literature, which means that these issues are actual.

Let us consider the ring ensemble N of the metallic nanoscale disks with the height H and the diameter D . We will assume that the radius of the ring (toroid) is equal to R (Fig. 1). The effective permittivity of such an ensemble in the Maxwell – Garnett approximation is determined by the relation

$$T_{\text{eff}} = \frac{NV_{\text{disk}}T_{\text{disk}} + (V_{\text{tor}} - NV_{\text{disk}})T_{\text{gap}}}{V_{\text{tor}}}, \quad (1)$$

where the volumes of the disk and torus are equal to

$$V_{\text{disk}} = \frac{\pi}{4}D^2H, \quad V_{\text{tor}} = \frac{\pi^2}{2}RD^2,$$

correspondingly, T_{gap} is the permittivity of the material of the gaps between the disks, and the dielectric function of the disk material within the frameworks of the Drude model is

$$T_{\text{disk}} = T^\infty - \frac{\omega_p^2}{\omega(\omega + i\gamma_{\text{eff}})}. \quad (2)$$

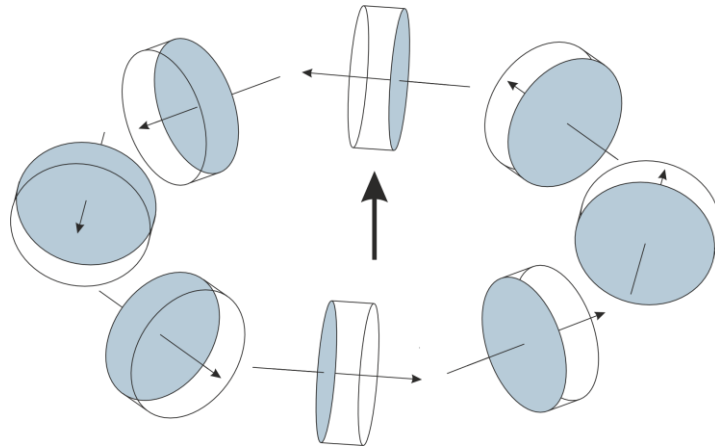


Fig. 1. Geometry of the problem

In formula (2) ω_p is plasma frequency; τ^∞ is the contribution of the interzone transitions into the permittivity of the disc material; γ_{eff} is the effective relaxation rate of electrons in the nanodisks.

Using the relations for the volumes, formula (1) can be rewritten as

$$T_{\text{eff}}(\omega) = T_{\text{gap}} + \frac{NH}{2\pi R} (T_{\text{disk}}(\omega) - T_{\text{gap}}). \quad (3)$$

Since $V_{\text{tor}} > NV_{\text{disk}}$, then the following inequality should be true for the geometric parameters

$$2\pi R > NH. \quad (4)$$

In order for the medium with the ring ensembles of the metallic nanodisks to be a metamaterial, the following condition must be satisfied:

$$\operatorname{Re} T_{\text{eff}}(\omega) < 0. \quad (5)$$

Taking into account the relations (2) and (3), when the influence of the relaxation processes ($\gamma_{\text{eff}} \rightarrow 0$) can be neglected, we obtain the following inequality for the frequencies at which the condition (5) is satisfied:

$$\omega < \omega^* = \frac{\omega_p}{\sqrt{T^\infty + \left(\frac{2\pi R}{NH} - 1\right)T_{\text{gap}}}}. \quad (6)$$

Thus, the lower the permittivity of the medium between the discs and the greater their number in the assembly, the higher the maximum frequency at which condition (5) is still satisfied.

[1]. Wu T., Evlyukhin A.B., Tuz V. Separation of a Toroidal Mode in Clusters of Dielectric Particles. *Progress In Electromagnetics Research*. 2024. V. 180. P. 103-113.

Selective laser melting of Al-Cu-Fe based alloys using elemental powder blends

Shtablavyi I., Kulyk Yu., Pauk A., Popilovskyi N., Yatsevych M., Mudry S.

¹ Ivan Franko National University of Lviv, Lviv, Ukraine, ihor.shtablavyi@lnu.edu.ua

3D metal printing technologies are extremely promising for replacing traditional manufacturing methods. Among them, laser sintering or melting of metal powders are at the forefront. In this case, powders with a composition corresponding to the alloy from which the product is to be obtained are used to form three-dimensional objects. Quite often, additional requirements are imposed on the powders used, relating to their geometry and elemental composition, which makes them really expensive. In view of this, studies related to the use of elementary powders in laser 3D printing to form bulk objects based on the required alloys is a top priority.

Currently, there are studies related to the technology of 3D printing of metal alloys using elemental powders [1, 2]. However, these works mainly concern the production of simple alloys and intermetallic compounds, and the results obtained in them have limited application.

In this work, we obtained ternary alloys of the Al-Cu-Fe system by selective laser melting under different processing modes. A mixture of aluminum, copper, and iron powders in the required ratios was used as the raw material for synthesis. Laser treatment was performed at a beam power of 20 to 45 W and a scanning speed of 1000 mm/s. The resulting alloys were studied using scanning electron microscopy and X-ray phase analysis. As a result of investigations, synthesis modes have been found under which non-porous alloys with quasi-crystalline phases are formed, contributing to the improvement of their mechanical properties.

[1]. Kang N., Coddet P., Dembinski L, Liao H., Coddet Ch. Microstructure and strength analysis of eutectic Al-Si alloy in-situ manufactured using selective laser melting from elemental powder mixture *Journal of Alloys and Compounds*. 2017. V. 691. P. 316-322

[2]. Glerum J. A, Kenel Ch., Sun T., Dunand D. C. Synthesis of precipitation-strengthened Al-Sc, Al-Zr and Al-Sc-Zr alloys via selective laser melting of elemental powder blends *Additive Manufacturing*. 2020. V. 36, P. 101461

Acknowledgments

This work was supported by the National Research Foundation of Ukraine (Project No 2025.06/0016).

Simulation of the X-ray topographic imaging of microdefects under impact of combined strain field

M. Borch, S. Novikov, Ya. Garabazhiv, D. Fedortsov, I. Yanchuk, S. Honcharuk

¹ *Yuriy Fedkovych Chernivtsi National University, Chernivtsi, Ukraine*
m.borcha@chnu.edu.ua

Microdefects and dislocations are typical defects in silicon, which can significantly change electrical properties in semiconductor devices. Structural diagnostics, where combination of X-ray and ultrasonic waves are using and combined strain field is formed consisting of strains from defects and ultrasound in the Si sample [1]. Special attention is paid to coherent and diffuse components of X-ray scattering at the condition of the X-ray acoustic resonance.

To identify the conditions under which ultrasound enhances the contrast of microdefects on X-ray topograms, we conducted simulations for microdefect concentrations from $n=10^5 \text{ cm}^{-3}$ to $n=10^7 \text{ cm}^{-3}$ (Fig.1) and for dislocations randomly distributed in different scattering planes with a density 10^3 cm^{-3} in the Si crystal of different thickness t . The MoK α -radiation and (001) surface, (220) and (440) reflections were used. Microdefects were defined as a spherically symmetric elastic displacement field. Dislocation loops considered with various geometric shapes and crystallographic orientations of Burgers vectors \vec{b} . The anisotropy of the crystal lattice was taken in account.

| | $\mu t=3, n=10^7 \text{ cm}^{-3}$ | $\mu t=6, n=10^5 \text{ cm}^{-3}$ | $\mu t=12, n=10^7 \text{ cm}^{-3}$ |
|------------------------|-----------------------------------|-----------------------------------|------------------------------------|
| $U_0=0$ | | | |
| $U_0=0.01 \text{ \AA}$ | | | |

Fig.1. Influence of ultrasound field on defect images under condition of X-ray and acoustic resonance. μ is X-ray absorption coefficient, t is sample thickness, n is microdefect concentration, U_0 is amplitude of acoustic wave.

The analysis of simulated topographs reveals that condition of X-ray and acoustic resonance is the most suitable to determine the defect size, their density/concentration and distribution. The quantitative relationship between macroscopic parameters of ultrasound and microscopic characteristics of defects is established. Therefore, it is demonstrated that the X-ray and acoustic resonance is a promising tool for material structural diagnostics.

[1]. Fodchuk I. X-ray acoustic topography of defects in Si crystals / I. Fodchuk, S. Novikov, D. Fedortsov // Phys. Stat. Sol. (a). – 2004. – Vol. 201, No. 4. – P. 711-717.

Structural and optical studies of nanocomposites based on Nd-substituted copper ferrite

Mokliak, M.G.¹, Mazurenko, J.S.², Kaykan, L.S.², Mokliak, V.V.^{2,3}

¹ Vasyl Stefanyk Carpathian University, Ivano-Frankivsk, Ukraine, mariamoklyak@gmail.com

² G. V. Kurdyumov Institute for Metal Physics, NAS of Ukraine, Kyiv, Ukraine

³ Ivano-Frankivsk National Technical University of Oil and Gas, Ivano-Frankivsk, Ukraine

Nanocomposites based on Nd-substituted copper ferrite $\text{CuNd}_x\text{FeO}_4$ ($x = 0.00$ – 0.11) were synthesized via the sol-gel auto-combustion method [1]. The effect of Nd^{3+} substitution on phase composition, lattice parameters, and optical band gap was studied using X-ray diffraction (XRD), UV-Vis spectroscopy.

XRD analysis confirmed the formation of a cubic spinel structure as the dominant phase (from 81.8% to 87.5%) for all samples, with varying amounts of secondary phases such as FeCuO_2 and CuO . Quantitative phase analysis showed that Nd^{3+} substitution promotes the stabilization of the spinel matrix. The content of FeCuO_2 decreased, while CuO became more pronounced with increasing Nd content, particularly above $x = 0.05$. This trend indicates that moderate Nd substitution enhances the formation of a pure spinel structure by suppressing intermediate or metastable phases.

The optical band gap (E_g) was evaluated using Tauc plot analysis. The E_g values exhibited a monotonic dependence on Nd content (Figure): a decrease from 2.86 eV to 2.76 eV at $x = 0.01$, a gradual increase to 2.88 eV at $x = 0.11$. At low Nd content ($x = 0.01$ – 0.03), the band gap narrows, which attributed to enhanced defect states or intermediate phase contributions (e.g., FeCuO_2). This correlates with the presence of ~12–18% FeCuO_2 and CuO phases, which can introduce localized states near the band edges, effectively narrowing the optical gap. At $x = 0.03$ – 0.11 , a marked increase in E_g is observed. In this range, the $\text{Fd}3\text{m}$ spinel phase reaches its highest content (~87.5%), while FeCuO_2 is nearly suppressed. This reduces defect-related sub-band states and restores intrinsic band structure features, resulting in a widening of the optical band gap.

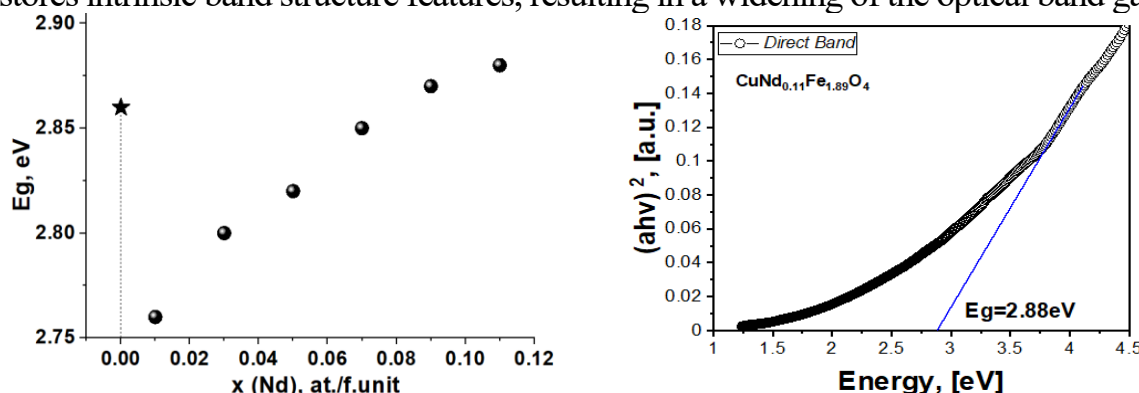


Figure – Tauc plot extrapolation for optical band gap estimation.

The correlation between increasing phase $\text{Fd}3\text{m}$ content and E_g widening suggests that elimination of parasitic phases enhances optical quality, while structural disorder and multiphase character tend to reduce the band gap.

Structure, phase composition, morphology, and magnetism of heavily Cr⁺-implanted CdTe layers for spintronic applications

Popovych, V.D.^{1,2}, Popovych, A.V.¹, Stolyarchuk, I.D.¹, Böttger, R.³, Heller, R.³
Dluzewski, P.⁴, Żywczak, A.⁵, Mroczka, R.⁶, Gołębiowski, M.⁷, Sagan, P.⁷, Zdyb,
R.⁷, Kuzma, M.⁸

¹ *Ivan Franko Drohobych State Pedagogical University, Drohobych, Ukraine,*
vpopovych@dspu.edu.ua

² *Lviv Polytechnic National University, Lviv, Ukraine*

³ *Helmholtz-Zentrum Dresden-Rossendorf, Dresden, Germany*

⁴ *Institute of Physics, Polish Academy of Science, Warsaw, Poland*

⁵ *AGH University of Science and Technology, Krakow, Poland*

⁶ *The John Paul II Catholic University of Lublin, Lublin, Poland*

⁷ *Maria Curie-Skłodowska University, Lublin, Poland*

⁸ *University of Rzeszow, Rzeszow, Poland*

Implantation of CdTe single crystals by 500 keV Cr⁺ ions with fluences from 10¹⁶ to 5·10¹⁷ cm⁻² was performed. The dopant depth profiles through SIMS measurements agree with the theoretical prediction using the Schulz-Wittmaack formalism, except for the accumulation of projectile ions at the sample's surface due to their out-diffusion. Strong target sputtering was observed, limiting Cr incorporation into the host lattice. XRD, HRTEM, and EDXS experiments revealed phase separation upon implantation, resulting in the formation of nanocrystals of metallic α-Cr nanoprecipitates with (110)_{Cr}||(110)_{CdTe} orientation relationship, as well as nanoparticles of chromium telluride compounds. As follows from the RBS spectra, the near-surface layers of the implanted samples were almost not damaged, whereas irradiation-induced disorder extends much further into the crystals than expected from the SRIM calculations. SEM and AFM studies indicated progressive coarsening and increased roughness of the irradiated surfaces as the ion fluence rose. In contrast, RHEED and LEED patterns, and also Raman spectra of the implanted samples, demonstrated improvement of the top-most layers due to the sputtering of the amorphized overlayer, created by the chemo-mechanical polishing of the samples, upon Cr⁺ ion bombardment. Magnetization measurements indicate ferromagnetic behavior for all the implanted crystals, both at liquid nitrogen and room temperature, revealing round-shaped hysteresis loops with a small coercive force, characteristic of soft magnetic materials. The thermomagnetic curves' non-monotonous character suggested several magnetic phases in the materials under study.

In summary, although a much higher dopant content was introduced compared to the conventionally grown CdTe:Cr crystals, the second phase separation and the disorder induced are substantial obstacles to the production of CdTe-based DMS by Cr ion implantation. However, this technique can be used to obtain the perspective magnetic composite, consisting of nanoprecipitates of ferromagnetic chromium tellurides embedded in a semiconducting CdTe medium.

Surface effects in neutron-irradiated CdSb crystals

Fedosov S.A., Panasyuk L.I., Yashchynskiy L.V., Shymchuk S.P., Urban O.A.

Lutsk National Technical University, Lutsk, Ukraine,
s.fedosov@lntu.edu.ua

At high doses of irradiation, the concentration of radiation defects exceeds the concentration of uncontrolled impurities and the role of radiation defects in the formation of the physical properties of crystals becomes dominant. Neutron irradiation of undoped *p*-CdSb crystals with a dose 2×10^{18} n/cm² leads to a conversion of the conductivity type, forming defects of the donor type with an ionization energy $E_C - 0.16$ eV.

When storing neutron-irradiated crystals, their resistance at nitrogen temperature decreased over time, while at room temperature the changes were practically imperceptible. The study of the spatial distribution of shallow donors (formed during storage of irradiated crystals) showed that they are mainly concentrated in the near-surface layer of the crystal with a thickness of $60 \div 80$ μm .

The change in the resistance of the surface layer during storage of irradiated crystals did not depend on the atmosphere in which they were stored. This phenomenon can be explained by the diffusion of radiation defects from the bulk of the crystal to its surface.

From the dependence of time (during which the resistance of the freshly treated surface decreased by $e = 2.7$ times) on the storage temperature of the irradiated crystals, the activation energy of the process was determined to be 0.36 ± 0.03 eV.

During isochronous annealing, the resistance of the irradiated crystals slowly decreased over a wide temperature range (up to 100 °C). At this stage of annealing, the decay of defect clusters formed by neutron radiation occurs. As a result, the lattice is enriched with shallow (ionized at $T = 78$ K) donor-type defects, which reduce the resistance of the crystal at low temperatures. Some of these defects migrate from the bulk to the crystal surface (with a migration energy of 0.36 eV), creating a low-resistance near-surface layer.

Starting from the annealing temperature of 80 °C, deep donors with $E_C - 0.16$ eV are annealed in the irradiated crystals. During annealing, shallow acceptors ionized at $T = 78$ K are formed, which leads to a decrease in the crystal resistance and a change in its conductivity type. After annealing at 130 °C, the irradiated crystals were converted from *n* to *p*-type conductivity, as before irradiation. Neutron-irradiated crystals annealed at a temperature of 200 °C practically did not differ in electrical and optical properties from unirradiated CdSb crystals.

It should be noted that simultaneously with the annealing of centers with $E_C - 0.16$ eV, the photosensitivity of the crystals at low temperatures increases. This fact confirms that these deep donors act as fast recombination centers.

Technologies and models for effective cleaning of rolling bearings from various types of operational contaminants

Shymchuk S.P.¹, Kostyunik R.E.², Mikosianchyk O.O.², Stelmakh A.U.^{2,3},
Kushchev A.V.², Fedosov S.A.¹, Zaichuk N.P.¹, Shymchuk O.P.¹

¹*Lutsk National Technical University, Lutsk, Ukraine,*

²*State University “Kyiv Aviation Institute”, Kyiv, Ukraine,*

³*Beijing Institute of Technology, Beijing, China,*

Fedosov.Serhiy@gmail.com, s.shimchuk@lntu.edu.ua

Ensuring the required cleanliness of rolling bearings is a very complex and important scientific, industrial and economic problem. The solution of which makes it possible to increase the accuracy of machines and equipment, which include rolling bearings, and significantly improve their operational properties and durability. As a result, such an approach leads to a reduction in the use of metal, lubricants and energy resources, noise and vibrations. Ensuring technological cleanliness is relevant for both new bearings and those bearings that have been in operation and are reused. The main types of contamination are metal particles (microchips formed during cutting or wear products), corrosion products, polymerization products of lubricants or accidental contamination that falls from the external environment.

The most widely used in industry are ultrasonic cleaning methods, the effectiveness of which is well documented in the special scientific literature, but insufficient to remove existing contaminants. Therefore, they, like the turbulent pulse-magnetic methods widely studied by the team of authors of this work, have a number of disadvantages.

Therefore, to ensure the required industrial cleanliness of bearings, it is necessary to design special equipment and develop appropriate methods, models, and technologies.

In this work, the authors propose technological solutions for the implementation of the rolling bearing cleaning process and a process model based on the use of ultrasonic fields and electromagnetic fields in the working fluid environment (aviation gas, heated water). To ensure the effectiveness of cleaning, the physical fields used are created by appropriate sensors and electromagnets of different power. This allows for a cleaning effect that consists in reducing the forces of adhesion and electromagnetic interaction between contaminants and working surfaces, softening and useful degradation of contaminants (flaking, chipping and possible erosion). After which such contaminants are removed from the working surfaces of the bearings into the filtration zone of the cleaning device using turbulent flows.

Cleaned bearings are subject to conservation or reuse.

The effect of mechanical processing on the structural and electrochemical properties of oxide nanocomposites

Yurii Yavorskyi¹, **Myroslav Karpets**¹, **Igor Vladymyrskyi**¹,
Yaroslav Zaulychnyy¹

¹*E.O. Paton institute material science an welding, National Technical University of Ukraine
“Kyiv Polytechnical Institute”, 37 Beresteiskyi Pros., Kyiv 03056, Ukraine,
yar-yra@ukr.net.*

It is widely recognized that the characteristics of nanoscale materials are determined by factors such as their structural and morphological features, electronic configuration, degree of development, surface defects, and more. One of the most promising and cost-effective methods for optimizing these parameters is mechanical processing of nanocomposites in a vibratory mill (MBT) [1-4]. We first examined the effect of 5-minute mechanical ball treatment (MBT) on the structure of individual metal and transition metal oxides [5], finding no significant changes. Further studies on composites of amorphous SiO₂ with crystalline Al₂O₃, TiO₂, and Fe₂O₃ [1–3] showed that an 80% SiO₂ / 20% crystalline oxide ratio yields optimal structural and electrochemical properties. Finally, the effect of MBT duration (3 - 20 min) on these properties was examined, and it was established that the optimal treatment duration is 5 min.

[1]. Effect of Mechanical Activation of Highly Disperse SiO₂/α-Fe₂O₃ Mixtures on Distribution of Valence Electrons / Ya. V. Zaulychnyy et all // Metallofiz. Noveishie Tekhnol. – 2015. – V. 37, № 8. – P. 1063-1075. <https://doi.org/10.15407/mfint.37.08.1063>

[2]. Effect of mechanical treatment on distribution of valence electrons and characteristics of lithium current sources in nanocomposite (SiO₂)_x(Al₂O₃)_{1-x} (x=0.8, x=0.7) cathode / Ya.V. Zaulychnyy et all // Applied Surface Science 494 (2019) 1013–1022. <https://doi.org/10.1016/j.apsusc.2019.07.206>

[3]. The dependence between the structural-morphological features mixes SiO₂/TiO₂ and discharge capacities of lithium power sources / Yavorsky Yu.V. et all // Journal Of Nano- And Electronic Physics – 2019. – Vol. 11 No 6, 060012 (6pp). [https://doi.org/10.21272/jnep.10\(6\).06012](https://doi.org/10.21272/jnep.10(6).06012)

[4]. Influence of the mechanosynthesis duration on the structural, electronic and electrochemical characteristics of SiO₂/TiO₂ nanocomposite / Yaroslav Zaulychnyy et all // Journal of The Electrochemical Society, 2025, 172, 010525 <https://doi.org/10.1149/1945-7111/ada644>

[5]. Influence of Mechanical Treatment on Structural and Morphological Characteristics and Distribution of Valence Electrons of Aluminum, Silicon, Iron and Titanium Oxides / Yu.V. Yavorsky, Ya.V. Zaulychnyy, V.M. Gunko, M.V. Karpets // Journal Of Nano- And Electronic Physics – 2018. – Vol. 10 No 6, 06005(8pp). [https://doi.org/10.21272/jnep.10\(6\).06005](https://doi.org/10.21272/jnep.10(6).06005)

The essence of diffusion in a non-homogeneous three-dimensional system

Chernova M.Ye¹.

¹Doctor of Technical Sciences, Professor, Professor of the Department of Physical and Mathematical Sciences, Ivano-Frankivsk National Technical University of Oil and Gas, Ivano-Frankivsk, Ukraine,
myroslava.chernova@nung.edu.ua

Objective: Monte Carlo simulation of the diffusion process in a three-dimensional two-phase system, provided that the diffusion coefficients in arbitrary phases are sufficiently different.

Methodology. The calculation is carried out using computer modeling using the Modelica 4.0 language as a base [1,2].

Results. The dependence of the concentration profiles of the diffusing substance under different percentages of unblocked nodes and the dependence of the average concentration of the diffusing substance under different percentages of unblocked nodes were obtained.

Scientific novelty. The dependence of the average concentration of the impurity substance on the percentage of unblocked nodes has been established.

Practical significance. The obtained data for calculating the dependence of the impurity concentration on the distance to the saturation surface of blocked lattice sites will help to obtain metallic and non-metallic alloys with predetermined diffusion characteristics.

Conclusions: 1). To study the phenomenon of diffusion in highly heterogeneous systems, it is worth using Monte Carlo simulation.

2). In a two-phase system, and in one of the phases the diffusion coefficient is higher, at a concentration that becomes close to the percolation limit (in our case ~ 31%), there is a sharp increase in the diffusion rate, which is interpreted as reaching the percolation limit.

3). Under the condition of a large number of unblocked nodes, the concentration changes insignificantly, and under the condition of a decrease in the number of unblocked nodes, the concentration changes are significant.

4). In a three-dimensional two-phase heterogeneous system in the presence of large concentration gradients, it is impossible to use the effective diffusion coefficient, which describes the distribution of the average concentration in depth.

[1]. Tokovyy Y. (2024). Stationary Temperature Fields in Radially Inhomogeneous Hollow Cylinders. In: Altenbach, H., Bogdanov, V., Grigorenko, A.Y., Kushnir, R.M., Nazarenko, V.M., Eremeyev, V.A. (eds) *Selected Problems of Solid Mechanics and Solving Methods. Advanced Structured Materials*, vol 204. Springer, Cham. URL: https://doi.org/10.1007/978-3-031-54063-9_31

[2]. Samoilenco A.M., Kushnir R.M. (2018) Modern problems of mechanics and mathematics: collection of scientific works in 3 volumes. *Institute of Applied Problems of Mechanics and Mathematics named after Ya.S. Pidstryhach, NAS of Ukraine. Lviv.– Vol. 3. 284 c.* URL: http://www.iapmm.lviv.ua/mpmm2018/Volume_3.pdf

The influence alloying of Hf and Ta on the mechanical properties of the ZhS3DK-VI alloy produced from remelting of scrap metal

Krapivka M.O.¹, Brodnikovskyi M.P.¹, Rokytska O.A.¹, Dudka O.I.², Hornostai V.V.², Syrotiuk A.V.², Slipchenko V.V.²

¹ Frantsevich Institute for Problems of Materials Science, National Academy of Sciences of Ukraine, 3 Omelyana Pritsaka Str., Kyiv, 03142, o.rokytska@ipms.kyiv.ua

² National Technical University of Ukraine “Igor Sikorsky Kyiv Polytechnic Institute”, 37 Beresteiskyi Ave, Kyiv, 03056, Ukraine

Despite ongoing intensive research aimed at developing sixth-generation gas turbine engines, all previous generations have operated exclusively on nickel-based alloys. Today, the issue of recycling worn components made of such alloys is particularly pressing, since conventional remelting makes it difficult to restore the initial chemical composition. This is due to the introduction of non-metallic elements from scrap, such as oxygen or carbon. Excess oxygen can be removed by deoxidizing the alloy with active rare earth elements, forming oxides that float to the ingot surface as slag. A more complex case occurs when the alloy contains excess carbon: during scrap remelting the carbon content may exceed the nominal value by more than a hundred times (2.2 wt.%), and such excess substantially reduces both low- and high-temperature strength.

Given the negative effects of excess carbon, we considered several approaches to restoring the ZhS3DK-VI alloy properties to nominal levels. Among them: additional remelting in an atmosphere with increased partial oxygen pressure to ensure carbon burn-off, or the introduction of a more effective carbide-forming element (in our case, Hf), which forms single-element carbides while maintaining the optimal matrix composition. Hf is one of the elements that, when added to heat-resistant nickel alloys, improves both strength and ductility. In addition, Ta was introduced as an alloying element to stabilize the γ' -phase and increase creep resistance. Although Ta is not a strong carbide former, in our case it contributed both to solid-solution strengthening of the matrix and to the kinetics of carbide precipitation.

Restoration of mechanical properties was monitored via microhardness values as well as compression and tensile testing in the temperature range of 20–800 °C. For example, while the initial ZhS3DK-VI alloy exhibits $H_v = 470 \text{ kg/mm}^2$, the introduction of 6 wt.% Ta increased microhardness to 508 kg/mm^2 , and alloying with 2 wt.% Hf raised the value to 514 kg/mm^2 .

Thus, using Ta or Hf as alloying elements demonstrates that the properties of the carbon-enriched ZhS3DK-VI alloy can be improved—and in some cases even surpassed—without major complications in the remelting process.

The influence of different types of microdefects on total integral reflectivity of CdTe:Cl single crystals

Fodchuk I.M., Kuzmin A.R., Dovganyuk V.V., Hutsuliak I.I.,
Solodky M.S., Zaplitny R.A.

Yuriy Fedkovych Chernivtsi National University, Chernivtsi, Ukraine,
a.kuzmin@chnu.edu.ua

This study utilizes a combination of methods, namely high-resolution X-ray diffractometry and the total integrated reflectivity (TIR) method, developed by V. B. Molodkin basing on dynamical theory, for the diagnosis of complex defect structures [1]. This method allows for the evaluation of the concentration and size of various types of microdefects.

The objects of investigation were a set of (111) high-resistivity CdTe single-crystal samples from Acrorad Co., Ltd. These samples were grown by the traveling heater method and had dimensions of $5 \times 5 \times 0.5$ mm³.

Experimental investigations were conducted using a Panalytical Philips X'Pert PRO diffractometer.

Two combinations of different defect types were considered in our analysis:

1. Disk-shaped clusters, defined as relatively large CdTe grains surrounded by dislocation loops of corresponding sizes, and small spherical clusters, which are small CdTe grains located in the spaces between the large grains.

2. Disk-shaped clusters, defined as relatively large CdTe grains, and dislocation loops.

The best results were obtained with the first model, which included three types of dominant defects: disk-shaped clusters – relatively large CdTe grains surrounded by dislocation loops of corresponding sizes – and small spherical clusters, which are small CdTe grains in the spaces between the larger grains. This model enabled the determination of the characteristics (concentration and size) of the dominant defects in the crystals.

[1]. Molodkin, V.B., Nizkova, A.I., Olikhovs'ky, S.J at all, Metallofizika i Noveishie Tekhnologii, 2003, 25 (1), pp. 107-116.
<https://www.scopus.com/record/display.uri?eid=2-s2.0-0344198058&origin=recordpage>

Acknowledgments

This work was partially supported by the Ministry of Education and Science of Ukraine (grant No. 0125U000832, authors A. R. Kuzmin, M. S. Solodkyi; grant No. 0125U001483, authors I. M. Fodchuk, I. I. Hutsuliak, V. V. Dovganyuk).

The structural state of the FeCoNiCrMoWB alloy after oxidation at 1000 °C

Karpets M.V.¹, Naumenko M. P.², Rokytska O. A.³, Solonchuk D.O.¹,
Holovkin K.A.¹

¹*National Technical University of Ukraine "Igor Sikorsky Kyiv Polytechnic Institute", Kyiv, Ukraine.*

²*E.O. Paton Electric Welding Institute of the NAS of Ukraine, Kyiv, Ukraine,
maksimnaumenko43@gmail.com*

³*Frantsevich Institute for Problems of Materials Science NAS of Ukraine, Kyiv, Ukraine*

High-entropy alloys (HEAs) are a new class of materials that attract significant attention due to their unique physico-mechanical properties, such as high strength, thermal stability, and resistance to corrosion and wear. One of the promising directions for improving HEAs is alloying with boron. Of particular interest is the FeCoNiCrMoWB alloy.

The oxidation resistance of the high-entropy alloy was studied in an electric resistance furnace in static air at a temperature of 1000 °C, with periodic weighing after 1, 2, and 3 hours.

X-ray analysis of the FeCoNiCrMoWB alloy in the as-cast state revealed the formation of five types of boride phases: (MoW)B, MeB₂, Fe₂B, Ni₃B, and Ni₂₁Mo₂B₆ (Table 1). After oxidation, the oxide layer showed the formation of NiMoO₄ oxide and an oxyborate of the type (Co_{1.5}Me_{0.5})(BO₃)O with an orthorhombic structure. After complete removal of the oxide layer, the matrix of the alloy was found to contain a W₂CoB₂-type boride, while the Fe₂B-type boride remained in approximately the same quantity as in the initial state.

Table 1. Phase composition and lattice parameters of the matrix phases before and after oxidation of the FeCoNiCrMoWB alloy

| Condition | Phase composition | Lattice parameters | | |
|------------------------|---|--------------------|--------|--------|
| | | a, nm | b, nm | c, nm |
| Before oxidation | (MoW)B | 0,3137 | 0,8371 | 0,3062 |
| | MeB ₂ | 0,3276 | - | 0,3278 |
| | Fe ₂ B | 0,5086 | - | 0,4259 |
| | Ni ₃ B | 0,5265 | 0,6678 | 0,4422 |
| | Ni ₂₁ Mo ₂ B ₆ | 1,0672 | - | - |
| Oxide scale | (Co _{1,5} Me _{0,5})(BO ₃)O | 0,9181 | 0,3103 | 0,9362 |
| | NiMoO ₄ | 1,0491 | 0,9535 | 0,7157 |
| Matrix after oxidation | CoWO ₄ | 0,4704 | 0,5696 | 0,4962 |
| | W ₂ CoB ₂ | 0,7000 | 0,4555 | 0,3159 |
| | Fe ₂ B | 0,5076 | - | 0,4232 |

Thermal conductivity of PbSnTe solid solutions

Halushchak M.O.¹, Matkivskyi O.M.²

¹*Ivano-Frankivsk National Technical University of Oil and Gas, Ivano-Frankivsk, Ukraine.*

²*Vasyl Stefanyk Carpathian National University, Ivano-Frankivsk, Ukraine,*

ostap.matkivskyi@pnu.edu.ua

A^4B^6 compounds are well-known thermoelectric materials. Improvement of their operational parameters can be achieved by creating solid solutions. First of all, this leads to a decrease in the thermal conductivity of the material, which has a positive effect on the thermoelectric factor Z ($Z=S^2\sigma/k$, where S is the Seebeck coefficient, σ and k are electrical conductivity and coefficient of thermal conductivity, T is the absolute temperature). The creation of solid solutions leads to a change in a number of fundamental characteristics of the material, in particular, the width of the band gap, the effective mass of carriers, etc. Thus, it is important to establish the influence of each of these factors on the magnitude of k , which will allow effective implementation of the technique of creating solid solutions to reduce the thermal conductivity of the base material. Since the coefficient of thermal conductivity of conductors can be represented as the sum of the coefficients of the electronic and lattice subsystems ($k = k_{el} + k_{lat}$), the calculation of the coefficient of thermal conductivity k is usually reduced to two separate problems. The calculation of the electronic component is almost always based on the use of the Wiedemann-Franz law. Due to the complexity of calculating k_{lat} of solid solutions, often the analysis of the influence of the composition of the solution on the value of k is reduced to the sequential calculation of the electronic component, and then the calculation of the lattice component of thermal conductivity, by subtracting the theoretically calculated k_{el} in various approximations from the experimental values of k_{exp} .

In this work, the electronic and lattice thermal conductivity of PbSnTe solid solutions were calculated with a sequential analysis of the influence of the accuracy of the determination of the listed parameters and some model assumptions on the obtained results. One of the main tasks that was set at the same time was to analyze the sufficiency of taking into account the scattering of phonons on phonons and phonons on substitution atoms for the interpretation of experimental data $k(T)$ for PbSnTe solid solutions. This task is due to the fact that other important mechanisms of phonon scattering and the participation of optical phonons in heat transfer processes are often discussed in the literature. In addition, in the work, the concentration of intrinsic charge carriers in solutions was calculated and their influence on the thermoelectric factor was discussed.

[1]. O.Z Khshanovska, M.O. Halushchak, O.M. Matkivskyi, I.V. Horichok. Analysis of heat conductivity mechanisms in PbSnTe solid solutions // Physics and Chemistry of Solid State V. 24, No. 3 (2023) pp. 564-577. DOI: [10.15330/pcss.24.3.564-577](https://doi.org/10.15330/pcss.24.3.564-577).

Ti₃SiC₂ MAX phase synthesized mechano-chemically from initial powder reactants: effect of Zr and V doping

Korablov D.S.¹, Ershova O.G.¹, Koval O.Yu.¹, Kopan A.R.¹,
Solonin Yu.M.¹

¹*Frantsevich Institute for Problems of Materials Science, NAS of Ukraine, Kyiv, Ukraine,*
finejima@gmail.com

Layered ternary carbides (MAX phases) are large collection of oxygen-free ceramic materials exhibit a unique combination of properties characteristic of both metals and ceramics. MAX phases are hard materials which are metallically conductive and thermally conductive. Such materials have low density, Young's modulus values on the order of 300 GPa, excellent corrosion resistance in aggressive liquid media, resistance to high temperature oxidation and have high melting point. Among the many MAX phases synthesized to date, the greatest interest from the standpoint of the level of their properties represents such material based on titanium as Ti₃SiC₂.

Synthesis of MAX phases is carried out mainly by methods of hot isostatic pressing, self-propagating high-temperature synthesis (SHS) and by spark plasma sintering (SPS) method. These techniques require high temperatures, utilization of complex and expensive equipment for the synthesis Ti₃SiC₂ MAX phase of high purity, while the yield of MAX phase reveals to be low. At the same time, in order to obtain MXenes it is desirable to pre-synthesize MAX phases in the form of a dispersed powder to improve etching of A-element layers. Thus, high-energy milling of the initial components in a planetary mill was applied as a promising synthesis route for the preparation of Ti₃SiC₂ MAX phase powder with a view to improve the quality and purity of resultant MXene.

In the present investigation the milling of reactants was performed in argon atmosphere in a planetary mill AIR-015M. The phase composition of the samples was examined by XRD using a diffractometer "DRON 3" (Cu K α radiation). Qualitative and quantitative X-ray phase analysis was conducted and the parameters of the unit cells of the Ti₃SiC₂ and TiC phases were determined. Using SEM was studied the microstructure of the synthesized MAX phase.

As a result of mechanically activated self-propagating synthesis, from the initial mixture of Ti, Si, and C powders or a mixture of Ti, Si, and C powders with the addition of 5 wt. % Zr or with the addition of 5 wt. % V, the MAX phase Ti₃SiC₂ was obtained. The effect of doping the MAX phase Ti₃SiC₂ with zirconium and vanadium on the degree of its formation was investigated. It was found that doping the MAX phase Ti₃SiC₂ with 5 wt. % V led to an increase in its amount and, accordingly, a decrease in the amount of the secondary TiC phase in the final product. When doping the MAX phase with 5 wt. % Zr, on the contrary, its amount decreased, and the amount of the TiC phase increased.

Tunable Emission in Dy³⁺/Tb³⁺ Co-Doped Borate Glasses for Multicolor Light Applications

M. Kushlyk¹, D. Slobodzyan¹, Y. Shpotyuk^{1,2}, M. Prokopchuk¹, I. Medvid¹,
J. Szlezak², B. Mahlovanyi^{1,2}, A. Luchekho¹

¹ Department of Sensor and Semiconductor Electronics, Ivan Franko National University of Lviv, 107, Tarnavskoho st., 79017 Lviv, Ukraine

E-mail: markyan.kushlyk@lnu.edu.ua; kushlykmarik@gmail.com

² Institute of Physics, University of Rzeszow, 1, Pigionia st., 35959 Rzeszow, Poland

Borate glasses activated by rare-earth ions are of great interest as promising luminescent materials for optoelectronic and photonic devices. Particular attention is focused on their application in energy-efficient lighting systems and in special-purpose light sources, including those used for agriculture, where blue-green emission bands can stimulate photosynthetic activity and plant growth. The ability to control emission colour through co-doping strategies offers new opportunities for designing advanced glass-based phosphors with different optical properties.

In this work, the (B₂O₃)₅₉–(ZnO)₁₀–(SrO)₁₀–(CaO)₁₀–(MgO)₁₀ glass samples were synthesised and investigated under different doping conditions: singly doped with 1.0 mol% Dy³⁺, 1.0 mol% Tb³⁺, and co-doped with 0.5 mol% Dy³⁺ + 0.5 mol% Tb³⁺. Transmission spectra revealed the characteristic absorption bands of Dy³⁺ and Tb³⁺ ions, confirming their successful incorporation into the borate matrix. PL excitation and emission spectra were recorded, enabling the identification of the main energy transitions responsible for light generation. The Dy³⁺-doped glasses exhibit four emission maxima at 478, 580, 663, and 753 nm, corresponding to ⁴F_{9/2}→⁶H_{15/2}, _{13/2}, _{11/2}, _{9/2} transitions, with the strongest yellowish emission arising from the 580 nm band. Tb³⁺-doped glasses show characteristic emissions at 490, 542, 585, and 622 nm, assigned to ⁵D₄→⁷F₆₋₃ transitions, where the dominant 542 nm band produces an intense green emission. In co-doped samples, Dy³⁺→Tb³⁺ energy transfer enhances the Tb³⁺ emission intensity, especially under Dy³⁺-related excitation, yielding spectra similar to Tb³⁺ single-doped glass but with improved efficiency. As the result, an energy level diagram of Dy³⁺ and Tb³⁺ ions was constructed, demonstrating the excitation pathways and the energy transfer mechanism between the two activators in co-doped samples.

Furthermore, the emission properties were analysed in terms of chromaticity. A colour diagram was constructed, illustrating how the emission colour depends on both the type of doping ion and the excitation wavelength. The results show that co-doping with Dy³⁺ and Tb³⁺ ions allows for tunable multicolour emission, opening the way for the development of borate glass-based PL materials for multifunctional and application-specific light sources.

[1]. This work was performed within the framework of the IMPRESS-U project supported by the NAS (USA, STCU Grant # 7112), NAWA (Poland, Grant # BPN/NSF/2023/1/00002/U/00001), and NSF (USA, Grant # OISE-2106457).

Wavelet analysis of X-ray curves obtained from CdTe crystals

Fodchuk I.M., Balovskyak S.V., Yakovliev I.S.

Yuriy Fedkovych Chernivtsi National University, Chernivtsi, Ukraine
i.fodchuk@chnu.edu.ua

Analysis of the intensity of X-ray rocking curves $I_h(\omega)$ allows obtaining information about the studied crystals: dislocation density, type and concentration of microdefects, magnitude of crystal lattice deformations, etc. X-ray diffractometry methods are used to study materials important for practical application, in particular, cadmium telluride crystals [1]. However, X-ray curves obtained from CdTe crystals have a complex shape (Fig. 1a), which complicates their processing. In particular, the shape of the curves is sensitive to the state of the surface layer of the crystals and the parameters of the metal films deposited on the crystal. Therefore, the work proposes to perform a wavelet analysis of X-ray curves by their continuous wavelet transform (CWT) (Fig. 1b). The wavelet coefficients $coef$ depend on the scale factors a and the shift b . The signal processing software was developed in Python.

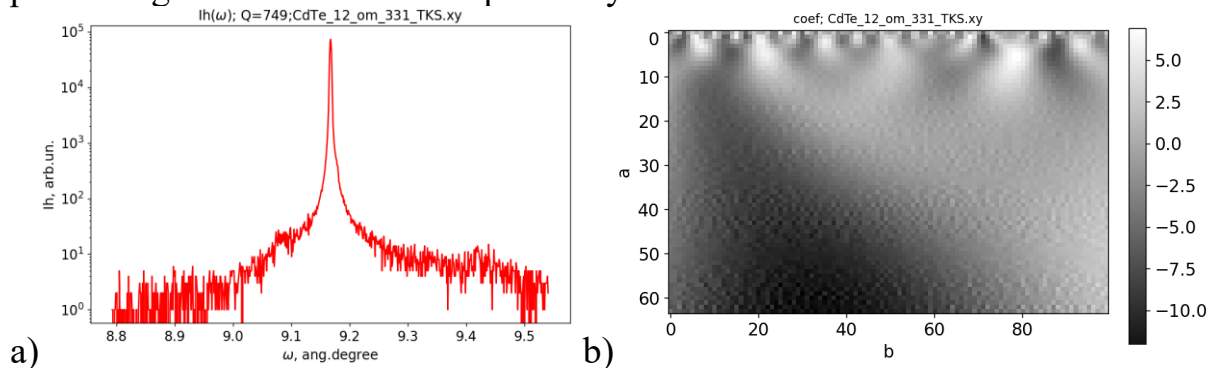


Fig. 1. Initial X-ray curve $I_h(\omega)$ (a) and a fragment of the matrix of wavelet coefficients $coef$ (b); a Gaussian wavelet of order 2 was used

The deposition of MoO_x films on the surface of CdTe crystals leads to deformations of the surface layer. Such deformations affect the shape of the X-ray curves and manifest themselves in the appearance of characteristic oscillations of wavelet coefficients. Therefore, the analysis of the matrix of wavelet coefficients allows to study the shape of the signal at different scales and obtain the most complete information about the studied crystalline samples.

[1]. Fodchuk I., Kuzmin A., Balovskyak S., Hutsuliak I., Solodkyi M., Maslynchuk O. The influence of the transition layer of CdTe:Cl/MoO_x heterostructures on the electrical and spectroscopic properties of detector systems. Proc. SPIE, Sixteenth International Conference on Correlation Optics. 2024. Vol. 12938. P. 129382H-1 – 129382H-5. doi: 10.1117/12.3015878.

XPS of heterostructures on (100) In₄Se₃ surface

Galiy P.V.¹, Nenchuk T.M.¹, Tuziak O.Ya.¹, Bolkot P.A.²,
Poplavskyy O.P.³, Dhingra A.⁴

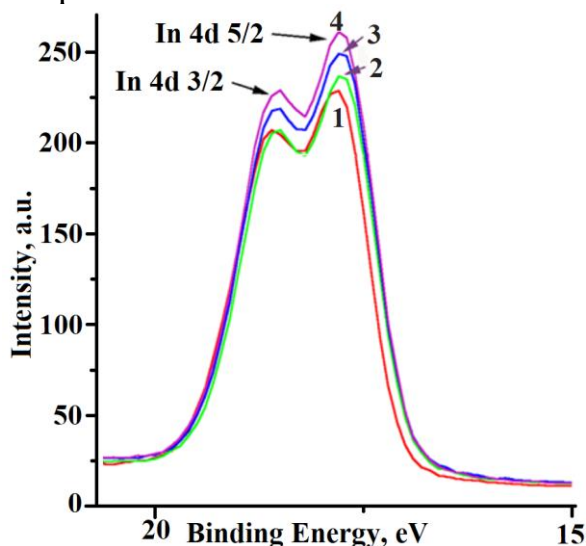
¹Ivan Franko Lviv National University, Lviv, Ukraine, pavlo.galiy@lnu.edu.ua

²Scientific Center of the Army Hetman Petro Sahaidachnyi National Army Academy, Lviv, Ukraine

³Vasyl Stefanyk Carpathian National University, Ivano-Frankivsk, Ukraine

⁴University of Nebraska–Lincoln, Lincoln, USA

A recent study [1] indicated that the clean (100) surfaces In₄Se₃ terminates in (as opposed to Se) which differed from the expected results of ground state density functional theory calculations. The possibility of In segregation on the surfaces (100) In₄Se₃ was, however, by no means excluded in that study. Here we probe the surface composition further and the effect of thermal motion at the (100) In₄Se₃ surface. We have used temperature dependent X-ray photoemission spectroscopy (XPS) in order to investigate the effective Debye temperature (which is one of the key descriptive parameters for the dynamic motion of the atoms) of the core-level In 4d5/2 and In 4d3/2 component at the system's surface and obtain an increase intensity this core-level with increase of the temperatures between 240 and 300 K.



The temperature dependent XPS measurements (Fig. 1) suggest that the In atoms on the surface (100) In₄Se₃ follow the Debye–Waller model while the In atoms in subsurface region do not.

Fig. 1. The XPS spectra of the temperatures dependence intensity of the low energy core-level In 4d5/2 and In 4d3/2 between 240 and 300 K: 1-250 K; 2-270 K; 3-280 K; 4-300 K.

This violation of the Debye–Waller model represented by increase in the surface component of the In 3d5/2 and core-level In 4d5/2 and In 4d3/2 XPS intensity with increasing temperature, implies that In segregates to the selvedge. There is now some reason to believe that the solubility of In in the subsurface region of (100) In₄Se₃ may be temperature dependent [2] and formation of In⁰/(100) In₄Se₃ heterostructures is possible.

[1]. Dhingra, A., Galiy, P.V. et al. Surface termination and Schottky-barrier formation of In₄Se₃(001). *Semicond. Sci. Technol.* 2020. V. 35, No 6. 065009.

[2]. Galiy P.V. et al. *Ukrainian conf. with intern. participation “Chem., Phys. and technol. of surf.” / Book of abst., 28–29 May 2025. Kyiv, 2025. P. 53.*

Aharonov–Bohm Effect in Lens-Shaped Quantum Dots

Holovatsky V.A., Mahanets O.M., Holovatsky I.V.

Yuriy Fedkovych Chernivtsi National University, Chernivtsi, Ukraine

v.holovatsky@chnu.edu.ua

Quantum dots grown by molecular beam epitaxy can have various shapes: dome-shaped, pyramidal, lenticular, hemispherical, and others. This study presents computer simulation of the electron energy spectrum in lenticular InAs/GaAs/AlAs quantum dots under the influence of magnetic and electric fields. The studied nanostructure is formed by self-organization of GaAs quantum dots on an AlAs substrate through a strained wetting layer and then an additional InAs layer. Such an architecture allows to localize the electron wave function in a hemispherical InAs film.

The Schrödinger equation is solved numerically using the finite element method in COMSOL Multiphysics. Ben-Daniel–Duke boundary conditions are applied at the InAs/GaAs and GaAs/AlAs heterointerfaces. The geometric configuration of the nanostructure is shown in Fig. 1.

Under the influence of an electric field perpendicular to the base of the quantum dot, the topology of the electron's ground-state wave function undergoes significant changes. As the field increases, the electron density becomes more compressed toward the base of the quantum dot, expanding the region near the axis where the wave function approaches zero. Thus, the electron density distribution becomes ring-shaped, which causes the Aharonov–Bohm oscillations of the ground state in the magnetic field (Fig. 2). The period of these oscillations depends on the strength of the applied static electric field.

These properties of lens-shaped quantum dots may be utilized in the development of advanced semiconductor nanodevices.

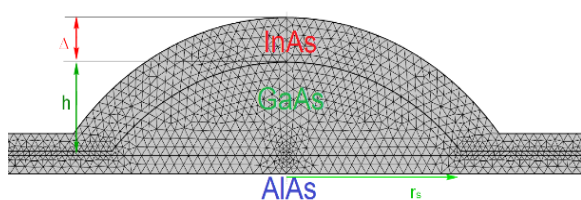


Fig. 1. Geometric scheme of an InAs/GaAs/AlAs quantum dot

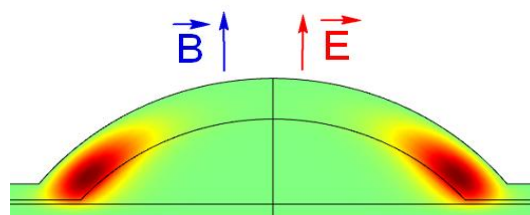


Fig. 2. Distribution of electron density in the ground state (b)

[1]. Holovatsky V., Holovatskyi I., Duque C. A. Electric field effect on the absorption coefficient of hemispherical quantum dots. *Mol. Cryst. Liq. Cryst.* 2024, 768 (14), 718.

[2]. Holovatsky V., Holovatsky I., Holovatska N. Electric field effect on the intraband optical absorption spectra in of the lens-shaped quantum dots. *J. of Thermoelectricity*. 2024, (1-2), 23-33.

Cobalt alloys with amorphous-nanocrystalline structure: corrosion behavior in alkaline solutions

Bodnar T.M.¹, Lopachak M.M.¹, Anton V. Nosenko², Dmytriv D.H.¹,
Boichyshyn L.M.¹

¹Chemistry Department, Ivan Franko National University of Lviv, 6 Kyryla i Mefodiya St.,
79005 Lviv, Ukraine¹

e-mail: bodnar.tanya99@gmail.com

²G. V. Kurdyumov Institute for Metal Physics of the N.A.S. of Ukraine, 36 Academician
Vernadsky Boulevard, UA-03142 Kyiv, Ukraine²

Amorphous and nanocrystalline cobalt alloys attract attention due to their unique electrochemical, magnetic, and mechanical properties. Their corrosion resistance in alkaline environments is of particular importance, which is critical for applications in energy, hydrogen, and electrochemical technologies [1, 2].

The aim of the study is to investigate the electrochemical behavior of amorphous and nanocrystalline cobalt alloys in alkaline solutions (1 M KOH) in order to evaluate their corrosion resistance and passivation mechanisms.

The objects of study are cobalt alloys with amorphous and nanocrystalline structures obtained by methods melt spinning and thermal annealing at the nanocrystallization temperature: Co₇₇Si₁₁B₁₂, Co₆₈Cr₉Si₁₁B₁₂, Co₇₂Fe₅Si₁₁B₁₂, Co₇₂Fe_{2.5}Cr_{2.5}Si₁₁B₁₂ (P4). Corrosion resistance was studied by cyclic voltammetry in a potentiodynamic mode in a 1 M aqueous KOH solution (Figure).

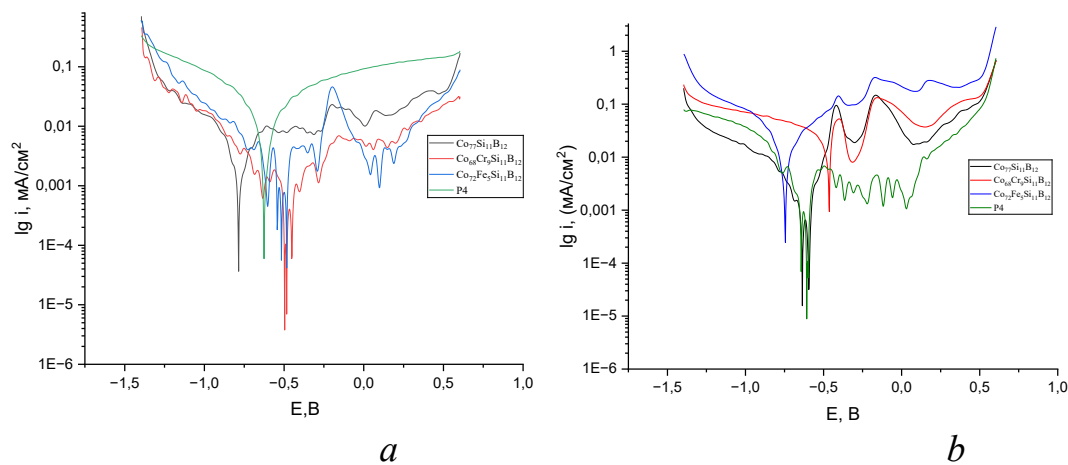


Figure. Voltammetric curves of initial and annealed cobalt-based AMA in 1 M aqueous KOH solution.

As shown by the analysis of the results presented in the table, AMA Co₆₈Cr₉Si₁₁B₁₂ after annealing has the highest corrosion current and the most positive corrosion potential value. A corrosion potential of -0.48 V indicates that AMA with Cr is thermodynamically more passive than Co₇₇Si₁₁B₁₂.

However, the high current ($\sim 10^{-2}$ mA/cm²) indicates low kinetic stability, i.e., the passivation film is thin, porous, and ineffective. Effective passivation

Topic 5

requires a combination of Cr with other elements (Si, B, Fe) or prolonged anodic oxidation to form a dense, stable oxide-hydroxide film.

Replacing Cr with Fe in AMA $\text{Co}_{72}\text{Fe}_5\text{Si}_{11}\text{B}_{12}$ improves corrosion resistance after annealing. AMA $\text{Co}_{77}\text{Si}_{11}\text{B}_{12}$ and $\text{Co}_{72}\text{Fe}_{2.5}\text{Cr}_{2.5}\text{Si}_{11}\text{B}_{12}$ show an increase in corrosion current after annealing. Annealing has different effects depending on the composition: Cr improves passivation, while Fe alloying leads to mixed effects.

Table. Corrosion parameters of cobalt-based AMA in 1 M KOH

| Alloy | Unannealed | | Annealed | |
|---|----------------|---------------------------------|----------------|---------------------------------|
| | E_{corr} , V | i_{corr} , mA/cm ² | E_{corr} , V | i_{corr} , mA/cm ² |
| $\text{Co}_{77}\text{Si}_{11}\text{B}_{12}$ | -0,63 | $4,78 \times 10^{-4}$ | -0,78 | $2,48 \times 10^{-3}$ |
| $\text{Co}_{72}\text{Fe}_5\text{Si}_{11}\text{B}_{12}$ | -0,75 | $4,34 \times 10^{-3}$ | -0,52 | $5,22 \times 10^{-4}$ |
| $\text{Co}_{68}\text{Cr}_9\text{Si}_{11}\text{B}_{12}$ | -0,48 | $1,03 \times 10^{-2}$ | -0,48 | $3,37 \times 10^{-4}$ |
| $\text{Co}_{72}\text{Fe}_{2.5}\text{Cr}_{2.5}\text{Si}_{11}\text{B}_{12}$ | -0,61 | $5,02 \times 10^{-4}$ | -0,63 | $3,39 \times 10^{-3}$ |

Thus, nanocrystalline alloys demonstrate better corrosion resistance, especially those containing Cr. Annealing changes the passivity of alloys: it can either improve or worsen their resistance depending on the composition. Nanostructuring increases the speed and uniformity of passivation layer formation, reduces local corrosion, and increases kinetic stability. The results are consistent with the literature, confirming the importance of nanostructuring for improving corrosion stability.

[1]. Mosaad Negem, H. Nady, M.M. El-Rabiei. Nanocrystalline nickel–cobalt electrocatalysts to generate hydrogen using alkaline solutions as storage fuel for the renewable energy. Int. J. Hydrogen Energy. 2019. Vol 44, 23. P. 11411-11420.

[2]. Xingyu Li, Jian Yu, Hongling Zhang, Guanyu Liu, Sen Luo, Jiangna Guo, Zequan Li, Yunhuai Zhang. Structural evolution of amorphous CoMo alloy in alkaline-based hydrogen evolution reaction. Applied Surface Sci. 2025. Vol. 699. P. 163161

Energy spectrum of side interface phonons in a semiconductor nanostructure quantum dot – quantum ring

Makhanets O.M., Holovatsky V.A., Konstantynovych I.A., Ivanochko M.M.

Yuriy Fedkovych Chernivtsi National University, Chernivtsi, Ukraine,
o.makhanets@chnu.edu.ua

Multilayer semiconductor nanostructures have been studied both theoretically and experimentally for quite some time. The unique properties of quasiparticles in such systems allow them to be used as basic elements in modern nanoelectronics devices [1, 2].

Semiconductor quantum rings occupy a special place among the various types of nanostructures. As a rule, they have cylindrical symmetry, just like quantum wires, but, unlike them, their height is finite and is on the order of several nanometers. Consequently, the movement of charge carriers in such nanostructures is limited in all three dimensions. Therefore, in this aspect, they are similar to cylindrical quantum dots.

The paper investigates the energy spectrum of side interface phonons in a nanostructure formed by a semiconductor thin film located in an external dielectric medium and containing a coaxially arranged cylindrical quantum dot and a quantum nanoring.

The calculation of interface phonon energies and corresponding polarization field potentials is performed in a dielectric continuum model in a cylindrical coordinate system suitable for this purpose for a nanostructure based on $\text{Al}_x\text{Ga}_{1-x}\text{As}$ semiconductors. At the same time, the functions describing the polarization field potential are obtained analytically exactly as solutions of Laplace's equation in all regions of the nanostructure. Next, boundary conditions are used for the normal components of the induction vector and the tangential components of the field intensity vector at all boundaries of the nanostructure.

It has been established that the energies of side interface phonons of nanostructures have insignificant dispersion of all branches at all values of quantum numbers. Regardless of the geometric dimensions of the nanostructure elements, all branches of SSO phonons are located between the energies of longitudinal phonons of the corresponding massive semiconductor crystals. The dispersion of interface phonons is noticeable only at low wave numbers near the center of the Brillouin zone.

[1]. [Young Joon Hong](#), [Rajendra K. Saroj](#), [Won Park](#), [Gyu-Chul Yi](#) One-dimensional semiconductor nanostructures grown on two-dimensional nanomaterials for flexible device applications // *APL Mater.* V.9, 060907 (2021).

[2]. M. Zervos Electronic properties of core-shell nanowire resonant tunneling diode // *Nanoscale Research Letters.* – 2014. – V. 9. – P. 509.

Thermal Modification of Biocarbon for Improved Adsorption Capacity

Vashchynskyi V.M.

Lviv Polytechnic National University, 12 S. Bandery Str., Lviv, Ukraine

v.vashchynskyi@gmail.com

Activated Carbon (AC) is one of the most widely used adsorbents for the treatment of wastewater contaminated with synthetic dyes. This is primarily due to its well-developed porous structure and high adsorption capacity. Among the numerous physical, chemical, and biological methods, adsorption has proven to be the most dominant and efficient technique for dye removal from aqueous solutions before their release into the ecosystem, owing to its low sensitivity to toxins, simplicity, and ease of operation.

The preparation of biocarbon adsorbents involved three stages: 1) carbonization of apricot shell biomass at 300–900 °C; 2) chemical activation with potassium hydroxide at a weight ratio of AC:KOH = 1:1; 3) thermal treatment in an argon flow at 900–920 °C, followed by washing and drying of the synthesized material.

Adsorption studies were carried out for an anionic dye (methyl orange, MO) and a cationic dye (methylene blue, MB). The equilibrium adsorption capacity, q_e (mg/g), was calculated according to equation (1)

$$q_e = \frac{(C_0 - C_e)V}{m} \quad (1)$$

C_0 and C_e (mg/L) are dye concentrations at initial and equilibrium, $V=0.025\text{L}$ is the volume of the solution, and m (g) is the mass of adsorbent used, respectively. When the optical density during experiments exceeded 0.8 a.u., 5 mL of the solution was diluted with deionized water to a final volume of 25 mL. The dilution factor was 20 for MB and 100 for MO.

Experimental results demonstrated that the sorption properties can be significantly improved by applying additional thermal modification, as this step enhances the porosity of biocarbon adsorbents. Adsorption kinetics indicated that the highest adsorption capacities were associated with an increased number of mesopores on the carbon surface. The obtained experimental isotherms were evaluated using the Langmuir and Freundlich adsorption models, according to which the adsorption process is monolayer for both types of dyes.

Diffusional and Structural Features of Titanium–Iron-Based Alloys

Makohin M.P., Umantsiv I.M., Yaremiy I.P., Andriichuk O.P.

Vasyl Stefanyk Carpathian National University, Ivano-Frankivsk, Ukraine,
yaremiyip@pnu.edu.ua

Titanium–iron-based alloys (Fe–Ti) are of significant interest to researchers due to their combination of high strength, heat resistance, corrosion resistance, and hydrogen absorption capability. Their structure is formed through the interaction between components, resulting in the formation of intermetallic phases such as FeTi, Fe₂Ti, and FeTi₂, which determine the physical and mechanical properties of the material. Therefore, the analysis of diffusion processes in such alloys is highly relevant, particularly in terms of the role of heat treatment and the potential of powder metallurgy.

The FeTi (B2 structure), Fe₂Ti (hexagonal Laves phase), and FeTi₂ phases are key to the microstructure of these alloys. They exhibit high thermal stability and hardness, although their plasticity is limited. The phase diagram of the Fe–Ti system reflects the formation of solid solutions and intermetallic compounds depending on the component ratio and temperature.

In powder compacts, the primary densification mechanism is diffusion: surface diffusion dominates at early stages, while bulk and grain boundary diffusion become significant at later stages. The activation energy for titanium diffusion in iron is relatively high, necessitating high-temperature sintering (1000–1300 °C). The extent of diffusion influences chemical homogeneity, particle bonding, and microstructure formation.

Fe–Ti alloys have hardness values up to 700 HV and tensile strength exceeding 1000 MPa, and they maintain their properties at temperatures up to 800–900 °C. Due to their ability to absorb hydrogen (FeTiH_x), these alloys are used in hydrogen energy systems. They are also employed as structural materials in aviation, metallurgy (ferrotitanium as a steel modifier), chemical industry (corrosion-resistant alloys), biomedicine (with up to 15% Ti alloying, biocompatibility is achievable), and catalysis.

Thus, diffusion and phase formation in the Fe–Ti system determine the performance characteristics of these alloys, combining the beneficial properties of both elements: high strength, thermal and chemical stability, and the ability to form hydrides. The application of powder metallurgy methods with controlled sintering regimes allows for the creation of materials with predictable microstructure and properties.

Influence of crystal symmetry on the electrochemical properties of nanoscale perovskites $\text{LaCr}_x\text{Fe}_{1-x}\text{O}_3$

Savchyn V.V., Yaremiy I.P., Yaremiy S.I.,
Kolkovskyi P.I., Mokhnatskyi M.L.

Vasyl Stefanyk Carpathian National University, Ivano-Frankivsk, Ukraine,
yaremiyip@pnu.edu.ua

Perovskite-type oxides with the general formula ABO_3 , in particular the $\text{LaCr}_x\text{Fe}_{1-x}\text{O}_3$ system, exhibit a wide range of functional properties including electrical conductivity, magnetism, and ferroelectricity. Due to the flexibility of cation substitution at both A and B sites, these materials are highly tunable for specific applications – in particular, as electrode materials for supercapacitors. One of the key factors affecting their electrochemical behavior is the crystal symmetry of the perovskite structure.

This study examines how the crystal structure symmetry influences charge storage mechanisms in $\text{LaCr}_x\text{Fe}_{1-x}\text{O}_3$ nanoparticles with sizes of 15–50 nm and coherence lengths of 15–20 nm. The symmetry strongly depends on the chemical composition (value of x), synthesis conditions, defect concentration, and particle size. It is shown that in the nanoscale regime, there is an increased tendency to deviate from bulk symmetries (e.g., orthorhombic Pbnm or trigonal $\text{R}-3\text{c}$) towards metastable or polar structures such as $\text{R}3\text{m}$, $\text{I}4/\text{mcm}$, $\text{R}-3$, or $\text{R}-3\text{m}$.

Symmetries associated with distorted BO_6 octahedra, lack of inversion centers, and local disorder (e.g., Pbnm , $\text{R}3\text{m}$) promote the emergence of pseudocapacitance via defect formation, variable valence states of $\text{Fe}^{3+}/\text{Fe}^{2+}$ and $\text{Cr}^{3+}/\text{Cr}^{2+}$, and local electric fields. Conversely, highly symmetric phases like $\text{Pm}-3\text{m}$ tend to be less effective, exhibiting mainly EDLC-type (electric double-layer capacitance) behavior.

Therefore, the crystal symmetry is a crucial parameter that determines the performance of $\text{LaCr}_x\text{Fe}_{1-x}\text{O}_3$ perovskites as electrode materials for supercapacitors, and should be considered when designing these materials for energy storage applications.

Morphological and electrophysical features of carbazole derivative films prepared by spin coating on silicon substrate

Roshchina N.¹, Kuznetsova D.¹, Smertenko P.¹, Kolomzarov Yu.¹,
Mamykin S.¹, Olkhovik G.¹, Blazevicius D.², Blazeviciute B.², Sasnauskaite I.²,
Grigalevicius S.²

¹V. Lashkaryov Institute of Semiconductor Physics, National Academy of Science of Ukraine,
41, Prospekt Nauky, 03028 Kyiv, Ukraine

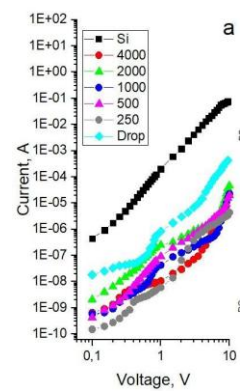
²Department of Polymer Chemistry and Technology, Kaunas University of Technology,
Radvilenu plentas 19, LT50254 Kaunas, Lithuania

Thin films of 4-(9H,9'H-[3,3'-bicarbazol]-9-yl)benzonitrile (DB-58) derivative were deposited on micro-profiled Si substrates by spin coating at rotation speeds (RS) ranging from 250 rpm to 4000 rpm. For comparison, the drop casting method was also used to form the film. The film thickness for spin coating was 20 – 70 nm, and for drop casting it was approximately 270 nm. Some morphological features of obtained films were studied by optical microscope and AFM. Fig. 1 demonstrates experimental results at RS 250, 500, 1000, 2000 and 4000 rpm. As anticipated, increasing the spin coating speed resulted in reduced film thickness. Concurrently, the size of the DB-58 material

| | Spin coating | | | | | Drop casting |
|---------------------|--------------|----------|----------|---------|---------|--------------|
| | 4000 rpm | 2000 rpm | 1000 rpm | 500 rpm | 250 rpm | |
| Optical image, 1 μm | | | | | | |

Fig. 1. DB-58 films morphology on Si substrate.

clusters also diminished. No self-organisation phenomenon was observed in for these films. When applying the film via the drop-casting method, the self-organization took place with the presence of a fibrous structure. The forward dark current-voltage characteristics (CVC) exhibited the expected behaviour: as the spin-coating speed decreased, the conductivity of spin-coating films decreased correspondingly while the film thickness increases (see Fig2).



In spite the thickness of drop-casting films is thicker their conductivity is higher due to self-organization. The fine CVC analysis by dimensionless sensitivity $DS = d \lg I / d \lg V$ shown the wider range of bimolecular recombination with $DS=1.5$ for films obtained by the rotation speed 500 rpm and 1000 rpm. The rectification ranges with $DS=0.5$ observed for films with RS 2000 rpm, 1000 rpm and 250 rpm. So, the spin-coating films obtained at SR=500 rpm is more appropriate for further experiments.

Fig. 2. CVCs of DB-58 films on Si substrate with various rotation per minute.

Acknowledgements. This work was financially supported by the Research Council of Lithuania (Grant No. S-LU-24-7), bilateral Ukraine-Lithuania project (M/54-2024).

Topic 6

Nano- and Thin films: History of inventions and features of University's educational programs

Designing a physics lesson based on universal design principles

Voitkiv H.V.

*Vasyl Stefanyk Precarpathian National University, Ivano-Frankivsk, Ukraine,
h.voitkiv@gmail.com*

In the context of modern educational challenges, especially inclusive education, there's a pressing need to develop effective pedagogical tools. Universal Design for Learning (UDL) stands out as an innovative model that helps address the challenges of adapting the learning process to the diverse needs of students [1, 3]. Research shows that despite legislative progress in Ukraine, the implementation of inclusive practices at the level of the physics teacher remains largely unregulated. This is due to a lack of systematic methodological guidelines, which forces educators to independently overcome barriers related to the abstract and complex nature of the subject [4].

Unlike «reasonable accommodation», which is a reactive response to a specific child's needs, UDL is a proactive approach. It involves the deliberate, advance planning of a lesson to be accessible and effective for all students, regardless of their individual characteristics. This concept is built upon three key principles: multiple means of representation, multiple means of action and expression and multiple means of engagement [2]. Implementing these principles in physics instruction helps lower educational barriers.

Therefore, the structure of an inclusive lesson should be comprehensive, combining macro-, micro-, and integrated components. The macro-elements correspond to the main stages of the lesson; micro-elements are the specific methodological tools that incorporate UDL principles; and the integrated components focus on health promotion and socialization. This approach not only ensures the acquisition of academic knowledge but also contributes to the development of life skills, which are essential for students' adaptation to society [4]. Ultimately, UDL transforms the physics lesson into a flexible, dynamic, and student-centered educational environment that is strategically vital for the effective implementation of inclusion.

- [1]. Kolupaeva A. A., Taranchenko O. M. Inclusion: step by step for teachers: educational and methodological manual. Kyiv, 2023. 232 p.
- [2]. Universal design in education: manual / ed. N. Z. Sofiy. Kyiv: LLC «Pleyady Publishing House», 2015. 76 p.
- [3]. James W., Bustamante C., Lamons K., Scanlon E., Chini J.J. Disabling barriers experienced by students with disabilities in postsecondary introductory physics. Physical Review Physics Education Research. 2020. Vol. 16, No. 2. P. 020111.
- [4]. Formation of key competencies of students through physics: civic and social competence / edited by O. V. Liskovich. Mykolaiv: Center for Editorial and Publishing Activities of the MOIPPO, 2024. 140 p.

Features of teaching children with special educational needs in an inclusive environment

Mandiuk A.

*Vasyl Stefanyk Precarpathian National University, Ivano-Frankivsk, Ukraine,
andrii.mandiuk.21@pmu.edu.ua*

Inclusive education is a systematic approach that ensures the integration of children with special educational needs (SEN) into the general education space. In Ukraine, this process is regulated by law, including the Law on Inclusive Education, which guarantees the right to free education and provides for the development of individual learning plans (ILPs) and the provision of psychological and pedagogical support. Inclusion contributes to the socialization of students with SEN and the formation of tolerance and empathy among all students.

Despite significant progress, the implementation of inclusion in Ukraine faces serious challenges. These include insufficient material and technical resources, a shortage of qualified correctional educators, and the psychological unpreparedness of teachers. For effective teaching, especially of physics, it is necessary to adapt the educational process to the specific needs of different categories of students. This involves using visual and multimodal methods for children with hearing and visual impairments, structured learning for students with autism, and incorporating art therapy for children with Down syndrome.

Key tools for ensuring quality inclusive education are individual learning plans (ILPs) and portfolios. ILPs allow for the determination of unique learning goals for each child, while a portfolio serves as a comprehensive tool for tracking the dynamics of their development. A portfolio helps to document not only academic achievements but also progress in correctional and developmental work, which is critically important for objective assessment and the adjustment of learning strategies. Constant interaction with specialists (psychologists, speech therapists) and parents ensures the effectiveness of this process.

The successful implementation of inclusive education depends on solving systemic problems. Further improvement of the material and technical base, better staffing, and professional development for educators are necessary. The use of ILPs and portfolios is effective, but it requires continuous self-improvement from the teacher. In the future, inclusion should become not just a formal requirement, but the foundation for creating a learning environment that promotes the full development and socialization of every child.

- [1]. Polhun, K. V. Challenges in organizing inclusive education and ways to overcome them. *Pedagogical Kryvorizhzhia: Pedagogical Almanac*, 2016, P. 72–75.
- [2]. Ashytok, N. I. Modernization of education for persons with psychophysical developmental disorders. *Scientific Journal: Educational Space of Ukraine*, 2018, P. 203–208.

Information Technologies in Molecular Physics and Thermodynamics

Klanichka V.M., Klanichka Yu.V.

Vasyl Stefanyk Precarpathian University, Ivano-Frankivsk, Ukraine

v.klanichka@gmail.com

Molecular physics and thermodynamics are fundamental branches of physics that study the microscopic properties of matter and the regularities of thermal processes. Their development is closely linked with the emergence of new research methods, among which information technologies hold a special place. Today, IT is applied not only as an auxiliary tool but also as a full-fledged method of scientific inquiry.

The first attempts to use computational technology in physics date back to the mid-20th century, when the first electronic computers were created. They made it possible to perform complex calculations that had previously taken weeks or even months. A breakthrough occurred in the 1960s–1970s, when numerical methods began to be actively applied to the modeling of molecular systems. In subsequent decades, the development of computer hardware and software led to the creation of specialized packages for simulations and statistical analysis.

One of the most widespread areas is numerical modeling. The molecular dynamics method makes it possible to reproduce the motion of atoms and molecules over time, while the Monte Carlo method statistically studies the behavior of systems under various conditions. These approaches allow the study of phase transitions, the investigation of the structure of liquids and gases, and the analysis of heat transfer processes. Modern software packages such as LAMMPS, GROMACS, NAMD, and Gaussian are the main tools of researchers in this field.

Examples of practical applications include the study of protein structures in biophysics, the development of new nanomaterials, and the analysis of complex systems under extreme temperatures and pressures. Such models help predict the properties of matter even before conducting experiments, which significantly saves resources and time.

Experiments in molecular physics and thermodynamics generate large volumes of data: spectroscopic signals, calorimetric measurements, and X-ray diffraction results. Processing these data requires the use of digital signal processing algorithms, statistical methods, and modern visualization tools.

Recently, machine learning algorithms have been actively applied. They make it possible to uncover hidden dependencies, classify experimental results, and predict the behavior of systems. The use of artificial intelligence is gradually becoming a new stage in the development of thermodynamic research.

Modeling complex many-particle systems often requires enormous computational resources. Supercomputers such as Summit, Fugaku, as well as Blue Gene clusters, perform billions of operations per second. This makes it

possible to investigate processes that cannot be reproduced in the laboratory. Cloud technologies make powerful computations accessible to a wide range of researchers.

Visualization of simulation and experimental results plays an important role in scientific research. Computer graphics not only enable the creation of three-dimensional models of molecules but also the animation of heat transfer, diffusion, and phase transition processes. This greatly facilitates the analysis of results and promotes a better understanding of complex phenomena.

In education, virtual laboratories and simulators (e.g., PhET, Molecular Workbench) are actively used, allowing students to conduct experiments in a virtual environment. This is especially important when real experiments require expensive equipment or involve risks.

Information technologies are being actively integrated into the educational process. Electronic textbooks, multimedia presentations, and virtual experiments enable students to study material more deeply. Moreover, IT connects molecular physics and thermodynamics with other sciences — chemistry, biology, and engineering.

In the future, a special role will be played by quantum computing, which opens up new opportunities for modeling complex molecular systems. Big Data will allow simultaneous analysis of billions of experimental results, while artificial intelligence will help discover new patterns. All this will lead to the creation of fundamentally new approaches in research.

The use of information technologies in molecular physics and thermodynamics is one of the most important factors in the development of these sciences. They make it possible to model complex processes, process large volumes of data, create virtual laboratories and educational simulators. In the future, the role of IT will only increase due to the development of quantum technologies and artificial intelligence.

- [1]. Frenkel D., Smit B. Understanding Molecular Simulation. Academic Press, 2002.
- [2]. Allen M. P., Tildesley D. J. Computer Simulation of Liquids. Oxford University Press, 2017.
- [3]. McQuarrie D. A. Statistical Mechanics. University Science Books, 2000.
- [4]. Lukianenko O. I. Thermodynamics and Molecular Physics. Kyiv: KNU Publishing, 2019.
- [5]. Matveev A. N. Molecular Physics. Moscow: Nauka, 2005.
- [6]. Jensen F. Introduction to Computational Chemistry. Wiley, 2017.
- [7]. Kalos M. H., Whitlock P. A. Monte Carlo Methods. Wiley, 2008.
- [8]. High Performance Computing in Science and Engineering. Springer, 2021.
- [9]. Gross D. Statistical Thermodynamics. World Scientific, 2020.
- [10]. Ukrainian Institute of Scientific and Technical Information. Information Technologies in Science. Kyiv, 2022.

Photovoltaic Systems Based on CdTe and Their Methodical Application in the Educational Process

Inna Kos, I.M. Lishchynskyi, L.I. Nykyruy

Vasyl Stefanyk Carpathian National University, Ivano-Frankivsk, Ukraine

The modern development of renewable energy is driven by the need to identify efficient and economically viable technologies for generating electricity from renewable sources. Photovoltaics is one of the key areas in this process, since solar energy is an inexhaustible and environmentally clean resource. Among the wide range of semiconductor materials used for solar cell production, cadmium telluride (CdTe) occupies a special place due to its physicochemical properties, making it one of the most promising thin-film photovoltaic materials.

The laboratory efficiency of CdTe solar cells has reached over 22%, compared to ~27% for monocrystalline silicon. Recent studies indicate the potential of tandem CdTe–perovskite structures to surpass the Shockley–Queisser limit and achieve efficiencies above 30%. The initial selection of input parameters for developing competitive materials is often best carried out through simulation in professional software environments.

This work presents methodological principles of applying photovoltaic conversion in the educational process, based on modeling in the **SCAPS-1D** environment [1]. Using this simulator allows one to study the influence of various parameters on solar cell characteristics (V_{oc} , J_{sc} , FF, η), analyze defects, and optimize structures without expensive experimental equipment.

To assist young researchers, laboratory exercises in SCAPS-1D have been developed, including:

- *Optimization of CdTe absorber and CdS buffer layer thickness:* students analyze the dependence of efficiency (η) on layer thickness, study the balance between optical and electrical losses, learn to construct graphs, and draw conclusions regarding optimal design parameters.
- *Investigation of temperature dependence of CdTe cell characteristics:* experimental–model analysis of temperature effects on V_{oc} , FF, and η helps students understand physical mechanisms of recombination, thermal losses, and solar cell stability.
- *Influence of defects on solar cell characteristics:* students simulate bulk and interface defects, analyze their effects on recombination, short-circuit current, and fill factor, and learn to draw conclusions about the need for passivation and quality control of thin films.

[1]. SCAPS-1D: Solar Cell Capacitance Simulator. University of Gent. – <https://scaps.elis.ugent.be/>.

Scientific and methodological achievements of Professor Bohdan Ostafiychuk in the context of physics teacher training

M.M. Ilyn.

Vasyl Stefanyk Carpathian National University, Ivano-Frankivsk, Ukraine,

mykola.ilyn.23@pnu.edu.ua

In the current context of school education development in Ukraine, updating the content and teaching methods of natural science and mathematics disciplines, particularly physics, is of particular importance. In this context, there is a need to comprehend and rethink the scientific and methodological heritage of leading Ukrainian physicists, in particular those who contributed to the training of a whole cohort of physics teachers at the Ivano-Frankivsk Pedagogical Institute and One of the prominent figures in this field is Bogdan Ostafiychuk, Corresponding Member of the National Academy of Sciences of Ukraine, Doctor of Physical and Mathematical Sciences, Professor.

The examination of B. K. Ostafiychuk's scholarly and methodological contributions makes it possible to distinguish a number of principles and approaches that may serve as a foundation for improving the content of educational programs and the methods of preparing future physics teachers.

It should be emphasized that Professor Ostafiychuk was not a methodologist in physics in the narrow sense of the term; however, his academic works play a crucial role in the training of prospective physics educators. His research and publications establish the groundwork for developing students' professional, pedagogical, and methodological competencies within the natural and mathematical sciences. Consequently, these insights and approaches, albeit indirectly, exert a significant influence on the quality of physics instruction in institutions of general secondary education, contributing to the advancement of students' competencies, particularly critical thinking, scientific literacy, and the ability to apply knowledge in practical contexts.

The scholarly interests of Professor Ostafiychuk encompassed the physics of magnetic materials, nanoscale systems, and next-generation energy generators and storage devices, which repeatedly demonstrated superiority over global counterparts. He is the author of more than 200 scientific papers, four monographs, several textbooks and teaching manuals, as well as inventions with practical applications.

Under the supervision of B. Ostafiychuk, 43 PhD and 10 doctoral dissertations were successfully defended, attesting to the scale and influence of his scientific school. Alongside his research activities, he actively advanced the educational and organizational spheres—serving as Rector of Vasyl Stefanyk Precarpathian National University from 2005 to 2012. His leadership was directed toward the modernization of the university's technical infrastructure, the development of scientific personnel, and the consolidation of high-quality education. Professor Ostafiychuk left behind a profound scientific and educational legacy that continues to shape future generations of scholars and educators.

The institutional and scientific legacy of Dmytro Freik, founder of the scientific school of semiconductor materials science in Ivano-Frankivsk

M.M. Ilyn, I.M. Lishchynskyy, M.V. Rubinsky.

Vasyl Stefanyk Carpathian National University, Ivano-Frankivsk, Ukraine,
mykola.ilyn.23@pnu.edu.ua

Dmytro Freik (1943–2015) was one of the scientists who shaped Ukrainian physics in the second half of the 20th century and early 21st century. His name is closely associated with the development of semiconductor materials science, solid state physics, and thin film and nanostructure technology, as well as with the formation of a world-class scientific school at Vasyl Stefanyk Precarpathian National University.

Dmytro Freik established research directions that combined fundamental approaches to the study of the physicochemical properties of semiconductors with applied tasks in modern electronics, optoelectronics, and thermoelectrics. His works addressed the physics of semiconductor compounds, thin-film materials, nanostructures, and functional coatings based on tin and lead chalcogenides. Owing to his initiatives, a strong scientific infrastructure was created in Ivano-Frankivsk, which not only ensured the training of highly qualified specialists but also produced significant results that gained international recognition.

Particular attention should be given to the initiative of D. Freik, which brought Ukrainian physical science onto the international stage. In 1979, upon his proposal, the International Conference on Physics and Technology of Thin Films and Nanosystems was launched. From its very inception, this scientific event was intended to serve as a platform for the exchange of experience, scholarly debate, discussion of research findings, and the establishment of academic collaborations among a broad community of scientists working in the fields of physics, chemistry, and materials science.

After D. Freik's death in 2015, the scientific community honored his memory in the best way possible—by naming subsequent conferences after him. Thus, in 2017, 2019, 2021, and 2023, the International Freik Conferences on Physics and Technology of Thin Films and Nanosystems were held. This name change was symbolic – it cemented Dmitry Freik's authorship and founding role in the creation of this prestigious scientific forum. This year's scientific event is the twentieth anniversary.

Today, the Freik Conference is one of the leading scientific forums in the field of thin-film materials science and nanotechnology. It continues the traditions initiated by Professor Freik, while also shaping new research directions, engaging young scholars, and demonstrating the integration of Ukrainian science into the global academic community.

The Methods of Co-operative Learning during Studying of Physics in the Inclusive Classroom

Piatko M.-B.B., Lishchynskyy I.M., Yablon L.S.

Vasyl Stefanyk Carpathian University, Ivano-Frankivsk, Ukraine,
mariia-bohdana.piatko.19@pnu.edu.ua

In the recent years inclusive education in Ukraine has been undergoing great development, which is confirmed by the statistics of the Ministry of Education and Science of Ukraine. Increasing of the quantity of inclusive classes and pupils with special educational needs (SEN) necessitates the search of new effective approaches of teaching school subjects, particularly Physics. These approaches take into consideration individual needs of each pupil and promote the formation of positive attitude towards learning. The methods of co-operative learning obtain special importance. They promote the development of communicative skills, increase in studying motivation and involving of pupils in the process (which is particularly important for pupils with S E N). Such methods help to avoid social isolation, activate social interaction and form an inclusive educational environment. The effectiveness of co-operative learning depends on the skills of the teacher to organize effectively the work of groups and the ability of pupils to organize themselves and build competently the process of their learning (to combine particularly individual work with pair work and group work). Pupils must understand that it is a mutual activity, in which everyone has his/her own face, expresses his/her own individuality and influences the results group. [1].

For this reason with the aim of practical implementing of the specified approach, we have made out lessons plans in Physics for the seventh form (according to the new programme NUS, chapter 2 "Mechanical movement"). In these lessons plan it is demonstrated the usage of methods of co-operative learning during different stages of the lesson; special coloured tabs are adapted for pupils with S E N (autism 3rd - 4th level of support). It is an example of realization of the inclusive approach in teaching Physics. The given plans of lessons help teachers to create a favorable learning environment, where every pupil (independently of the peculiarities of the development) feels being involved in the mutual work - a part of the group. The work in groups, which is provided by the method of collective learning, allows pupils with different educational needs to interact, to develop social skills, to enrich their knowledge in comfortable conditions and to be supported by their coevals. Co-operative learning also promotes the formation of the atmosphere of tolerance, mutual respect and help. That is incredibly important for successful integration of children with S E N into the modern society.

[1]. M. Voron. Methodical work in the conditions of co-operative learning.
URL: <https://osvita.ua/school/method/technol/1501/>

The role of artificial intelligence in improving the quality of modern education

Maksymchuk Serhii

*Vasyl Stefanyk Precarpathian National University, Ivano-Frankivsk, Ukraine,
serhii.maksymchuk.23@pnu.edu.ua*

The development of artificial intelligence (AI) is significantly transforming the educational process. The use of intelligent technologies opens up new prospects for personalized learning, automated assessment, the creation of adaptive environments, and learning analytics [1; 2]. At the same time, it raises a number of challenges and risks related to academic integrity, knowledge standardization, the loss of interpersonal interaction, and security threats [3; 4].

The purpose of this study is to analyze the opportunities and risks accompanying the integration of AI technologies into the educational space, as well as to outline the prospects for improving the quality of education through the use of intelligent tools.

At its core, AI offers a powerful set of tools for personalizing learning. Through adaptive environments and intelligent tutors, AI systems can tailor content to an individual student's pace, style, and proficiency. This capability allows for targeted support and remediation, ensuring that students receive the specific help they need to master complex concepts. Furthermore, AI streamlines administrative tasks through automated assessment and learning analytics, freeing up valuable teacher time to focus on mentorship, creative lesson planning, and direct student interaction. These tools also support inclusive education by offering features like language translation and assistive technologies, thereby broadening access to learning for diverse student populations.

However, the rapid integration of AI is not without its challenges. There are legitimate concerns about a potential decrease in student motivation and an increased risk of social isolation, as technology mediates more of the learning process. The issue of academic integrity becomes more complex with the rise of AI-powered tools that can generate written work or solve problems. Furthermore, the reliance on algorithms introduces threats such as inherent bias in data, and a general lack of preparedness among educators to effectively integrate and manage these intelligent systems. These issues underscore the need for a balanced approach that respects the foundational role of the teacher. Looking ahead, the future of AI in education lies in a symbiotic relationship between human and machine. AI will serve as a powerful facilitator, but the teacher will remain the mentor and guide. A sustainable and ethical framework for AI integration requires the development of clear ethical principles, alongside dedicated programs to enhance teachers' digital competence. Ultimately, the goal is to harness the transformative power of AI to create a more equitable,

Topic 6

efficient, and engaging educational experience without compromising the essential human connection at the heart of learning.

- [1]. Concept of Artificial Intelligence Development in Ukraine. Kyiv, 2020.
- [2]. Luckin R. Machine Learning and Human Intelligence: The Future of Education for the 21st Century. London: UCL IOE Press, 2018.
- [3]. Holmes W., Porayska-Pomsta K., & Holstein K. Ethics of AI in Education. London: Springer, 2022.
- [4]. UNESCO. Artificial Intelligence in Education: Challenges and Opportunities. Paris, 2021.

The scientific and methodological legacy of Ivan Klymyshyn as a factor in shaping future physics teachers

M.M. Ilyn, I.M. Lishchynskyy, A.M. Oleniuk.

Vasyl Stefanyk Carpathian National University, Ivano-Frankivsk, Ukraine,
mykola.ilyn.23@pnu.edu.ua

Current trends in general secondary education necessitate a rethinking of approaches to the teaching of natural and mathematical disciplines, particularly physics and astronomy. One of the factors that can introduce innovation into the methods of studying the natural sciences in general, and the methodology of teaching astronomy in particular, is the exploration of the scientific and pedagogical legacy of Ukrainian scholars.

Of particular interest is the scientific and pedagogical legacy of the Precarpathian School of Physics and Astronomy. One of its most prominent representatives is Ivan Antonovych Klymyshyn, a renowned astronomer, educator, and science popularizer.

I. A. Klymyshyn's scientific interests cover a wide range of issues in astronomy and astrophysics. His research focuses in particular on the propagation of shock waves in inhomogeneous media and in stellar envelopes. Among his scientific works, the monograph "Shock Waves in Inhomogeneous Media" stands out in particular, laying the foundations for further research in the field of relativistic astrophysics. Another important area of I. A. Klymyshyn's scientific activity is the history of astronomy. In particular, he focused on the study of the development of astronomical ideas, chronology, and calendars. These studies are reflected in the works *Calendar and Chronology and History of Astronomy*.

One of the notable chapters in the scientific biography of I. A. Klymyshyn is his contribution to the methodology of teaching physics and astronomy. His textbooks and instructional manuals were widely used in schools and higher education institutions across Ukraine. Among his most popular works are *Astronomy of Our Days*, *Astronomy Yesterday and Today*, *Relativistic Astronomy*, *School Astronomical Handbook*, *Star Map*, *Interesting Astronomy*, *The Sky of Our Planet*, *Pearls of the Starry Sky*, *Atlas of the Starry Sky*, and *The Starry Sky of Ukraine*.

Thus, the scientific and methodological legacy of Professor Klymyshyn holds exceptional value for the contemporary system of school and academic education, particularly in the fields of astronomy and physics teaching. His works combine fundamental scholarly rigor, profound pedagogical intuition, and worldview sensitivity, making them a universal tool for shaping both subject-specific and key competencies of students. We consider it advisable to incorporate I. A. Klymyshyn's contributions into the curricula for the training of future teachers of physics and astronomy. His legacy is not merely instructional content but also a source of pedagogical inspiration, cultural memory, and scientific humanism capable of shaping generations of responsible and knowledgeable citizens.

Modeling the wave scattering on fractal surfaces

Krainova M.D.¹, Saliy Ya.P.¹

¹ Vasyl Stefanyk Carpathian National University, Ivano-Frankivsk, Ukraine

Interaction of waves with fractal systems is a powerful method for studying the morphology of complex surfaces. In particular, the scattering of X-ray, neutron, or electron radiation is sensitive to the fractal geometry of the surface due to multiple scales and resonant effects. It is known that in the case of surface fractals, the scattering intensity is described by a power law.

$$I(q) = A \cdot \frac{\Gamma(5-D_s) \sin\left[\frac{\pi(3-D_s)}{2}\right]}{3-D_s} \cdot q^{-6+D_s},$$

where D_s — fractal dimension of a surface, A - a constant proportional to the surface area of the scattering elements and the scattering contrast. However, for a correct description, it is necessary to take into account the shape of the unit elements and the correlation function of the height distribution [1, 2]. A simplified presentation of the model that allows taking into account these effects and using it for the analysis of experimental data is considered.

The concept of modeling wave scattering on fractal surfaces, taking into account not only the standard power-law behavior, but also the correlation function and the shape of the elements, is demonstrated. The model opens the way to a deeper analysis of the morphology of fractal systems with a high number of parameters and can be used as a basis for further research and optimization in applied problems.

- [1]. Ya.P. Saliy, I.I. Chavyak, I.S. Bylina, D.M. Freik, Topological features of para-phase SnTe nanostructures on polyamide/*Journal of Nano- and Electronic Physics*, Vol. 6, No. 4, 04020(6cc) (2014).
- [2]. Ya.P. Saliy, D.M. Freik, I.S. Bylina, M.O. Halushchak, Crystallographic and orientational nature of nanocrystals in thin-film PbTe-Bi₂Te₃ condensates on sitall/*Journal of Nano- and Electronic Physics*, Vol. 7, No. 2, 02020(8cc) (2015).

AUTHORS INDEX

- Akselrud L.G. 206
Aksimentyeva O.I. 99, 200
Andriichuk O.P. 232
Andrushchak A.S. 144
Anikina N.S. 70, 71, 178, 185, 190, 199
Aniołek K. 118
Antonin S.V. 100
Antonov V.N. 37
Apopii V.H. 15, 89
Azhniuk Y. M. 92, 103, 111, 198
Babenko A.V. 101
Bachynsky O.I. 114
Balabai R.M. 42
Balayeva N. 31, 113
Balovskyak S.V. 193, 225
Bandura A.I. 184
Bandura H.Ya. 74
Barchuk N. 85
Baturin V.A. 32
Bedriy T.R. 160
Bekenov L.V. 37
Belous A.G. 86
Benko T. 134, 136
Berezhnyi O. Yu. 58
Bereznykov O.V. 38
Berezovska N.I. 133, 204
Bersirova O.L. 18
Bezsmertna V. I. 185, 187, 190
Bielinskyi A.O. 105
Bihun R.I. 15, 89
Bilogorodskyy Yu.S. 46
Bilynskyi I.V. 44, 74
Blazevicius B. 234
Blazevicius D. 234
Bodnar T.M. 228
Boichyshyn L.M. 110, 118, 228
Bolkot P.A. 226
Borch M. 193, 212
Borchuk D.S. 160
Bordun I.O. 84
Bordun O.M. 84
Borovyi M.O. 24
Borysenko M.V. 150
Böttger R. 116, 214
Bovgyra O.V. 50
Boychuk V.M. 49, 86, 156, 188
Bratus O.L. 100
Brodnikovskiy M.P. 219
Brytan V. 201
Budnyak T.M. 181
Budzuliak I. I. 56, 176, 179
Budzuliak I. M. 176, 179
Bukartyk N. M. 28
Bychko I. B. 67
Chava M. 118
Chehil Yu.I. 12
Chekaylo M.V. 85, 206
Chelyadyn V.L. 157
Chepela L.I. 24, 125
Cherniushok O. 165
Chernivchan V.Ya. 87
Chernova M.Ye. 218
Cholewa M. 49
Cieniek B. 26, 85
Csík A. 164
Danylenko I. 29
Dan'kiv O.O. 114, 175
Datsenko O.I. 115, 191
Demchyna O.I. 122
Demianenko E.M. 178, 187, 194, 199
Demkiv T. 96
Dhingra A. 226
Diskovskyi I.S 144
Dluzewski P. 116, 214
Dmytriv D.H. 228
Dmytruk A.M. 91, 120

- Dmytruk I.M. 133, 204
Doga P.G. 101
Dombrovskyi S.V. 11
Donyk H. 165
Dovganyuk V.V. 172, 220
Dranchuk M.V. 32
Dremliuzhenko K.S. 13
Druzhinin A. 152
Dubikovskyi O. 98
Dudka O.I. 219
Dusheiko M.G. 32
Dyachenko A.G. 119
Dzeryn M.R. 99
Dzhagan V.M. 98, 115, 120
Dzikovskyi V.Ye. 50
Dziuba V.I. 76
Dzundza B.S. 11, 20
Eliseev E.A. 38
Eremenko A.M. 150
Ershova O.G. 223
Evans D.R. 38
Evtukh A.A. 100
Fareniuk A. 89
Fedenko V.Y. 20, 25
Fedorchenco S. 148
Fedortsov D. 212
Fedosov S.A. 80, 82, 168, 215, 216
Filep M.J. 103, 198, 205
Filonenko O.V. 65
Fochuk P.M. 163, 180
Fodchuk I.M. 172, 193, 220, 225
Frolyak V. 188
Gabdullin M.T. 70, 71, 178, 185,
187, 190, 194, 199
Galiy P.V. 76, 226
Garabazhiv Ya. 212
Gavrilyuk N.A. 70, 71, 178, 185,
187, 190, 194, 199
Gleb V.F. 25
Gomonnai A. V. 92, 103, 111, 198
Gorelov B.M. 202
Gołębiowski M. 116, 214
Grigalevicius S. 234
Gudymenko O.Yo. 120
Halushchak M.O. 157, 162, 222
Hasynets S. M. 92, 111, 198
Havryliuk M.V. 23, 146
Heller R. 116, 214
Hertsyk O.M. 110
Hladun R. 56
Hleb V.F. 117
Hnylytsia I.D. 124
Hoivanovych N.K. 154
Holovatsky I.V. 227
Holovatsky V.A. 227, 230
Holovkin K.A. 221
Honcharuk S. 212
Horbenko Yu.Yu. 99, 200
Horichok I.V. 162, 167
Hornostai V.V. 219
Horyn A.M. 197
Hovdiak V. 167
Hoy.V. 188
Hrabovskyi Ye.S. 133
Hryha L. 129
Hryha V. 128, 129, 135
Hula V. 129
Hutsuliak I.I. 193, 220
Ievtushenko A.I. 29, 32
Ilchuk H.A. 60
Ilnytskyi N. 56
Ilnytskyi R. 56
Ilyn M.M. 241, 242, 246
Isaeva O.F. 13
Isaiev M.V. 24, 125
Ivakh M.S. 51, 140
Ivakhno-Tsehelnyk O. 115
Ivanichok N.Ya. 86, 151, 160
Ivanitska V.G. 163
Ivanochko M.M. 230
Ivanovskyi A.V. 43
Ivanyshyn I.P. 156
Izai V. Y. 103
Kachurak Y.M. 51, 140
Kalyuzhnyi D.Y. 24
Kapush O.A. 120

- Karachevtseva L.A. 34, 36, 169
Karlash A. 91
Karolus M. 118
Karpets M.V. 217, 221
Karpii V.R. 196
Karpyna V.A. 29, 32
Kartel M.T. 63, 169
Kashuba A.I. 25, 60, 203
Kavetskyy T.S. 31, 52, 105, 154
Kaykan L.S. 213
Kazakova O.O. 41
Khatsevych O. 148
Khora O.V. 178, 187, 194, 199
Khoverko Yu. 152
Khrushchyk Kh. 118
Khyyzhun O.Y. 32
Kindrat V. 49
Kinzerska O.V. 88, 183
Kiv A.E. 52, 105, 154
Klanichka V.M. 238
Klanichka Yu.V. 238
Klepko V.V. 143, 153
Klishevich G.V. 202
Klymyuk M. 188
Kochubei H. 31, 113
Koflyuk I.M. 84
Kohut I. 128, 145
Kokhan O.P. 205
Kolbasov G.Ja. 150
Kolkovska H.M. 86
Kolkovskyi P.I. 86, 156, 233
Kolomiiets D. I. 195
Kolomys O.F. 32, 150
Kolomzarov Yu. 234
Kondratenko S.V. 115, 191
Konstantynovych I.A. 68, 230
Koplak O.M. 15
Kopylova L.I. 187, 194, 199
Korablov D.S. 223
Korbityak D.V. 13, 28, 204
Korchovyi A.A. 32, 98
Kordan V.M. 30, 118, 200
Korichev S. 29
Korobeinyk A.V. 181
Korochkova T.E. 70, 71, 194
Korolkov R. Yu. 58, 207, 209
Korostil A.M. 17
Korotchenkov O.O. 202
Korotun A.V. 58, 61, 72, 170, 207, 209
Korotysh V.O. 52
Kos I. 240
Kosinov O.G. 13
Kostyukevich S. 113
Kostyunik R.E. 216
Kosulya O.A. 120
Kotliar D.A. 70, 71, 178, 185, 187, 190, 194, 199
Kotsuybynsky V.O. 49, 86, 156, 188
Kovalenko M.V. 50
Kovalenko O.V. 204
Koval O.Yu. 223
Kovalskyi Y.P. 29, 200
Koval V.M. 32
Koval Yu.V. 168
Koziarskyi D.P. 121
Koziarskyi I.P. 121
Krainova M.D. 247
Kramar A.S. 68, 119
Krapivka M.O. 219
Kravchuk A.V. 178, 187, 190, 194
Kremen O. S. 63, 67
Kremer I.P. 51, 140
Krivushchenko O.Y. 70, 71, 178, 185, 190, 199
Kroitor O. 193
Krupa M.M. 17, 21
Krychovetskyi M.V. 22, 25
Kryshenik V. M. 92, 103, 111, 198
Kshevetskyi O.S. 112
Kukharskyi I.Yo. 84
Kukhazh Y.Y. 154
Kukusta D.A. 37
Kulbachynskyi O. 98
Kulchytskyi B.N. 13
Kulyk O.H. 162

- Kulyk Yu. 211
Kunytska L.R. 143
Kurbatsky V.P. 170
Kurta S. 148
Kuryliuk A.M. 202
Kushchev A.V. 216
Kushlyk M. 224
Kushmeliuk C. 148
Kutnjak Z. 38
Kuzma M. 116, 214
Kuzmin A.R. 193, 220
Kuznetsova D.A. 14, 234
Kuzyk O.V. 114, 175
Kvyk M.V. 44
Leonov D. 89
Lepikh Ya.I. 158
Leshko O.V. 44
Leshko R.Ya. 44, 74
Levchenko B.I. 50
Linnik O.P. 119
Lishchuk P.O. 24, 125
Lishchynskyi I.M. 159, 240, 242, 243, 246
Lisnykh D. 152
Lisovskiy R.P. 160
Lobanov V.V. 63, 65, 67
Lopachak M.M. 228
Lopushansky V. V. 92, 103, 111, 198
Los M.V. 69
Loya V. Y. 92, 111, 198
Luchechko A. 224
Lukiienko I. 19
Lysiv T.O. 151, 160
Lysko V.V. 23, 126, 146
Lytvynenko O.O. 169
Lytvyn P.M. 32, 98, 120, 191
Magunov I.R. 101
Mahanets O.M. 227
Mahlovanyi B. 224
Mastruk E.V. 121
Makhanets O.M. 230
Makohin M.P. 232
Makovshyn V.I. 102
Maksymchuk S. 244
Malakhovska T.O. 205
Malanych G.P. 81, 137
Mamroha V. 136
Mamykin S.V. 14, 32, 234
Mandiuk A. 237
Mandzyuk V.I. 139
Manko D.Yu. 12
Manoryk P.A. 133
Marchuk O. 165
Martyniuk V. 128, 129, 135
Martynova K.V. 174
Mar'yan M. 47
Mashira V.A. 185, 187, 190, 194
Mateik H.D. 94
Matkivskyi O.M. 167, 222
Matskiv O.I. 105
Mazurenko J.S. 213
Mazur M.P. 27, 87, 94, 107, 138, 184
Mazur N.V. 13, 115, 120
Mazur T.M. 27, 87, 88, 94, 107, 138, 183, 184
Medvid I.I. 84, 224
Melnyk Ya.Yu. 44
Mentynskyi N. 49
Mikosianchyk O.O. 216
Mironyuk I. F. 124
Mokhnatskyi M.L. 233
Mokliak M.G. 151, 157, 213
Mokliak V.V. 151, 157, 206, 213
Molnar K.A. 205
Morgun A.V. 11
Moroz H.V. 170
Morozovska A.N. 38
Mozkova O.V. 101
Mroczka R. 116, 214
Mudry S. 30, 211
Muryi Ya.Yu. 100
Mykytyn I.M. 124, 148
Mykytyuk Z.M. 51, 140, 144

- Myroniuk D.V. 32
Myroniuk L. 29
Nadtochiy A.B. 202
Nagirna N.I. 139
Naumenko M. P. 221
Nenchuk T.M. 226
Nenchuk T.N. 76
Nesin S.D. 143
Nikolaienko A. 91
Nosenko A.V. 228
Novak E. V. 172
Novikov S. 212
Nykyrui L.I. 95, 240
Nykyrui Yu. 30
Ocheretyanyi A.O. 44
Odnodvorets L.V. 108
Oleniuk A.M. 246
Olifan O.I. 29, 32
Olikh O. Ya 14, 24
Olkhovik G.P. 14, 234
Onyshchenko V.F. 34, 36
Orletskyi I.G. 121
Ostrauskaite J. 105
Ovsiannikova L.I. 32
Ovsiienko I. V. 125, 186
Padalka I. 26
Panasyuk L.I. 215
Pandiak N.L. 110
Parashchuk T. 131, 165
Pasichnyy M. O. 195
Pauk A. 211
Pavlovskyy Yu. 201
Pavlyshche N.I. 72
Pavlyuk M. 135
Pecherkin M. 180
Pedan R. 83
Peleshchak R. 175
Penyukh B. 89
Permyakova N.M. 143, 153
Petrik I.S. 150
Piatko M.-B. B. 243
Pihel V. 118
Plyushchay A.I. 186
Plyushchay I.V. 24, 186
Podolian A.O. 202
Podust H.P. 133
Pogodin A. I. 103, 205
Politanskyi R.L. 144
Pomytkin A.P. 70, 71, 178, 185, 190, 199
Popilovskyi N. 211
Popiuk K.V. 24
Poplavskyy I.P. 159
Poplavskyy O.P. 159, 226
Pop M. 141
Popov M.Yu. 44
Popovych A.V. 114, 116, 196, 214
Popovych M. 113
Popovych V.D. 116, 196, 214
Potera P. 26, 85, 196
Potiatynnyk T. S. 167
Prokopchuk M. 224
Protsak M.V. 84
Protsenko I.Yu. 108
Pryshliak O.S. 42
Prystaiko A. 128, 145
Pushak A. 96
Pylypez M.M. 156
Pylypko V.G. 163
Pylypov A.I. 100
Pylypova O.V. 100
Rachiyl B.I. 86, 151, 156, 160
Radchenko T.M. 69
Razinkov V.V. 23, 146
Rehei M. 175
Reva V.I. 207
Riabovol V.M. 65
Rogachova O.I. 64, 109, 174
Rokytska O.A. 219, 221
Romaka L.P. 197
Romaka V.A. 197
Romanchuk O.M. 43
Romankevych V. F. 172
Romanovska N.I. 133
Romanyuk V.R. 32
Roshchina N.M. 14, 234

- Rubinsky M.V. 242
Rubish V.M. 61
Rusavsky A. 98
Rybak O.V. 203
Rylova A.K. 108
Sadova N. M. 158
Sagan P. 116, 214
Sahalianov I.Yu. 69
Sakhniuk P.V. 54
Sakhnyuk V.E. 43
Saliy Ya.P. 75, 127, 247
Samarchuk O. 128, 145
Sasnauskaite I. 234
Šauša O. 52, 105, 154
Savchyn V.V. 233
Savenko A.F. 70, 71, 178, 185, 187, 190, 194
Savenko O.F. 199
Schur D.V. 70, 71, 178, 185, 187, 190, 194, 194
Seben V. 47
Sembratovych N. 30
Semeniuk M.V. 110
Semkiv I.V. 25, 60
Sergeeva A. 80, 82
Shaposhnikova T.I. 71, 178, 185, 190
Shender I.O. 205
Shevchenko V.B. 24
Shevchuk O.M. 28
Shirinyan A.S. 46
Shmyhelskyi Y.V. 117
Shpotyuk Y. 224
Shtablavyi I. 211
Shtepliuk I.I. 32
Shtun M.V. 11
Shumakova N.I. 108
Shvets V. 96
Shymchuk O.P. 216
Shymchuk S.P. 215, 216
Shymchyshyn M.O. 51, 140
Shyrokopoias O.O. 207
Sklepova S.-V. S. 160
Sklyarchuk V. 180
Skubenych K. 141
Slipchenko V.V. 219
Slobodnyj V.A. 110
Slobodyanik M.S. 189
Slobodzyan D. 224
Slusarenko M.A. 52
Slynko V.E. 164
Slyotov M.M. 27, 87, 88, 183
Slyotov O.M. 87
Smertenko P.S. 14, 234
Smirnova N.P. 115
Smitiukh O. 165
Solodky M.S. 193, 220
Solomovskyi R.V. 139
Solonchuk D.O. 221
Solonenko D. 92
Solonin Yu.M. 223
Soloviev V.M. 52, 105, 154
Solovyov M.V. 203
Stadnyk Yu.V. 197
Starik S.P. 29, 32
Stasiuk Yu.Yu. 205
Stefanuik I. 26, 114
Stelmakh A.U. 216
Stievenard M. 105
Stoliarchuk I.D. 114, 116, 175, 196, 214
Stoliarchuk N.V. 181
Stolyarchuk A.I. 114, 175
Strelchuk V.V. 29, 32
Strikha M.V. 38
Strizhak P. E. 67
Stronski A. 31, 113
Strusovskiy K.I. 23, 146
Švajdlenková H. 105, 154
Svezhentsova K. 98
Synhaivs'kyi O.F. 137
Syrotiuk A.V. 219
Syrovatko Yu.V. 35
Szlezak J. 224
Tatarenko V.A. 69
Terebilenko K.V. 189

- Tkachenko O. 181
Tkach V.M. 32
Tokarev V.S. 28
Tomashyk V.M. 81, 37
Tomyn Ya.I. 10
Trishchuk L.I. 13
Tsehelnyi V.A. 125
Tsizh B.R. 99
Tuzhykov A.V. 52, 154
Tuziak O.Ya. 76, 226
Tymkiv A. 201
Uhlíř V. 19
Ulyanytskiy K.S. 121
Umantsiv I.M. 232
Urban O.A. 215
Valakh M.Ya. 120
Vashchynskyi V.M. 232
Vashchyshak I.R. 139
Vashchyshak S.P. 139
Vasiliev O.O. 78
Vasin A. 98
Vasylyeva H.V. 124, 142
Vekeryk D.V. 10
Vintoniak V. 129
Virt I. 26, 85
Vistak M.V. 144
Vladymyrskyi I. 83, 217
Voitkiv H.V. 236
Vorobets V.S. 150
Vorovsky V.Yu. 204
Voynarovych I. M. 92, 103
Warowna J. 154
Wieczorek D. 165
Wiendlocha B. 165
Wojciechowski K.T. 165
Yablon L.S. 176, 179, 243
Yakovenko O.S. 125
Yakovliev I.S. 225
Yanchuk I. 212
Yaremii H.I. 10
Yaremiy I.P. 10, 86, 232, 233
Yaremiy S.I. 10, 233
Yashchynskyi L.V. 169, 215
Yatsevych M. 211
Yavorovsky O.P. 65
Yavorska L.O. 22, 95
Yavorskyi R.S. 22, 25
Yavorskyi Y.S. 117, 217
Yefanov V.S. 120
Yeshchenko O.A. 133
Yevchuk I.Yu. 122
Yukhymchuk V.O. 120, 202, 204
Yurkovych N. 47
Yuryev S.O. 206
Yushchuk S.I. 206
Zahn D.R.T. 92, 115
Zaichuk N.P. 216
Zakharchuk D.A. 168
Zamurujeva O.V. 43, 54
Zaplitny R.A. 220
Zaporozhets A. 141
Zapukhlyak R. 188
Zaulychnyy Ya. 217
Zayachuk D.M. 164
Zdyb R. 114, 116, 214
Zelinskiy A.V. 197
Zgardzińska B. 154
Zhyhalo M.M. 122
Zhytskyi A.K 200
Zinchenko V.F. 101
Zolotarenko A.D. 70, 71, 178, 185, 187, 190, 194, 199
Zolotarenko O.D. 70, 71, 178, 185, 187, 190, 194, 199
Zozulia V.O. 189
Zubrytska O.V. 105, 106
Żywczak A. 116, 214

Наукове видання
ФІЗИКА І ТЕХНОЛОГІЯ ТОНКИХ ПЛІВОК ТА НАНОСИСТЕМ
Матеріали XX Міжнародної Фреїківської конференції

МКФТПН-XX

PHYSICS AND TECHNOLOGY OF THIN FILMS AND NANOSYSTEMS
Materials of XX International Freik Conference

ICPTTFN-XX

Технічна редакція:
Тетяна Потятинник, Маргарита Крайнова, Ілона Міщук
Відповідальний за випуск Любомир Никируй

Усі матеріали подано у авторський редакції

Підписано до друку 26.09.2025.
Гарнітура «Times New Roman».

Видавець
Карпатський національний університет
імені Василя Стефаника,
вул. С. Бандери, 1, м. Івано-Франківськ, 76000.
Тел. (0342) 71-56-22.

*Свідоцтво суб'єкта видавничої справи
ДК №2718 від 12.12.2006.*